DEPARTAMENTO DE ASTROFÍSICA

Universidad de La Laguna

Search for Super-Jupiters Around Young Nearby Stars

Memoria que presenta
Dña. Patricia Chinchilla Gallego
para optar al grado de
Doctor por la Universidad de La Laguna.

INSTITUTO Đ ASTROFISICA Đ CANARIAS
xxxxx de 2020

Examination date: xxxx, 2021
Thesis supervisors: Dr. Víctor J. Sánchez Béjar

ISBN: xx-xxx-xxxx-x
Depósito legal: TF-xxxx/2021

A Rebe,

Resumen

La multiplicidad es un aspecto muy importante en los modelos de formación estelares y subestelares. La evidencia observacional de la población de binarias jóvenes a diferentes edades proporciona información muy útil sobre la frecuencia y la evolución de las binarias en sus fases iniciales. Los objetos subestelares se enfrían con el tiempo, y son más brillantes y fáciles de detectar cuando son jóvenes. Algunas de sus propiedades, como la luminosidad y la temperatura efectiva, evolucionan con el tiempo, y es necesaria una estimación de sus edades para obtener sus masas. Encontrar objetos subestelares en asociaciones jóvenes con edades bien determinadas nos permite caracterizar completamente sus propiedades físicas.

El objetivo de esta tesis es explorar la población de compañeros subestelares a gran separación de estrellas jóvenes cercanas. Para alcanzar este objetivo, hemos realizado una búsqueda astrométrica y fotométrica de compañeros con movimiento propio común utilizando datos de VISTA Hemisphere Survey (VHS), el cual cubre el hemisferio sur completo en las bandas J y Ks del infrarrojo cercano, en combinación con otros catálogos astrométricos y fotométricos. Las búsquedas han sido realizadas en la asociación joven Upper Scorpius (USco; 5–10 Myr, d$\sim$145 pc), y en cuatro grupos jóvenes de movimiento (YMGs): AB Doradus (AB Dor; $\sim$150 Myr, d$\sim$30 pc), Tucana-Horologium (THA; $\sim$40–50 Myr, d$\sim$50 pc), β Pictoris (β Pic; $\sim$20–30 Myr, d$\sim$30 pc) y TW-Hydrae (TWA; $\sim$10 Myr, d$\sim$60 pc). Nuestro objetivo es determinar la frecuencia de compañeros subestelares a gran separación para edades jóvenes, e investigar sus propiedades físicas y espectroscópicas.

Hemos compilado una lista de miembros de las asociaciones jóvenes seleccionadas de la literatura. Para la búsqueda en la asociación USco, hemos correlado el catálogo VHS con UKIDSS GCS en un área circular de $60''$ alrededor de cada miembro compilado, lo que corresponde a separaciones físicas proyectadas de hasta 8700 UA. También hemos utilizado fotometría de Pan-STARRS

y astrometría de *Gaia* DR2 para filtrar nuestros candidatos. El rango de masas explorado para los candidatos es 0.01 $M_\odot$ < M < 0.2 $M_\odot$. Para la búsqueda en los YMGs, hemos correlado VHS con el catálogo fotométrico 2MASS en un área circular correspondiente a una separación máxima proyectada de 50 000 UA alrededor de cada miembro compilado. También hemos utilizado los catálogos DENIS, AllWISE y *Gaia* DR2 para descartar contaminantes y alineamientos casuales. El rango de masas explorado varía entre los cuatro YMGs, con límites superiores entre 0.23–0.45 $M_\odot$ y límites inferiores entre 0.008–0.011 $M_\odot$. También hemos obtenido espectroscopía de baja resolución en el óptico y/o infrarrojo cercano de aquellos componentes (primarias o secundarias) que no tenían una caracterización espectroscópica previa en la literatura. Para ello, hemos utilizado los instrumentos NTT/SofI, WHT/LIRIS, NOT/ALFOSC, duPont/B&C, GTC/OSIRIS, VLT/FORS2 y VLT/X-shooter en varias campañas de observación.

En la búsqueda en USco, hemos obtenido 39 compañeros a gran separación con $J > 12.5$ mag en 38 sistemas, en nuestra búsqueda en torno a 1195 miembros de USco. 21 de ellos han sido reportados como compañeros previamente, 16 son miembros de USco que no han sido relacionados como compañeros, y 2 son nuevos descubrimientos. De los 39 compañeros, 22 son probablemente subestelares. La frecuencia de compañeros subestelares en USco es 1.8±0.4% en el rango estudiado de separaciones. Nuestra búsqueda es completa hasta 11 M_{Jup}. Sólo podemos establecer un límite inferior de 0.08% para la frecuencia de compañeros de masa planetaria a gran separación, y por tanto esta frecuencia puede ser mucho mayor.

En AB Dor, hemos identificado 12 candidatos a compañeros en 11 sistemas en nuestra búsqueda en torno a 154 miembros, ninguno de los compañeros es subestelar. En THA, hemos identificado 11 compañeros en torno a 281 miembros, 2 de ellos son subestelares. En β Pic, hemos encontrado 9 compañeros en 7 sistemas en torno a 109 miembros, 3 de los compañeros son subestelares. Por último, en TWA hemos identificado 3 compañeros en torno a 55 miembros, 2 de ellos son subestelares. Las frecuencias de compañeros subestelares obtenidas en los cuatro grupos de movimiento son: 4.3±3.0% en TWA, 3.2±1.8% en β Pic, 0.7±0.5% en THA, y <1.4% en AB Dor.

La caracterización espectroscópica de los compañeros nos ha permitido determinar tipos espectrales entre M temprano y L temprano. También hemos detectado rasgos de juventud en los espectros, como emisión intensa en Hα, líneas alcalinas debilitadas, y una forma triangular en el pseudo-contínuo de la banda H en el infrarrojo cercano en los tipos espectrales más tardíos.

Encontramos que los compañeros subestelares a gran separación en sistemas jóvenes son raros, con frecuencias entre 1–4%. También encontramos

una tendencia en la frecuencia con la edad en el rango de edades estudiado y en comparación con el campo. Sin embargo, los pocos casos encontrados para este tipo de sistemas llevan a obtener incertidumbres elevadas en la determinación de las frecuencias, y estos resultados deben ser tomados con prudencia. Los resultados observacionales indican que el mecanismo de formación para binarias subestelares a muy alta separación puede ser similar al de las estrellas de baja masa.

Entre los compañeros identificados, hemos encontrado varios objetos con masas en torno o por debajo del límite de la quema del deuterio, como USco1621 B, USco1556 B y 2MASS J0249−0557 c. Estos objetos son análogos a los planetas gigantes en órbitas cercanas, y proporcionan una oportunidad única para investigar las propiedades físicas y atmosféricas de los exoplanetas, las cuales son muy difíciles de caracterizar de otro modo.

Abstract

Multiplicity is a very important aspect for stellar and substellar formation models. The observational evidence of the young binary population at different ages provides useful information about the frequency and the evolution of binaries in their early stages. Substellar objects cool down with time, and they are brighter and easier to detect when they are young. Some of their properties, such as luminosity and effective temperature, evolve with time, and an age estimation is needed to derive their masses. Finding substellar objects in young associations with well constrained ages allow for the full characterisation of their physical properties.

The aim of this thesis is to search for the population of wide substellar companions to young nearby stars. To reach this objective, we performed an astrometric and photometric search for common proper motion companions using data from the VISTA Hemisphere Survey (VHS), which covers the whole southern hemisphere in the near-infrared J and Ks bands, in combination with other astrometric and photometric catalogues. The searches were performed in the young nearby Upper Scorpius association (USco; 5–10 Myr, d∼145 pc), and in four young moving groups (YMGs): AB Doradus (AB Dor; ∼150 Myr, d∼30 pc), Tucana-Horologium (THA; ∼40–50 Myr, d∼50 pc), β Pictoris (β Pic; ∼20–30 Myr, d∼30 pc) and TW-Hydrae (TWA; ∼10 Myr, d∼60 pc). Our aim is to determine the frequency of wide substellar companions at young ages, and to investigate their physical and spectroscopic properties.

We compiled a list of members of the selected young associations from the literature. For the search in the USco association, we cross-correlated the VHS catalogue with UKIDSS GCS in a circular area of $60''$ around each compiled member, corresponding to projected physical separations up to 8700 AU. We also made use of Pan-STARRS photometry and *Gaia* DR2 astrometry to further constrain our candidates. The explored range of companion masses is 0.01 $M_\odot$ < M < 0.2 $M_\odot$. For the search in the YMGs, we cross-correlated the VHS

catalogue with the 2MASS photometric survey in a circular area corresponding to a maximum physical separation of 50 000 AU around each compiled member. We also made use of the DENIS, AllWISE and *Gaia* DR2 catalogues to discard contaminants and chance alignments. The explored masses vary between the four YMGs, with high thresholds between 0.23–0.45 $M_{\odot}$ and low thresholds between 0.008–0.011 $M_{\odot}$. We also obtained low-resolution optical and/or near-infrared spectroscopy of the components (primaries or secondaries) with no previous spectroscopic characterisation in the literature. For this task, we made use of the instruments NTT/SofI, WHT/LIRIS, NOT/ALFOSC, duPont/B&C, GTC/OSIRIS, VLT/FORS2 and VLT/X-shooter in several observing campaigns.

In the USco search, we obtained 39 wide companions with $J > 12.5$ mag in 38 systems, in our search around 1195 USco members. 21 of them were previously reported as companions, 16 were known USco members which were not related as companions, and 2 are new discoveries. Of the 39 companions, 22 are likely substellar. The substellar companion frequency in the USco region is 1.8±0.4% in the studied range of separations. Our search is complete down to 11 M_{Jup}. We can only impose a lower limit of 0.08% for the frequency of wide planetary mass companions, and hence this binarity fraction can be much higher.

In AB Dor, we identified 12 candidate companions in 11 systems in our search around 154 members, none of the companions is substellar. In THA, we identified 11 candidate companions around 281 members, 2 of them are substellar. In β Pic, we found 9 candidate companions in 7 systems around 109 members, 3 of the companions are substellar. Finally, in TWA we identified 3 candidate companions around 55 members, 2 of them are substellar. The corresponding derived frequencies for substellar companions in the four YMGs are 4.3±3.0% for TWA, 3.2±1.8% for β Pic, 0.7±0.5% for THA, and <1.4% for AB Dor.

The spectroscopic characterization of our companions allowed to determine spectral types between early-M and early-L. We also found features of youth in their spectra, such as a strong Hα emission, weaker alkali lines, and a triangular shape in the H-band pseudo-continuum in the near-infrared for the latest spectral types.

We find that substellar companions in wide orbits in young systems are rare, with frequencies around 1–4%. We also find a tendency in the frequency of companions with age among the range of studied ages and in comparison with the results in the field. However, the low occurrence of this kind of systems leads to high errors in the frequency determination, and these results should be taken with caution. The observational results indicate that the formation

mechanism for very wide substellar binaries may be similar to that of low-mass stars.

Among the identified wide companions, we found several objects with masses around and below the deuterium burning minimum mass, such as USco1621 B, USco1556 B and 2MASS J0249−0557 c. These objects are analogues of close-in gas giant planets and provide a unique opportunity to investigate the physical and atmospheric properties of exoplanets, which are otherwise very difficult to characterize.

Contents

1

Introduction

"'Cause I have found,
all that shimmers in this world is sure to fade"
— *"Shimmer"*, Fuel.

1.1 Substellar objects

1.1.1 Concept and definitions

Substellar objects are celestial bodies which are not massive enough to maintain stable nuclear fusion processes in their interiors and become stars. This category includes brown dwarfs and exoplanets.

The existence of a minimum mass for stable hydrogen burning was first predicted by Kumar (1963). He modeled the internal structure of these theoretical entities, as there was no observational evidence of their existence yet, and determined that the matter in the interior of these objects would become degenerate as they contract during their formation. He placed a minimum stellar mass limit in 0.07–0.09 $M_{\odot}$, which depended on the metallicity. In the same year, Hayashi & Nakano (1963) also predicted that "stars" less massive than 0.08 $M_{\odot}$ would contract and reach a high electron-degeneracy configuration without burning hydrogen.

Kumar (1963) called the objects not able to fuse hydrogen in a stable manner "black" dwarfs. But this name was not adequate, as it was also used to refer white dwarfs in their theoretical final cooling stage (Mestel & Ruderman

1967). Several other names were proposed for substellar objects, as "Lillipution Stars" (Shapley 1958), "Infrared Dwarf" (Davidson 1975), "Super-Jupiters" or "Extreme Red Dwarfs". In 1975, Jill Tarted suggested the most accepted name today, "Brown Dwarfs" (Tarter 1975).

Brown dwarfs were thought to be the responsible for the missing Dark Matter in our Galaxy (e.g. Stevenson 1978; Hawkins 1986; Daly & McLaughlin 1992; Kerins & Carr 1994), one of the biggest open questions of the modern astrophysics. Back in those days, some Initial Mass Function (IMF) estimations, as the famous Salpeter power-law mass function (Salpeter 1955), pointed to a very high proportion of Brown Dwarfs compared to stars. Nevertheless, nowadays it is known that brown dwarfs are not so numerous to be the responsibles for the missing matter in our Galaxy (e.g. Alcock et al. 1996, 1998).

There is a strong debate regarding the difference between brown dwarfs and planets. One of the proposed criteria to distinguish these two populations is the ability to burn deuterium in their interiors: objects with masses above the deuterium burning minimum mass would be called "brown dwarfs", and objects with masses below this limit would be called "planets" (Basri 2000). Another proposed classification scheme for substellar objects based on their formation process. According to this scheme, objects formed in isolation or in systems from the collapse of a cloud, and not able to fuse hydrogen in a stable way, would be called "brown dwarfs", regardless of their mass. Only objects formed in a protoplanetary disk around a star would be called "planets" (Chabrier et al. 2005). This classification is problematic because sometimes it is not possible to determine the formation process leading to a low-mass substellar object found for example in isolation, or as a companion to another star in a wide orbit, because it may have been formed in any of the two proposed scenarios. As a working definition, the IAU in 2003 adopted the following criteria: objects with masses above the deuterium burning minimum mass would be called "brown dwarfs", objects below this threshold that are found orbiting stars would be called "planets", and objects below the deuterium burning mass limit found in isolation would be called "planetary-mass objects", "free-floating planets" or any other appropriate name.

1.1.2 First observational discoveries

The observational discovery of brown dwarfs came decades after their theoretical prediction, in the year 1995, when two groups published almost simultaneously their genuine discoveries. The first one, Teide 1, was a young isolated brown dwarf belonging to the Pleiades star association, discovered in a photometric survey conducted by Rafael Rebolo, M. Rosa Zapatero Osorio and

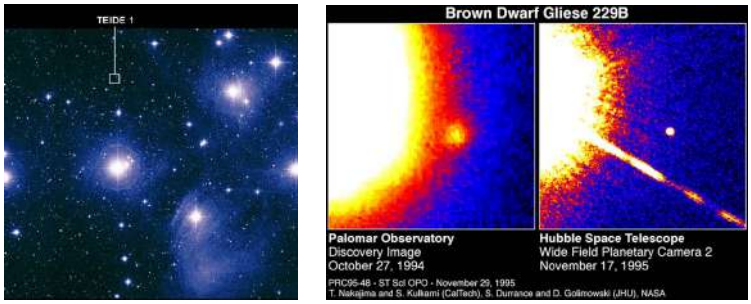

(a) (b)

Figure 1.1: The first observed brown dwarfs, Teide 1 (Left panel, Rebolo et al. 1995, image credit: IAC) and GJ 229B (Right panel, Nakajima et al. 1995, image credit: NASA).

Eduardo Martín (Rebolo et al. 1995). The second one, GJ 229B, was a brown dwarf companion to an M-type star discovered using coronography by Tadashi Nakajima and collaborators (Nakajima et al. 1995).

The first observed exoplanets came surprisingly in the same years. Three years before the observations of the first brown dwarf, in the year 1992, Aleksander Wolszczan and Dale Frail reported the discovery of two planets with several times the mass of the Earth orbiting the pulsar PSR 1257+12, from the small and periodic time variations in the pulsar emissions (Wolszczan & Frail 1992). Two years later, in 1994, Wolszczan published the discovery of a third "moon-mass" object in the system (Wolszczan 1994). Later, in the year 1995, the first planet orbiting a solar-type star was discovered by Michel Mayor and Didier Queloz through the radial velocity method: 51 Pegasi b (Mayor & Queloz 1995). It was a Jupiter-like object in a close orbit to the G-type star 51 Pegasi. This discovery led them to receiving the Nobel Prize in Physics in the year 2019. Nowadays, more than 4000 planets have been discovered and confirmed, and several thousands of planet candidates are waiting for confirmation. At the same time, thousands of brown dwarfs (and free-floating planets) have been identified in the field, in open clusters and star forming regions and as companions to stars or other substellar objects.

1.2 Formation mechanisms and evolution of substellar objects

The substellar mass regime includes a wide variety of objects, from the highest mass brown dwarfs, in the frontier with very low-mass stars, to, for example, the planets in our Solar System. These objects do not seem to be formed in a unique formation scenario. On one hand, low-mass stars (and stars in general) are formed from the gravitational collapse of molecular clouds of interstellar gas. On the other hand, the planets in our Solar System were formed in a protoplanetary disk that surrounded our recently-formed Sun in its first evolutionary stages. Since brown dwarfs are the link between planets and low mass stars, it is a priori plausible for them to be formed in a similar way to any of them. Understanding the characteristics of the different formation scenarios for substellar objects is nowadays one of the main open questions in astronomy, and strong efforts are being made, both from the theoretical and observational perspectives, to shed light on this problem. We present here a summary of the main proposed formation mechanisms for very low mass objects.

1.2.1 Gravoturbulent cloud fragmentation

Cloud fragmentation occurs when a molecular cloud of interstellar gas collapses due to the Jeans instability. The Jeans instability is produced when the cloud mass is too high for its gas pressure to overcome the gravitational self-attraction and prevent its collapse. The minimum mass required to trigger this collapse is called the "Jeans mass", and depends on the density and temperature of the cloud. The Jeans mass for the temperatures and densities found in an average star-forming cloud is around one or several solar masses (Larson 1985; Padoan & Nordlund 2004).

Forming a low mass object from the collapse of an ordinary cloud requires a small, very dense and very cold environment, in which the self-gravitational collapse could be triggered with very little mass. This can be achieved in the gravoturbulent fragmentation scenario. In this scenario, the inner fluctuations of the density inside a collapsing cloud can create small and overdense clumps which can produce lower mass objects, as brown dwarfs. The supersonic turbulence as the reason for the presence of sub-structures of the density field in gas clouds was proposed by Padoan et al. (1997). A subsequent work by Padoan & Nordlund (2002) showed through theoretical simulations that this formation scenario could reproduce the observed stellar initial mass functions (IMF), and that it could also lead to the formation of objects with substellar masses (see also Padoan & Nordlund 2004). Many other studies have analysed the theoretical outcome of the turbulent fragmentation of gas clouds through simulations,

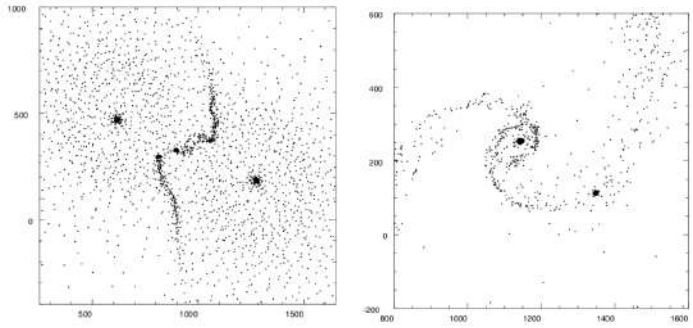

Figure 1.2: Particle plots from a coplanar disk-disk interaction simulation, from Watkins et al. (1998a). Left panel shows the fragmentation of the shock layer in the interaction. Right panel shows the primary star with a newly-born companion.

and shown results consistent with the observed stellar IMFs (e.g. Bate et al. 2002; Jappsen et al. 2005; Hennebelle & Chabrier 2008; Bate 2009, 2012; Jones & Bate 2018). One of the predictions of this mechanism is that the fraction of substellar objects to stars depends on the different physical properties of the star forming regions (density, temperature, turbulence, etc.) and, hence, the IMF distribution is not universal.

The opacity limited minimum mass is the smallest gravitationally bound mass which is able to radiate the energy produced by its compression. An object with a mass below this threshold would not be able to form by gravitational collapse, and, hence, an object with this mass cannot divide into smaller fragments (Low & Lynden-Bell 1976; Rees 1976; Silk 1977). The size of these smallest fragments is a figure of great significancy, as any observed object with a lower mass would need an alternative explanation for its formation, different than gravitational collapse. A few examples of the theoretical estimations of the opacity limited minimum mass are 0.007 $M_{\odot}$ by Low & Lynden-Bell (1976), around 0.010 $M_{\odot}$ by Silk (1977), 0.010 $M_{\odot}$ by Boss (1987, 1988), 0.004 $M_{\odot}$ by Bate (2009), 0.001–0.004 $M_{\odot}$ by Whitworth & Stamatellos (2006), and 0.003 $M_{\odot}$ by Whitworth (2018). [1]

1.2.2 Dynamical interactions between protostars

Besides the ordinary gravitational collapse of molecular clouds, there are some other phenomena which can lead to the formation of substellar objects. One of them is the dynamical interaction of protostars in their early forming stages.

One of the possible effects of these interactions is the premature ejection of a stellar embryo Reipurth & Clarke (2001); Bate et al. (2003). In this scenario, a collapsing fragment is expelled due to dynamical interactions with other objects before it can accrete the mass from its surroundings. This way, a potential star can become a substellar object if the ejection occurs before the protostar is able to accrete the minimum necessary mass for stable hydrogen burning. Premature ejections are favoured in environments with high (proto-) stellar densities Bate (2012).

Watkins et al. (1998a,b) also proposed that substellar objects can be formed in the dynamical interaction between the massive circumstellar disks of close protostars, which could lead to new fragmentations in the interacting material. According to their simulations, this new fragmentations would lead to lower-mass companion objects, including substellar objects. Figure 1.2 shows two frames of one of the coplanar disk-disk interactions simulations from Watkins et al. (1998a), where the shock layer in the interaction leads to high-density clumps where substellar objects can be generated.

1.2.3 Photo-erosion

This formation scenario occurs when the presence of nearby massive stars alters the medium that surrounds a forming protostar. In this case, a group of recently formed OB stars ionise the surrounding gas and form an H II region. The ionizing radiation of these massive stars can erode the outer layers of nearby pre-stellar cores, removing the envelope and disk of the protostars, and preventing them from accreting further material (Hester et al. 1996). Through this mechanism, substellar objects can be formed if their accreting envelopes are ionized before they reach a stellar mass (Whitworth & Zinnecker 2004).

1.2.4 Planetary disks formation

During their formation process, protostellar cores develop circumstellar disks of material around them. These disks can host the formation of further objects around the central protostar. There are two different formation mechanisms in protostellar disks:

[1] $1\ M_{\odot} = 1047.57\ M_{Jup}$.

- Disk fragmentation. If the disk is massive and cool enough to become gravitationally unstable, it can form objects by gravitational collapse, in a similar way as clumps collapse and form stars from an interstellar gas cloud (Boss 1997, 2001; Bate et al. 2002; Bate 2012). The fragmentation most likely happens in the outer regions of the disk, where the material temperature is cooler. After the collapse of the fragment is triggered, the newly-formed object can accrete more material from the protostellar disk, becoming more massive.

  Another mechanism that can trigger the fragmentation of a disk is the infall of further material from the external environment (parent cloud Kratter et al. 2008, 2010). The objects formed by fragmentation can also be later ejected from the disk by dynamical interactions with other disk objects or with nearby stars, and become isolated (Stamatellos & Whitworth 2009; Basu & Vorobyov 2012). Once the object is expelled from the disk, it will not be able to accrete more material, and it will not be able to become more massive. Some authors have pointed out that the presence of a massive companion can influence the fragmentation of a protostellar disk. However, the results on this influence are contradictory: while Boss (2006) explains that the presence of a companion may trigger the instabilities more easily, Nelson (2000); Mayer et al. (2005) and Lodato et al. (2007) find the opposite.

  Unstable disks which are prone to fragmentation are usually massive. For this reason, the objects formed through this mechanism are most likely brown dwarfs, or even low-mass stars if the disk is massive enough, and disk fragmentation does not favour the formation of objects with very low masses, below the deuterium burning mass limit. However, some studies have proposed that this mechanism could produce objects as small as rocky planets (Boss 1997; Nayakshin 2010).

- Core accretion. This formation scenario leads to rocky planets and gas giant planets. When the disk gets colder, the particles in it start to condensate, forming dust grains. These dust grains then begin to adhere through collisions and gravitational attraction, forming small bodies which can further grow in size by sticking to more material, and become planetesimals (Pollack et al. 1996). If the planetesimal accretes enough mass, it can start to clean the zones belonging to their orbits, attracting all the material in their influence zone and becoming rocky proto-planets. These proto-planets can become gas giant planets if they grow massive enough to accrete and also retain the gas from the disk. The objects

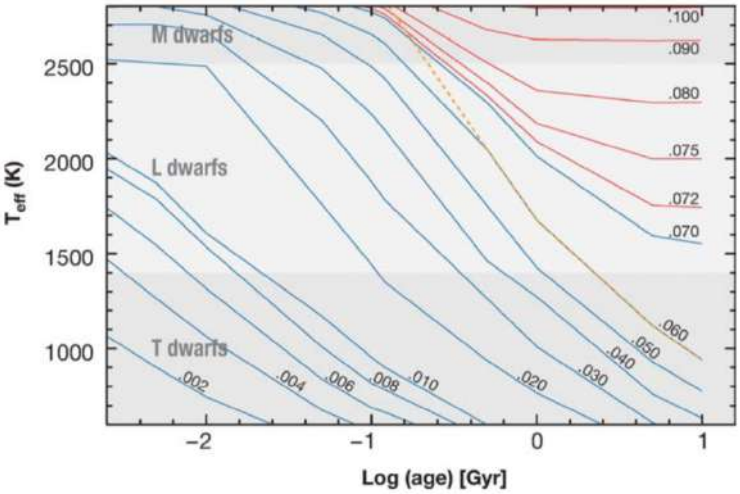

Figure 1.3: Effective temperature vs. time diagram for very low-mass objects from Kirkpatrick (2005). Isomass lines for different masses are shown as solid lines. The masses are indicated above each line, in solar units. Stars are marked in red, substellar objects are marked in blue. The boundary at which lithium is 50% depleted is shown as a yellow dashed line. Evolutionary tracks for temperatures higher than 1500 K come from Chabrier et al. (2000), using the AMES-dusty models of citetAllard2001. Evolutionary track for temperatures cooler than 1500 K come from Baraffe et al. (2003), using the AMES-cond evolutionary models of Allard et al. (2001).

formed by core accretion can also suffer from dynamical perturbations from other disk objects and be moved to different orbits, or ejected.

1.2.5 Evolution of substellar objects

In their early evolution, very low-mass objects (including stars and substellar objects) contract due to self-gravity, increasing the density and temperature in their interior. Then, this contraction stops, due to the onset of thermonuclear reactions if the object is massive enough to reach the required core temperature, or because of the electron degeneracy if the object is not. Stevenson (1978) shows a very comprehensive description of the phases in the evolution of a brown dwarf:

- **Collapse phase:** In its formation, the brown dwarf follows the Hayashi

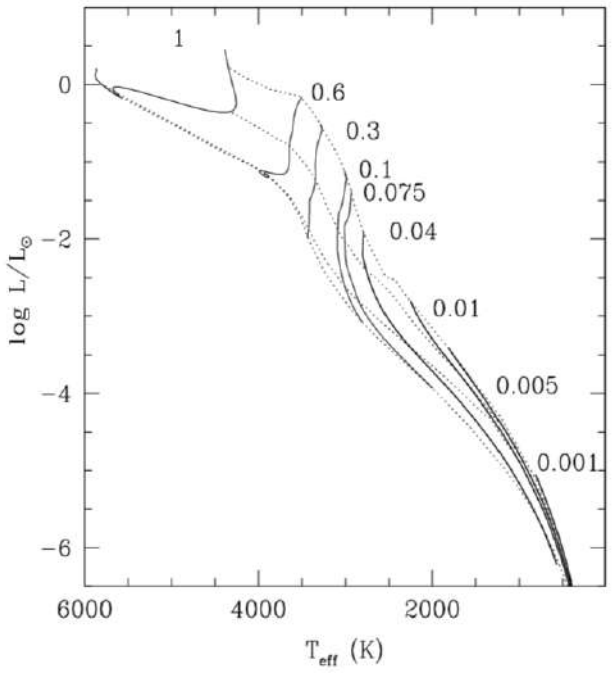

Figure 1.4: Hertzsprung-Russel (HR) diagram including the evolutionary tracks for very low-mass objects, from Chabrier & Baraffe (2000). The isomasses are marked as solid lines, and each mass is shown in solar units. The isochrones corresponding to 1 Myr, 10 Myr, 100 Myr and 5 Gyr are shown as dotted lines, from right to left.

line at a roughly constant effective temperature, and contracts, progressively decreasing its luminosity. During this phase, the interior is fully convective, and contraction occurs in an adiabatic way.

- **Deuterium Burning:** If the object has a mass above 0.013 $M_{\odot}$, it enters a pseudo-main sequence phase, in which Deuterium is burnt. During this phase, luminosity enters a relatively stable phase.

- **Degenerate Cooling:** After the Deuterium Burning phase is finished, the brown dwarf starts cooling down again and contracting, and its luminosity starts decreasing again.

Low-mass stars, which are capable of hydrogen burning, reach the Main Sequence (MS) and stay in it for most of their lives. More massive stars reach the MS faster, and spend very little time in the early contraction phase, while low-mass stars need more time to start burning hydrogen in their interiors. On the other hand, substellar objects, which are not able to reach these central temperatures, keep on cooling down with time as they contract. One of the consequences of this is that their effective temperature and spectral type evolve with their age, as they never reach stability. This is a problem when we try to characterise their physical properties, like their masses, as, in contrast to main sequence stars, it is a priori not possible to correctly identify the mass of a substellar object based on their temperature, spectral type and/or luminosity alone. In fact, in their early evolution, high-mass brown dwarfs have temperatures and spectral types which are very similar to those of low-mass stars. Figure 1.3 shows the evolution of the effective temperature with time for very low-mass objects. This Figure clearly shows the huge degeneracy in mass for the ultracool spectral types. Any late-M or early-L dwarf can be either of stellar or substellar nature, depending on its age. The latest L-dwarfs and the T-dwarfs are always substellar, but they can also present a great variety of masses, depending on their age. Figure 1.4 shows the Hertzsprung-Russel (HR) diagram with the evolutionary tracks for low-mass stars and substellar objects, from (Chabrier & Baraffe 2000). In this diagram we can see the huge decrease in luminosity suffered by substellar objects as they move to lower effective temperatures with time.

1.3 The interior and atmospheric properties of substellar objects

1.3.1 The interior of substellar objects

In their formation, low-mass stars contract increasing their core temperature and density, until they reach high enough temperatures and pressures in their interior to start the ignition of the PPI chain.

$$\begin{aligned} p + p &\longrightarrow d + e^{+} + \nu_e \\ p + d &\longrightarrow {}^{3}He + \gamma \\ {}^{3}He + {}^{3}He &\longrightarrow {}^{4}He + p + p \end{aligned} \tag{1.1}$$

This creates a radiative and thermal pressure which stops the contraction of the newborn star, as it enters the MS. At lower masses, the contraction is slower, and higher densities are required to reach the temperatures necessary for the onset of the hydrogen burning phase. For masses below $\sim$0.1 $M_{\odot}$, the density of the core becomes high enough to cause the electron degeneracy. If the mass of the object is too low, it will reach a high level of degeneracy capable of stopping the further contraction of its core before the needed temperature for hydrogen burning is reached, and the object will not become a star but a brown dwarf.

The hydrogen burning minimum mass limit is set around $\sim$0.07–0.08 $M_{\odot}$ for a solar metallicity according to theoretical models (Chabrier & Baraffe 1997). However, this threshold depends on features like the metallicity: for a lower metallicity, the hydrogen burning minimum mass would be higher, as the more transparent atmospheres would lead to a more efficient radiative transfer, and more mass would be needed to reach the required temperature in the core. Other facts as the rotation of the object can also affect this threshold. Objects with masses below the hydrogen burning minimum mass limit will not be able to fuse hydrogen in their interiors in a stable way, and will cool down and shrink over time. Nevertheless, the most massive brown dwarfs are able to fuse hydrogen in their interiors for a limited amount of time.

Substellar objects can, however, burn some other elements. Figure 1.5 shows the evolution with time of the central temperature for very low-mass objects, the minimum core temperature required to burn each element, and the minimum masses which are able to meet these requirements. If their central temperature reaches values higher than $\sim 0.5 \cdot 10^{6}$ K, they are able to fuse deuterium through the second line of the PPI chain, until the initial abundance of this element in the interior of the object is exhausted. The minimum mass

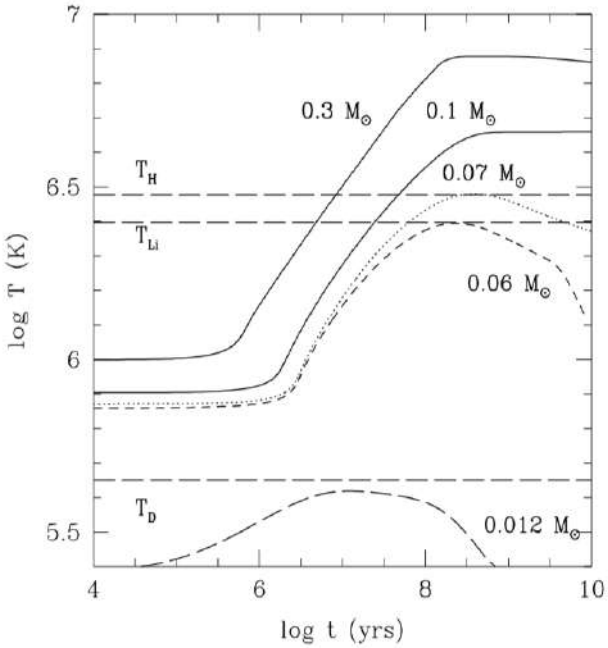

Figure 1.5: Evolution of the central temperature of very low-mass objects with time, from Chabrier & Baraffe (2000). The minimum temperatures for deuterium, lithium and hydrogen are marked as dashed horizontal lines. The tracks for the objects with the minimum required mass to burn each of these elements are also shown.

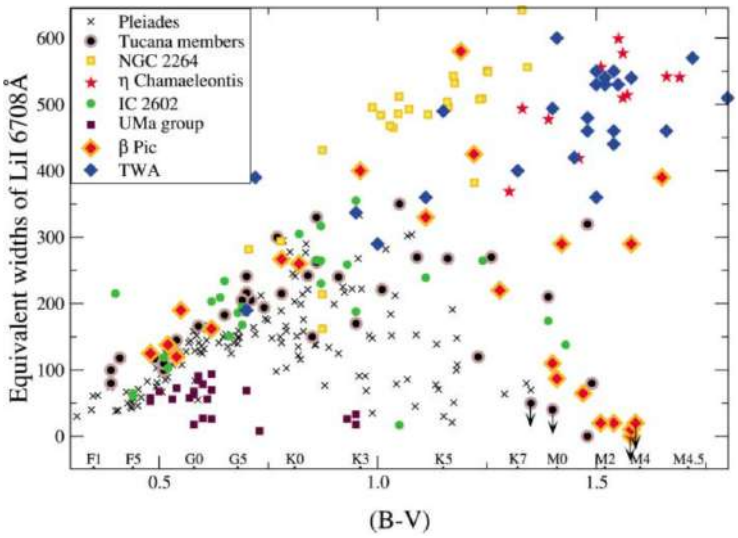

Figure 1.6: Pseudo-equivalent widths (pEW) of the lithium doublet at 6708 Å for members of young moving groups of different ages, from Zuckerman & Song (2004). The pEW is measured in mÅ.

needed to reach this central temperature is around 0.012 $M_\odot$, and objects with masses lower than this threshold will not be able to fuse deuterium in their interiors (Saumon et al. 1996; Burrows et al. 1997; Chabrier & Baraffe 2000). The deuterium-burning phase of substellar objects lead to a pseudo-main sequence in which their contraction is halted for a short period of time.

Another light element which can be fused by substellar objects is lithium. This element can be fused in the interior of objects with masses above 0.06 $M_\odot$, which are able to reach core temperatures above $\sim 2.5 \cdot 10^6$ K (Chabrier et al. 1996), as shown in Figure 1.5. Lithium is burnt through the process:

$$^7Li + p \longrightarrow {}^4He + {}^4He \tag{1.2}$$

As in the case of the deuterium, the primordial abundance of this element is destroyed through its fusion reaction, until the element is exhausted. This fact lead to the establishment of the so-called "lithium test" (Rebolo et al. 1992; Magazzu et al. 1993; Martin et al. 1994) to determine the substellar nature of very low-mass objects through the detection and measurement of the Li I doublet at 6708 Å. The fully-preserved presence of this element would indicate that the object is not massive enough to fuse it and is, hence, substellar. This test is, however, not useful to determine the substellar nature of brown dwarfs with masses above ~ 0.06 $M_\odot$, as they are capable of destroying their lithium, and for ages below ~ 120 Myr, because very low-mass stars can also preserve lithium until that age. Another useful capability of the lithium test is the age determination of a group of simultaneously-formed objects, as the amount of lithium still present in the low-mass stars (and high-mass brown dwarfs) indicates the life time of the group, acting as a stellar hourglass. Figure 1.6 shows the pseudo-equivalent width of the lithium doublet at 6708Å for members of young moving groups of different ages.

In an average picture, the interior of a substellar object consists of a fully ionized H^+ / He^{++} plasma, with a correlated, partially degenerate electron gas. In it, the energy is transported mainly by convection. The core is completely convective, and behaves as a $n = 3/2$ polytrope. The detailed thermodynamical description of the interior of these objects is a complex problem of dense matter physics, and requires a deep comprehension of strongly correlated, polarisable, partially degenerate classical and quantum plasmas, and partial ionization due to pressure. Metals do not affect substantially the structure and evolution of brown dwarfs, due to their small abundance (Chabrier & Baraffe 1997), although they do affect their atmospheric properties and effective temperature, and the hydrogen burning minimum mass limit.

1.3.2 Spectroscopic properties of substellar objects

The atmospheres of brown dwarfs are thin and composed of molecules and grains. Their radiative regions represent a very small fraction in size of the object. Their surface temperatures are around and below 3500 K, and they emit most of their energy in the near-infrared wavelength range.

Brown dwarfs emit most of their energy in the infrared wavelength range. The spectral energy distribution for brown dwarfs is dominated by the collision-induced absorption of H_2 and $H_2 - He$ and strong molecular absorption bands like TiO, VO, H_2O, CO or CH_4. Also, below 2400 K, grains condense out and contribute to the opacity. Although the atmosphere of a brown dwarf is dominated by molecular hydrogen and neutral helium, there are other ionized species present, like H_2^-, H^- and He^-. We can also find hydrides, oxides, magnesium silicates, carbides and iron grains (Burrows & Liebert 1993).

Substellar objects present very late spectral types. As we have already presented, these objects cool down with time, and their spectral types and spectral features are highly dependent not only on their mass, but also on their age. The youngest and/or most massive brown dwarfs show spectral types as early as mid-M.

The M-type spectral type is characterized by strong molecular band absorptions in the optical, mainly from TiO and VO, which are the main source of opacity, and also by MgH, CaH, FeH and CaOH in late-M dwarfs. H_2O and CO features are dominant in the infrared. These features leave practically no space for a true continuum. The most common way to classify M-type objects is by their TiO and VO strength index, up to spectral types of ∼M7 (Kirkpatrick et al. 1991). For spectral types between M7–M9.5, TiO weakens and VO saturates. For this reason, pseudo-continua spectral indices were introduced as a classification method by Martín et al. (1999).

The discovery of objects cooler than the M-stars required the expansion of the commonly used stellar spectral-type classification sequence; *OBAFGKM* (Cannon & Pickering 1901); with the establishment of new spectral types. Martin et al. (1997) proposed the use of the letter "L" for the recently discovered objects whose spectra showed cooler features not compatible with the M spectral type. Later, Kirkpatrick et al. (1999) analysed the available alphabet letters, and agreed on the use of the letters "L" and "T" for the objects cooler than "M", and established a classification based on spectral standards in the optical for the subtypes L0 to L8. Almost simultaneously, a similar classification scheme for L-dwarfs was presented by Martín et al. (1999).

L-type spectral type corresponds to effective temperatures of $T_{\rm eff}$=2200–1500 K. Their main spectroscopic features are:

- The TiO and VO bands weaken compared to the M-dwarfs. These features are present in the early L-types, and disappear from mid-L on due to the formation of dust grains.
- The alkali lines (Na I, K I, Rb I, Cs I) strengthen. The Na I and K I lines remarkably grow stronger in mid- and late-L dwarfs.
- The hydrides bands (CrH, FeH) also strengthen.
- The H_2O absorption bands also grow strong in the infrared. This absorption becomes stronger in late-L dwarfs.

The cooler spectral type "T" was firstly proposed by Kirkpatrick et al. (1999) to define objects similar to Gliese 229B, which was cooler than the L-dwarfs and showed strong methane (CH_4) absorption in its spectrum. A couple of years later, Burgasser et al. (2002) defined a classification scheme for the subtypes T0–T8. This proposed classification was performed in the near-infrared, as the optical emission of these very cool objects is very low, and the most remarkable spectral features, useful for their spectral typing, are present in the near-infrared. Nevertheless, Burgasser et al. (2003) also presented an optical classification scheme for T-dwarfs.

The T-type spectral type transition is characterized by the disappearance of the CO and the formation of methane, and the clearing of condensate clouds and sedimentation of condensed species below the photosphere. For the late-T types, ammonia molecules (NH_3) start to appear (Saumon et al. 2012). The effective temperatures associated to T type objects range between T_{eff}=1500–600K. The main spectroscopic features of the T dwarfs are:

- Strong CH_4 absorption bands appear in the infrared, between 1.0 and 1.2 μm.
- H_2O absorption bands are very strong.
- The combination of the strong CH_4 and H_2O absorptions, and the H_2 collision-induced absorption lead to a bluer $J-Ks$ color in the infrared.
- The Na I and K I lines dominate the pseudo-continuum in the optical, and by late-T these lines begin to supress the pseudo-continuum between them.

Figure 1.7, extracted from Kirkpatrick (2005), shows the classification schemes in the optical and the near-infrared of the new cool spectral types "L" and "T", where the main spectral features of these spectral types can be distinguished.

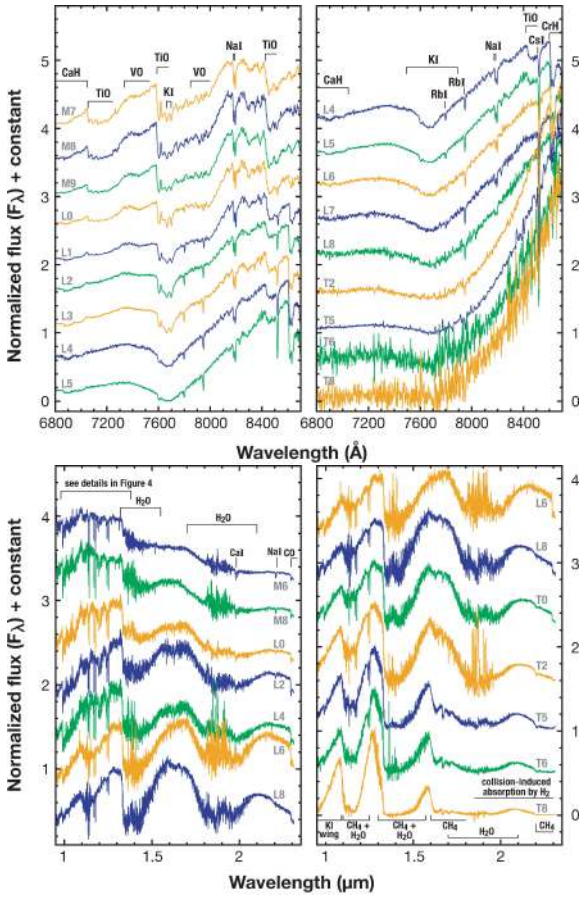

Figure 1.7: Upper panel: Optical spectra of standard M7–T8 objects. Lower panel: Near-infrared spectra of standard M7–T8 objects. Both adapted from Kirkpatrick (2005).

Some years later, in the early 2010's, two objects cooler than the latest-type T-dwarf were discovered. They were WD 0806−661B b Luhman et al. (2011), found as a wide comoving companion to a white dwarf, and CFBDSIR J1458+1013B Liu et al. (2011), a close companion to another brown dwarf, found by adaptive optics imaging. The expected effective temperature of these companions was around 300–400 K. Unfortunately, the first object was too faint and the second one was too close to its primary to achieve a successful spectral characterisation. However, 13 similar objects which could be spectroscopically characterised were soon discovered by Cushing et al. (2011) and Kirkpatrick et al. (2012) using the new Wide-field Infrared Survey Explorer (WISE; Wright et al. 2010) survey data. This lead to the definition of the coolest spectral class up to date: the "Y" dwarfs.

The Y spectral type corresponds to objects with effective temperature lower than 600 K. There is still little knowledge about Y dwarfs, as only around 30 Y dwarfs have been found yet. Their spectral features in the near-infrared appear to smoothly extrapolate the tendency of late T-dwarfs. Figure 1.8 shows some examples of low-resolution spectra of early Y-dwarfs (figure from Cushing 2014), and the comparison of an Y0 dwarf with some late-T dwarfs (figure from Cushing et al. 2011). Some remarkable features of the Y-dwarfs are:

- Very strong H_2O and CH_4 absorption bands in the near-infrared. This produces very thin J and H pseudo-continuum bands.
- Possible presence of ammonia (NH_3) absorption bands in the infrared, which is not so evident due to some overlapping with the CH_4 bands.
- Very red optical/near-infrared to mid-infrared colors. These objects emit most of their light in the mid-infrared wavelengths.
- Accused drop of the absolute magnitude in *J, H, K* bands in the T/Y transition.

The spectral type Y is the coolest spectral type proposed to date. With its inclusion, the complete updated spectral-type classification sequence, in a natural temperature-based order, becomes *OBAFGKMLTY*. [2]

[2] There has not been yet a consensual update on the commonly-used and widely known in the astronomical community mnemonic rule "Oh Be A Fine Guy/Girl Kiss Me", an example could be: "Oh Be A Fine Guy/Girl Kiss Me Later, Thank You".

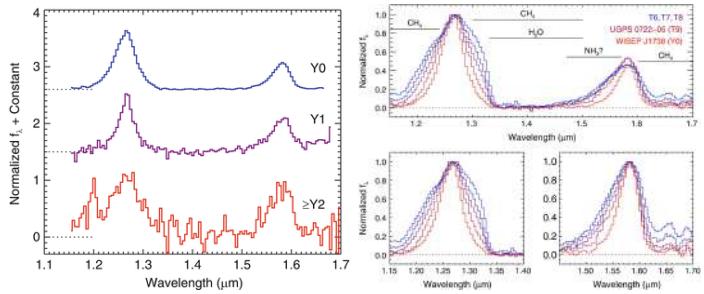

Figure 1.8: *Left panel*: Low-resolution near-infrared spectra of Y-type dwarfs. Adapted from Cushing (2014). *Right panel*: Comparison between T and Y spectra. It can be noted how Y0 spectral type follows the late T tendency naturally. Adapted from Cushing et al. (2011).

1.4 Stellar and substellar binaries, and wide companions.

Back in the 18th century, Michell (1767) was intrigued by the fact that many "fixed" stars were very close to each other in the sky. He determined that the probability that many of these relative positions were coincidental was very small, proposing the real existence of clusters, and what he called "satellite" stars orbiting other "fixed" stars. He remarked that, if measured, their periods and separations would provide the mass relation between the two components, allowing to understand the relation between the mass and the brightness of the stars, which was then unknown. Some decades after, in 1803–1804, Herschel traced some part of the orbits of several proposed binaries, and found out that they followed Newton's gravitation laws, confirming the existence of binary stars.

The formation and evolution of stellar and substellar binaries is nowadays a matter of study and debate. Although the theoretical formation models and simulations of collapsing gas clouds are capable of reproducing the observed initial mass function in stellar formation, the frequency and characteristics of stellar binaries is a more complex problem. The results obtained from theoretical simulations need to be compared and supported by observational evidence, which can provide very useful constraints to the models.

1.4.1 The formation of binaries

Theoretical models and simulations show that there are several possibilities for the formation of binaries. The first one is the early fragmentation of a

protostellar clump, prior to its collapse (e.g. Boss 1988; Pringle 1989; Fisher 2004; Goodwin et al. 2004; Offner et al. 2010; Bate 2012; Offner et al. 2016). In this scenario, two or more clumps are formed close to each other. In this case, the maximum separation of the binary would be related to the initial size of the fragmented clump. In addition, in star-forming regions, the gas clouds can present substructures in the shape of elongated filaments (e.g. Shu et al. 1987; Arzoumanian et al. 2011; Könyves et al. 2015; Marsh et al. 2016; Könyves et al. 2020), which can also be responsible for the birth of very wide binaries (Kraus et al. 2011).

The second possibility for binary formation is the fission of a protostellar core after its initial collapse. However, hydrodynamical simulations do not agree with this scenario, and thus it seems unlikely (see the review by Tohline 2002, and references therein).

The third possibility is the fragmentation of the accretion disk surrounding the central protostar (e.g. Toomre 1964; Adams et al. 1989; Bonnell 1994; Bonnell & Bate 1994; Whitworth et al. 1995; Matsumoto & Hanawa 2003; Stamatellos & Whitworth 2009; Kratter et al. 2010; Zhu et al. 2012), in which the companion object may even reach a similar mass to the central protostar (Bonnell 1994; Matsumoto & Hanawa 2003). In the disk fragmentation scenario, the maximum separation of the produced binary would be determined by the size of the disk, which is typically around 50–100 AU. Moreover, the disk fragmentation mechanism seems to be more easily produced in the outer regions of the protostellar disks, where the cooling processes are more efficient, rather than in the inner regions (e.g. Rafikov 2005; Matzner & Levin 2005; Whitworth & Stamatellos 2006; Stamatellos et al. 2007). Once the fragmentation is triggered, the proto-companion would start accreting material, carving a gap in the disk. Inwards migration can then be produced, resulting in a much closer binary, which could not be explained with an in-situ formation.

1.4.2 The frequency of binaries

Observational studies show that the majority of the Solar-mass stars, ∼50–60%, are formed in binary systems (Duquennoy & Mayor 1991; Raghavan et al. 2010; Tokovinin 2014; Moe & Di Stefano 2017). The evidence also shows that this frequency is lower for low-mass stars and brown dwarfs, but still a significant proportion of M-type stars, around ∼20–30%, are also part of multiple systems (Leinert et al. 1997; Reid & Gizis 1997; Delfosse et al. 2004; Lada 2006; Allen et al. 2007; Ward-Duong et al. 2015; Cortés-Contreras et al. 2017). The frequency is similar or lower for late-M and later spectral types (Koerner et al. 1999; Reid et al. 2001; Bouy et al. 2003; Burgasser et al. 2003; Close et al. 2003;

Gizis et al. 2003; Siegler et al. 2003, 2005; Fontanive et al. 2018).

In young sparse associations and star forming regions, like Taurus and Upper Scorpius, the frequency of binaries tends to be higher than the field, by a factor 2–4. For example, Ghez et al. (1993) find a binary frequency among T-Tauri stars in Taurus and Ophiucus of 60±17%, 4 times higher than in main sequence stars. Leinert et al. (1993) find a multiplicity rate of 42±6% in Taurus, twice the frequency obtained in field stars by Duquennoy & Mayor (1991). Chen et al. (2013) find a mutiplicity frequency of 64±8% in a sample of nearby (<500 pc) Class 0 protostars, two times higher than for a sample of Class I protostars, and 3 times higher than main-sequence stars. Furthermore, Tobin et al. (2016) find a multiplicity fraction of 57±9% for Class 0 protostars, and 23±8% for Class I protostars in Perseus, also showing a notable difference in the very early evolution of protostars. In addition, a recent result by Zúñiga-Fernández et al. (2020) points to a dependence with the age on the frequency of spectroscopic binaries (SB). They find a SB fraction of around 20–30% for the youngest studied associations (η Cha, β Pictoris and TW Hydrae), and ∼10% or lower for the oldest studied associations (with ages between 35–125 Myr). On the other hand, the frequency of binaries in denser cluster is similar to the field. It is not clear whether these differences are due to the older age of the dense clusters, and hence have an evolutionary explanation related to the disruption due to interactions with external bodies (Raghavan et al. 2010) or due to dynamical evolution of higher order systems (e.g. Reipurth & Mikkola 2012; Elliott & Bayo 2016); or the differences may be due to different initial conditions in the formation stage of dense and sparse associations.

Regarding higher order multiples, a very interesting study by Reipurth & Mikkola (2012) show how stars born in triple systems tend to form tight binaries with a third component, frequently the less massive one, orbiting at wide separations due to dynamical interactions between the three objects. For the stable bound triple systems that they find in their simulations, the typical separations of the close binary go from 10–100 AU, and the wide component shows typical orbits of around 1000–10 000 AU, although there are some systems showing separations up to more than 1 000 000 AU. Wide binaries which are formed this way need some time to reach the apastron for the first time (half the orbital period). Objects in very wide orbits take tens to hundreds of Myr to reach this point. During this "unfolding time", they are less likely to being disrupted by external perturbers than if they were originally born in these wide separations.

1.5 Looking for brown dwarfs and planetary-mass companions: current search methods

There are different techniques to search for substellar companions to stars. One of them is the direct detection of the objects through imaging. This method is limited by the faintness of substellar objects compared to the primaries and by the angular separation between the two components, and only the brightest and most widely separated substellar companions can be detected through direct imaging. To solve this problem, other indirect detection methods have been developed, as radial velocity, transits or microlensing.

1.5.1 Direct imaging

The direct imaging method consists on the direct detection of the light coming from the companion through imaging. This method is useful only for relatively bright and widely-separated companions. The limitations of this method depend on the resolution and depth of the images. For very close companions, where high contrast is needed, this method can be aided by the coronography, interferometry adaptive optics and lucky imaging techniques.

- Coronography consists on the removal of the host star's light, by obscuring it through an internal mask and a pupil stop, or through an external occulter or "star shade". This allows for the detection of close objects which otherwise would be hidden by the PSF of the primary star.
- Interferometry consists on the use of two or more separated telescopes to increase the observing resolution. A special case is the nulling-interferometer (Bracewell 1978), which collects the segments of the wavelength front and applies a half-wavelength path delay before combining them, to block out the light of the central object (usually the primary star) and allow the detection of fainter off-axis objects, in a similar way to a coronograph. An example of this is the Keck Interferometer Nuller (KIN; Colavita et al. 2009).
- Adaptive optics is used to increase the resolution of the images taken with ground-based telescopes, in particular for large diameter telescopes, removing the effects of the atmospheric turbulence, and allowing to obtain nearly diffraction limited images and to resolve close objects more easily. This method is based on a fast measurement of distortions in the arriving light wavefront, and the compensation of these distortions through actuators that can alter the shape of the deformable mirrors in real time to correct the distortions.

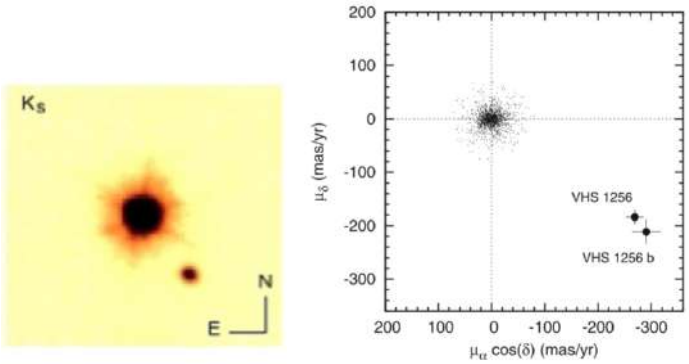

Figure 1.9: *Left panel:* Finding chart of the VHS 1256−0557 system, which was found through direct imaging and proper motions. The field of view is $30'' \times 30''$, and the orientation is north up and east to the left. *Right panel:* Proper motion diagram of the VHS 1256−0557 system. Both components are labeled. Other objects within 1^o around the primary are shown as black dots. Both diagrams from Gauza et al. (2015).

- Lucky imaging techniques consist on acquiring very short exposures with fast cameras so that the changes in the atmospheric conditions above the telescope remain practically unchanged during the exposures. Some of these images may not be significantly altered by atmospheric turbulence, and then they are nearly diffraction limited. The best quality images (called "lucky" images) are selected, and shifted and added, and the result is a high resolution final image.

The direct imaging technique also allows for the search of substellar companions through their proper motion (PM). When two objects are gravitationally bound, they travel together through space, and we measure the same apparent movement in the sky for both. For this method, we need astrometric measurements of the bound objects in different epochs. The precision of the measurement depends on the precision of the astrometry of the different epochs and the time baseline between them. This method is useful for intrinsically fast moving objects, and objects with low heliocentric distances (which have higher apparent movements). Figure 1.9 shows the finding chart and PM diagram of VHS 1256−0557 B (Gauza et al. 2015), a substellar companion identified through this method. The PM diagram shows that the high PM of the two components is very similar, and remarkably stands out compared to the PM of the other objects in the same field of view, thus confirming them as com-

panions. The recent *Gaia* mission has also contributed to the identification of many PM companions, providing not only precise PM for the targets, but also very accurate parallaxes, which help to constrain the companionship of wide binaries.

Another possible method for the detection or confirmation of substellar companions to any target stars through direct imaging is through their photometric colours, and magnitudes. When two objects are physical companions, they must be certainly placed at the same heliocentric distance from our point of view, and they must share a similar age and metallicity, assuming that they were formed at the same time and have been traveling together through space since their formation. If they fulfill these conditions, then they will show colours and apparent magnitudes which follow the photometric sequence of the corresponding age, displaced to their heliocentric distance. This method is frequently used not only to search and confirm candidate companions, but also to search for members of young associations (e.g. Lodieu et al. 2007; Luhman et al. 2018). Figure 1.10 shows an example of the use of a colour-magnitude diagram to separate a group of coeval objects which are placed at the same heliocentric distance, from Lodieu et al. (2007). In this case, this diagram was used to obtain candidate members of the Upper Scorpius association. In the diagram we can distinguish the photometric sequence of the members, brighter and redder than the background objects, and the photometric cut that was used to perform the candidate selection. Although some non-members (contaminants) partially overlap with the photometric sequence of the association, most of the selected objects are good candidates.

In contrast to most of the indirect methods, direct imaging also allows for the spectroscopic characterisation of the substellar companions, especially in the cases where the angular separation of the components is large. In the case of high-contrast imaging (e.g. through AO or coronography), the acquisition of spectroscopy is complicated, but it still can be often performed at least in the wavelength ranges where the contrast of the components is lower (e.g. Chauvin et al. 2004, 2005b; Janson et al. 2010; Chilcote et al. 2017). Spectroscopy provides us with very valuable information about the substellar companion properties, as its spectral type, temperature, gravity, metallicity, radial velocity, activity or element abundances, which can help to constrain crucial parameters such as the age and mass of the objects. Besides, planetary mass objects found in isolation or as wide companions can serve as analogs to close-orbit giant planets, which are normally very difficult to characterise due to the proximity to their parent stars.

Direct imaging is also favoured in the search for young substellar objects. As these objects cool down with time, they are brighter and easier to detect

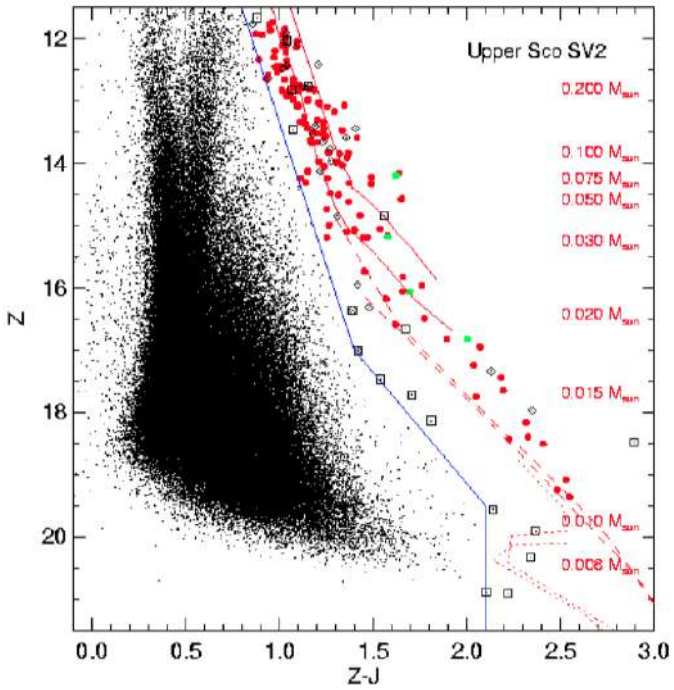

Figure 1.10: Colour-magnitude diagram selection in Z vs $Z - J$ for the objects in the USco region, from Lodieu et al. (2007). Green and red objects are USco members, following the photometric sequence of the association. Background contaminants are marked as black dots. Other contaminants which partially overlap with the photometric sequence are shown as black open markers. Some theoretical isochrones are shown as red lines. The theoretical corresponding masses for each Z magnitude are labeled in red. The photometric cut used to select the candidates is shown as a blue line.

at young ages. Old substellar objects are intrinsically very faint, and their detection is a very challenging task. As an example, we have not been yet able to detect nor discard the presence of the so-called "Planet 9", a hypothetical wide substellar companion of our own Sun, which presumably could be the responsible of the peculiar clustering of the orbits of trans-Neptunian objects (de La Fuente Marcos & de La Fuente Marcos 2014; Trujillo & Sheppard 2014; Batygin & Brown 2016). Due to the intrinsically faintness of this hypothetical object, it could have remained so far unnoticed despite its proximity (e.g. Linder & Mordasini 2016).

1.5.2 Indirect methods

1.5.2.1 Radial velocity

When binary systems are not resolved, radial velocity measurements can help us to reveal the binary nature of a system. Stars are gravitationally affected by the presence of a massive and close object, which makes them move around a common center of mass. This movement is reflected in their spectrum thanks to the Doppler effect. There are two main ways to detect the presence of a companion using radial velocity method:

- Detecting periodical displacements of the main lines in the spectrum of a star. This indicates a periodical change in the velocity of the star, due to this movement around the common center of mass.
- Detecting the periodic occurrence of double lines. This indicates that the spectrum is in fact the addition of the spectra of two different objects moving with different velocities. These binaries are known as "double-lined spectroscopic binaries". The detection of double lines is only possible if the companion has a similar brightness to the primary star.

This method is used for the detection of binary stars and the presence of close-orbit brown dwarfs and exoplanets. Some examples are the first discovered exoplanet orbiting a solar type star, 51 Pegasi b (Mayor & Queloz 1995), the earth-mass planet orbiting α Centauri B (Dumusque et al. 2012), the multiple planetary system found in Upsilon Andromedae (Butler et al. 1999), or the multiple planetary system with 7 planets HD 10180 (Lovis et al. 2011), which was found to have 9 planets in a later analysis by Tuomi (2012). The effect in this method is stronger for closer and more massive companions, but the Doppler displacement of the lines in the spectrum can also be used to detect smaller bodies if the precision of the radial velocity measurements is high

enough. Some remarkable examples of instruments involved in the detection of substellar objects through radial velocity are the HARPS spectrograph at La Silla 3.6m telescope (Mayor et al. 2003), the CARMENES spectrograph (Quirrenbach et al. 2010) on the Calar Alto 3.5m telescope, the HIRES spectrograph (Vogt et al. 1994) on the Keck-I telescope, the SOPHIE spectrograph (Bouchy & Sophie Team 2006) on the Observatoire de Haute- Provence 1.93-m telescope, the ESPRESSO spectrograph (Pepe et al. 2010) on the VLT, SPIRou (Artigau et al. 2014) on the Canada-France-Hawaii Telescope, MAROON-X (Seifahrt et al. 2018) on the Gemini North Telescope, or IRD (Kotani et al. 2014) on the Subaru Telescope.

1.5.2.2 Precision astrometry

As in the radial velocity method, this procedure is also based in measuring the gravitational effect produced by the presence of a high-mass close companion to the host star. The displacements of the primary star around the common center of mass can be detected astrometrically. This method is useful when the target star has a large proper motion and if the companion is not bright enough to be visually detected.

Only a few substellar companion candidates have been detected so far with this technique (Muterspaugh et al. 2010; Sahlmann et al. 2013, 2014; Curiel et al. 2020). However, the *Gaia* mission is expected to allow for the detection of thousands of companions through this method (Perryman et al. 2014).

1.5.2.3 Microlensing

Gravitational lens effect consists on the deviation and amplification of the light coming from a distant source due to the presence of a massive object passing in front of it in our line of sight. Then, the image that we receive from the distant source is distorted and its flux is magnified.

Gravitational lens events created by low mass objects acting as lenses can also be detected. If the lens object is not very massive, the deviation of the light cannot be easily measured, but we can measure the flux variations of the distant source. When the (low-mass) lens passes in front of the source, we observe a peak in the photometric brightness of the background source. The presence of a companion of a star which acts as gravitational lens will be revealed as a small second peak in the flux magnification of the distant source.

Currently, over 80 planets have been discovered through microlensing. Some examples are OGLE 2003–BLG–235/MOA 2003–BLG–53 (Bond et al. 2004), a 2.6 M_{Jup} object which was the first confirmed exoplanet found through this

method, the super-Earth OGLE–2005–BLG–390Lb found by Beaulieu et al. (2006) or the multi-planetary systems OGLE–2006-BLG–109L (Gaudi et al. 2008) and OGLE–2012–BLG–0026 (Han et al. 2013).

Microlensing events are not very frequent, as the lenses and sources must be perfectly aligned in our line of sight. A fruitful option to increase the probability of a detection is to photometrically monitor dense regions of the sky, as stellar or galaxy clusters. Another problem of microlensing method is that observations can hardly be repeated for a specific object, as they normally are unique events.

1.5.2.4 Transits

The transits method is one of the most successfully used in the detection of exoplanets. When a planet crosses in front of its host star, it blocks part of the light that we receive from it. This "eclipse" is detectable as a slight variation in the stellar flux, that we can measure. The shape of the light-curve during the transit gives us information about the planet size and orbit.

We can only detect transits in those stellar systems whose orbital plane is oriented nearly "edge-on". The transit probability is higher for objects orbiting in close orbits (short periods). For objects with long periods the transits occur less frequently, and hence finding them is less probable. Furthermore, when found, their characterization is more tedious as measurements cannot be repeated so frequently. The first detections of transiting planets were accomplished by Charbonneau et al. (2000), Konacki et al. (2003) and Alonso et al. (2004). Some later remarkable projects involving transiting exoplanets are the space missions CoRoT (Baglin et al. 2006; Auvergne et al. 2009), Kepler (Borucki et al. 2010) and TESS (Ricker et al. 2014), and the future mission PLATO (Rauer et al. 2014); and the ground-based projects HAT (Bakos et al. 2004), MEarth (Nutzman & Charbonneau 2008; Irwin et al. 2009), SuperWASP (Pollacco et al. 2006), TRAPPIST (Jehin et al. 2011) and SPECULOOS (Delrez et al. 2018).

The transits method also allows the performance of transmission spectroscopy, a technique based on the detection of small variations in the stellar spectrum during a transit, due to the absorption in the transiting object's atmosphere. With this technique we can obtain information about the planet atmosphere composition and temperature (e.g. Seager & Sasselov 2000).

1.6 The search for wide substellar companions through direct imaging

The first wide substellar companion discovered by direct imaging was also one of the first discovered brown dwarfs: the T-dwarf companion Gl 229 B (Nakajima et al. 1995). Since then, many other substellar companions have been found through direct imaging. Some of the most remarkable examples are the late T-dwarf companion in a quadruple system Gl570 D (Burgasser et al. 2000), the brown dwarf companion to one of the nearest stars ϵ Indi B (Scholz et al. 2003; McCaughrean et al. 2004), the first planetary-mass companion imaged orbiting a brown dwarf 2M1207−39 b (Chauvin et al. 2004, 2005a), and many other wide substellar companions with masses below or around the planetary mass boundary: DH Tau B (Itoh et al. 2005), AB Pic b (Chauvin et al. 2005b), CHXR 73 B (Luhman et al. 2006), UScoCTIO 108 B (Béjar et al. 2008), Fomalhaut b (Kalas et al. 2008), 1RXS J160929.1−210524 b (Lafrenière et al. 2008), HR8799 bcde (Marois et al. 2008, 2010), FU Tau AB (Luhman et al. 2009), GJ 758 B (Thalmann et al. 2009), β Pic b (Lagrange et al. 2010), 2M J044144 B (Todorov et al. 2010), Ross 458 (AB)c (Goldman et al. 2010), GSC 06214−00210 b (Ireland et al. 2011), CFBDSIR 1458+10 b (Liu et al. 2011), HIP 78530 b (Lafrenière et al. 2011), SR 12 ABc (Kuzuhara et al. 2011), WD 0806−661 B (Luhman et al. 2011), κ And b (Carson et al. 2013), 2M0103−55 (AB)b (Delorme et al. 2013), ξ UMA b (Wright et al. 2013), HD 95086 b (Rameau et al. 2013b), GJ 504 b (Kuzuhara et al. 2013), 2M0122−24 B (Bowler et al. 2013), GU Psc b (Naud et al. 2014), 2M0441+2301 AabBab (Bowler & Hillenbrand 2015), VHS 1256−1257 B (Gauza et al. 2015), 2MASS J2126−8140 (Deacon et al. 2016), 2MASS J0249−0557 c (Dupuy et al. 2018), and SDSS 2131−0119 (Gauza et al. 2019).

Only a few of the substellar companions found through direct imaging have extremely wide separations of more than 1000 AU. Table 1.6, published in Chinchilla et al. (2020b), shows a compilation of the known substellar companions with the highest projected physical separations from their primaries.

Name	Short Name	RA	DEC	Age (Gyr)[a]	Projected Sep. (AU)[a]	Companion Mass (M_{Jup})[a]	Ref.[c]
2MASS J160251.16−240150.2	USco 1602−2401 B	16:02:51.17	−24:01:50.45	0.005–0.010	1000	19–67	1
SR12 C	SR12 C	16:27:19.51	−24:41:40.1	0.0003–0.010	1083	6–21	2
ULAS J130041+122114	Ross 458 c	13:00:41.73	+12:21:14.7	<1	1168	5–14	3
ULAS J150457.65+053800.8	HIP 73786 B	15:04:57.66	+05:38:00.8	>1.6	1260	... [b]	4, 5
2M1348−1344B	2M1348−1344B	13:48:02.90	−13:44:07.1	4–10	1400	31–79	6, 7
2MASS J06462756+7935045	HD 46588 B	06:46:27.56	+79:35:04.5	1.3–4.3	1420	47–75	8
ε Indi Ba	ε Indi Ba	22:04:10.52	−56:46:57.7	1.3	1459	37–57	9, 10
ε Indi Bb	ε Indi Bb	22:04:10.52	−56:46:57.7	1.3	1459	21–35	9, 10
2MASS J14571501−212148	Gl 570D	14:57:15.04	−21:21:49.82	2–10	1525	30–70	11
HIP 38939 B	HIP 38939 B	07:58:01.61	−25:39:01.4	0.3–2.5	1630	18–58	12
2MASS J04414489+2301513 Ba	2M0441+2301 Ba	04:41:45.65	+23:01:58.0	0.001–0.003	1800	16–22	13, 14
2MASS J04414489+2301513 Bb	2M0441+2301 Bb	04:41:45.65	+23:01:58.0	0.001–0.003	1800	8–12	13, 14
2MASS J02495436−0558015	2MASSJ0249−0557 [c]	02:49:54.36	−05:58:01.5	0.016–0.028	1950	10.6–12.9	15
Gl 417B	Gl 417B	11:12:25.7	+35:48:13	0.63–0.9	1970	50–56	16, 17, 18
Gl 417C	Gl 417C	11:12:25.7	+35:48:13	0.63–0.9	1970	45–52	16, 17, 18
GU Psc b	GU Psc b	01:12:36.48	+17:04:31.8	0.07–0.13	2000	9–13	19
WD 0806-661 B	WD 0806-661 B	08:07:14.68	−66:18:48.7	1.5–2.5	2500	6–9	20, 21
SDSS J2249+0044A	SDSS J2249+0044A	22:49:53.47	+00:44:04.6	0.012–0.790	2600	11–73	22
SDSS J2249+0044B	SDSS J2249+0044B	22:49:53.47	+00:44:04.6	0.012–0.790	2600	9–68	22
WISEP J142320.86+011638.1	BD +01° 2920B	14:23:20.86	+01:16:38.1	>2.3	2630	20–50	23
SDSS J175805.46+463311.9	SDSS J1758+4633	17:58:05.46	+46:33:11.9	0.5–1.5	2685	21–37	24
2MASS J16212830−2529558	USco1621 B	16:21:28.31	−25:29:56.1	0.005–0.010	2900	14–18	25
WISE J200520.38+542433.9	Wolf 1130C	20:05:20.38	+54:24:33.9	>2	3150	>52	26
HIP 77900B	HIP 77900B	15:54:30.47	−27:19:57.51	0.005–0.010	3200	15–27	1
2MASS J15562344−2541056	USco1556 B	15:56:23.43	−25:41:05.7	0.005–0.010	3500	12–17	25
2MASSW J1523226+301456	Gl 584C	15:23:22.6	+30:14:56	1.0–2.5	3600	47–79	16
SDSS J213154.43−011939.3	SDSS 2131−0119	21:31:54.43	−01:19:39.3	>1	3800	52–73	27
WISE J111838.70+312537.9	WISE 1118+31	11:18:38.70	+31:25:37.9	2–8	4100	14–38	28
VVV J151721.49−585131.5	β Cir B	15:17:21.60	−58:51:30.0	0.37–0.50	6656	51–66	29
2MASS J21265040−8140293	2MASS J2126−8140	21:26:50.40	−81:40:29.3	0.010–0.045	6900	11.6–15	30
HIP 70849B	HIP 70849B	14:28:42.32	−05:10:20.9	1–5	9000	... [b]	31
ULAS J133943.79+010436.4	HD 118865B	13:39:43.79	+01:04:36.4	1.5–4.9	9200	42–68	32
ULAS J145935.25+085751.2	ULAS J1459+0857	14:59:35.25	+08:57:51.2	>4.8	∼20 000	63–79	33

Table 1.1: Known wide substellar companions with projected separations above 1000 AU. Table published in Chinchilla et al. (2020b). *(a)*Data compiled from the literature. *(b)*Classified as a T dwarf. *(c)* References: (1) Aller et al. (2013); (2) Kuzuhara et al. (2011); (3) Goldman et al. (2010); (4) Scholz (2010); (5) Murray et al. (2011); (6) Mužić et al. (2012); (7) Deacon et al. (2012b); (8) Loutrel et al. (2011); (9) Scholz et al. (2003); (10) McCaughrean et al. (2004); (11) Burgasser et al. (2000); (12) Deacon et al. (2012a); (13) Todorov et al. (2010); (14) Bowler & Hillenbrand (2015); (15) Dupuy et al. (2018); (16) Kirkpatrick et al. (2001); (17) Bouy et al. (2003); (18) Dupuy et al. (2014); (19) Naud et al. (2014); (20) Luhman et al. (2011); (21) Luhman et al. (2012); (22) Allers et al. (2010); (23) Pinfield et al. (2012); (24) Faherty et al. (2010); (25) Chinchilla et al. (2020b); (26) Mace et al. (2013); (27) Gauza et al. (2019); (28) Wright et al. (2013); (29) Smith et al. (2015); (30) Deacon et al. (2016); (31) Lodieu et al. (2014); (32) Burningham et al. (2013); (33) Day-Jones et al. (2011).

1.6.1 Systematic surveys for substellar companions

Some systematic high-contrast searches have used AO to search for substellar companions and binaries in a systematic way. One of the pioneering ones was conducted by Oppenheimer et al. (2001) around a sample of stars with heliocentric distances closer than 8 pc. This search made use of the adaptive optics coronographic technique. However, and although this survey was sensitive up to the most massive brown dwarfs considering an age of 5 Gyr, the only substellar object identified was the already known brown dwarf Gl 229B.

Another coronographic search for substellar companions was performed with the Keck Telescope by McCarthy & Zuckerman (2004) around more than 100 stars closer than 25 pc, and almost 200 stars with the 3m Shane Telescope and the 2.3m Bok Telescope. They were sensitive to companion masses down to 10 M_{Jup} at separations between 75–300 AU in the first campaign, and to companion masses down to 30 M_{Jup} at separations between 140–1200 AU in the second campaign. They found only one candidate companion in the brown dwarf mass regime, and no planetary mass objects, leading to a companion frequency of 1±1% for brown dwarfs in the explored range of separations.

Metchev & Hillenbrand (2009) found a substellar companion frequency of $3.2^{+3.1}_{-2.7}$% to solar-like nearby stars of all ages at separations between 28–1590 AU, using the Palomar and Keck telescopes. Kraus et al. (2011) identified five brown dwarf companion candidates in their search around 129 members of Taurus-Auriga at separations between 5–5000 AU, corresponding to a substellar companion frequency of $3.9^{+2.6}_{-1.2}$%, also using AO with the Palomar and Keck telescopes. Later, Daemgen et al. (2015) surveyed a sample of 64 stars in the same region using NIRI on Gemini North, and obtained a substellar companion frequency of ∼3.5–8.8% between 10–1500 AU. Vigan et al. (2012) found a brown dwarf companion frequency of 2.0–8.9% around 42 young A-type stars at separations between 10–300 AU, and a planetary-mass companion frequency of 5.9–18.8% between 5–320 AU. Bowler et al. (2015) surveyed a sample of 122 young M-dwarfs using AO and coronography with the Keck and Subaru telescopes, and found a frequency for brown dwarf companions of $2.8^{+2.4}_{-1.5}$% between 10–100 AU, and a model-dependent lower limit of 10.3–16.0% for planetary-mass objects. Lannier et al. (2016) observed 58 young nearby M-dwarfs using the NAOS-CONICA (NaCo) instrument on the VLT, and derived a frequency of $4.4^{+3.2}_{-1.3}$% for companions with masses 2–80 M_{Jup} at separations between 8–400 AU, and $2.3^{+2.9}_{-0.7}$% for planetary-mass companions.

Many other similar studies have also made use of the high-contrast imaging to search for substellar companions, as for example the speckle imaging survey around members of Praesepe and α Persei by Patience et al. (2002) using

the Palomar Hale and Keck telescopes, the lucky-imaging search for young substellar companions by Neuhäuser et al. (2003) using the speckle camera Sharp-I and the Son of Isaac imager (SofI) on the NTT, the Gemini Deep Planet Survey (GDPS Lafrenière et al. 2007), the aperture-masking interferometry search for companions in Upper Scorpius by Kraus et al. (2008) using the Keck and Palomar telescopes, the Strategic Explorations of Exoplanets and Disks with Subaru (SEEDS, Tamura 2009), or the Gemini/NICI Planet-Finding campaign (Liu et al. 2010; Biller et al. 2013; Nielsen et al. 2013; Wahhaj et al. 2013). Many surveys were performed using AO with NaCo on the VLT, as the search for substellar companions to members of η Chamaeleontis by Brandeker et al. (2006), the search for substellar companions to Tucana and β Pictoris members by Kasper et al. (2007), the searches performed by Chauvin et al. (2010, 2012, 2015) around members of young associations and isolated nearby brown dwarfs, or the search for substellar companions around young nearby stars by Rameau et al. (2013a).

Some other studies have made use of space telescopes to reach a higher contrast in the search for substellar companions. For example, Dieterich et al. (2012) searched for substellar companions to 255 stars within 10 pc using NICMOS on the Hubble Space Telescope (HST), and obtained an L- and T-type companion frequency of $2.3^{+5.0}_{-0.7}$% for separations between 10–70 AU. Another examples are the study of T-dwarf companions around M-, L- and T-dwarfs performed by Carson et al. (2011) using the Infrared Array Camera (IRAC) on the Spitzer Space Telescope, which did not found any substellar companion, and many other searches performed with the HST, as the survey of several stars within 13 pc by Schroeder et al. (2000), the search for binary L-dwarfs by Reid et al. (2001), the substellar companions search performed by Neuhäuser et al. (2002) to a sample of young objects belonging to the Chameleon association, or the searches for binarity in M-, L- and T-dwarfs by Burgasser et al. (2003) and Gizis et al. (2003).

Other studies have focused in wider separations, using regular imaging or survey data to look for wide companions. However, most of them were focused on the search for stellar binaries and not many of them have focused on the search for substellar objects. Some examples are the search for stellar and substellar companions to white dwarfs through near-infrared imaging with the Bok telescope by Farihi et al. (2005), which did not find any substellar companion, reporting an upper limit of <0.5% for separations between 50–5000 AU. The search for wide companions in Upper Scorpius by Aller et al. (2013) using UKIDSS and Pan-STARRS survey data lead to a substellar companion frequency of $\sim 0.6 \pm 0.3$% for separations between 400–4000 AU. Deacon et al. (2014) searched for low-mass (stellar and substellar) companions to a sample

of more than 87 000 stars using 2MASS and Pan-STARRS and found 88 wide M- and L-type companions at separations wider than ∼300 AU. The search for stellar and substellar companions to YMG members using 2MASS survey data and proper motion catalogues by Elliott et al. (2016) found that many systems containing wide stellar and substellar companions in β Pictoris were part of triple and higher order systems. Finally, the survey for large-separation planetary mass companions to YMG ultracool members by Naud et al. (2017) using GMOS on the Gemini telescope obtained a wide planetary-mass companion frequency of $0.84^{+6.73}_{-0.66}$% for separations between 500–5000 AU around young K5–L5 stars and brown dwarfs.

2

Aims and Observations

2.1 Aims

The aim of this work is to look for the wide substellar companion population at very young ages (5–200 Myr). With this study we will determine the frequency of low-mass companions, we will obtain the statistics for their masses and separations, and we will be able to compare these distributions with the age. This will provide observational constraints for the different formation and migration models. Furthermore, substellar objects in very wide orbits are very useful benchmarks, as they are analogues to the giant gas planets placed in close orbits. They share similar properties like effective temperatures, gravity and possibly composition, and hence they share similar magnitudes, colours and spectroscopic properties. Wide substellar companions allow for a detailed spectroscopic characterisation, which is very difficult to perform for the close-orbit objects. In this work we will also provide optical and near-infrared spectra of some of these analogues.

We carried out our study in the young Upper Scorpius association (5–10 Myr, d∼145pc), and in four young moving groups: Beta Pictoris (20–30 Myr, d∼50pc) Tucana-Horologium (40–50 Myr, d∼50 pc), TW Hydrae (5–15 Myr, d∼70pc) and AB Doradus (120–200 Myr, d∼50pc). For this purpose, we used direct imaging from the new near-infrared survey VHS covering the whole southern hemisphere, in combination with other near-infrared surveys, namely UKIDSS GCS and 2MASS. Combining these data, we looked for wide companions to a list of known members of the mentioned young associations. We used the astrometry from these catalogues to select the candidate companions that

share a common proper motion with the primaries. Then, we used the available photometry, from these and other photometric catalogues (e.g. PanSTARRS, AllWISE), to discard possible contaminants. We also made use of the very recent *Gaia* DR2 astrometry to get rid of possible chance alignments among our brightest candidates.

2.2 Survey data

In this section we will list and describe the most important surveys involved in this work: VHS, UKIDSS GCS and 2MASS. Table 2.1 shows the main technical information about these surveys and other surveys used in this work.

Survey	Coverage [deg^2]	Filters	Depth	Astrom. precision	Epoch
VHS	20 000	J, Ks	J=20.2, Ks=18.1	$<0.1''$	2009–2020
UKIDSS GCS	1600	Z, Y, J, H, K	J=19.1, Ks=18.4	$<0.1''$	2005–2013
2MASS PSC	All sky	J, H, K	J=15.8, Ks=14.3	$<0.1''$	1997–2001
Pan-STARRS	30 000	g, r, i, z, y	r=23.2, i=23.1, z=22.3	$\sim 0.005''$	2010–??
Gaia DR2	All sky	G, G_{BP}, G_{RP}	G=17	$<0.002''$	2014–2016

Table 2.1: Basic information from the main photometric and astrometric surveys used in this work.

2.2.1 VHS

The Visible and Infrared Survey Telescope for Astronomy (VISTA) Hemisphere Survey (VHS; McMahon et al. 2013) is a near-infrared survey which images the entire southern hemisphere in the J and Ks bands (central wavelength $\sim$1.26 μm and $\sim$2.16 μm, respectively; filter width $\sim$0.17 μm and $\sim$0.31 μm, respectively). It is carried out by the VISTA telescope, a 4m diameter quasi-Ritchey-Chretien telescope placed at Cerro Paranal Observatory (Chile) and owned by the European Southern Observatory (ESO). The VHS reaches 5σ point source limiting magnitudes of J=20.2 and Ks=18.1 (Vega system), around 3–4 magnitudes deeper than the previous near-infrared surveys 2MASS (Skrutskie et al. 2006) and DENIS (Epchtein et al. 1997). Figure 2.1 shows the sky coverage of the VHS, together with other VISTA surveys, and the completeness diagram in the J and Ks bands.

The VISTA's near-infrared camera, VISTA InfraRed CAMera (VIRCAM), provides a field of view of 1.65 degree diameter using a mosaic of 16 detectors, arranged in a 4×4 rectangular grid, adding a total of 67 million pixels with

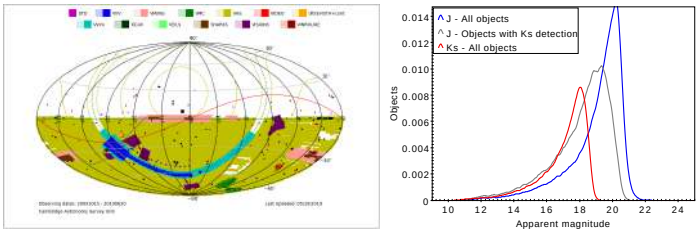

Figure 2.1: Left panel: Aitoff projection of the VISTA surveys sky coverage, updated on 5 October 2019. The VHS coverage is shown in gold colour. Right panel: Completeness diagram of VHS, showing the histogram of the number of detected objects per apparent magnitude.

a projected size in the sky of $0.339''\text{pix}^{-1}$ (Sutherland et al. 2015). Each detector covers a field of $11.6' \times 11.6'$. The separation between the detectors is $10.4'$ and $4.9'$ in the X and Y axes, respectively. To obtain the complete images, the observations are performed using a pattern of 6 separate pointings, or "pawprints", taken in different positions assuring that each point in the sky is imaged by at least two of the pawprints. Two or more exposures are taken at each pointing, with a small dithering offset of a few arcseconds, to correct for small-scale cosmetics. The pawprints are then aligned and combined to form the final image, called "tile", with a total size of $1.5^o \times 1.0^o$.

The astrometric solution of VHS is provided by the VISTA Data Flow System pipeline (Irwin et al. 2004; Lewis et al. 2010) at the Cambridge Astronomical Survey Unit (CASU). This pipeline, written using C and Perl, performs reset, dark, linearity, flat-field and sky background corrections, destripe, interleaving, jittering, catalogue generation, astrometric and photometric calibration, and tiling. The median astrometric rms is $0.1''$, with 99% of the images having a rms better than $0.2''$. The photometric calibration is based on the 2MASS Point Source Catalog. The 2MASS magnitudes of the imaged sources, which are around 200 2MASS sources per pointing, are converted to VISTA magnitudes using colour equations, including terms to correct from interstellar reddening. Then these magnitudes are used to estimate the zeropoints in each image to perform the photometric calibration. The VISTA photometric precision is better than 2% in the $YJHKs$ filters, and better than 3% in the Z filter. A detailed description on the photometric calibration of the VISTA data can be found in González-Fernández et al. (2018).

2.2.2 UKIDSS

The United Kingdom Infrared Telescope Infrared Deep Sky Survey Galactic Clusters Survey (UKIDSS GCS) is a near-infrared survey performed by the 3.8m United Kingdom Infrared Telescope (UKIRT), located on the summit of Maunakea in Hawai'i. The UKIDSS GCS covers an area of ∼1600 deg^2 around 10 Galactic open clusters and star-forming associations, in the *ZYJHK* filters, up to completeness magnitudes of $J \sim 19.1$, $K \sim 18.4$.

The UKIRT telescope is equipped with the UKIRT Wide Field Camera (WFCAM; Casali et al. 2007). This instrument is equipped with four 2048×2048 HgCdTe Rockwell Hawaii-2 infrared detectors, with a pixel size of 18 microns and a plate scale of $0.40''\text{pix}^{-1}$. It provides a field of view of 0.9 degrees. The astrometric and the photometric calibrations are performed by CASU in a similar way to VISTA, with an astrometric rms accuracy per source better than $0.1''$, and a photometric accuracy of ∼2% (Hambly et al. 2008; Hodgkin et al. 2009).

2.2.3 2MASS

The Two Micron All-Sky Survey (2MASS; Skrutskie et al. 2006) is a near-infrared all-sky photometric survey carried out between 1997 and 2001 by two 1.3-m telescopes: one placed in the northern hemisphere, at Mt. Hopkins, USA; and the second one placed in the southern hemisphere, at Cerro Tololo Inter-American Observatory (CTIO), Chile. The catalogue includes photometry in three near-infrared broadband filters, J (∼1.25 μm), H (∼1.65 μm), and Ks (∼2.17 μm), down to completeness magnitudes (SNR∼10) of J ∼15.8, H ∼15.1 and Ks ∼14.3. The 2MASS Point Source Catalog (PSC) contains around 500 million sources, including sources down to SNR∼7. The Extended Source Catalog (XSC; including mostly galaxies) contains around 2 million objects. Figure 2.2 shows the completeness diagram of the 2MASS catalogue.

Both 2MASS telescopes were equipped with a three-channel camera to observe the sky in their three near-infrared filters simultaneously. Each channel was equipped with a 256×256 NICMOS3 HgCdTe array detector, with a pixel size of $2.0''$. The astrometric calibration of the 2MASS catalogue was performed using the Tycho-2 Reference Catalog (Høg et al. 2000) astrometry as a reference, reaching an astrometric accuracy better than $0.1''$at 1σ for objects with $Ks < 14$. The photometric calibration was performed through the observation of $1^o\times 8.5'$calibration fields containing fiducial standard stars, drawn mostly from the Near-Infrared Camera and Multi-Object Spectrometer (NICMOS) calibrators (Persson et al. 1998). In the southern facility, one calibration

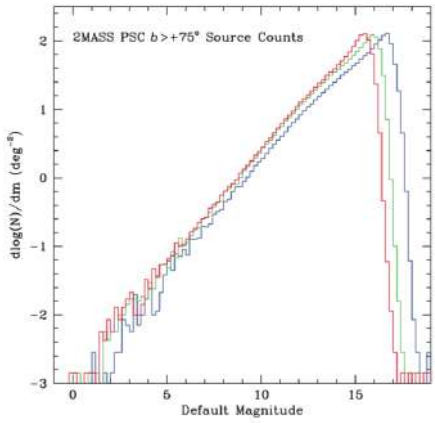

Figure 2.2: Completeness diagram for the 2MASS point source catalogue, showing the number of detected sources per apparent magnitude, from Skrutskie et al. (2006). Blue, green and red lines represent the J, H and Ks photometric bands, respectively.

field was observed every hour, each night. In the northern facility, at the beginning, two calibration fields were observed every 2 hours each night. Lately, the observing strategy changed to one calibration field every hour, like in the southern one.

2.3 Follow up observations and data reduction

We obtained near-infrared and/or optical spectroscopy for previously unknown candidates, and for those with no spectroscopic information in the literature. We aim to characterise them spectroscopically and look for youth features in their spectra. These objects were observed in several observational campaigns using mainly two low-resolution near-infrared spectrographs: NTT/SofI and WHT/LIRIS. Some of these objects were also observed using other low-resolution optical and near-infrared spectrographs, like NOT/ALFOSC, duPont/B&C, GTC/OSIRIS, VLT/X-shooter, and VLT/FORS2. The list of the spectroscopic campaigns involved in this work is shown in Table 2.2, and the instrumental configurations and number of observed objects with each instrument are shown in Table 2.3. The observing logs of all the observed candidates are shown in Table 3.3 for the USco search, and Table 5.2 for the YMG search. In the fol-

Date	Instrument	Wavelengths	Nights/hours	PI
Apr 2017	NTT/SofI	NIR	3n	P. Chinchilla
May 2017	GTC/OSIRIS	OPT	-[a]	N. Lodieu
Jun 2017	WHT/LIRIS	NIR	3n	P. Chinchilla
Jun 2018	NTT/SofI	NIR	3n	P. Chinchilla
Jun 2018	WHT/LIRIS	NIR	2.5n	P. Chinchilla
Jun 2018	VLT/X-shooter	OPT+NIR	4.2h	P. Chinchilla
Sep 2018	WHT/LIRIS	NIR	2n	P. Chinchilla
Oct 2018	NOT/ALFOSC	OPT	1n	P. Chinchilla
Nov 2018	NTT/SofI	NIR	3n	P. Chinchilla
Jan 2019	GTC/OSIRIS	OPT	1.5h	P. Chinchilla
Mar 2019	duPont/B&C	OPT	-[a]	B.Gauza
Jul 2019	VLT/FORS2	OPT	-[a]	M.R. Zapatero
Oct 2019	duPont/B&C	OPT	-[a]	B.Gauza

Table 2.2: Spectroscopic campaigns involved in this work.

[a] External campaign. Some data obtained in collaboration.

lowing sub-sections, we describe the instrumentation involved in this work, the observing strategy, and the data reduction process for each instrument.

2.3.1 NTT/SofI

The Son of ISAAC (SofI) instrument (Moorwood et al. 1998) is a near-infrared imager and spectrograph mounted on the Nasmyth A focus of the ESO 3.5 m New Technology Telescope (NTT) in La Silla Observatory, Chile. It had its first light in December 1997, and will be decommissioned at the end of this year 2020, when it will be replaced with the new Son of X-shooter (SoXS) spectrograph. The SofI spectrograph has spectral resolutions between 600–2200, and covers the near-infrared wavelengths between 0.93–2.54 μm. It is equipped with fixed width slits of 0.6″, 1.0″ and 2″. It has a Hawaii HgCdTe 1024x1024 CCD detector with a pixel size of 18.5 μm, and a plate scale of 0.288″pix^{-1}. The instrument includes also a polarimetric observing mode.

2.3.1.1 Observations

We applied for observing time with NTT/SofI in the ESO P099, P101 and P102 periods (P.I. P. Chinchilla). All the requested runs were accepted, and

we were awarded with 3 nights of observation in each period, in visitor mode. The 3 observing campaigns were successfully completed, with very little time lost due to some occasional high clouds, high wind peaks or technical problems which never lasted for more than a couple of hours in each occasion.

For all the objects observed in the NTT/SofI campaigns, we used Long Slit spectroscopy mode with the 1.0″ wide slit, and the low-resolution Red and Blue grisms (GR and GB, wavelength ranges 1.53–2.52 μm and 0.95–1.64 μm respectively, resolving power 600, nominal dispersion 10.22 and 6.96 Å pix^{-1}, respectively). The exposures were taken using an ABBA nodding pattern along the slit, with individual exposure times in each position adjusted depending on the brightness of the source. We also observed some telluric standards after each target, at similar airmasses, to correct for telluric absorption in each observation. To perform the flat-field correction and wavelength calibration, we also acquired continuum lamps images and Xe arc-lamp images every afternoon, prior to the observations.

2.3.1.2 Data reduction

For most of the objects, we obtained the 2D reduced and combined images through the SofI pipeline recipes provided by ESO, using the GASGANO file manager (Gebbinck & Sforna 2007) available at the telescope. The pipelines perform the bias, flat-field and dark corrections, and they align and combine the individual images to produce the final 2D spectral image.

Nevertheless, due to a sporadical problem in the SofI detector, some of the individual exposures presented a noticeable noise which occupied a remarkable surface of the images. Most of the time, this problem was detected during the observations, so the failure could be repaired and the observations could be repeated. However, some of the failures went unnoticed. For this reason, all the individual exposures were carefully inspected in the reduction process. Whenever an object presented this noise in any of its exposure, the noisy exposures were removed from the datasets, and the data were reduced "by hand" using IRAF standard routines. The exposures were flat-field corrected, then we subtracted the images corresponding to the A-B positions, aligned and combined them to produce the 2D final image. The dark current was not removed from the flat-field images, but due to the high number of counts in these images, the contribution of the dark current is negligible.

After obtaining the 2D images, either through GASGANO or through IRAF standard routines, the spectra were extracted from the combined 2D images using APALL routine in IRAF. Then, they were wavelength-calibrated using the arc images, through IDENTIFY and DISPCOR routines. For the telluric

correction, we removed manually the lines in the telluric standards spectra using SPLOT task. Then, we divided the telluric spectra by a black body corresponding to their effective temperature. Finally, we divided the targets spectra by these telluric spectra to obtain the final results. We combined the Blue and Red sides of the spectra by scaling them using the overlapping region at ∼1.5–1.6 μm.

Instrument	n. obj	Gratings	Wav. range [μm]	Pl. scale [$''$pix^{-1}]	Disp. [A pix^{-1}]	Res. power*
NTT/SofI	48	GB, GR	0.95–1.64, 1.53–2.52	0.29	6.96, 10.22	600, 600
WHT/LIRIS	18	lr_zj, lr_hk	0.89–1.53, 1.39–2.42	0.25	6.1, 9.7	460, 460
NOT/ALFOSC	11	gr5, gr17	0.50–1.07, 0.63–0.69	0.21	3.5, 0.26	400, 5000
VLT/X-shooter	2	VIS, NIR	0.55–1.02, 1.02–2.48	0.16, 0.25	0.16, 0.77	5400, 3600
GTC/OSIRIS	2	R300R, R500R	0.48–1.00	0.25	7.74, 4.88	210, 350
duPont/B&C	24	600/7500	0.59–9.11	0.70	1.6	3200
VLT/FORS2	1	GRIS_300I	0.60–1.10	0.25	1.62	660

Table 2.3: Instrumental configurations used in the spectroscopic observations. (*) Resolving power considering a $1''$ slit.

2.3.2 WHT/LIRIS

The Long-slit Intermediate Resolution Infrared Spectrograph (LIRIS; Manchado et al. 1998) is a near-infrared imager and spectrograph mounted on the Cassegrain focus of the 4.2m William Herschel Telescope (WHT) in Roque de los Muchachos Observatory in La Palma, Spain. The spectrograph can perform long-slit spectroscopy with low resolutions (600–2500), using fixed-width slits of $0.65''$, $0.75''$, $1.0''$, $2.5''$, $5''$ and $10''$. The instrument offers also a Multi-Object Spectroscopy (MOS) mode, and a polarimetric mode. Similar to NTT/SofI, it is also equipped with a Hawaii HgCdTe 1024x1024 detector with a pixel size of 18.5 μm (pixel scale of $0.25''$pix^{-1}), which covers the near-infrared between 0.9–2.5 μm.

2.3.2.1 Observations

We applied for observing time with WHT/LIRIS in semesters 2017A, 2018A and 2018B (P.I. P. Chinchilla). All the requested observing time was approved, and we were awarded with 7.5 nights in total, in visitor mode. The weather conditions in the three campaigns were adequate for observations, with clear skies most of the time (occasional thin high clouds), and average seeings around and below $1''$. All the observations were successfully completed.

The observations with WHT/LIRIS were performed in the Long Slit Spectroscopy mode, using the 0.75″ or 1″ wide slits, depending on the seeing conditions of the night. We used the low resolution ZJ and HK grisms (lr_zj and lr_hk, wavelength ranges 0.89–1.53 μm and 1.39–2.42 μm respectively, resolving power ∼700, nominal dispersion 6.1 and 9.7 Å pix^{-1}, respectively). Similarly to the NTT/SofI observations, the exposures were taken using an ABBA nodding pattern along the slit, with individual exposure times in each position depending on the brightness of the source. We also observed some telluric standards after each target, at similar airmasses, to correct for telluric absorption in each observation. To perform the flat-field correction and wavelength calibration, we also acquired continuum lamps images, and Ar and Xe arc-lamp images, every afternoon before starting the observations.

2.3.2.2 Data reduction

The WHT/LIRIS data reduction was performed using standard IRAF tasks. The raw images were flat-field corrected. Then, we subtracted the A-B images to perform the sky subtraction, and then aligned and combined them to produce the 2D final image. The spectra were extracted using the APALL routine, and finally they were wavelength-calibrated using Argon and/or Xenon arcs. For the telluric correction, we removed the intrinsic lines of the telluric standard spectra using the SPLOT task, and then divided them by a black body corresponding to their effective temperature. Then, the target spectra was divided by this telluric spectra to obtain the final result.

In the case of WHT/LIRIS, combining the zj and hk regions of the spectra was more complicated than the case of NTT/SofI. We found that the overlapping region of the zj and hk spectra was not always reliable, partly due to the presence of deep telluric absorptions in this region, and partly due to the loss in the flux transmission of the grisms at the border of the spectral range coverage. To overcome this problem, we estimated the most reliable wavelength range to perform the overlap. For this task, we used some observed objects with known spectral types. We visually aligned their spectra by comparing to their corresponding spectral templates, and estimated the best region of the overlapping zone, which is 14 500–14 850 Å. We used this wavelength range to scale and combine all the remaining spectra. Nevertheless, although this overlapping region fitted the spectra of most of the objects with known spectral types, it was not perfect for all of them. Therefore, we must take the zj+hk combination of the WHT/LIRIS spectra of some of these objects with caution. Fortunately, for most of these objects we have additional near-infrared and/or optical spectroscopy to confirm our spectral type classification.

2.3.3 NOT/ALFOSC

The Alhambra Faint Object Spectrograph and Camera (ALFOSC) is an optical imager and spectrograph mounted on the 2.5-m Nordic Optical Telescope (NOT) in the island of La Palma, Spain. The spectrograph is equipped with a variety of grisms covering wavelengths between 3200–11 000 Å, with resolutions between 200–10 000; and vertical and horizontal slits with a variety of widths, from 0.4″ to 40″. It also includes an echelle mode, multi-object spectroscopy mode (MOS), and a polarimetric mode both in imaging and spectroscopy. It is equipped with a E2V CCD231-42-g-F61 detector with 2048×2064 pixels, and a pixel size of 15μm (pixel scale of 0.214″pix^{-1}).

2.3.3.1 Observations

We were awarded with one night of observations with NOT/ALFOSC, on the 2 October 2018. We observed our targets in long slit spectroscopy mode, with the gr5 grism and the 1″ slit (covering 5000–10 700 Å, resolution ∼400) for a full optical low-resolution spectrum, and the gr17 grism and the 1″ slit (covering 6330–6870 Å, resolution ∼5000) for a higher resolution spectrum in the Hα and lithium region. For the low-resolution gr5 grism, two exposures were taken, in an AB nodding pattern with an offset of 10″ along the slit. For the higher resolution gr17 grism, two exposures were also taken, but both in the same position. The spectrophotometric standard star BD+17 4708 was also observed to correct for the instrumental response. Some continuum lamps images and Ne-He arc-lamp images were also acquired to perform the flat-field correction and wavelength calibration. For the higher resolution gr17 grism, arc-lamp and continuum lamp images were taken immediately after each target exposure at the same telecope position, for an accurate correction and calibration.

2.3.3.2 Data reduction

The data reduction for NOT/ALFOSC was performed using standard IRAF routines. The raw images were corrected for bias using the overscan region of the images, and they were flat-field corrected. Then, the images were aligned and combined. The spectra were extracted from the combined 2D images using the APALL routine. The spectra were wavelength calibrated using the Ne-He arc images. Then, the spectra were corrected for instrumental response and flux-calibrated using the spectrophotometric standard spectrum. Since the spectra are in the optical, they were not corrected for atmospheric telluric absorptions.

2.3.4 VLT/X-shooter

X-shooter is a multi-wavelength medium-resolution spectrograph mounted on the UT2 Cassegrain focus at the Very Large Telescope (VLT) in Paranal Observatory, Chile. It is a three arms spectrograph, each one being an independent cross-dispersed echelle spectrograph, which operate at the same time: UVB, VIS and NIR, covering wavelength ranges of 0.30–0.56, 0.56–1.02 and 1.02–2.48 μm respectively. Each spectrograph is equipped with a different set of slits of different widths, between $0.5''$–$1.6''$, $0.4''$–$1.5''$ and $0.4''$–$1.2''$ for the UVB, VIS and NIR arms respectively, leading to resolving powers of ∼3000–18 000, depending on the arm and slit configuration. The CCD detectors used in X-shooter are a 4k x 2k E2V CCD44-82 for the UVB arm, a 4k x 2k MIT/LL CCID 20 detector for the VIS arm, and a 2k x 2k Hawaii 2RG for the NIR arm.

2.3.4.1 Observations

We requested X-shooter time to observe two very faint Upper Scorpius candidates in the period P101 (I.P. P. Chinchilla). The two objects were observed in service mode in June 2018.

These observations were performed in the three arms (UVB, VIS and NIR), using an ABBA nodding pattern. We selected the $1.2''$ slits for VIS and NIR arms and the $1.3''$ for the UVB arm. The acquisition in the three arms is simultaneous, although the readout times are different, so taking this into consideration we chose different exposure times (270s in the UVB arm, 280s in the VIS arm, and 300s in the NIR arm for each exposure, for both objects) to match the total time spent in each of the two A,B nodding positions and maximize the exposure times. A spectrophotometric standard was also observed right after the targets at a similar airmass to correct for atmospheric telluric absorption.

2.3.4.2 Data reduction

The objects have a negligible emission in the UVB wavelength range, so these data were ignored, and only the VIS and NIR arms were taken into consideration.

To obtain the reduced spectra, the reduced 2D images of the targets and the telluric standards were obtained using the X-shooter reduction pipeline (Modigliani et al. 2010). This pipeline performs bias and dark subtraction; flat-fielding, non-linearity and instrument flexure correction; instrument response and wavelength calibration; and spectral orders combination. For one of the objects, this was performed through the ESO REFLEX environment (Freudling

et al. 2013), which is based on the open source workflow engine Kepler. For the other object, the reduced 2D images were directly downloaded from ESO Science Archive, which make use of the same reduction pipeline.

Then, the spectra were extracted using the IRAF APALL routine. To perform the telluric correction, we manually removed the characteristic spectral lines of the telluric star spectrum, divided the spectrum of the target by the telluric standard spectrum, and then multiplied the result by a black body of the corresponding temperature of the telluric standard.

2.3.5 Other observations

Some of the obtained candidates were observed in the optical in other observational campaigns carried out by our collaborators using different instruments.

Some of our targets were observed by Dr. B. Gauza using the Boller and Chivens Spectrograph (B&C) on the 2.5-m Irenee du Pont telescope, in Las Campanas observatory, Chile. This spectrograph provides low and medium-resolution spectroscopy through different gratings, with resolutions ∼300–1200, in the optical wavelength range, between 3500–9000 Å. In the observations, the 600/7500 grism was used, together with the 1″ wide slit, providing a resolution of ∼3200 at 7500 Å.

Our faintest candidate in the USco search was also observed in the optical in collaboration with Dr. M.R. Zapatero Osorio, during her VLT/FORS2 campaign in July 2019. The observations were performed using the GRIS_300I grism and the 1″ wide slit.

Furthermore, one of the USco companions published in Chinchilla et al. (2020b) was also observed with GTC/OSIRIS in collaboration with Dr. N. Lodieu, through his 2017 GTC filler programme. These observations used the R300R grism and the 1″ wide slit, providing a resolution of ∼210. Another YMG companion, published in Chinchilla et al. (2020a) was also observed with GTC/OSIRIS through the program GTC06-18BDDT, using the R500R grism and the 0.8″ wide slit, which provided a resolution of ∼440.

3

Search For Companions in Upper Scorpius

3.1 Introduction

Upper Scorpius (USco; Bertiau 1958; Blaauw 1964) is the youngest subgroup of the nearby young stellar Scorpius-Centaurus association (Sco-Cen), which also includes Upper Centaurus-Lupus (UCL) and Lower Centaurus-Crux (LCC) (de Zeeuw et al. 1999). Figure 3.1 shows the distribution of the subgroups of the Sco-Cen association. USco's central coordinates are RA=16:12:00.0, DEC=−23:24:00 (de Zeeuw et al. 1999). It is located at a mean heliocentric distance of 146±3±6 pc (Galli et al. 2018), where the second term in the uncertainty refers to systematic errors, and the mean proper motion of its members is $(\mu_\alpha \cos\delta, \mu_\delta) = (-10, -23) \pm 6$ mas yr^{-1} (Fang et al. 2017). The current census of USco includes more than a thousand members and candidate members (Luhman et al. 2018).

The age of USco is under debate, and the estimated ages range between 5–15 Myr. One of the first estimations by Preibisch et al. (2002) suggested a very young age of 5 Myr, regarding the position of the members in the HR diagram. For this study, they used the USco population from 0.1 $M_\odot$ to 20 $M_\odot$. Given the very small age dispersion derived from their study, and that the low- and high-mass members follow the same isochrones, these authors suggested that the USco association was formed in a mini-starburst, possibly triggered by a close supernova. However, a later study by Pecaut et al. (2012), suggested an older age of around 11 Myr. This age was estimated from the HR diagram

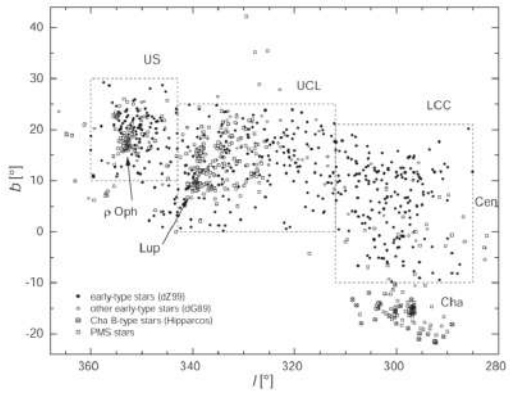

Figure 3.1: Map of the Scorpius-Centaurus association, including Upper Scorpius (US), Upper Centaurus-Lupus (UCL) and Lower Centaurus-Crux (LCC). The Rho Ophiuchi (ρ Oph), Lupus (Lup) and Chameleon (Cha) star-forming regions are also marked. Stars from de Zeeuw et al. (1999) and de Geus et al. (1989) are indicated as dZ99 and dG89 (filled and unfilled circles, respectively), stars from Sartori et al. (2003) are indicated as "PMS stars" (unfilled squares) and "Cha B-type stars" (crossed squares). Figure from Sartori et al. (2003).

position of the high-mass USco members, through isochrones, and through the analysis of the ZAMS in the photometric sequence of the USco members. They also estimated the minimum age of USco through its kinematic expansion, and found a minimum age of 10.5 Myr. They found a spread in ages for the USco members indicating that most of them were formed over a time span of 2–6 Myr. Pecaut & Mamajek (2016) suggested that the whole Sco-Cen region presents spatial substructures regarding the age, and found a turnoff age of around 7 Myr for USco. Rizzuto et al. (2016) found that the high-mass and low-mass populations of USco follow different isochrones, the high-mass members ($\sim$ G-type) following a $\sim$11.5 Myr isochrone, and the low-mass members ($\sim$M-type objects) following an isochrone of around 7 Myr. They suggest that this may be an indicator of problems in the current pre-main sequence evolutionary models of low-mass objects. More recently, David et al. (2019) performed a new estimation based on the location of eclipsing binaries in the mass-radius diagram, and they found an age of 5–7 Myr using several pre-main sequence models, and 9–10 Myr using models which take into account magnetic fields and star spots (see also Feiden 2016).

The Ophiucus star-forming region is placed very close to USco, and partially

Reference	Age [Myr]	Method
Blaauw (1978)	5	Kinematic
de Zeeuw & Brand (1985)	6–8	Isochrones
de Geus et al. (1989)	5–6	Isochrones
Preibisch & Zinnecker (1999)	∼5	Isochrones
Preibisch et al. (2002)	∼5	Isochrones
Slesnick et al. (2008)	5±3	Isochrones
Pecaut et al. (2012)	11±3	Isochrones
Pecaut et al. (2012)	>10.5	Kinematic
Herczeg & Hillenbrand (2015)	∼4	Isochrones
Pecaut & Mamajek (2016)	10±3	Isochrones
Rizzuto et al. (2016)	7–11.5	Isochrones
David et al. (2019)	5–7	Isochrones

Table 3.1: Age estimations of the USco association in the literature.

overlaps with it in a small portion of the sky. The Ophiucus region still contains dense gas clouds where active star formation is taking place. These dark clouds weaken and redden the objects within and behind them. The Ophiucus complex contains more than 300 known members and candidate members (Wilking et al. 2008; Esplin & Luhman 2020), with ages around and above 1 Myr, which are younger than USco.

Due to its young age and proximity, USco has been the object of study of many direct imaging searches for stellar and substellar companions, through direct imaging (e.g. Kraus et al. 2005; Kraus & Hillenbrand 2007a; Béjar et al. 2008; Aller et al. 2013), speckle interferometry (e.g. Köhler et al. 2000; Tokovinin & Briceño 2018, 2020), or adaptive optics techniques (e.g. Kraus et al. 2008; Lafrenière et al. 2008; Biller et al. 2011; Ireland et al. 2011; Lafrenière et al. 2011).

In this Chapter, we are presenting an astrometric and photometric search for wide substellar companions around previously known USco members, using VHS data.

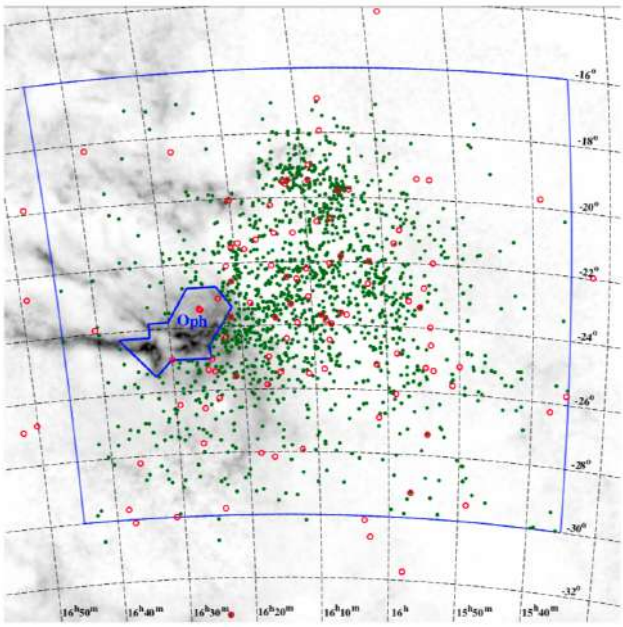

Figure 3.2: Map of the USco region. Stars from de Zeeuw et al. (1999) are marked as red unfilled circles. Candidate members from Luhman et al. (2018) are marked as green dots. The ρ Oph region is marked with a blue line. The extinction map from Dobashi et al. (2005) is marked in grey. Figure from Luhman et al. (2018).

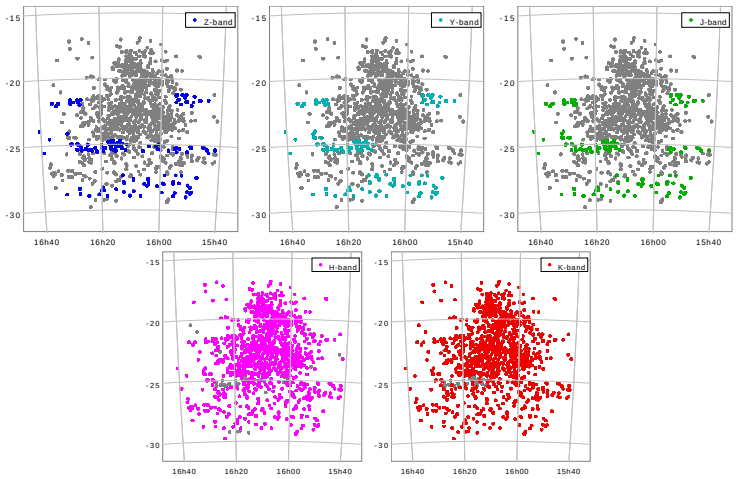

Figure 3.3: UKIDSS coverage of the USco region. Markers are bigger than the actual size of the individual studied regions.

3.2 Search Method

The USco region's low negative declination provides the advantage of being reached by both the southern hemisphere VHS and the northern hemisphere UKIDSS GCS. The latter covered most of the USco region in the H and K bands, and some of it in Z, Y and/or J bands. Figure 3.3 shows the photometric coverage of USco in the different UKIDSS bands. The UKIDSS GCS is similar in depth to the VHS, and although they are recent surveys, they observed the USco region in different epochs, being the mean time baseline between their observations around seven years. Therefore, combining VHS and UKIDSS GCS data for our correlations is an optimal choice regarding photometric depth and proper motion determination.

The procedure used in our search is detailed in the following sub-sections.

3.2.1 USco members compilation

First, we compiled a list of USco confirmed members and candidate members obtained from the existing searches in the literature. Our compilation includes the targets provided by Walter et al. (1994); Preibisch et al. (1998); Ardila

et al. (2000); Martín et al. (2004); Lodieu et al. (2006); Slesnick et al. (2006); Lodieu et al. (2007); Findeisen & Hillenbrand (2010); Dawson et al. (2011); Lodieu et al. (2011); Luhman & Mamajek (2012); Dawson et al. (2013); Lodieu (2013); Rizzuto et al. (2015); Best et al. (2017). The final compilation includes 1300 individual objects.

3.2.2 Data download

We downloaded the VHS proprietary data from the VISTA Science Archive (VSA) website[1]. We requested to download all the data within an area of $60''$ around each member of our compilation.

We also carried out a similar download from the UKIDSS WFCAM Science Archive website[2]. The USco field was visited by UKIDSS GCS in several occasions. We are interested only in the first epochs for the proper motion determination, as the time baseline between GCS and VHS will be larger, and then we will obtain a more precise measurement. Therefore, for this download we selected the DR7 instead of the latest release, corresponding to the earliest epochs (∼2005, 2008) and hence we are avoiding the astrometric data from the observations performed in the years 2011 and later. Nevertheless, we will later use the photometric data from the DR10 release.

For the downloaded VHS data, we faced the inconvenience that the tables did not include the epoch data. This information is very important to obtain the proper motions of all the targets in the downloaded fields. To overcome this, we also downloaded the Detection Table, which is the unmerged catalogue, with separate entries for the exposures in the different photometric bands. This Detection Table includes the epoch information of the observations. Then, we cross-matched the VHS Source Table and the Detection Table, with a cross-match radius of $1''$. We selected the correct matches imposing a coincidental photometric measurement either in the J or Ks filters. We noticed that, in all cases, the J-band and the Ks-band observations were carried out with a time difference of less than 10 minutes, so either the J or Ks epoch can be assigned to the targets.

Some of the objects from the USco compilation do not have available data either in the VHS or the UKIDSS GCS catalogues in their surroundings. In some cases, they are candidate members placed further away from the central region of USco, so they are out of the region covered by UKIDSS GCS (∼50 objects). Others are objects catalogued as candidate members of USco which are in the Rho Ophiuci region, which is not available in VHS (∼30 objects).

[1] `http://horus.roe.ac.uk/vsa/index.html`
[2] `http://wsa.roe.ac.uk/index.html`

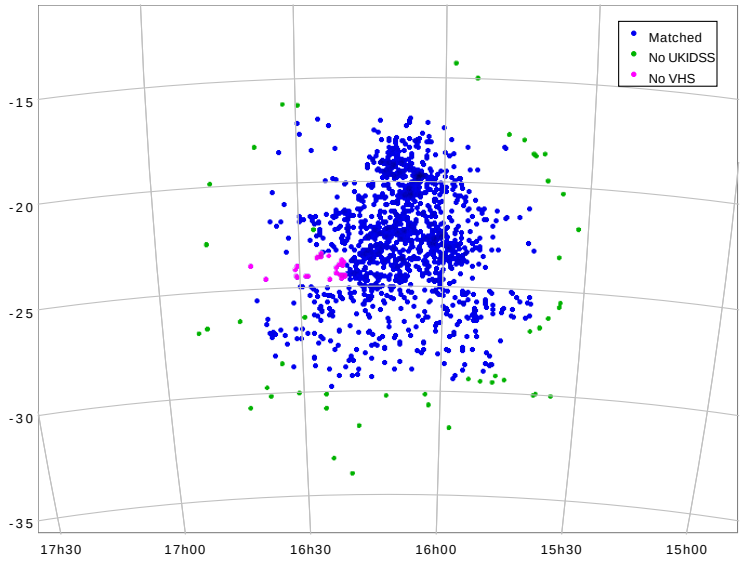

Figure 3.4: Sky projection of the USco compiled members with available data in both VHS and UKIDSS GCS catalogues (blue), only VHS but no GCS (green) and only GCS but no VHS data (magenta).

Figure 3.4 shows the USco region and the missing objects either in the VHS or UKIDSS GCS catalogues. The number of objects and systems included in both catalogues is 1195.

3.2.3 VHS vs UKIDSS GCS cross-correlation

Previous to the catalogues cross-correlation, we performed an internal cross match separately to the VHS and GCS downloaded tables to remove any duplicated source. Some USco compiled members have neighbors closer than $60''$, so their $60''$ fields may coincide partially, and as a result all the objects in these coincidental sections will be duplicated in our downloaded tables. Furthermore, objects placed in the overlapping areas of the VHS "pawprints" are duplicated in the catalogue.

After removing the duplicates, we cross-correlated the two tables using TOPCAT. The cross-match radius was $1''$, and we kept all the matches. The relatively large cross-match radius takes into account the astrometric uncertainties of the catalogues and the motion of the possible USco members over the interval of 7 years ($\sim$0.15–0.20$''$), which is the mean time baseline between the two surveys.

To remove any possible mismatch or artifact, we imposed that the cross-matched objects have similar J or Ks magnitudes both in VHS and GCS. We required that either the J or Ks magnitude differ in less than 0.75 mag, which corresponds to the magnitude difference for a resolved versus non-resolved equal-mass binary.

3.2.4 Proper motion determination and astrometric selection

Our first selection will be based on the proper motion of the matched objects. Any wide companion candidate will share the same apparent movement in the sky as their primary star. All the objects in the USco association have similar proper motions, so we can impose that the candidates proper motion is compatible with that of the association.

We estimated the proper motions of all the matched targets, using the coordinates and epoch from VHS and UKIDSS catalogues. We computed the mean proper motion of the association using VHS and UKIDSS GCS astrometry of 246 known USco members from the compilation with magnitudes in either the VHS J band or the VHS Ks band or both higher than 12.5, to make sure that they are not saturated. Figure 3.5 shows the proper motion diagram of these 246 known members. Using TOPCAT statistics option, we obtained a mean proper motion of $\mu\alpha\, cos\delta, \mu\delta = (-7.46, -19.82)$ mas yr^{-1}, with a stan-

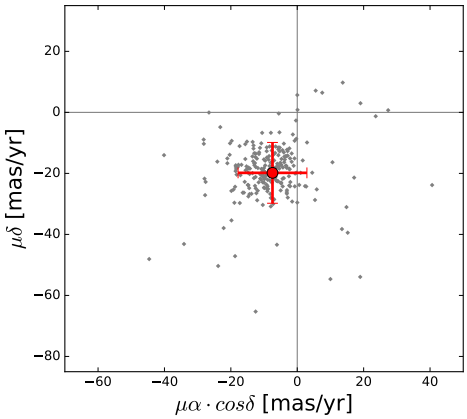

Figure 3.5: Proper motion diagram of the USco members. The 246 primaries are marked as grey dots. The mean proper motion of the association is marked as a red circle. The error bars correspond to the standard deviation of the mean proper motion.

dard deviation of 10.37 and 9.96 mas yr^{-1}, respectively (see Table 3.2). This proper motion is compatible with the mean proper motion obtained by Fang et al. (2017), and it will be used as the mean proper motion for the candidates selection.

	mean	SD
PM RA (mas yr^{-1})	−7.45705	10.3689
PM DEC (mas yr^{-1})	−19.8226	9.96411

Table 3.2: USco mean Proper Motions obtained from the primaries.

In order to astrometrically select our companion candidates, we also have to take into account the uncertainties in the PM determination. We estimated the error for the selection from the dispersion of all background non-moving objects. To obtain it, we used the whole VHS vs GCS 1″ cross-correlation. By using this, we are overestimating the astrometric uncertainty, as the correlation also includes objects that actually move (like the USco members) up to 1 arcsec between epochs, and extended objects whose coordinates may slightly differ in

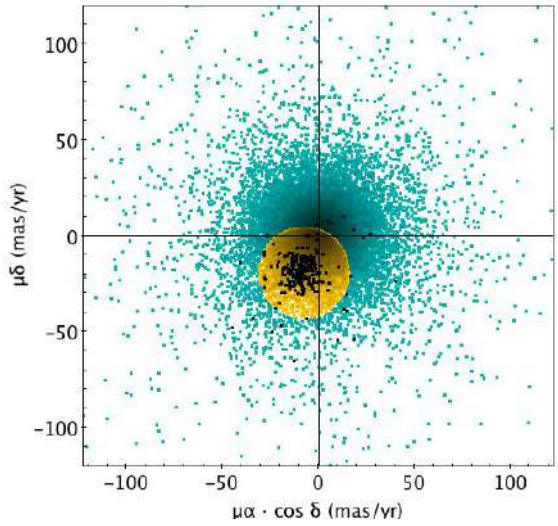

Figure 3.6: Proper motion diagram of the selection. The selected objects are marked in yellow. Objects discarded as contaminants are marked in blue. Some of the USco primaries are marked in black.

the two surveys.

The mean proper motion that we obtain in the whole correlation is close to zero, as expected (−0.200, 0.286 mas yr^{-1} in RA and DEC, respectively), and the standard deviations in the PM are 16.660 and 16.636 mas yr^{-1}, for RA and DEC respectively. These will be the error values considered for the proper motion selection of the candidates.

In order to include all the objects with proper motions in RA and DEC up to the SD of the correlations, we accepted all the targets with PM differences with respect to the mean value of USco within a radius of 23.544 mas yr^{-1} ($\sqrt{16.660^2 + 16.636^2}$). Since the USco proper motion is not very high, and our selection radius is generous, we still obtain a lot of contaminants after this first selection, including many non-moving objects. Figure 3.6 shows the performed proper motion selection. Roughly the 45% of the cross-matched objects fulfill this condition. Table 3.4 shows the number of remaining candidates after each step of the search.

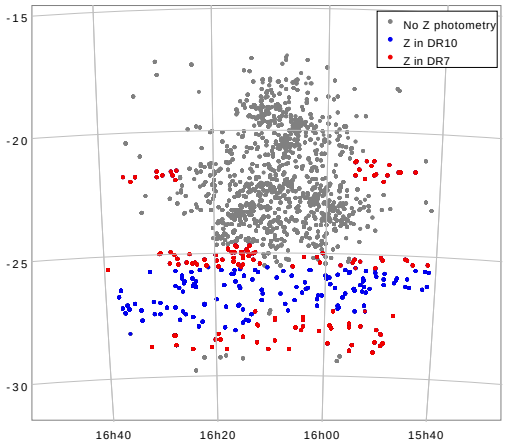

Figure 3.7: Sky projection of cross-matched objects with and without Z filter information from UKIDSS GCS in data releases DR7 and DR10.

3.2.5 Photometric selection using UKIDSS GCS

To filter out the contaminants, we performed a photometric selection using J vs. $J-Z$ colour-magnitude diagrams, using Z-band from UKIDSS GCS and J-band from VHS, for the regions covered by GCS in the Z filter.

The UKIDSS GCS DR7 data release, which we used for the proper motion estimations, does not include all the Z filter measurements. Therefore, to obtain all the available photometry, we downloaded the GCS DR10 data release and cross-correlated it with our data. Figure 3.7 shows the UKIDSS GCS coverage in Z filter in our objects.

Around 30% of the objects selected by proper motion have Z photometry in UKIDSS GCS. The remaining 70% of the objects lack of Z photometry, and we will use another catalogue for the photometric selection in following sections.

For the 30% of objects with Z photometry, we built the J vs. $J-Z$ colour-magnitude diagram, using J photometry from VHS and Z photometry from UKIDSS GCS. In this diagram, we can clearly distinguish the USco photometric sequence, placed above the further and fainter field objects. To separate the new companion candidates from the field contaminants, we identified some of the USco members of the compilation in this diagram and used them as a reference. From the lower envelope of their photometric sequence, we defined

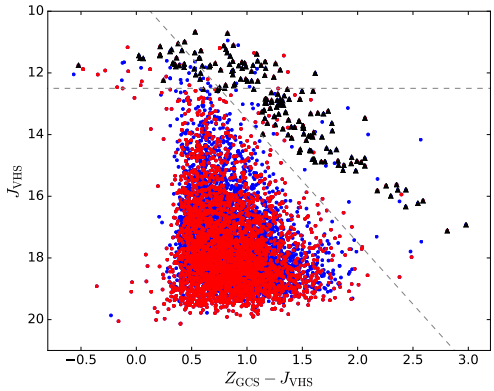

Figure 3.8: J vs $Z - J$ colour-magnitude diagram for the selection using VHS and GCS photometry. Objects with Z photometry from UKIDSS GCS DR7 are shown in red, objects with Z photometry from UKIDSS GCS DR10 are shown in blue. Some USco known members from the compilation with available Z photometry in UKIDSS GCS are marked as black triangles. The $J > 12.5$ and $J < 4(Z - J) + 9.5$ cuts are shown as grey dashed lines.

the following colour and magnitude cut: $J < 4 * (Z - J) + 9.5$. All the objects brighter and redder than this limit were selected as companion candidates. We also cut the objects with J magnitudes brighter than 12.5 mag, to avoid targets affected by saturation. Figure 3.8 shows the UKIDSS GCS J vs. $J-Z$ colour-magnitude diagram of the selection. Through this selection we obtained 150 objects. After removing those with coordinates matching the primaries from the compilation, we obtained 44 candidates. As the recovered primaries can also be candidate companions to other primaries in the compilation, we also verified if any of them is placed closer than $60''$ from another compiled member. None of them was found to be a companion.

In addition, to discard some of the contaminants and mismatches among the selected candidates, we built a J vs $J - K_s$ colour-magnitude diagram using VHS photometry. Figure 3.9 shows this J vs $J - K_s$ colour-magnitude selection. In this case, we also used some USco members in the compilation as a guide. The colour cut used was $J < 6 * (J - K_s) + 10$. From the candidates, 10 objects not following the USco photometric sequence in this diagram were marked as contaminants and discarded. At the end of this step, we obtained 34 candidates.

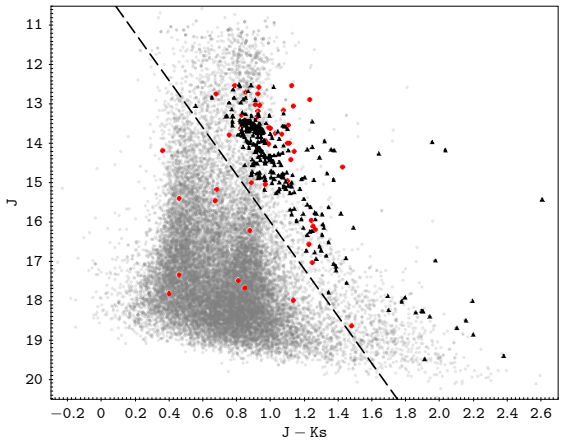

Figure 3.9: J vs $J-K_s$ colour-magnitude diagram for the Z-UKIDSS selected objects. Objects passing the J vs $Z-J$ selection are shown in red. The location of background contaminants is shown in grey, as a guide. Some USco known members from the compilation with available J and K_s photometry in VHS are marked as black triangles. The selection cut is shown as a dashed line.

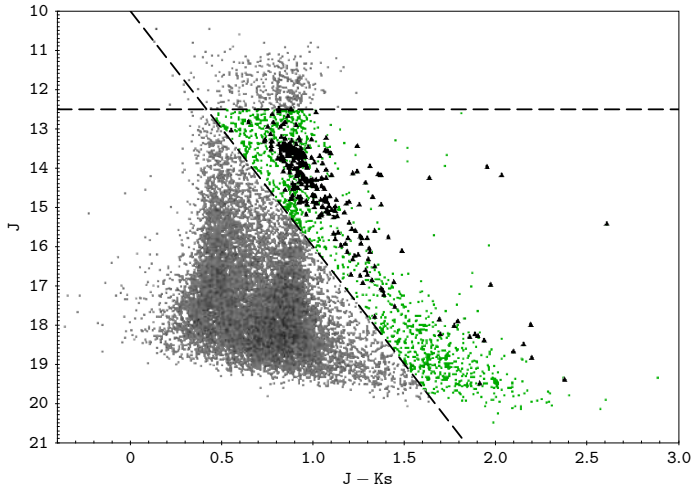

Figure 3.10: J vs $J-K_s$ colour-magnitude diagram for the objects without Z photometry in UKIDSS GCS. Objects selected in this step are marked in green, objects discarded as contaminants are marked in grey. Some USco known members from the compilation with available J and K_s photometry in VHS are marked as black triangles. The selection cuts are shown as dashed lines.

3.2.6 Photometric selection using Pan-STARRS

For the ∼70% of matched objects without Z photometry in UKIDSS GCS, we used Pan-STARRS photometry. Pan-STARRS covered the USco region in the optical, in the g, r, i, z and y filters. We decided to use the z filter photometry to perform a similar selection as the one performed using UKIDSS GCS.

Prior to the cross-correlation, as a first filter, we built a J vs. $J-K_s$ colour-magnitude diagram using the VHS photometry of the objects to discard obvious contaminants. Figure 3.10 shows the J vs. $J-K_s$ colour-magnitude diagram for this set of objects. In this filtering, we used the same colour cut used for the Z-UKIDSS set. We discarded 90% of the objects as contaminants.

The remaining objects were cross-correlated with the Pan-STARRS database to obtain their z filter photometry, with a $3''$ matching radius, and All-Matches selection. Then, we built a J vs $z-J$ colour-magnitude diagram and we placed some USco known members as a guide, to perform the colour cut. The equation of the lower envelope used for this selection was $J < 3.3*(z-J)+7.7$. Figure

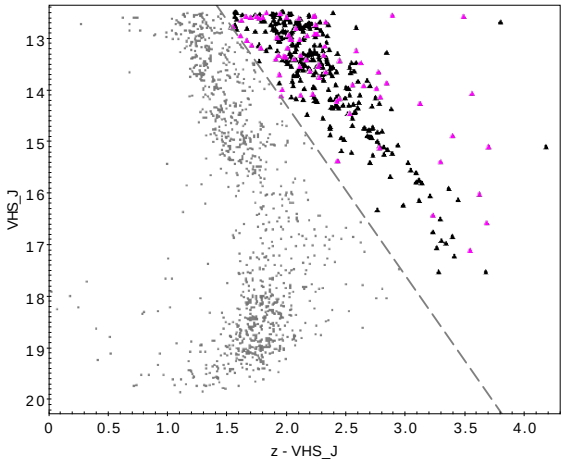

Figure 3.11: J vs $Z - J$ colour-magnitude diagram for the Pan-STARRS selection. The selected objects are marked as pink triangles. Some USco known members from the compilation with available J and z photometry are marked as black triangles. Objects discarded as contaminants are shown as grey dots. The selection cut is shown as a grey dashed line.

3.11 shows the J vs $z - J$ colour-magnitude diagram of the selection.

After removing those with positions corresponding to the primaries in our compilation, we obtained 89 entries. Some objects were duplicated, so we performed an internal match using their VHS coordinates, and we obtained 60 individual objects. Similarly to the Z-UKIDSS selection, we also verified if the retrieved primaries were placed closer than $60''$ from another primary of the compilation, as they would be also considered as candidate companions in that case. We found 7 compiled members recovered in our search that were placed close to another compiled member.

3.2.7 Constraining the candidates: Gaia DR2 and additional photometry.

The result of the selection is 111 (34+60+7) candidates with $J > 12.5$ which needed further investigation. To verify that they are bona fide candidates, they were visually inspected, and information available from other surveys, especially from Gaia DR2, was used to discard the contaminants.

The Gaia Data Release 2 in April 2018 provided a very valuable information

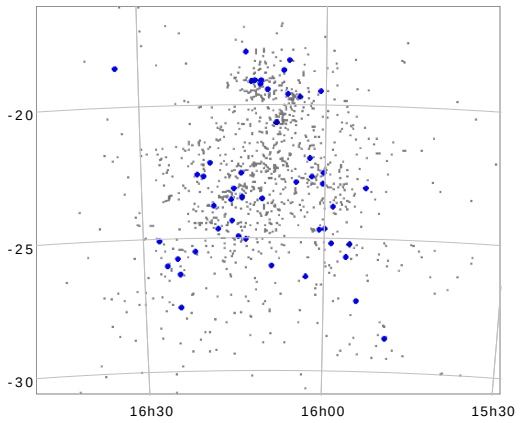

Figure 3.12: Position in the sky of the found candidate companions (blue circles). USco compiled members are shown as grey dots.

to assess the USco membership of our candidates. The precise astrometry from Gaia provides proper motions and parallaxes for the brightest candidates, up to $J \sim 16$, allowing to discard many contaminants prior to the spectroscopic follow-up observations. We cross-correlated our list of candidates with Gaia DR2, using a $3''$ cross-match radius, and keeping all the matches.

95 of our 111 candidates had a complete *Gaia* 5-parameter astrometric solution, which includes a parallax measurement. We selected all of the objects compatible with being placed at a distance of around or lower than 250 pc (parallax < 4 mas). In this selection, we obtained the following:

- 53 candidates presented Gaia DR2 parallaxes which were not compatible with being placed at a distance of around or lower than 250 pc. Many of these objects barely passed our astrometric and colour-magnitude selections, but are not really placed at a heliocentric distance compatible with belonging to the USco association.
- 42 objects presented Gaia DR2 parallaxes compatible with being placed at a distance of around or lower than 250 pc. These objects were kept as good companion candidates.

14 of the 111 candidates did not have a complete *Gaia* 5-parameter astrometric solution, or did not have any detection in *Gaia* at all. We used further

photometric data to select or discard these objects. In particular, we used the photometry from the Pan-STARRS i- and r-bands, and the *Gaia* G-band. We obtained the following:

- 7 candidates were rejected regarding their Pan-STARRS and/or *Gaia* photometry. They were faint objects which also barely passed our previous photometric selections, but which presented J magnitudes and colours in $i-J$, $r-i$ and/or $G-J$ which did not follow the USco photometric sequence.
- 7 candidates presented magnitudes and colours compatible with the USco photometric sequence. These objects were kept as good companion candidates.

As a summary, 49 candidates were kept as good candidate companions. Two of the found candidates belong to the same multiple system, so we obtained 48 final systems. We performed an exhaustive revision of the literature to collect all the available information on them. Some of them were previously-known wide companions that we recovered in our search. Some others were not previously found, or not considered as companions to other USco members. The list of these 48 candidate wide systems is shown in Table 3.5. A detailed description of the individual systems can be found in Appendix A.

3.2.8 Spectroscopic follow-up

Those components (either candidates or primaries) without a previous spectral characterization in the literature were scheduled for near-infrared and/or optical spectroscopic observations in our campaigns, to obtain their spectral types and look for youth features in the spectra. The candidates in this search were observed using several instruments: NTT/SofI, WHT/LIRIS, VLT/X-shooter, VLT/FORS2 and GTC/OSIRIS. The details on the spectroscopic campaigns, the instruments, observing methods and data reduction can be found in Section 2.3. The observing log of our candidates is shown in Table 3.3.

We obtained the spectral types of our targets comparing them with spectral templates. For the near-infrared spectra, we used main sequence star spectra from the IRTF Spectral Library (Cushing et al. 2005; Rayner et al. 2009) to classify all the targets with expected spectral types earlier than M9. This library includes spectra obtained with the SpeX spectrograph (Rayner et al. 2003), mounted on the NASA Infrared Telescope Facility (IRTF) at Mauna Kea Observatory. For our faintest objects (USco 1621−2529 B, USco 1556−2541 B and USco 1611−1906 c), with expected spectral types of early-L, we performed

RA	DEC	Range	Instrument	Date	Grating	Slit	Expt
15:49:24.85	−28:43:51.6	NIR	NTT/SofI	14 Apr 2017	GB, GR	1″	4x150s,4x150s
15:49:25.08	−28:43:52.7	NIR	NTT/SofI	14 Apr 2017	GB, GR	1″	4x150s,4x150s
15:55:47.88	−25:12:17.3	NIR	NTT/SofI	21 Jun 2018	GB, GR	1″	4x150s,4x150s
15:56:23.44	−25:41:05.6	OPT	VLT/X-shooter	15 Jun 2018	VIS	1.2″	10x280s
15:56:23.44	−25:41:05.6	NIR	VLT/X-shooter	15 Jun 2018	NIR	1.2″	10x300s
15:58:53.97	−25:11:51.8	NIR	WHT/LIRIS	28 Jun 2018	lr_zj, lr_hk	1″	4x150s,4x150s
15:59:57.94	−24:38:13.3	NIR	WHT/LIRIS	27 Jun 2018	lr_zj, lr_hk	1″	4x150s,4x150s
15:59:58.99	−24:38:15.3	NIR	WHT/LIRIS	27 Jun 2018	lr_zj, lr_hk	1″	4x150s,4x150s
16:00:15.33	−22:31:57.5	NIR	WHT/LIRIS	08 Jun 2017	lr_zj, lr_hk	0.75″	4x150s,4x150s
16:00:15.68	−22:31:58.0	NIR	WHT/LIRIS	08 Jun 2017	lr_zj, lr_hk	0.75″	4x150s,4x150s
16:00:17.66	−22:56:53.6	NIR	WHT/LIRIS	27 Jun 2018	lr_zj, lr_hk	1″	4x150s,4x150s
16:00:52.79	−24:40:35.5	NIR	WHT/LIRIS	28 Jun 2018	lr_zj, lr_hk	1″	4x150s,4x150s
16:00:52.84	−24:40:38.0	NIR	WHT/LIRIS	28 Jun 2018	lr_zj, lr_hk	1″	4x150s,4x150s
16:02:09.63	−22:40:58.0	NIR	WHT/LIRIS	27 Jun 2018	lr_zj, lr_hk	1″	4x150s,4x150s
16:03:02.35	−26:26:16.5	NIR	WHT/LIRIS	28 Jun 2018	lr_zj, lr_hk	1″	4x150s,4x150s
16:06:47.94	−18:41:43.8	NIR	WHT/LIRIS	08 Jun 2017	lr_zj, lr_hk	0.75″	4x150s,4x150s
16:06:47.98	−18:41:48.1	NIR	WHT/LIRIS	08 Jun 2017	lr_zj, lr_hk	0.75″	4x150s,4x150s
16:07:57.13	−20:40:17.6	NIR	NTT/SofI	20 Jun 2018	GB, GR	1″	4x150s,4x150s
16:08:44.38	−26:02:14.0	NIR	NTT/SofI	20 Jun 2018	GB, GR	1″	4x150s,4x150s
16:10:21.74	−19:04:06.7	NIR	WHT/LIRIS	27 Jun 2018	lr_zj, lr_hk	1″	4x150s,4x150s
16:10:21.78	−19:04:02.4	NIR	WHT/LIRIS	27 Jun 2018	lr_zj, lr_hk	1″	4x150s,4x150s
16:11:56.90	−19:06:47.0	OPT	VLT/FORS2	29 Jul 2019	GRIS_300I	1″	3x1800s,4x150s
16:11:56.90	−19:06:47.0	NIR	VLT/X-shooter	15 Jun 2018	NIR	1.2″	10x300s
16:13:01.89	−25:01:41.3	NIR	WHT/LIRIS	28 Jun 2018	lr_zj, lr_hk	1″	4x150s,4x150s
16:13:40.26	−22:33:19.4	NIR	NTT/SofI	21 Jun 2018	GB, GR	1″	4x150s,4x150s
16:13:40.46	−22:33:15.6	NIR	NTT/SofI	21 Jun 2018	GB, GR	1″	4x150s,4x150s
16:17:30.57	−24:38:37.3	NIR	WHT/LIRIS	28 Jun 2018	lr_zj, lr_hk	1″	4x150s,4x150s
16:18:11.69	−23:47:26.5	NIR	WHT/LIRIS	28 Jun 2018	lr_zj, lr_hk	1″	4x150s,4x150s
16:19:51.41	−22:41:26.8	NIR	WHT/LIRIS	27 Jun 2018	lr_zj, lr_hk	1″	4x150s,4x150s
16:20:49.26	−22:35:13.3	NIR	NTT/SofI	21 Jun 2018	GB, GR	1″	4x300s,4x300s
16:21:28.32	−25:29:56.0	OPT	GTC/OSIRIS	29 May 2017	R300R	1″	2x600s
16:21:28.32	−25:29:56.0	NIR	NTT/SofI	10 Abr 2017	GB, GR	1″	4x300s,4x300s
16:24:01.19	−26:20:36.0	NIR	NTT/SofI	20 Jun 2018	GB, GR	1″	4x300s,4x300s
16:26:02.36	−26:00:36.4	NIR	NTT/SofI	21 Jun 2018	GB, GR	1″	4x300s,4x300s
16:27:15.86	−25:04:04.7	NIR	NTT/SofI	14 Apr 2017	GB, GR	1″	4x150s,4x150s
16:33:34.73	−18:32:54.8	NIR	NTT/SofI	21 Jun 2018	GB, GR	1″	4x150s,4x150s
16:33:34.97	−18:32:54.0	NIR	NTT/SofI	21 Jun 2018	GB, GR	1″	4x150s,4x150s

Table 3.3: Observations log for USco candidate systems.

a comparison with several L-type USco members obtained with GNIRS spectrograph (Elias et al. 2006b,a) on the Gemini North telescope by Lodieu et al. (2008), and with the X-shooter spectrograph (Vernet et al. 2011) on the VLT telescope by Lodieu et al. (2018). These comparisons are shown in Figure 3.18. For a proper comparison, the spectra with higher resolutions were convolved with gaussians to match the lower resolution ones. The adopted spectral types for the observed targets are included in Table 3.5. The spectral types obtained here are highlighted in boldface in this table. The spectral types of the observed targets range between M2–L1. In the near-infrared, the main spectral feature of our candidates is the strong water vapor absorptions, mainly present at both sides of the H-band wavelength region ($\sim$1.4μm and $\sim$1.9μm), which are growing in intensity as we move to later spectral types. We can also see that the flux in the K-band is higher for later spectral types. For the late-M spectra, we can distinguish youth features like weaker alkali lines in the J-band, like the 1.169 / 1.177 μm and 1.243 / 1.252 μm K I doublets, and a triangular

shape in the H-band pseudo-continuum due to a strong water absorption at the sides of this band, stronger than the usually seen in higher gravity objects (e.g. Lucas et al. 2001; Allers & Liu 2013). A close-up display of the J-band wavelength range of the spectra is also shown in Figure 3.19.

Our faintest companions were also observed in the optical, using GTC/OSIRIS (USco 1621−2529 B), VLT/X-shooter (USco 1556−2541 B) and VLT/FORS2 (USco1611−1906 c). We obtained their optical spectral types through comparisons with optical spectra of USco members obtained with GTC/OSIRIS by Lodieu et al. (2018). The plots with these comparisons are shown in Figure 3.20. For the comparisons, the spectra with higher resolutions were convolved with gaussians to match the lower resolution ones. The adopted optical spectral types are also included in Table 3.5, and highlighted in boldface. These candidates show spectral types of M8.5 (USco 1621−2529 B and USco 1556−2541 B) and M9.25 (USco1611−1906 c) in the optical. The spectra show an overall red shape, with a much higher flux in the red wavelengths than for the blue wavelengths. We can distinguish several prominent oxide molecular bands, as TiO and VO, and some alkali lines such as the KI and NaI doublets (7665 / 7699 Å, and 8183 / 8195 Å, respectively). These alkali lines are very weak in our spectra, which is a consequence of the low gravities of the objects, and hence a remarkable youth feature. We cannot distinguish any strong Hα emission in our spectra. The presence of Hα emission is another remarkable sign of youth, commonly associated with chromospheric activity or accretion (Hawley et al. 1996; Gizis et al. 2000; Barrado y Navascués & Martín 2003; Mohanty & Basri 2003; Muzerolle et al. 2003; Jayawardhana et al. 2003; White & Basri 2003; Mohanty et al. 2005; Caballero et al. 2006), and it is present in most of the young late-M objects. However, there are several cases of young late-M or early-L objects which do not show this emission, being the Hα emission a sufficient but not necessary indicator of youth (e.g. Martín et al. 2010; Lodieu et al. 2018).

3.2.9 Chance alignments within USco

Constraining the companionship of our candidates in the USco region presents another difficulty. We can find USco members which, due to projection effects, are placed at separations lower than 60″ from our primaries by chance, and are not really physically close to each other in a 3D picture.

The precision of the *Gaia* DR2 PM measurements is better than the intrinsic dispersion of velocities of the association, and allows to distinguish truly bound companions from chance alignments within unbound members of USco. In the left panel of Figure 3.13 we show the differences in proper motion and parallax

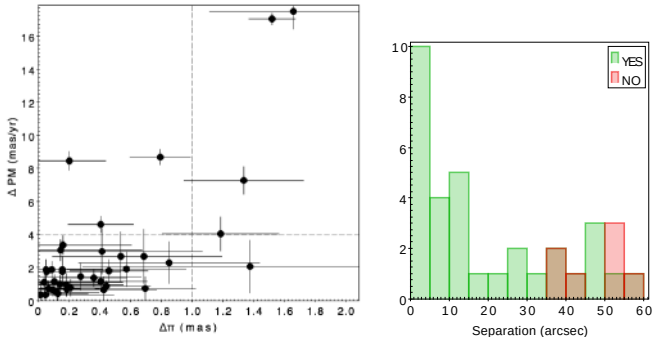

Figure 3.13: Left panel: Differences in *Gaia* proper motion and parallax for the candidate pairs with available and reliable 5-parameter astrometric solutions in this catalogue. Dashed lines show the adopted astrometric cuts to discard chance alignments. Right panel: Histogram of the angular separation of the candidate pairs with complete 5-parameter astrometric solutions. Pairs accepted ("YES") and rejected ("NO") regarding their PM and parallax differences are marked in green and red, respectively.

of our pairs of candidate companions which present complete and good quality *Gaia* astrometric data. Most of the pairs are concentrated in a region close to zero, showing differences in PM and parallax smaller than 4 mas yr^{-1} and 1mas, respectively, and only few of them show differences much larger than these values, so we considered as good companions all the pairs with differences in *Gaia* proper motion lower than these thresholds. These cuts are shown as dashed lines in the Figure. All the pairs with differences higher than these values are probably chance alignments and we will consider them as not truly-bound pairs. Objects with not-matching *Gaia* astrometry but suspected to be close binaries were not discarded in this step, as close binarity may seriously affect *Gaia* DR2 astrometry.

We analysed the angular separations of the candidates with complete *Gaia* astrometry. For this analysis, we did not include all the objects which are possible close binaries. The right panel of Figure 3.13 shows the distribution of the separations of the pairs with reliable *Gaia* DR2 astrometry. This distribution shows that all the pairs flagged as chance alignments due to their PM or parallaxes have angular separations above 35″, while all the pairs with separations lower than 35″ have consistent PM and parallax. Pairs with separations between 35″–50″ have a moderate probability of being chance alignments (∼33% probability). And pairs with separations above 50″ are most likely chance align-

ments (∼66% probability). We used these separation criteria to flag the rest of the pairs (15), which do not have *Gaia* DR2 PM and parallaxes, or which have an unreliable astrometry, to classify them as likely bound or likely not-bound.

Table 3.5 shows the final classification of our candidate pairs. Pairs with reliable and matching *Gaia* astrometry, and pairs previously confirmed in the literature, are marked as true companions ("y"). Pairs with any of the members having no *Gaia* astrometry or having unreliable *Gaia* astrometry, and showing separations lower than 35″ are marked as most-likely companions ("y?"). Pairs with any of the members having no *Gaia* astrometry or having unreliable *Gaia* astrometry, but having separations higher than 35″ are marked as possible chance alignments ("n?"). Finally, pairs having reliable but non-matching *Gaia* astrometry are marked as chance alignments ("n"). The pair of candidate companions which do not seem to belong to the association are also included in the table, but flagged as not belonging to USco ("nUsc").

Selection criteria	Cand. left
PM	∼20 000
CMD	111
Gaia DR2	49
Final candidate comp.	42
Bona fide ("y")	31
Likely ("y?")	8
Dubious ("n?")	3

Table 3.4: Summary of the remaining candidates in each step of the search.

Table 3.5: USco companion candidates.

RA	DEC	Jmag[a]	Sep ['/']	SpT Opt.	Ref[b]	SpT NIR	Ref[b]	Parallax[c] [mas]	pmra[c] [mas yr^{-1}]	pmdec[c] [mas yr^{-1}]	Comp?
15:49:25.08	−28:43:52.7	10.619 ± 0.03		M2	2	**M2**	1	7.6919 ± 0.0521	−20.533 ± 0.103	−25.112 ± 0.072	y
15:49:24.85	−28:43:51.6	12.7152 ± 0.0011	3.2	–	–	**M4**	1	7.3313 ± 0.165	−21.459 ± 0.323	−24.077 ± 0.241	y
15:53:18.82	−23:06:39.5	12.133 ± 0.023		–	–	–	–	11.3452 ± 0.0968	3.293 ± 0.166	−38.349 ± 0.098	y-nUsc
15:53:18.63	−23:06:31.3	13.0571 ± 0.0012	10.6	–	–	–	–	11.3662 ± 0.1249	2.81 ± 0.216	−36.57 ± 0.127	y-nUsc
15:54:30.11	−27:20:19.1	6.234 ± 0.019		B6	3	–	–	6.6037 ± 0.1196	−13.357 ± 0.187	−25.272 ± 0.11	y
15:54:30.47	−27:19:57.5	14.9801 ± 0.004	22.3	–	–	M9	4	5.2279 ± 0.9696	−13.908 ± 1.517	−23.265 ± 1.097	y
15:55:48.82	−25:12:24.1	8.756 ± 0.032		G3	6	–	–	6.9503 ± 0.0406	−15.851 ± 0.100	−23.555 ± 0.055	y
15:55:48.40	−25:12:17.4	10.956 ± 0.037	9.0	M2.5	5	–	–	8.9942 ± 0.2221*	−15.59 ± 0.441*	−22.233 ± 0.264*	y?
15:55:47.88	−25:12:17.3	13.3792 ± 0.0014	14.6	–	–	**M5**	1	7.0055 ± 0.1578	−15.645 ± 0.313	−21.788 ± 0.185	y
15:56:24.92	−25:41:20.3	11.373 ± 0.023		M3	2	–	–	7.0835 ± 0.0827	−18.446 ± 0.129	−22.386 ± 0.076	y
15:56:23.44	−25:41:05.6	16.1660 ± 0.010	24.8	**M8.5 vlg**	**7**	**L0.5 vlg**	**7**	–	–	–	y
15:58:36.21	−23:48:02.0	11.110±0.023		M3 VB	5	–	–	8.1656±0.0850	−15.433±0.159	−25.428±0.101	y
15:58:35.98	−23:48:13.6	12.9512±0.0011	12.2	M4	23	–	–	8.0709±0.1460	−15.587±0.276	−26.071±0.174	y
15:58:53.52	−25:12:33.4	10.548 ± 0.026		M1	6	–	–	9.2554 ± 0.0614	−21.567 ± 0.095	−34.207 ± 0.065	n?
15:58:53.97	−25:11:51.8	13.0352 ± 0.0012	42.2	–	–	**M4.5**	1	–	–	–	n?
15:59:58.99	−24:38:15.3	12.6197 ± 0.0009		–	–	**M4**	1	6.9899 ± 0.1248	−17.473 ± 0.229	−21.638 ± 0.132	y
15:59:57.94	−24:38:13.3	12.6848 ± 0.0010	14.6	M4.5	8	**M4**	1	7.131 ± 0.1343	−18.428 ± 0.251	−21.265 ± 0.145	y
16:00:15.68	−22:31:58.0	11.365 ± 0.023		M4	8	–	–	6.8808 ± 0.1043	−11.462 ± 0.17	−24.434 ± 0.094	y?
16:00:15.33	−22:31:57.5	14.1265 ± 0.0028	5.0	–	–	–	–	–	–	–	y?
16:00:17.66	−22:56:53.6	13.4473 ± 0.0018		–	–	**M7 vlg**	1	7.2356 ± 0.2442	−12.936 ± 0.446	−25.912 ± 0.275	y
16:00:19.44	−22:56:29.0	14.4779 ± 0.0036	35.0	M8	9	–	–	6.8203 ± 0.4089	−10.133 ± 0.758	−24.882 ± 0.476	y
16:00:49.89	−19:28:00.4	10.673 ± 0.024		M1.5	2	–	–	7.4061 ± 0.1289	−10.274 ± 0.302	−22.152 ± 0.16	y?
16:00:50.65	−19:27:50.4	12.6138 ± 0.0008	15.1	M6.5 vlg	10	–	–	–	–	–	y?
16:00:52.84	−24:40:38.0	11.322 ± 0.036		M3.5	8	**M3**	1	6.8126 ± 0.0797	−12.201 ± 0.15	−24.232 ± 0.092	y
16:00:52.79	−24:40:35.5	12.5168 ± 0.0008	3.0	–	–	**M4**	1	6.6841 ± 0.115	−11.808 ± 0.217	−24.002 ± 0.133	y
16:02:10.45	−22:41:28.0	8.866 ± 0.023		K5	11	–	–	–	–	–	y?
16:02:09.63	−22:40:58.0	13.3408 ± 0.0017	32.4	–	–	**M5**	1	8.8558 ± 0.2023	−22.034 ± 0.353	−29.432 ± 0.192	y?
16:02:34.18	−22:00:35.6	12.7047 ± 0.0012		M6	8	–	–	6.3878 ± 0.1976	−12.915 ± 0.349	−22.014 ± 0.226	y
16:02:32.27	−22:00:48.7	13.2599 ± 0.0016	29.7	M5.75	8	–	–	6.2066 ± 0.1755	−11.942 ± 0.313	−22.117 ± 0.207	y
16:03:01.78	−26:26:21.9	10.624 ± 0.024		M0	2	–	–	6.8978 ± 0.0755	−16.325 ± 0.08	−23.489 ± 0.046	y
16:03:02.35	−26:26:16.5	13.1390 ± 0.0012	9.7	–	–	**M5**	1	6.4539 ± 0.2099	−15.991 ± 0.267	−22.669 ± 0.154	y
16:04:17.40	−19:42:28.7	11.443 ± 0.044		M3.5	8	–	–	6.2022 ± 0.0946	−9.703 ± 0.189	−21.632 ± 0.09	y
16:04:17.62	−19:42:33.2	12.206±0.026	5.5	–	–	–	–	6.1335 ± 0.1136	−9.132 ± 0.233	−21.155 ± 0.110	y
16:04:17.92	−19:41:50.8	13.4192 ± 0.0014	38.8	M5	8	–	–	6.0465 ± 0.1684	−8.264 ± 0.331	−22.834 ± 0.163	y
16:04:42.70	−22:54:52.8	13.4752±0.0015		–	–	–	–	4.6478±0.1752	−1.643±0.269	−8.935±0.166	n
16:04:40.26	−22:54:32.5	14.2900±0.0024	39.6	M6	8	–	–	6.3048±0.3724	−12.796±0.704	−22.497±0.391	n
16:05:53.94	−18:18:42.7	13.3998 ± 0.0015		M7	12	M7	12	6.9306 ± 0.2409	−10.156 ± 0.454	−20.618 ± 0.26	y
16:05:54.09	−18:18:49.1	16.4548 ± 0.0147	4.6	M9.5	12	–	–	–	–	–	y
16:06:11.99	−19:35:33.1	12.013±0.026		M5+M5	24	–	–	7.2912±0.1351	−11.944±0.329	−21.727±0.188	y
16:06:11.44	−19:35:40.7	13.0090±0.0011	10.8	M5	24	–	–	7.1691±0.1389	−11.518±0.347	−21.942±0.196	y
16:06:47.94	−18:41:43.8	9.886 ± 0.022		M0	2	–	–	6.4456 ± 0.0502	−8.336 ± 0.098	−21.082 ± 0.075	y
16:06:47.98	−18:41:48.1	13.9277 ± 0.0026	4.2	–	–	–	–	5.873 ± 0.3365	−9.734 ± 0.72	−19.737 ± 0.595	y
16:07:57.97	−20:40:08.7	11.061 ± 0.023		M1	5	–	–	5.041 ± 0.2026*	−7.149 ± 0.262*	−26.306 ± 0.183*	y?
16:08:00.51	−20:40:28.9	12.325 ± 0.023	41.1	M5	14	–	–	6.1450 ± 0.1971	−9.500 ± 0.328	−22.608 ± 0.169	y
16:07:57.13	−20:40:17.6	12.6308 ± 0.0012	14.5	–	–	**M5.5**	1	6.3052 ± 0.2488	−10.286 ± 0.348	−25.904 ± 0.242	y
16:07:58.50	−20:39:48.8	13.5173 ± 0.0020	21.5	M6	13	–	–	6.1596 ± 0.2818	−9.079 ± 0.416	−22.906 ± 0.273	y

16:08:43.41	−26:02:16.8	8.55 ± 0.02	13.4	G9	15	–	–	6.4184 ± 0.1164	−10.47 ± 0.309	−26.269 ± 0.231	y
16:08:44.38	−26:02:14.0	13.9967 ± 0.0024		M8.25	8	**M7.5 vlg**	1	7.1046 ± 0.3913	−12.233 ± 1.044	−24.262 ± 0.738	y
16:09:20.89	−19:27:25.9	7.587±0.023	49.4	A0	25	–	–	6.6402±0.0792	−7.790±0.133	−23.428±0.095	y
16:09:20.54	−19:26:32.1	12.9797±0.0012		M5.5	8	–	–	7.0442±0.2229	−8.766±0.386	−24.032±0.260	y
16:10:20.88	−23:31:55.7	12.005 ± 0.027	50.8	M5.5	16	–	–	7.3809 ± 0.1571	−15.771 ± 0.254	−27.202 ± 0.196	n
16:10:19.43	−23:31:09.0	13.5607 ± 0.0014		M5.75	16	–	–	6.0455 ± 0.2316	−10.067 ± 0.412	−22.684 ± 0.299	n
16:10:21.74	−19:04:06.7	10.679 ± 0.03	4.6	M3	17	**M2-3**	1	7.4634 ± 0.0598	−9.413 ± 0.144	−24.072 ± 0.096	y
16:10:21.78	−19:04:02.4	12.9254 ± 0.0012		–	–	**M5 vlg**	1	7.2774 ± 0.1508	−9.25 ± 0.356	−24.758 ± 0.228	y
16:10:31.95	−19:13:06.1	10.026 ± 0.026	5.8	K7	–	–	–	7.496 ± 0.0718	−9.342 ± 0.206	−23.591 ± 0.111	y
16:10:32.33	−19:13:08.7	13.8834 ± 0.0020		M9	4	–	–	6.96 ± 0.3719	−7.043 ± 1.112	−24.982 ± 0.576	y
16:11:23.05	−19:05:23.2	10.508±0.027	54.5	M3	14	–	–	7.1525±0.0874	−9.911±0.173	−25.709±0.120	y
16:11:19.35	−19:05:08.2	13.6461±0.0017		M6.5	2	–	–	7.3104±0.2901	−8.803±0.616	−24.348±0.431	y
16:11:59.27	−19:06:53.4	8.981 ± 0.023	3.3	K2+M4	11	–	–	7.2867 ± 0.0415	−12.506 ± 0.101	−22.658 ± 0.067	y
16:11:59.23	−19:06:56.2	9.148 ± 0.077		M1	19	–	–	7.2374 ± 0.01854	−10.879 ± 0.403	−21.737 ± 0.272	y
16:11:56.90	−19:06:47.0	17.1249 ± 0.0261		**M9.25 vlg**	1	**L1 vlg**	1	–	–	–	y?
16:12:48.93	−18:00:52.5	11.351 ± 0.026	3.2	M3	18	–	–	6.3156 ± 0.0747	−7.418 ± 0.161	−21.148 ± 0.112	y
16:12:48.97	−18:00:49.6	14.1463 ± 0.0024		M8.5	4	–	–	6.0413 ± 0.3224	−7.002 ± 0.698	−19.738 ± 0.512	y
16:13:02.34	−25:01:46.0	10.423 ± 0.024	7.8	M2	8	–	–	7.1186 ± 0.2456*	−11.259 ± 0.501*	−22.501 ± 0.326*	y?
16:13:01.89	−25:01:41.3	12.6019 ± 0.0010		–	–	**M3**	1	6.2855 ± 0.0819	−10.698 ± 0.169	−22.39 ± 0.107	y?
16:13:36.89	−23:27:29.8	11.807±0.028	8.0	M4.5	16	–	–	6.6303±0.0829	−12.612±0.150	−23.516±0.112	y?
16:13:36.48	−23:27:35.3	12.196±0.028	54.3	M5.75	16	–	–	–	–	–	y?
16:13:34.77	−23:28:15.8	13.2999±0.0014		M5.75	16	–	–	6.2251±0.1278	−9.308±0.239	−20.277±0.178	n
16:13:40.46	−22:33:15.6	13.0595 ± 0.0012	4.4	M5.5	8	**M6.5 vlg**	1	6.3417 ± 0.22	−9.759 ± 0.326	−25.081 ± 0.234	y
16:13:40.26	−22:33:19.4	13.5666 ± 0.0015		M6.5	8	**M7 vlg**	1	6.3804 ± 0.2901	−10.589 ± 0.429	−24.315 ± 0.306	y
16:14:12.59	−24:54:28.8	10.836 ± 0.026	53.8	M0.5	2	–	–	6.0107 ± 0.0314	−11.586 ± 0.065	−20.31 ± 0.043	n
16:14:15.73	−24:55:01.4	13.5960 ± 0.0018		–	–	–	–	7.532 ± 0.1191	−21.42 ± 0.232	−34.276 ± 0.154	n
16:14:52.69	−23:08:02.6	10.569±0.026	52.5	M3.5	2	–	–	7.1322±0.1553*	−12.972±0.254*	−22.140±0.185*	n?
16:14:51.31	−23:08:51.7	12.584±0.0009		M5	21	–	–	5.8984±0.1304	−7.651±0.203	−21.063±0.148	n?
16:15:12.39	−24:20:09.3	13.0315 ± 0.0012	17.9	M4	5	–	–	6.5114 ± 0.1256	−12.132 ± 0.241	−20.314 ± 0.165	y
16:15:11.16	−24:20:15.3	14.1589 ± 0.0023		M6	13	–	–	6.9383 ± 0.2159	−11.513 ± 0.447	−20.085 ± 0.31	y
16:15:20.25	−23:33:58.9	11.995 ± 0.032	4.8	M4	8	–	–	6.5802 ± 0.0766	−8.809 ± 0.153	−22.538 ± 0.101	y
16:15:20.09	−23:33:54.6	12.9239 ± 0.0011		M5.75	16	–	–	6.5344 ± 0.1686	−8.477 ± 0.332	−22.382 ± 0.217	y
16:17:30.32	−24:38:39.0	10.832 ± 0.035	3.9	M0	2	–	–	6.3881 ± 0.0361	−12.03 ± 0.08	−21.101 ± 0.056	y
16:17:30.57	−24:38:37.3	12.5763 ± 0.0010		–	–	**M4 vlg**	1	6.1798 ± 0.1638	−11.284 ± 0.34	−20.924 ± 0.24	y
16:18:15.68	−23:47:08.4	12.425 ± 0.026	57.6	M5.5	20	–	–	6.7991 ± 0.1861	−10.11 ± 0.439	−23.308 ± 0.263	y
16:18:11.69	−23:47:26.5	12.9670 ± 0.0012		–	–	**M6 vlg**	1	6.1045 ± 0.1421	−10.358 ± 0.339	−22.589 ± 0.222	y
16:18:43.23	−22:09:34.5	12.9968 ± 0.0011	37.3	M5.5	8	–	–	5.9425 ± 0.1336	−6.348 ± 0.297	−22.563 ± 0.204	y?
16:18:40.74	−22:09:48.2	13.6873 ± 0.0017		M6	8	–	–	7.1292 ± 0.2453	−9.695 ± 0.566	−24.839 ± 0.37	y?
16:19:51.41	−22:41:26.8	13.1608 ± 0.0014	6.6	M5.5	21	**M7 vlg**	1	7.0688 ± 0.1574	−8.613 ± 0.329	−21.593 ± 0.214	y
16:19:51.44	−22:41:33.3	14.4781 ± 0.0032		M6.75	8	–	–	6.2187 ± 0.4299	−10.93 ± 0.914	−21.495 ± 0.576	y
16:20:50.23	−22:35:38.8	8.032 ± 0.023	28.9	A9	22	–	–	6.9482 ± 0.0552	−10.718 ± 0.165	−19.766 ± 0.085	y
16:20:49.26	−22:35:13.3	14.1170 ± 0.0024		M5.5	8	**M7 vlg**	1	7.4088 ± 0.1966	−12.414 ± 0.444	−19.146 ± 0.281	y
16:21:29.53	−25:29:43.1	11.175 ± 0.024	20.8	M2.5	2	–	–	7.2232 ± 0.0504	−6.138 ± 0.101	−25.617 ± 0.073	y
16:21:28.32	−25:29:56.0	15.9422 ± 0.010		**M8.5 vlg**	**7**	**L0 vlg**	**7**	–	–	–	y
16:23:57.24	−26:20:24.5	11.188 ± 0.021	54.4	M4.5	2	–	–	–	–	–	n?
16:24:01.19	−26:20:36.0	13.9110 ± 0.0018		–	–	**M7 vlg**	1	6.0961 ± 0.6186	−11.793 ± 1.144	−24.862 ± 0.877	n?
16:23:59.02	−27:36:03.8	10.327 ± 0.024	12.6	M3.5	2	–	–	–	–	–	y?
16:23:58.53	−27:35:52.9	13.5897 ± 0.0014		–	–	–	–	3.4197 ± 0.7419	−10.698 ± 1.326	−20.362 ± 1.038	y?
16:24:15.52	−25:44:34.5	10.711 ± 0.022	11.4	M0	2	–	–	8.9951 ± 0.2257*	−14.398 ± 0.593*	−21.697 ± 0.318*	y?
16:24:16.15	−25:44:27.3	14.9278 ± 0.0051		–	–	–	–	7.213 ± 0.5254	−11.454 ± 1.394	−19.474 ± 0.779	y?

16:25:57.91	−26:00:37.5	9.575 ± 0.024	59.8	G8	2	–	–	6.3162 ± 0.0442	−14.84 ± 0.094	−23.779 ± 0.07	n
16:26:02.36	−26:00:36.4	14.3946 ± 0.0032		–	–	**M6 vlg**	1	6.5180 ± 0.1921	−22.761 ± 0.4	−26.779 ± 0.282	n
16:27:12.74	−25:04:01.8	10.553 ± 0.023	42.6	M1	2	–	–	7.1826 ± 0.0531	−5.713 ± 0.124	−26.971 ± 0.071	n
16:27:15.86	−25:04:04.7	12.8693 ± 0.0013		–	–	**M5.5**	1	6.3908 ± 0.1434	−10.935 ± 0.296	−20.022 ± 0.201	n
16:33:34.97	−18:32:54.0	11.314 ± 0.03		M3.5	2	**M3**	1	8.3578 ± 0.0819	−16.71 ± 0.146	−28.546 ± 0.077	y
16:33:34.73	−18:32:54.8	13.3447 ± 0.0013	3.3	–	–	**M6 vlg**	1	8.2545 ± 0.1303	−15.91 ± 0.232	−27.708 ± 0.132	y

Table 3.5: *(a)* J magnitudes from VHS for targets fainter than J=12.5, and from 2MASS for targets brighter than J=12.5.
(b) References: (1) This work, (2) Rizzuto et al. (2015), (3) Garrison (1967), (4) Aller et al. (2013), (5) Kraus & Hillenbrand (2009), (6) Kunkel (1996), (7) Chinchilla et al. (2020b), (8) Luhman et al. (2018), (9) Martín et al. (2004), (10) Martín et al. (2010), (11) Mathieu et al. (1989), (12) Béjar et al. (2008), (13) Slesnick et al. (2006), (14) Preibisch et al. (2001), (15) Torres et al. (2006), (16) Lodieu et al. (2011), (17) Walter et al. (1994), (18) Preibisch et al. (2002), (19) Martín et al. (1998), (20) Slesnick et al. (2008), (21) Esplin et al. (2018), (22) de Zeeuw et al. (1999), (23) Ardila et al. (2000), (24) Kraus & Hillenbrand (2007b), (25) Houk & Smith-Moore (1988)
(c) Astrometric data from *Gaia* DR2. Data marked with an asterisk (*) correspond to suspected close binaries and may not be reliable.

3.3 Results: Wide binary systems in USco

We found 48 candidate companions with J >12.5 placed in 47 candidate wide systems, in our search around 1195 known members; plus one candidate companion in one system which does not seem to belong to USco regarding its astrometry. Of the 48 pairs, we have confirmed that 31 companions in 30 systems are physically bound companions using Gaia DR2 astrometry. 8 pairs do no have reliable Gaia DR2 astrometry in one of the components but are located at angular separations closer than 35″, and hence have a low probability of being a chance alignment. Another 3 pairs are located at large separations (>35″), and hence have a significant probability (∼50%) of being chance alignments. Finally, we discarded 6 pairs as chance alignments, due to large differences in PM and parallax in their Gaia DR2 astrometry. In summary, we have identified 39 bona fide companions with J >12.5, in 38 systems, around our sample of 1195 members of the USco association. From these 39 objects, 21 were already reported as candidate companions in the literature, 16 were reported as candidate USco members but not related as companions,[3] and 2 are newly discovered objects.

Our search covers separations between 3″–60″, which corresponds to physical projected separations of 400–8700 AU at the mean distance of USco (145 pc). We are complete between magnitudes $12.5 < J < 17.3$, which corresponds to masses between $0.01\,M_\odot < M < 0.2\,M_\odot$ approximately.

We obtain that **3.2**±0.5% of the USco members have a wide low-mass companion in the studied range of masses and separations. There is a possibility that any of the 3 companions which we considered as possible chance alignments may be actually bound, in that case this ratio would be up to **3.4**%, which is slightly larger, but within the error bars.

Tables 3.6 and 3.7 show the luminosities, masses, effective temperatures and binding energies of the components of our systems considering an age of 5 Myr and 10 Myr, respectively. The luminosities were calculated using the J magnitude of the components, and the USco bolometric corrections from Lodieu et al. (2011) for objects later than M3.5. For objects earlier than M3.5, we used the bolometric corrections of Pecaut & Mamajek (2013) for young objects. For the massive primaries (earlier than F0), we obtained the bolometric corrections from the updated version of the table of stellar color and effective temperature sequence from Pecaut & Mamajek (2013), available on-

[3] Two of these objects, USco1556 B and USco1621 B, were published in Chinchilla et al. (2020b). Nevertheless, as their discovery is a part of this search, we count them as newly reported companions here.

line.[4] For the distance determination, we used the most precise *Gaia* parallax measurement among the components of each system. The *Gaia* parallaxes of suspected binaries were not used. Masses and effective temperatures were obtained from the theoretical evolutionary models from Baraffe et al. (2015) based on the BT-Settl atmospheric models from Allard et al. (2012). These models do not cover masses above 1.4 $M_{\odot}$, so the masses and temperatures for the brightest primaries were obtained using the Pisa pre-main sequence models (Tognelli et al. 2011). The luminosity of the wide planetary mass companion USco 1611−1906c was also not covered by BT-Settl for an age of 5 Myr, so we used the AMES-Cond models (Allard et al. 2001; Baraffe et al. 2003) to obtain its mass and temperature at this age.

From the 39 companions, 17 have masses which are likely above the stellar/substellar boundary. 22 wide companions in 22 systems have masses which are likely below this threshold. This means a ratio of **1.8**±0.4% of the USco members having a wide substellar companion in the studied range of separations. Furthermore, 2 of the unlikely-bound candidate companions are also likely substellar. If any or both of them is truly bound, this ratio could increase up to 2.0%.

Only one of the candidate wide companions has a mass which is likely below the deuterium burning mass limit. This implies a lower limit of **0.08**% occurrence for planetary mass objects at very wide separations to USco members. But regarding that our search is not complete for masses lower than 11 $M_{\rm Jup}$, the ratio of wide planetary mass companions may be much higher.

The distribution of companion masses and physical separations are shown in Figure 3.14. The left panel shows that the frequency of the wide companions increases as the companion mass decreases. We note that the first bin of this histogram is not complete due to our photometric detection limits, and many undetected planetary mass companions may exist, if this tendency extends to lower masses. Therefore, we can discard the existence of a minimum mass for widely separated companions within our detection limits. The right panel in this Figure shows the separation distribution of the systems. Wide companions are more frequently found at shorter separations, and their occurrence decreases when we move to wider separations.

The comparison of mass-ratios with the primary mass and with the separations is shown in Figure 3.15. The left panel of this Figure shows the mass ratio of the wide binaries compared to the primary mass, and the photometric boundaries of our search. The mass-ratios for low-mass primaries seem well distributed, and we do not notice a preference for equal-mass binaries for them.

[4] `https://www.pas.rochester.edu/~emamajek/EEM_dwarf_UBVIJHK_colors_Teff.txt`

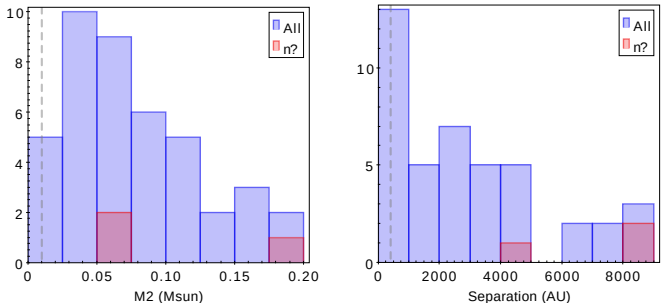

Figure 3.14: Left panel: Histogram of the companion masses for the discovered systems. Companions with a moderate probability of being chance alignments are marked in red. The completeness low limit in mass is marked as a dashed grey line. Right panel: Histogram of the separations for the discovered systems. Possible chance-alignment pairs are also marked in red, and the lower limit on separations is marked as a dashed grey line.

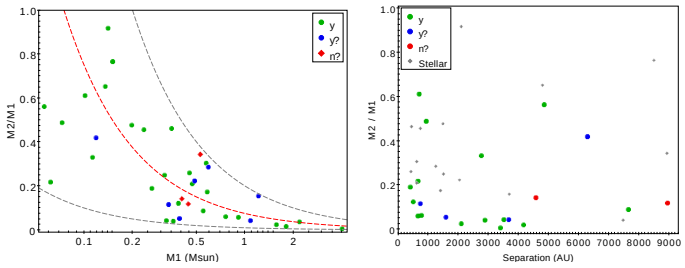

Figure 3.15: Left panel: Mass ratio vs. primary mass of the USco candidate systems. Grey dashed lines mark the photometric limits of the search. Red dashed line marks the stellar/substellar boundary. Green, blue and red colours stand for confirmed candidate companions, high-probability companions, and companions with moderate probability of chance alignment, respectively. Candidate companions belonging to triple or cuadruple systems are not included. Right panel: Mass ratio vs. separation of the candidate systems. Substellar companions are marked as coloured circles, with the same colour code as the left panel. Low-mass stellar companions are marked as grey dots. Candidate companions belonging to triple or cuadruple systems are not included.

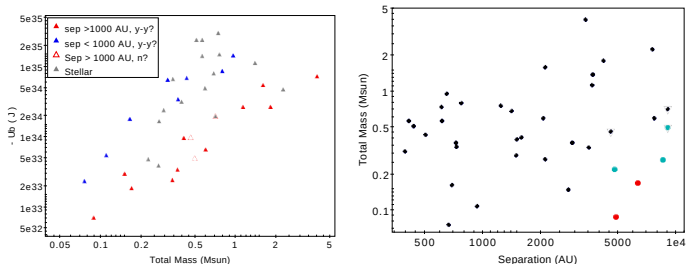

Figure 3.16: Left panel: Binding energy vs. total mass of the discovered systems. Systems with wide substellar companions at separations higher than 1000 AU are marked as red triangles. Systems with wide substellar companions at separations < 1000 AU are marked as blue triangles. Systems with low-mass stellar companions are marked as grey triangles. Systems with moderate probability of being chance alignments are marked as unfilled triangles. Candidate companions belonging to triple or cuadruple systems are not included. Right panel: Total mass vs. separation of the discovered systems. Systems more prone to disruption are marked in coloured circles. Systems with a moderate probability of being chance alignments are marked with a triangular contour. Candidate companions belonging to triple or cuadruple systems are not included.

However, due to the photometric restrictions of the search we cannot confirm this precisely. The right panel of this Figure shows the comparison of the mass-ratio and the separation of the binary systems. We do not observe any remarkable dependence between them, as we find binaries with any mass-ratio at any separation within our separation limits.

The left panel of Figure 3.16 shows the binding energy of the binary systems compared to the total mass of the binary. The right panel of this Figure shows the comparison between the total mass of the binaries and the separation. We computed the estimated disruption times for these binaries using the soft binary approximation from Binney & Tremaine (1987), following the procedure described in Chinchilla et al. (2020b). To estimate the actual density of objects in the USco region, we queried the *Gaia* DR2 database to obtain all the objects located inside a spherical volume of 5 pc radius around the centre of the association. We found 226 objects in this volume, leading to an object density of 0.43 obj pc^{-3}. We considered a mean perturber mass of 1 $M_{\odot}$, and a mean velocity dispersion of 3.20 km s^{-1} (Wright & Mamajek 2018). Most of our systems present disruption times above 100 Myr, far above the estimated dissipation time of USco. However, a few of the systems are more prone to disruption due to encounters with other stars. We marked these systems in coloured circles in Figure 3.16 right panel. The objects marked in red have

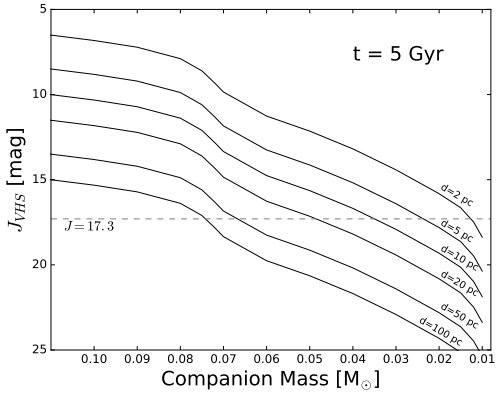

Figure 3.17: Photometric detectability in the VHS J band for substellar objects at different heliocentric distances considering an age of 5 Gyr.

estimated disruption times between 10–50 Myr, and those marked in light blue have estimated disruption times between 50–100 Myr. Considering a similar environment to the Solar vicinity after the dissipation of the association (few tens of Myr): 0.076–0.084 obj pc^{-3}, dispersion velocity 52.8 km s^{-1} (Zapatero Osorio et al. 2007; Henry et al. 2018; Chinchilla et al. 2020b,a), all of the systems are expected to survive for, at least, 1 Gyr. 14% of them have disruption times below 5 Gyr, but 86% of the systems are expected to survive for more than 5 Gyr.

At the age of our sun, these substellar companions will have become much fainter, and their detection would be challenging. Figure 3.17 shows the expected apparent magnitude of substellar objects placed at different heliocentric distances, computed using the AMES-Cond evolutionary models for the VHS photometry (Allard et al. 2001; Baraffe et al. 2003). Considering a detection limit similar to our search, we would not be able to find any old substellar companion placed at a distance larger than 100 pc from the Sun. For distances between 20–100 pc, it would be possible to detect only the most massive brown dwarfs, around of or more massive than 50 M_{Jup}. Finding an old 20 M_{Jup} companion would be possible only if it is placed closer than 5 pc from us. And an old 10 M_{Jup} wide companion would be accesible for us only at a distance of around 1 pc. A deeper search, capable of reaching objects with magnitude

of $J = 20$ would increase the number of accesible companions, but would still miss any 20 M_{Jup} object placed further than just 10 pc. Instruments like the James Webb Space Telescope, with its mid-infrared capabilities, or the Euclid Space Telescope could help finding and characterising these objects.

Table 3.6: Physical parameters for the companion candidate systems considering an age of 5 Myr.

RA	DEC	Jmag[a]	Sep ['/]	Sep [AU]	log(L/L$_\odot$)	Mass [M$_\odot$][b]	T$_{\rm eff}$ [K][b]	U$_{\rm b}$ [J]
15:49:25.08	−28:43:52.7	10.619 ± 0.03	3.2	416 ± 16	−0.884 ± 0.064	0.376 ± 0.036	3505 ± 60	−1.36E35 ± 2.3E34
15:49:24.85	−28:43:51.6	12.7152 ± 0.0011			−1.664 ± 0.017	0.085 ± 0.003	2976 ± 12	
15:54:30.11	−27:20:19.1	6.234 ± 0.019	22.3	3377 ± 76	2.3348 ± 0.100	3.967 ± 0.249*	14.544 ± 574*	−5.62E34 ± 6.0E33
15:54:30.47	−27:19:57.5	14.9801 ± 0.004			−2.321 ± 0.026	0.0271 ± 0.0006	2655 ± 11	
15:55:48.82	−25:12:24.1	8.756 ± 0.032	9.0	1294.9 ± 24	0.278 ± 0.033	1.579 ± 0.034*	4994.9 ± 49*	−5.46E35 ± 5.2E34
15:55:48.40	−25:12:17.4	10.956 ± 0.037		2101 ± 29	−1.130 ± 0.033	0.254 ± 0.014	3306 ± 22	−6.10E34 ± 7.5E33
15:55:47.88	−25:12:17.3	13.3792 ± 0.0014	14.6		−1.907 ± 0.054	0.046 ± 0.004	2817 ± 23	
15:56:24.92	−25:41:20.3	11.373 ± 0.023	24.8	3501 ± 55	−1.090 ± 0.026	0.271 ± 0.011	3333 ± 17	−1.90E33 ± 1.5E32
15:56:24.44	−25:41:05.6	16.166 ± 0.01			−3.059 ± 0.0245	0.0139 ± 0.0003	2245 ± 21	
15:58:36.21	−23:48:02.0	11.11 ± 0.023	12.2	1494 ± 28	−1.108 ± 0.026	0.263 ± 0.011	3321 ± 17	−1.61E34 ± 2.2E33
15:58:35.98	−23:48:13.6	12.9512 ± 0.0011			−1.842 ± 0.017	0.052 ± 0.004	2850 ± 21	
15:58:53.52	−25:12:33.4	10.548 ± 0.026	42.2	4560 ± 41	−0.952 ± 0.0348	0.338 ± 0.019	3442 ± 32	−5.10E33 ± 7.2E32
15:58:53.97	−25:11:51.8	13.0352 ± 0.0012			−1.9946 ± 0.0649	0.039 ± 0.003	2780 ± 24	
15:59:58.99	−24:38:15.3	12.6197 ± 0.0009	14.6	2089 ± 52	−1.5848 ± 0.017	0.112 ± 0.005	3051 ± 9	−9.46E33 ± 1.13E33
15:59:57.94	−24:38:13.3	12.6848 ± 0.0010			−1.628 ± 0.017	0.100 ± 0.005	3028 ± 9	
16:00:15.68	−22:31:58.0	11.365 ± 0.023	5.0	727 ± 26	−1.069 ± 0.026	0.279 ± 0.011	3346 ± 17	−1.98E34 ± 1.8E33
16:00:15.33	−22:31:57.5	14.1255 ± 0.0028			−2.233 ± 0.018	0.0292 ± 0.0004	2691 ± 7	
16:00:17.66	−22:56:53.6	13.4473 ± 0.0018	35.0	4837 ± 177	−2.018 ± 0.014	0.0383 ± 0.0006	2771 ± 5	−3.63E32 ± 2.6E31
16:00:19.44	−22:56:29.0	14.4779 ± 0.0036			−2.367 ± 0.020	0.0260 ± 0.0005	2636 ± 8	
16:00:49.89	−19:28:00.4	10.673 ± 0.024	15.1	2039 ± 49	−0.832 ± 0.034	0.405 ± 0.0245	3554 ± 37	−2.74E34 ± 2.7E33
16:00:50.65	−19:27:50.4	12.6138 ± 0.0008			−1.7046 ± 0.009	0.0782 ± 0.0011	2953 ± 3	
16:00:52.84	−24:40:38.0	11.322 ± 0.036	3.0	440 ± 20	−1.039 ± 0.027	0.292 ± 0.011	3366 ± 18	−1.57E35 ± 1.9E34
16:00:52.79	−24:40:35.5	12.5168 ± 0.0008			−1.5048 ± 0.017	0.134 ± 0.005	3092 ± 9	
16:02:10.45	−22:41:28.0	8.866 ± 0.023	32.4	3659 ± 95	−0.177 ± 0.0347	1.029 ± 0.043	4342 ± 49	−1.72E34 ± 2.4E33
16:02:09.63	−22:40:58.0	13.3408 ± 0.0017			−2.0947 ± 0.054	0.0347 ± 0.00246	2743 ± 20	
16:02:34.18	−22:00:35.6	12.7047 ± 0.0012	29.7	4785 ± 151	−1.609 ± 0.054	0.106 ± 0.014	3038 ± 28	−2.38E33 ± 8.2E32
16:02:32.27	−22:00:48.7	13.2599 ± 0.0016			−1.806 ± 0.054	0.061 ± 0.011	2893 ± 41	
16:03:01.78	−26:26:21.9	10.624 ± 0.024	9.7	1406 ± 30	−0.707 ± 0.030	0.4949 ± 0.021	3688 ± 32	−4.59E34 ± 7.9E33
16:03:02.35	−26:26:16.5	13.139 ± 0.0012			−1.739 ± 0.054	0.074 ± 0.008	2939 ± 27	
16:04:17.40	−19:42:28.7	11.443 ± 0.044	5.5	887 ± 30	−1.006 ± 0.030	0.308 ± 0.017	3392 ± 28	−1.15E35± 2.3E34
16:04:17.62	−19:42:33.2	12.206 ± 0.026	38.8	6256 ± 112	−1.306 ± 0.075	0.188 ± 0.020	3196 ± 39	−5.47E33 ± 1.36E33
16:04:17.92	−19:41:50.8	13.4192 ± 0.0014			−1.7946 ± 0.053	0.063 ± 0.011	2902 ± 41	
16:05:53.94	−18:18:42.7	13.3998 ± 0.0015	4.6	664 ± 37	−1.961 ± 0.014	0.0414 ± 0.0011	2793 ± 6	−1.41E33 ± 1.5E32
16:05:54.09	−18:18:49.1	16.4548 ± 0.0147			−3.147 ± 0.027	0.0128 ± 0.0003	2169 ± 23	
16:06:11.99	−19:35:33.1	12.013 ± 0.026	10.8	1481 ± 41	−1.3948 ± 0.063	0.164 ± 0.017	3150 ± 33	−1.29E34 ± 3.8E33
16:06:11.44	−19:35:40.7	13.009 ± 0.0011			−1.779 ± 0.053	0.066 ± 0.011	2914 ± 41	
16:06:47.94	−18:41:43.8	9.886 ± 0.022	4.2	652 ± 21	−0.353 ± 0.029	0.819 ± 0.032	4103 ± 38	−8.42E34 ± 1.04E34
16:06:47.98	−18:41:48.1	13.9277 ± 0.0026			−2.0248 ± 0.0547	0.038 ± 0.002	2769 ± 20	
16:07:57.97	−20:40:08.7	11.061 ± 0.023	14.5	2300 ± 107	−0.629 ± 0.034	0.554 ± 0.026	3769 ± 35	−5.01E34 ± 1.23E34
16:07:57.13	−20:40:17.6	12.6308 ± 0.0012	21.5	3490 ± 176	−1.564 ± 0.066	0.114 ± 0.018	3062 ± 34	−2.29E34 ± 2.4E33
16:07:58.50	−20:39:48.8	13.5173 ± 0.002	41.1	6688 ± 231	−1.902 ± 0.054	0.046 ± 0.004	2819 ± 23	−2.48E34 ± 4.5E33
16:08:09.51	−20:40:28.9	12.325 ± 0.023			−1.371 ± 0.062	0.170 ± 0.017	3169 ± 22	
16:08:43.41	−26:02:16.8	8.85 ± 0.02	13.4	2088 ± 53	0.353 ± 0.021	1.654 ± 0.020*	5102 ± 29*	−4.16E34 ± 2.3E33
16:08:44.38	−26:02:14.0	13.9967 ± 0.0024			−2.210 ± 0.019	0.0298 ± 0.0005	2701 ± 8	
16:09:20.89	−19:27:25.9	7.587 ± 0.023			1.297 ± 0.134	2.174 ± 0.056*	6598 ± 604*	

16:09:20.54	−19:26:32.1	12.9797 ± 0.0012	49.4	7440 ± 104	−1.800 ± 0.066	0.062 ± 0.013	2898 ± 50	−3.20E34 ± 8.0E33
16:10:21.74	−19:04:06.7	10.679 ± 0.03			−0.857 ± 0.028	0.390 ± 0.016	3530 ± 26	
16:10:21.78	−19:04:02.4	12.9254 ± 0.0012	4.6	616 ± 18	−1.758 ± 0.053	0.070 ± 0.011	2929 ± 32	−7.82E34± 1.78E34
16:10:31.95	−19:13:06.1	10.026 ± 0.026			−0.516 ± 0.019	0.654 ± 0.019	3900 ± 24.5	
16:10:32.33	−19:13:08.7	13.8834 ± 0.002	5.8	774 ± 21	−2.131 ± 0.023	0.0332 ± 0.0010	2730 ± 8	−4.95E34 ± 4.3E33
16:11:23.05	−19:05:23.2	10.508 ± 0.027			−0.752 ± 0.027	0.463 ± 0.020	3640 ± 29	
16:11:19.35	−19:05:08.2	13.6461 ± 0.0017	54.5	7627 ± 107	−2.106 ± 0.011	0.0343 ± 0.0005	2739 ± 4	−3.67E33 ± 2.6E32
16:11:59.27	−19:06:53.4	8.981 ± 0.023			0.019 ± 0.033	1.261 ± 0.042	4600 ± 47	
16:11:59.23	−19:06:56.2	9.148 ± 0.077	3.3	456 ± 15	−0.178 ± 0.0549	1.027 ± 0.069	4340 ± 77	−5.01E36 ± 6.7E35
16:11:56.90	−19:06:47.0	17.1249 ± 0.0261	34.0	4666 ± 40	−3.459 ± 0.031	0.0090 ± 0.0003**	1886 ± 24.8**	−4.29E33 ± 3.2E32
16:12:48.93	−18:00:52.5	11.351 ± 0.026			−0.981 ± 0.027	0.322 ± 0.0149	3414.9 ± 24.9	
16:12:48.97	−18:00:49.6	14.1463 ± 0.0024	3.2	507 ± 22	−2.1248 ± 0.023	0.0334 ± 0.0010	2732 ± 8	−3.74E34 ± 4.5E33
16:13:02.34	−25:01:46.0	10.423 ± 0.024			−0.608 ± 0.035	0.502 ± 0.027	3698 ± 36	
16:13:01.89	−25:01:41.3	12.6019 ± 0.001	7.8	1241 ± 32	−1.477 ± 0.017	0.141 ± 0.0046	3107 ± 9	−1.01E35 ± 1.1E34
16:13:40.46	−22:33:15.6	13.0595 ± 0.0012			−1.744 ± 0.054	0.073 ± 0.008	2937 ± 27	
16:13:40.26	−22:33:19.4	13.5666 ± 0.0015	4.4	694 ± 40	−1.956 ± 0.014	0.0418 ± 0.0011	2795 ± 6	−7.76E33 ± 1.5E33
16:14:52.69	−23:08:02.6	10.569 ± 0.026			−0.778 ± 0.023	0.444 ± 0.017	3612 ± 25	
16:14:51.31	−23:08:51.7	12.584 ± 0.0009	52.5	8901 ± 214	−1.439 ± 0.053	0.152 ± 0.014	3127 ± 28	−1.34E34 ± 2.1E33
16:15:12.39	−24:20:09.3	13.0315 ± 0.0012			−1.688 ± 0.017	0.080 ± 0.003	2960 ± 11	
16:15:11.16	−24:20:15.3	14.1589 ± 0.0023	17.9	2749 ± 68	−2.262 ± 0.054	0.0285 ± 0.0013	2679 ± 22	−1.46E33 ± 1.6E32
16:15:20.25	−23:33:58.9	11.995 ± 0.032			−1.282 ± 0.029	0.194 ± 0.008	3208 ± 15	
16:15:20.09	−23:33:54.6	12.9239 ± 0.0011	4.8	729 ± 24	−1.716 ± 0.053	0.077 ± 0.007	2949 ± 20	−3.61E34 ± 6.0E33
16:17:30.32	−24:38:39.0	10.832 ± 0.035			−0.724 ± 0.034	0.483 ± 0.024	3671 ± 37	
16:17:30.57	−24:38:37.3	12.5763 ± 0.001	3.9	611 ± 19	−1.460 ± 0.017	0.146 ± 0.0047	3115 ± 9	−2.04E35 ± 2.3E34
16:18:15.68	−23:47:08.4	12.425 ± 0.026			−1.547 ± 0.075	0.122 ± 0.020	3070 ± 39	
16:18:11.69	−23:47:26.5	12.967 ± 0.0012	57.6	8472 ± 247	−1.674 ± 0.053	0.083 ± 0.011	2969 ± 35	−2.11E33± 6.9E32
16:18:43.23	−22:09:34.5	12.9968 ± 0.0011			−1.659 ± 0.065	0.086 ± 0.013	2980 ± 43	
16:18:40.74	−22:09:48.2	13.6873 ± 0.0017	37.3	6277 ± 158	−2.097 ± 0.054	0.0347 ± 0.00246	2742 ± 20	−8.39E32 ± 2.07E32
16:19:51.41	−22:41:26.8	13.1608 ± 0.0014			−1.875 ± 0.066	0.048 ± 0.005	2830 ± 28	
16:19:51.44	−22:41:33.3	14.4781 ± 0.0032	6.6	934 ± 35	−2.299 ± 0.016	0.0278 ± 0.0004	2664 ± 6	−2.52E33 ± 3.9E32
16:20:50.23	−22:35:38.8	8.032 ± 0.023			0.791 ± 0.042	1.952 ± 0.018*	5642 ± 56*	
16:20:49.26	−22:35:13.3	14.117 ± 0.0024	28.9	4159 ± 47	−2.298 ± 0.066	0.0277 ± 0.0016	2664 ± 27	−2.29E34 ± 1.8E33
16:21:29.53	−25:29:43.1	11.175 ± 0.024			−1.027 ± 0.026	0.297 ± 0.011	3374 ± 17	
16:21:28.32	−25:29:56.0	15.9422 ± 0.01	20.8	2880 ± 34	−2.986 ± 0.024	0.0147 ± 0.0003	2307 ± 21	−2.67E33 ± 1.9E32
16:23:59.02	−27:36:03.8	10.327 ± 0.024			−0.043 ± 0.024	1.186 ± 0.026	4516 ± 29	
16:23:58.53	−27:35:52.9	13.5897 ± 0.0014	12.6	3684.5 ± 829	−1.412 ± 0.019	0.159 ± 0.005	3141 ± 10	−9.03E34 ± 2.51E34
16:23:57.24	−26:20:24.5	11.188 ± 0.021			−0.893 ± 0.076	0.370 ± 0.042	3497 ± 70	
16:24:01.19	−26:20:36.0	13.911 ± 0.0018	54.4	8924 ± 922	−2.0545 ± 0.016	0.0366 ± 0.0007	2758 ± 6	−2.68E33 ± 6.3E32
16:24:15.52	−25:44:34.5	10.711 ± 0.022			−0.972 ± 0.031	0.326 ± 0.017	3423 ± 28	
16:24:16.15	−25:44:27.3	14.9278 ± 0.0051	11.4	1580 ± 129	−2.603 ± 0.057	0.0204 ± 0.0014	2538 ± 24	−7.42E33 ± 1.50E33
16:33:34.97	−18:32:54.0	11.314 ± 0.03			−1.214 ± 0.0246	0.219 ± 0.010	3251 ± 16	
16:33:34.73	−18:32:54.8	13.3447 ± 0.0013	3.3	394.8 ± 16	−2.087 ± 0.053	0.0351 ± 0.0024	2746 ± 19	−3.43E34 ± 5.3E33

Table 3.6: (a) Magnitude from VHS for objects with $J > 12.5$, and from 2MASS for objects with $J < 12.5$.
(b) Obtained through the BT–Settl models (Allard et al. 2012; Baraffe et al. 2015).
(*) Obtained through the Pisa pre-main sequence models (Tognelli et al. 2011).
(**) Obtained through the Ames–COND models (Allard et al. 2001; Baraffe et al. 2003).

Table 3.7: Physical parameters for the companion candidate systems considering an age of 10 Myr.

RA	DEC	Jmag[a]	Sep ($''$)	Sep (AU)	log($L/L_\odot$)	Mass ($M_\odot$)[b]	T_{eff} (K)[b]	U_b (J)
15:49:25.08	−28:43:52.7	10.619 ± 0.03			−0.884 ± 0.064	0.522 ± 0.054	3680 ± 70	
15:49:24.85	−28:43:51.6	12.7152 ± 0.0011	3.2	416 ± 16	−1.664 ± 0.017	0.151 ± 0.004	3148 ± 8	−3.34E35 ± 5.6E34
15:54:30.11	−27:20:19.1	6.234 ± 0.019			2.3348 ± 0.100	3.952 ± 0.249*	14 410 ± 552*	
15:54:30.47	−27:19:57.5	14.9801 ± 0.004	22.3	3377 ± 76	−2.321 ± 0.026	0.042 ± 0.002	2786 ± 16	−8.67E34 ± 1.15E34
15:55:48.82	−25:12:24.1	8.756 ± 0.032			0.278 ± 0.033	1.394 ± 0.017	5343 ± 54	
15:55:48.40	−25:12:17.4	10.956 ± 0.037	9.0	1294.9 ± 24	−1.130 ± 0.033	0.355 ± 0.018	3443 ± 26	−6.74E35 ± 5.5E34
15:55:47.88	−25:12:17.3	13.3792 ± 0.0014	14.6	2101 ± 29	−1.907 ± 0.054	0.091 ± 0.013	3023 ± 39	−1.07E35 ± 1.8E34
15:56:24.92	−25:41:20.3	11.373 ± 0.023			−1.090 ± 0.026	0.378 ± 0.014	3476 ± 21	
15:56:23.44	−25:41:05.6	16.166 ± 0.01	24.8	3501 ± 54.9	−3.059 ± 0.0245	0.0153 ± 0.0003	2274 ± 15	−2.91E33 ± 2.1E32
15:58:36.21	−23:48:02.0	11.11 ± 0.023			−1.108 ± 0.026	0.368 ± 0.014	3461 ± 21	
15:58:35.98	−23:48:13.6	12.9512 ± 0.0011	12.2	1494 ± 28	−1.842 ± 0.017	0.107 ± 0.004	3063 ± 8	−4.65E34 ± 4.4E33
15:58:53.52	−25:12:33.4	10.548 ± 0.026			−0.952 ± 0.0349	0.470 ± 0.0249	3608 ± 36	
15:58:53.97	−25:11:51.8	13.0352 ± 0.0012	42.2	4560 ± 41	−1.9948 ± 0.0649	0.078 ± 0.008	2980 ± 32	−1.42E34 ± 2.3E33
15:59:58.99	−24:38:15.3	12.6197 ± 0.0009			−1.5848 ± 0.017	0.171 ± 0.004	3185 ± 8	
15:59:57.94	−24:38:13.3	12.6848 ± 0.001	14.6	2089 ± 52	−1.628 ± 0.017	0.160 ± 0.004	3164.8 ± 8	−2.31E34 ± 1.7E33
16:00:15.68	−22:31:58.0	11.365 ± 0.023			−1.069 ± 0.026	0.389 ± 0.014	3492 ± 21	
16:00:15.33	−22:31:57.5	14.1255 ± 0.0028	5.0	727 ± 26	−2.233 ± 0.018	0.0497 ± 0.00148	2841 ± 11	−4.69E34± 4.8E33
16:00:17.66	−22:56:53.6	13.4473 ± 0.0018			−2.018 ± 0.014	0.0753 ± 0.0018	2968 ± 7	
16:00:19.44	−22:56:29.0	14.4779 ± 0.0036	35.0	4837 ± 177	−2.367 ± 0.020	0.038 ± 0.002	2749.9 ± 21	−1.04E33 ± 1.2E32
16:00:49.89	−19:28:00.4	10.673 ± 0.024			−0.832 ± 0.034	0.5647 ± 0.029	3735 ± 37	
16:00:50.65	−19:27:50.4	12.6138 ± 0.0008	15.1	2039 ± 49	−1.7047 ± 0.009	0.141 ± 0.002	3129± 4	−6.89E34 ± 6.2E33
16:00:52.84	−24:40:38.0	11.322 ± 0.036			−1.039 ± 0.027	0.408 ± 0.019	3519 ± 27	
16:00:52.79	−24:40:35.5	12.5168 ± 0.0008	3.0	440 ± 20	−1.5048 ± 0.017	0.191 ± 0.004	3223 ± 8	−3.12E35 ± 3.5E34
16:02:10.45	−22:41:28.0	8.866 ± 0.023			−0.177 ± 0.0348	1.124 ± 0.0248	4604 ± 53	
16:02:09.63	−22:40:58.0	13.3408 ± 0.0017	32.4	3659 ± 94.9	−2.0948 ± 0.054	0.066 ± 0.006	2928 ± 28	−3.58E34 ± 5.0E33
16:02:34.18	−22:00:35.6	12.7047 ± 0.0012			−1.609 ± 0.054	0.165 ± 0.013	3174 ± 25	
16:02:32.27	−22:00:48.7	13.2599 ± 0.0016	29.7	4785 ± 151	−1.806 ± 0.054	0.116 ± 0.013	3081 ± 25	−7.06E33 ± 1.6E33
16:03:01.78	−26:26:21.9	10.624 ± 0.024			−0.707 ± 0.030	0.669 ± 0.025	3869 ± 32	
16:03:02.35	−26:26:16.5	13.139 ± 0.0012	9.7	1406 ± 30	−1.739 ± 0.054	0.133 ± 0.013	3112 ± 25	−1.12E35 ± 1.7E34
16:04:17.40	−19:42:28.7	11.443 ± 0.044			−1.006 ± 0.030	0.431 ± 0.022	3553 ± 31	
16:04:17.62	−19:42:33.2	12.206 ± 0.026	5.5	887 ± 30	−1.306 ± 0.075	0.268 ± 0.031	3324 ± 38	−2.28E35 ± 4.6E34
16:04:17.92	−19:41:50.8	13.4192 ± 0.0014	38.8	6256 ± 112	−1.7947 ± 0.053	0.119 ± 0.013	3086 ± 25	−1.45E34 ± 2.6E33
16:05:53.94	−18:18:42.7	13.3998 ± 0.0015			−1.961 ± 0.014	0.083 ± 0.002	2996 ± 7	
16:05:54.09	−18:18:49.1	16.4548 ± 0.0147	4.6	664 ± 37	−3.147 ± 0.027	0.01457 ± 0.00017	2202 ± 24	−3.21E33 ± 2.9E32
16:06:11.99	−19:35:33.1	12.013 ± 0.026			−1.3948 ± 0.063	0.231 ± 0.026	3279 ± 32	
16:06:11.44	−19:35:40.7	13.009 ± 0.0011	10.8	1481 ± 41	−1.779 ± 0.053	0.123 ± 0.013	3093 ± 25	−3.38E34 ± 8.3E33
16:06:47.94	−18:41:43.8	9.886 ± 0.022			−0.353 ± 0.029	0.989 ± 0.024	4344 ± 42	
16:06:47.98	−18:41:48.1	13.9277 ± 0.0026	4.2	652 ± 21	−2.0248 ± 0.0548	0.074 ± 0.008	2964 ± 36	−1.98E35 ± 3.3E34
16:07:57.97	−20:40:08.7	11.061 ± 0.023			−0.629 ± 0.034	0.741 ± 0.034	3962 ± 45	
16:07:57.13	−20:40:17.6	12.6308 ± 0.0012	14.5	2300 ± 107	−1.564 ± 0.066	0.177 ± 0.016	3195 ± 31	−1.01E35 ± 1.8E34
16:07:58.50	−20:39:48.8	13.5173 ± 0.002	21.5	3490 ± 176	−1.902 ± 0.054	0.092 ± 0.014	3027 ± 39	−3.45E34 ± 8.6E33
16:08:00.51	−20:40:28.9	12.325 ± 0.023	41.1	6688 ± 231	−1.371 ± 0.062	0.241 ± 0.026	3291 ± 32	−4.71E34 ± 8.9E33
16:08:43.41	−26:02:16.8	8.55 ± 0.02			0.353 ± 0.021	1.453 ± 0.009*	5468 ± 30*	
16:08:44.38	−26:02:14.0	13.9967 ± 0.0024	13.4	2088 ± 53	−2.210 ± 0.019	0.053 ± 0.002	2857 ± 14	−6.51E34 ± 4.5E33
16:09:20.89	−19:27:25.9	7.587 ± 0.023			1.297 ± 0.134	2.132 ± 0.174*	9397 ± 650*	

16:09:20.54	−19:26:32.1	12.9797 ± 0.0012	49.4	7440 ± 104	−1.800 ± 0.066	0.118 ± 0.016	3083 ± 31	−5.96E34 ± 1.38E34
16:10:21.74	−19:04:06.7	10.679 ± 0.03			−0.857 ± 0.028	0.544 ± 0.024	3708 ± 31	
16:10:21.78	−19:04:02.4	12.9254 ± 0.0012	4.6	616 ± 18	−1.758 ± 0.053	0.128 ± 0.013	3103 ± 25	−1.99E35 ± 3.5E34
16:10:31.95	−19:13:06.1	10.026 ± 0.026			−0.516 ± 0.019	0.849 ± 0.017	4114.6 ± 26	
16:10:32.33	−19:13:08.7	13.8834 ± 0.002	5.8	774 ± 21	−2.131 ± 0.023	0.062 ± 0.003	2910 ± 12	−1.20E35 ± 1.1E34
16:11:23.05	−19:05:23.2	10.508 ± 0.027			−0.752 ± 0.027	0.632 ± 0.023	3821 ± 29	
16:11:19.35	−19:05:08.2	13.6461 ± 0.0017	54.5	7627 ± 107	−2.106 ± 0.011	0.0648 ± 0.0012	2922 ± 5	−9.47E33 ± 6.5E32
16:11:59.27	−19:06:53.4	8.981 ± 0.023			0.019 ± 0.033	1.255 ± 0.021	4917 ± 56	
16:11:59.23	−19:06:56.2	9.148 ± 0.077	3.3	456 ± 14.9	−0.178 ± 0.0549	1.123 ± 0.039	4602 ± 84	−5.45E36 ± 4.6E35
16:11:56.90	−19:06:47.0	17.1249 ± 0.0261	34.0	4666 ± 40	−3.459 ± 0.031	0.01260 ± 0.00019	1929 ± 27	−5.98E33 ± 2.4E32
16:12:48.93	−18:00:52.5	11.351 ± 0.026			−0.981 ± 0.027	0.449 ± 0.019	3578 ± 27	
16:12:48.97	−18:00:49.6	14.1463 ± 0.0024	3.2	507± 22	−2.1248 ± 0.023	0.063 ± 0.003	2913 ± 12	−9.84E34 ± 1.31E34
16:13:02.34	−25:01:46.0	10.423 ± 0.024			−0.698 ± 0.035	0.677 ± 0.029	3878 ± 37	
16:13:01.89	−25:01:41.3	12.6019 ± 0.001	7.8	1241 ± 32	−1.477 ± 0.017	0.198 ± 0.004	3236 ± 8	−1.91E35 ± 1.7E34
16:13:40.46	−22:33:15.6	13.0595 ± 0.0012			−1.744 ± 0.054	0.131 ± 0.013	3110 ± 26	
16:13:40.26	−22:33:19.4	13.5666 ± 0.0015	4.4	694 ± 40	−1.966 ± 0.014	0.083 ± 0.002	2998 ± 7	−2.76E34± 5.0E33
16:14:52.69	−23:08:02.6	10.569 ± 0.026			−0.778 ± 0.023	0.610 ± 0.019	3794 ± 24.7	
16:14:51.31	−23:08:51.7	12.584 ± 0.0009	52.5	8901 ± 214	−1.439 ± 0.053	0.213 ± 0.022	3256 ± 27	−2.57E34 ± 4.1E33
16:15:12.39	−24:20:09.3	13.0315 ± 0.0012			−1.688 ± 0.017	0.146 ± 0.004	3136 ± 8	
16:15:11.16	−24:20:15.3	14.1589 ± 0.0023	17.9	2749 ± 68	−2.262 ± 0.054	0.047 ± 0.0045	2823 ± 34	−4.40E33 ± 6.5E32
16:15:20.25	−23:33:58.9	11.995 ± 0.032			−1.282 ± 0.029	0.278 ± 0.012	3336 ± 14.9	
16:15:20.09	−23:33:54.6	12.9239 ± 0.0011	4.8	729 ± 24	−1.716 ± 0.053	0.139 ± 0.013	3123 ± 25	−9.35E34 ± 1.6E34
16:17:30.32	−24:38:39.0	10.832 ± 0.035			−0.724 ± 0.034	0.635 ± 0.029	3851 ± 36	
16:17:30.57	−24:38:37.3	12.5763 ± 0.001	3.9	611 ± 19	−1.460 ± 0.017	0.204 ± 0.007	3244.9 ± 9	−3.86E35 ± 4.2E34
16:18:15.68	−23:47:08.4	12.425 ± 0.026			−1.547 ± 0.075	0.181 ± 0.019	3203 ± 36	
16:18:11.69	−23:47:26.5	12.967 ± 0.0012	57.6	8472 ± 247	−1.674 ± 0.053	0.149 ± 0.013	3143 ± 25	−5.62E33 ± 1.24E33
16:18:43.23	−22:09:34.5	12.9968 ± 0.0011			−1.659 ± 0.065	0.153 ± 0.016	3150 ± 31	
16:18:40.74	−22:09:48.2	13.6873 ± 0.0017	37.3	6277 ± 158	−2.097 ± 0.054	0.066 ± 0.006	2927 ± 28	−2.84E33 ± 6.3E32
16:19:51.41	−22:41:26.8	13.1608 ± 0.0014			−1.875 ± 0.066	0.099 ± 0.016	3046 ± 48	
16:19:51.44	−22:41:33.3	14.4781 ± 0.0032	6.6	934 ± 34.9	−2.299 ± 0.016	0.0443 ± 0.0013	2800 ± 10	−8.28E33 ± 1.89E33
16:20:50.23	−22:35:38.8	8.032 ± 0.023			0.791 ± 0.042	1.606 ± 0.014*	6129 ± 83*	
16:20:49.26	−22:35:13.3	14.117 ± 0.0024	28.9	4159 ± 47	−2.298 ± 0.066	0.044 ± 0.006	2800 ± 41	−3.00E34 ± 4.7E33
16:21:29.53	−25:29:43.1	11.175 ± 0.024			−1.027 ± 0.026	0.416 ± 0.019	3531 ± 26	
16:21:28.32	−25:29:56.0	15.9422 ± 0.01	20.8	2880 ± 34	−2.986 ± 0.024	0.0161 ± 0.0003	2320 ± 15	−4.10E33 ± 3.1E32
16:23:59.02	−27:36:03.8	10.327 ± 0.024			−0.043 ± 0.024	1.217 ± 0.0149	4814 ± 40	
16:23:58.53	−27:35:52.9	13.5897 ± 0.0014	12.6	3684.5 ± 829	−1.412 ± 0.019	0.224 ± 0.008	3270 ± 10	−1.31E35 ± 3.6E34
16:23:57.24	−26:20:24.5	11.188 ± 0.021			−0.893 ± 0.076	0.514 ± 0.063	3669 ± 82	
16:24:01.19	−26:20:36.0	13.911 ± 0.0018	54.4	8924 ± 922	−2.0545 ± 0.016	0.0705 ± 0.0016	2948 ± 6	−7.16E33 ± 1.78E33
16:24:15.52	−25:44:34.5	10.711 ± 0.022			−0.972 ± 0.031	0.455 ± 0.022	3587 ± 31	
16:24:16.15	−25:44:27.3	14.9278 ± 0.0051	11.4	1580 ± 129	−2.603 ± 0.057	0.023 ± 0.002	2564 ± 39	−1.17E34 ± 2.5E33
16:33:34.97	−18:32:54.0	11.314 ± 0.03			−1.214 ± 0.0246	0.309 ± 0.014	3376 ± 20	
16:33:34.73	−18:32:54.8	13.3447 ± 0.0013	3.3	394.8 ± 16	−2.087 ± 0.053	0.067 ± 0.006	2932 ± 27	−9.25E34 ± 1.62E34

Table 3.7: (a) Magnitude from VHS for objects with $J > 12.5$, and from 2MASS for objects with $J < 12.5$.
(b) Obtained through the BT-Settl models (Allard et al. 2012; Baraffe et al. 2015).
(*) Obtained through the Pisa pre-main sequence models (Tognelli et al. 2011).

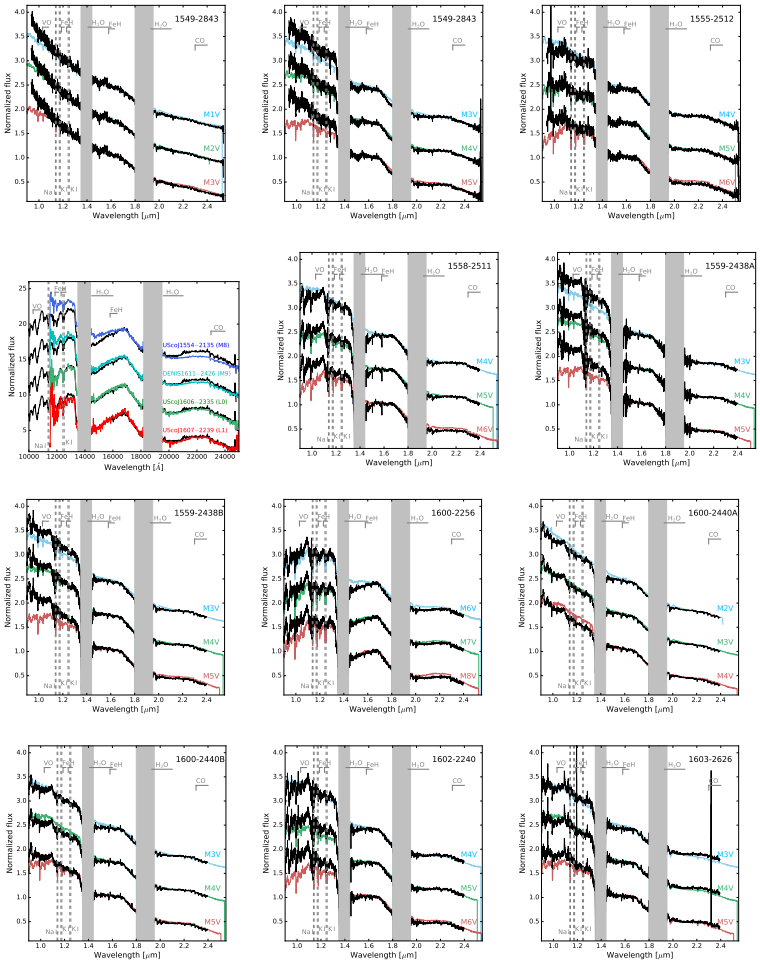

Figure 3.18: Near infrared spectra of the observed candidate companions. The candidate spectra are shown in black. Template spectra are shown in colours, for comparison. The spectra were normalised at 1.68 μm and shifted by a constant for clarity. Regions strongly affected by atmospheric telluric absorption are covered with grey bands. Some remarkable spectral features are marked in grey.

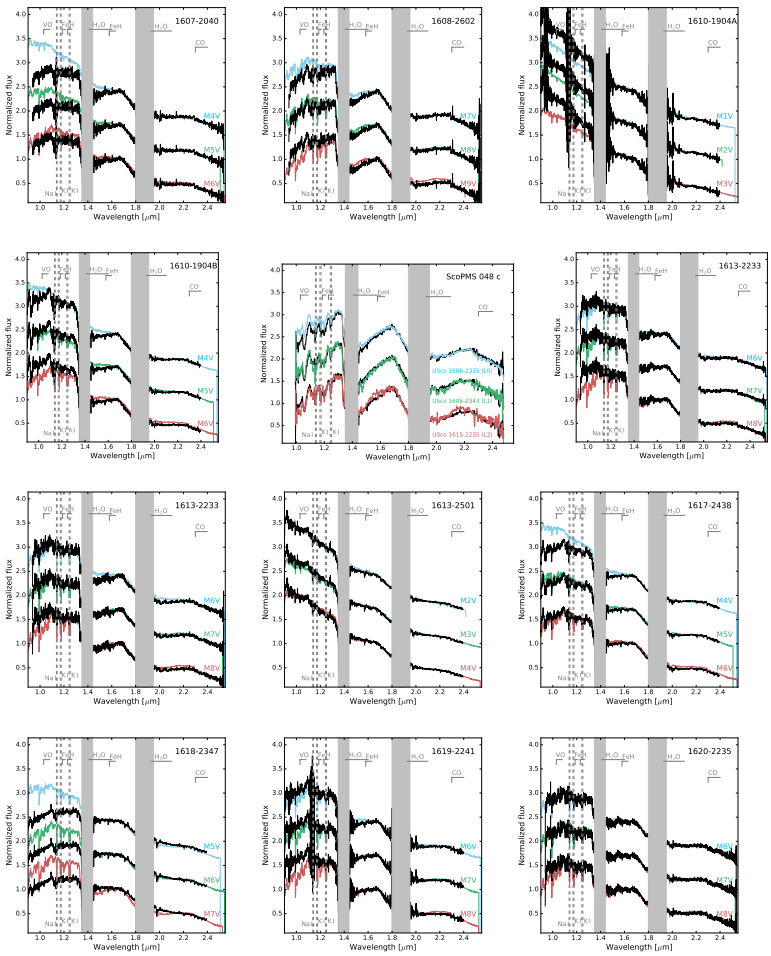

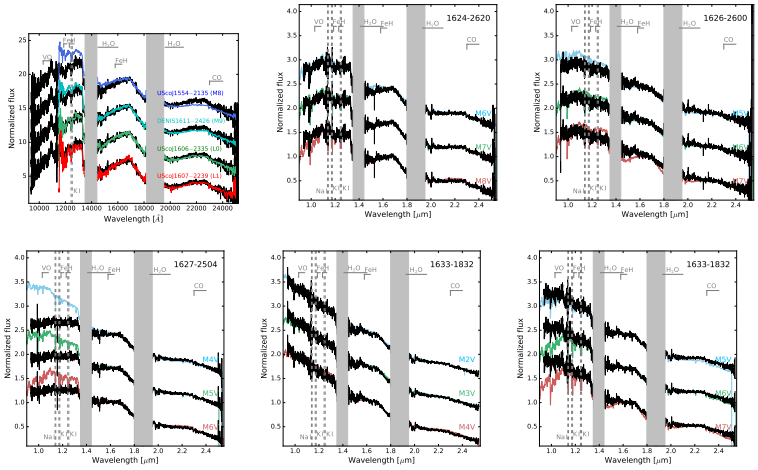

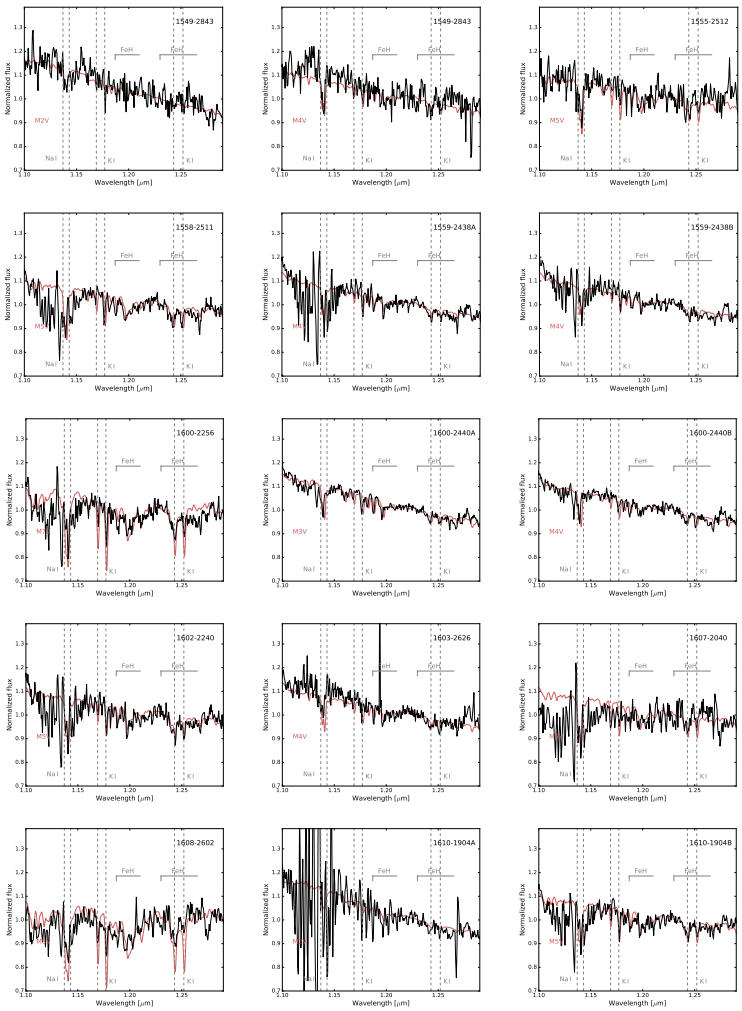

Figure 3.19: *J*-band close-up display of the near-infrared spectra. Candidate spectra is shown in black, template spectra for comparison is shown in red. Some remarkable spectral features are marked in grey.

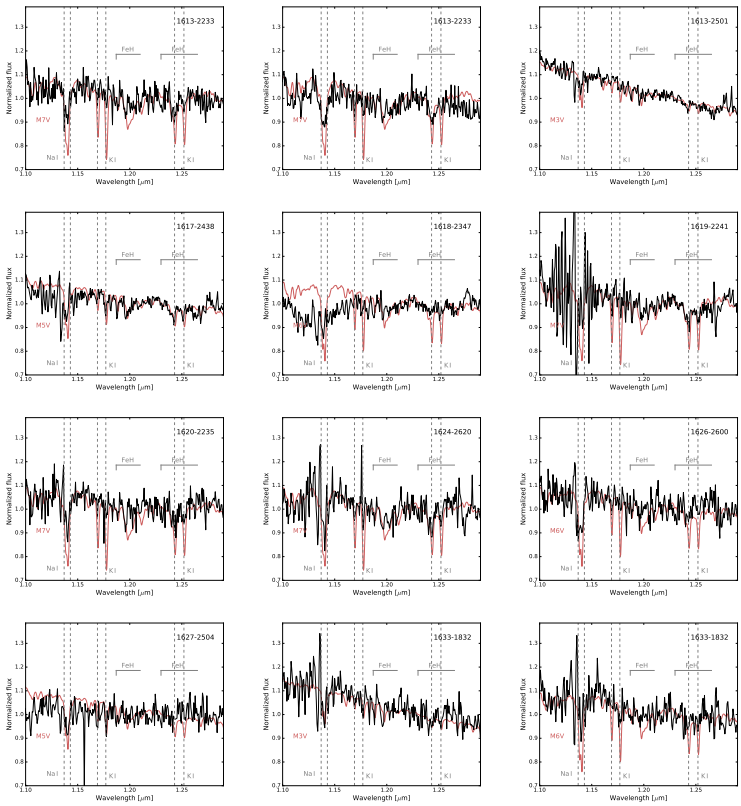

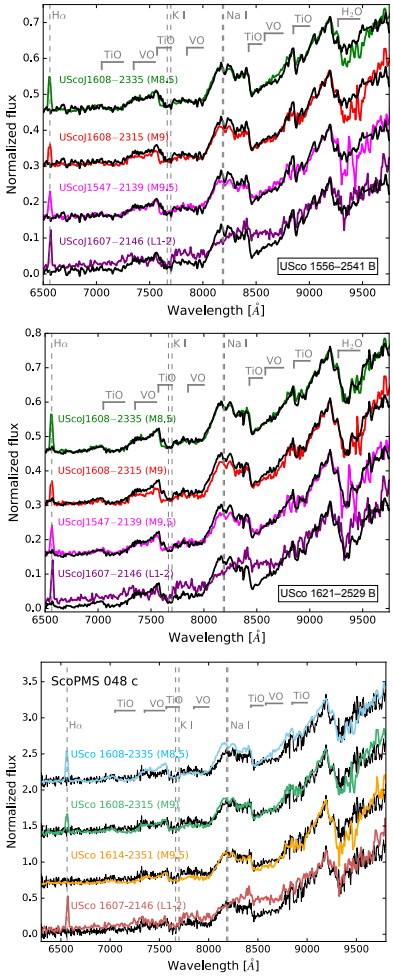

Figure 3.20: Optical spectra of the faintest candidate companions (USco 1556−2541 B, USco 1621−2529 B and USco1611−1906 c; black) compared with optical spectra of other USco members (coloured) from Lodieu et al. (2018). The spectra were normalised at ∼9200 Å, and shifted by a constant for clarity. Some remarkable spectral features are marked in grey.

4

USco1621 B and USco1556 B: Two wide companions at the deuterium-burning mass limit in Upper Scorpius.

In this chapter we present the discovery of two of the least massive companions found in the USco search: USco1621 B and USco1556 B. These results were published with the title "USco1621 B and USco1556 B: Two wide companions at the deuterium-burning mass limit in Upper Scorpius." in the peer-reviewed journal "Astronomy & Astrophysics", Volume 633, id.A152 (Chinchilla et al. 2020b). The article is included here in the original format of the journal.

Astronomy & Astrophysics manuscript no. Chinchilla2019˙forPublisher
December 9, 2019

USco1621 B and USco1556 B: Two wide companions at the deuterium-burning mass limit in Upper Scorpius

Patricia Chinchilla[1,2], Víctor J. S. Béjar[1,2], Nicolas Lodieu[1,2], Bartosz Gauza[3,4], Maria Rosa Zapatero Osorio[5], Rafael Rebolo[1,2,6], Antonio Pérez Garrido[7], Carlos Alvarez[8], and Elena Manjavacas[8]

[1] Instituto de Astrofísica de Canarias (IAC), Calle Vía Láctea s/n, 38200 La Laguna, Tenerife, Spain.
e-mail: pcg@iac.es
[2] Departamento de Astrofísica, Universidad de La Laguna (ULL), 38205 La Laguna, Tenerife, Spain.
[3] Departamento de Astronomía, Universidad de Chile, Camino El Observatorio 1515, Las Condes, Santiago, Chile.
[4] Janusz Gil Institute of Astronomy, University of Zielona Góra, Lubuska 2, 65-265 Zielona Góra, Poland.
[5] Centro de Astrobiología (CSIC-INTA), Ctra. de Ajalvir km 4, 28850 Torrejón de Ardoz, Madrid, Spain.
[6] Consejo Superior de Investigaciones Científicas (CSIC), Spain.
[7] Departamento de Física Aplicada, Universidad Politécnica de Cartagena, Campus Muralla del Mar, 30202 Cartagena, Murcia, Spain.
[8] W. M. Keck Observatory, 65-1120 Mamalahoa Highway, Kamuela, HI 96743, USA.

Received 18 June 2019 / Accepted 29 November 2019

ABSTRACT

Aims. Our objective is to identify analogues of gas giant planets, but located as companions at wide separations of very young stars. The main purpose is to characterise the binarity frequency and the properties of these substellar objects, and to elucidate their early evolutionary stages.
Methods. To identify these objects, we cross correlated the Visible and Infrared Survey Telescope for Astronomy (VISTA) Hemisphere Survey (VHS) and the United Kingdom Infrared Telescope Infrared Deep Sky Survey Galactic Clusters Survey (UKIDSS GCS) catalogues to search for common proper motion companions to 1195 already known members of Upper Scorpius (USco; age ∼5–10 Myr, distance ∼145 pc). We present the discovery and spectroscopic characterisation of two very wide substellar companions of two early-M stars in Upper Scorpius: USco1621 B and USco1556 B. We obtained optical and near-infrared low-resolution spectroscopy of the candidates to characterise their spectral energy distribution and confirm their youth and membership to the association. We also acquired adaptive optics images of the primaries and secondaries to search for signs of binarity and close companions.
Results. By comparison with field dwarfs and other young members of USco, we determined a spectral type of M8.5 in the optical for both companions, along with L0 and L0.5 in the near-infrared for USco1621 B and USco1556 B, respectively. The spectra of the two companions show evident markers of youth, such as weak alkaline Na I and K I lines, along with the triangular shape of the *H*-band. The comparison with theoretical evolutionary models gives estimated masses of 0.015±0.002 and 0.014±0.002 $M_{\odot}$, with temperatures of 2270±90 and 2240±100 K, respectively. The physical separations between the components of both systems are 2880±20 and 3500±40 AU for USco1621 and USco1556 systems, respectively. We did not find any additional close companion in the adaptive optics images. The probability that the two secondaries are physically bound to their respective primaries, and not chance alignments of USco members, is 86%, and the probability that none of them are physically related is 1.0%.

Key words. brown dwarfs – binaries:visual – Proper motions – Surveys – open clusters and associations: individual: Upper Scorpius – Stars: pre-main sequence

1. Introduction

Multiplicity is an important outcome of the formation processes giving rise to stars and planetary systems and is key to understand the stellar and substellar physics. Binarity is a common phenomenon and the latest results indicate that a large fraction of stars form as part of multiple systems (Tokovinin & Lépine 2012; Raghavan et al. 2010) and that the binary frequency and the separation between components decrease when the mass of the primary decreases (Luhman 2012; Cortés-Contreras et al. 2017, and references therein).

The substellar companions discovered at wide separations from their primaries allow for a detailed photometric and spectroscopic characterisation to be carried out, which is extremely difficult in the case of objects found at close orbits around their primaries. The identification of substellar objects in binary systems also allows for an inference with regard to the ages, distances, and metallicities from their brighter and easier to characterise primaries, and to determine the otherwise ambiguous luminosities, effective temperatures, and masses of the companions (e.g. Rebolo et al. 1998; Faherty et al. 2010; Deacon et al. 2014; Gauza et al. 2015). Young moving groups, stellar clusters and associations with well determined ages, metallicities and distances are also helpful in the determination of the physical parameters of substellar objects.

Low-mass companions at wide orbits typically have very low gravitational binding energies, so they are not expected to survive as bound systems for a long time, especially in dense environments since they can be easily disrupted by external dynamical perturbations (Kroupa 1995; Close et al. 2007). However, several substellar companions of all ages with orbital separations of more than a thousand AU have been found (see Table 1 and references therein).

Table 1. Known wide substellar companions with projected separations above 1000 AU

Name	Short Name	RA	DEC	Age (Gyr) [a]	Projected Sep. (AU) [a]	Companion Mass (M_{Jup}) [a]	Ref.[c]
2MASS J160251.16−240150.2	USco 1602−2401 B	16:02:51.17	−24:01:50.45	0.005–0.010	1000	19–67	1
SR12 C	SR12 C	16:27:19.51	−24:41:40.1	0.0003–0.010	1083	6–21	2
ULAS J130041+122114	Ross 458 c	13:00:41.73	+12:21:14.7	<1	1168	5–14	3
ULAS J150457.65+053800.8	HIP 73786 B	15:04:57.66	+05:38:00.8	>1.6	1260	... [b]	4, 5
2M13480290−1344071	2M1348−1344B	13:48:02.90	−13:44:07.1	4–10	1400	31–79	6, 7
2MASS J06462756+7935045	HD 46588 B	06:46:27.56	+79:35:04.5	1.3–4.3	1420	47–75	8
ε Indi Ba	ε Indi Ba	22:04:10.52	−56:46:57.7	1.3	1459	37–57	9, 10
ε Indi Bb	ε Indi Bb	22:04:10.52	−56:46:57.7	1.3	1459	21–35	9, 10
2MASS J1457150−212148	Gl 570D	14.57:15.04	−21:21:49.82	2–10	1525	30–70	11
HIP 38939 B	HIP 38939 B	07:58:01.61	−25:39:01.4	0.3–2.5	1630	18–58	12
2MASS J04414489+2301513 Ba	2M0441+2301 Ba	04:41:45.65	+23:01:58.0	0.001–0.003	1800	16–22	13, 14
2MASS J04414489+2301513 Bb	2M0441+2301 Bb	04:41:45.65	+23:01:58.0	0.001–0.003	1800	8–12	13, 14
2MASS J02495436−0558015	2MASSJ0249−0557 c	02:49:54.36	−05:58:01.5	0.016–0.028	1950	10.6–12.9	15
Gl 417B	Gl 417B	11:12:25.7	+35:48:13	0.63–0.9	1970	50–56	16, 17, 18
Gl 417C	Gl 417C	11:12:25.7	+35:48:13	0.63–0.9	1970	45–52	16, 17, 18
GU Psc b	GU Psc b	01:12:36.48	+17:04:31.8	0.07–0.13	2000	9–13	19
WD 0806-661 B	WD 0806-661 B	08:07:14.68	−66:18:48.7	1.5–2.5	2500	6–9	20, 21
SDSS J224953.47+004404.6A	SDSS J2249+0044A	22:49:53.47	+00:44:04.6	0.012–0.790	2600	11–73	22
SDSS J224953.47+004404.6B	SDSS J2249+0044B	22:49:53.47	+00:44:04.6	0.012–0.790	2600	9–68	22
WISEP J142320.86+011638.1	BD +01° 2920B	14:23:20.86	+01:16:38.1	>2.3	2630	20–50	23
SDSS J175805.46+463311.9	SDSS J1758+4633	17:58:05.46	+46:33:11.9	0.5–1.5	2685	21–37	24
2MASS J16212830−2529558	USco1621 B	16:21:28.31	−25:29:56.1	0.005–0.010	2900	14–18	25
WISE J200520.38+542433.9	Wolf 1130C	20:05:20.38	+54:24:33.9	>2	3150	>52	26
HIP 77900B	HIP 77900B	15:54:30.47	−27:19:57.51	0.005–0.010	3200	15–27	1
2MASS J15562344−2541056	USco1556 B	15:56:23.43	−25:41:05.7	0.005–0.010	3500	12–17	25
2MASSW J1523226+301456	Gl 584C	15:23:22.6	+30:14:56	1.0–2.5	3600	47–79	16
SDSS J213154.43−011939.3	SDSS 2131−0119	21:31:54.43	−01:19:39.3	>1	3800	52–73	27
WISE J111838.70+312537.9	WISE 1118+31	11:18:38.70	+31:25:37.9	2–8	4100	14–38	28
VVV J151721.49−585131.5	β Cir B	15:17:21.60	−58:51:30.0	0.37–0.50	6656	51–66	29
2MASS J21265040−8140293	2MASS J2126−8140	21:26:50.40	−81:40:29.3	0.010–0.045	6900	11.6–15	30
HIP 70849B	HIP 70849B	14:28:42.32	−05:10:20.9	1–5	9000	... [b]	31
ULAS J133943.79+010436.4	HD 118865B	13:39:43.79	+01:04:36.4	1.5–4.9	9200	42–68	32
ULAS J145935.25+085751.2	ULAS J1459+0857	14:59:35.25	+08:57:51.2	>4.8	~20 000	63–79	33

Notes. [a] Data compiled from the literature. [b] Classified as a T dwarf. [c] References: (1) Aller et al. (2013); (2) Kuzuhara et al. (2011); (3) Goldman et al. (2010); (4) Scholz (2010); (5) Murray et al. (2011); (6) Mužić et al. (2012); (7) Deacon et al. (2012a); (8) Loutrel et al. (2011); (9) Scholz et al. (2003); (10) McCaughrean et al. (2004); (11) Burgasser et al. (2000); (12) Deacon et al. (2012b); (13) Todorov et al. (2010); (14) Bowler & Hillenbrand (2015); (15) Dupuy et al. (2018); (16) Kirkpatrick et al. (2001); (17) Bouy et al. (2003); (18) Dupuy et al. (2014); (19) Naud et al. (2014); (20) Luhman et al. (2011); (21) Luhman et al. (2012); (22) Allers et al. (2010); (23) Pinfield et al. (2012); (24) Faherty et al. (2010); (25) This work; (26) Mace et al. (2013); (27) Gauza et al. (2019); (28) Wright et al. (2013); (29) Smith et al. (2015); (30) Deacon et al. (2016); (31) Lodieu et al. (2014); (32) Burningham et al. (2013); (33) Day-Jones et al. (2011)

Dedicated studies have also been performed to investigate the multiplicity at wide separations in young moving groups and associations. For example, Kraus et al. (2011) carried out a search for wide binaries in the Taurus-Auriga star-forming region, exploring separations of 3–5000 AU, finding that only 25–32% of the stars in the region are single, whereas the majority of them are part of a multiple system, either with stellar or substellar secondaries. Aller et al. (2013) explored the frequency of substellar companions between 15–60 M_{Jup} at orbital distances of 400–4000 AU in the Upper Scorpius (USco) region, finding a companionship rate of 0.6±0.3%. Elliott & Bayo (2016) studied the distribution of the binary population at wide separations in the β Pictoris moving group, finding stellar and substellar companion candidates up to physical separations of 100 000 AU. From a sample of 49 β Pictoris members and systems, they found 14 stellar systems (∼29%) with separations above 1000 AU, and seven stellar systems (∼14%) with separations above 10 000 AU. They also found four substellar companions with separations <1000 AU.

The USco region is part of the Scorpius Centaurus (Sco-Cen) Association, the nearest OB association to the Sun. USco has an estimated average age of ∼ 5–10 Myr (Preibisch et al. 2002; Slesnick et al. 2006; Lodieu et al. 2008; Pecaut et al. 2012; Song et al. 2012; Feiden 2016; Pecaut & Mamajek 2016; Rizzuto et al. 2016; Fang et al. 2017; David et al. 2019) and is located at a heliocentric distance of 146±3±6 pc, where the second term in the uncertainty refers to systematic errors (Galli et al. 2018). The mean proper motion of USco members is (μ_α cos δ, μ_δ) = (−10, −23) ± 6 mas yr^{-1} (Fang et al. 2017). Its youth and close distance make this association an ideal place for the study of substellar objects, as these objects cool down with time and are still relatively bright at such young ages. A number of wide low-mass substellar companions with masses below or close to the deuterium-burning mass limit (∼13 M_{Jup} for solar metallicities, Burrows et al. 1997, 2001) have been found in the USco region, such as GSC 06214-00210 (Ireland et al. 2011), and 1RXS1609b (Lafrenière et al. 2008). These companions orbit young K-type stars at physical separations below 500 AU. A less massive system, UScoCTIO 108 AB (Béjar et al. 2008), formed by a brown dwarf and a planetary-mass companion at the deuterium-burning mass limit was also found at the wider separation of 670 AU in this region.

We have performed a search for wide binaries in USco, at separations between ∼400–9000 AU, to assess the frequency of wide companions to young stars and compare with the companionship rate for different ages. Our main goal is

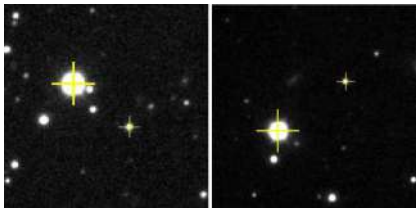

Fig. 1. VHS *J*-band images of USco1621 AB (left) and USco1556 AB (right). The primaries and secondaries are marked with crosses. The field of view is 1′×1′and the orientation is north up and east to the left.

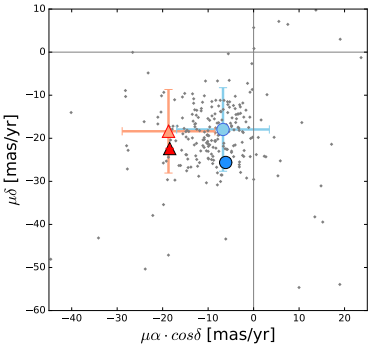

Fig. 2. Proper motion diagram of USco1621 A and B (blue circles) and USco1556 A and B (red triangles). The proper motions of USco known members from our VHS vs UKIDSS GCS cross-correlation are plotted with grey dots. The proper motions of the secondaries are calculated from the VHS and UKIDSS GCS astrometric data and plotted in lighter colours, while the proper motions of the primaries are obtained from *Gaia* DR2 and plotted in darker colours. The error bars of the *Gaia* DR2 measurements are smaller than the size of the symbols.

to provide observational constraints to evaluate the different wide-binary formation models and test general scenarios of substellar formation. In this work, we present the identification of 2MASS J16212830−2529558 (hereafter, USco1621 B) and 2MASS J15562344−2541056 (hereafter, USco1556 B) as two wide substellar companions to the previously-known low-mass stars of USco 2MASS J16212953−2529431 (hereafter, USco1621 A) and 2MASS J15562491−2541202 (hereafter, USco1556 A) (Rizzuto et al. 2015). In Section 2, we present the search method. Section 3 describes the follow-up observations of the systems, data reduction, and immediate results derived from these observations. In Section 4, we analyse the physical properties of the secondaries. Section 5 is dedicated to the discussion of the companionship of these pairs and the analysis of their formation and evolution. Finally, Section 6 corresponds to the summary and final remarks.

2. Two new young, low-mass systems

2.1. Astrometric and photometric search

We have performed a search for companions orbiting at wide separations from a list of 1195 known member candidates of the USco association compiled from the literature (Walter et al. 1994; Preibisch et al. 1998; Ardila et al. 2000; Martín et al. 2004; Lodieu et al. 2006; Slesnick et al. 2006; Lodieu et al. 2007; Findeisen & Hillenbrand 2010; Dawson et al. 2011; Lodieu et al. 2011; Luhman & Mamajek 2012; Dawson et al. 2013; Lodieu 2013; Rizzuto et al. 2015; Best et al. 2017). For this purpose, we have made use of proprietary data from the Visible and Infrared Survey Telescope for Astronomy (VISTA) Hemisphere Survey (VHS, McMahon et al. 2013) catalogue in combination with public data from the United Kingdom Infrared Telescope Infrared Deep Sky Survey (UKIDSS, Lawrence et al. 2007) Galactic Clusters Survey (GCS) catalogue.

The VISTA telescope (4m diameter quasi-Ritchey-Chretien telescope) is located at ESO's Cerro Paranal Observatory (Chile), and it is equipped with a near-infrared camera, VISTA InfraRed CAMera (VIRCAM), which provides a field of view of 1.65 degree diameter using a mosaic of 16 detectors, adding a total of 67 million pixels with a projected size in the sky of 0.34″pix^{-1} (Sutherland et al. 2015). The VHS is a near-infrared survey which images the entire southern hemisphere (~ 20 000 square degrees) in *J* and *Ks* bands. It also includes *H* band in 5000 square degrees in the South Galactic Cap, and *H* and *Y* bands in the remaining areas of high Galactic latitude ($|b| > 30°$). It reaches limiting magnitudes down to *J*=20.2 and *Ks*=18.1 (Vega system), around 4 magnitudes deeper than the previous infrared surveys 2MASS (Skrutskie et al. 2006) and DENIS (Epchtein et al. 1997). The astrometric solution of VHS is provided by the VISTA Data Flow System pipeline (Irwin et al. 2004; Lewis et al. 2010) at the Cambridge Astronomical Survey Unit (CASU), which uses the 2MASS Point Source Catalog astrometry as a reference, giving a relative accuracy that is better than 0.1″.[1]

The UKIDSS GCS is a survey performed by the 3.8m United Kingdom Infrared Telescope (UKIRT) which is located on the summit of Maunakea in Hawai'i. The UKIRT telescope is equipped with the UKIRT Wide Field Camera (WFCAM; Casali et al. 2007), which provides a field of view of 0.9 degree diameter, using four 2048×2048 HgCdTe Rockwell Hawaii-2 infrared detectors with a pixel size of 18 microns and a plate scale of 0.40″pix^{-1}. The UKIDSS GCS covers an area of ~ 1600 square degrees around several Galactic open clusters and star-forming associations, in the *ZYJHK* filters, up to limiting magnitudes of *J* ~ 19.1, *K* ~ 18.4. One of the regions covered by GCS is the USco region. The astrometric calibration is performed by CASU in a similar way to VISTA, giving an rms accuracy per source better than 0.1″(Hambly et al. 2008; Hodgkin et al. 2009).

Our compiled catalog contains 1306 individual members of USco, grouped in 1286 systems. 1195 of these 1286 systems are in the region of USco covered by both VHS and GCS catalogues. Companion candidates were identified as follows: we singled out all the detected sources in a circular area of 60″radius (corresponding to ~9000 AU at the USco distance) around each

[1] for further details, see `http://casu.ast.cam.ac.uk/surveys-projects/vista/technical`.

known USco member. We adopted this value as a compromise between the expected number of contaminants and the number of true companions. We cross-correlated the VHS and UKIDSS GCS catalogues using TOPCAT (Taylor 2005) but limiting the cross-correlation exercise to the aforementioned circular areas. The cross-match radius for the individual objects was 1″. This relatively large radius takes into account the astrometric uncertainties of the catalogues and the expected motion of USco members over the interval of seven years, which is the mean time baseline between the two surveys. In the 60″radius area around each USco member, we calculated the proper motions of all the cross-matched objects using VHS and GCS astrometry, and selected all the sources that have proper motions compatible with the mean USco motion (−7.46, −19.82, according to our measurement) with a maximum deviation of 23.5 mas yr^{-1} in the total proper motion. This astrometric threshold is defined by the quadratic sum of the dispersion of the proper motions in both axes of non-moving background objects, which is dominated by faint stars and unresolved galaxies, even fainter than our discoveries.

Besides sharing similar proper motions, we also imposed an additional condition on the astrometric candidates: they must follow the well-known USco photometric sequence in the J versus $Z-J$ and J versus $J-Ks$ colour-magnitude diagrams. We used the Z, J and Ks photometry of the USco known members in our compilation to determine a lower envelope limit for the candidate selection in each diagram. The photometric selection criteria were: $J_{VHS} < 4(Z_{GCS} - J_{VHS}) + 9.5$ and $J_{VHS} < 6(J_{VHS} - Ks_{VHS}) + 10$. For those regions not covered in the Z filter by UKIDSS GCS, we used Pan-STARRS (Chambers et al. 2016) z filter photometry to perform a similar selection. In this case, for the J versus $z-J$ selection, the criterium was $J_{VHS} < 3.3(z_P - J_{VHS}) + 7.7$.

Two of the faintest and reddest companion candidates found by this procedure are USco1621 B and USco1556 B. They were not identified in the search performed by Lodieu (2013), covering the same area but using only UKIDSS GCS data. USco1621 B was missed due to the lack of H filter photometry in UKIDSS GCS, and USco1556 B was missed because the proper motion in RA measured by UKIDSS GCS alone (−19.5 ± 2.97 mas yr^{-1}) deviates from the mean USco motion in RA (−8.6 mas yr^{-1}) by more than three times the estimated error. USco1621 B and USco1556 B were, however, recognised as USco candidates by the more recent work of Luhman et al. (2018), but these authors did not have spectroscopic information to determine their membership in the association. Figure 1 shows the VHS J-band image of both objects and their primaries. Table 2 presents astrometric and photometric information for the two pairs. The angular separations are 20.78±0.02 and 24.78±0.02 arcsec for USco1621 AB and USco1556 AB, corresponding to projected orbital separations of 2910±160 and 3530±180 AU, respectively, at the distance of the primaries measured by *Gaia* DR2 (Gaia Collaboration et al. 2016, 2018).

2.2. USco membership

USco1621 A and USco1556 A were discovered by Rizzuto et al. (2015) in their search for low mass members of this association. They performed a Bayesian membership selection using the photometry from 2MASS and the American Association of Variable Star Observers (AAVSO) Photometric All-Sky Survey (APASS; Henden & Munari 2014), and The fourth United States Naval Observatory (USNO) CCD Astrograph Catalog (UCAC4; Zacharias et al. 2013) proper motions (Rizzuto et al. 2011). They

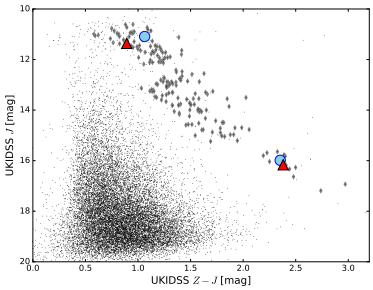

Fig. 3. UKIDSS GCS J vs Z-J colour-magnitude diagram. Previously-known members of USco are shown as grey diamonds. Field contaminants are indicated with black dots. USco1621 A and B are marked as light blue circles, and USco1556 A and B are marked as red triangles.

also carried out spectroscopic follow-up observations to confirm their membership. They determined a spectral type of M2.5 for USco1621 A and M3.0 for USco1556 A in the optical, and measured their Hα and Li 6708 Å equivalent widths (EWs), finding an EW(Hα) of −4.29 Å and a EW(Li) of 0.29 Å for the former, and an EW(Hα) of −5.67 Å and a EW(Li) of 0.27 Å for the later, which are values compatible with the age of USco.

Gaia DR2 recently provided a more precise determination of the proper motions of USco1621 A and USco1556 A, in addition to parallactic distances of 138±1 and 141±2 pc, respectively. These proper motions and distances fit perfectly with those of the USco association.

Rebull et al. (2018) measured the rotation periods of USco1621 A and USco1556 A using their photometric light curves from the Kepler space telescope K2 mission (Howell et al. 2014) and find rotation periods of 2.06 and 4.67 days, respectively. They assigned the highest probability of membership in USco to both primaries in their study. These values indicate a fast rotation, which is a hallmark of youth, since late-K and early-M dwarfs typically have rotation periods greater than 10 days for ages older than ∼ 100 Myr (e.g. Marcy & Chen 1992; Kiraga & Stepien 2007; Engle & Guinan 2011; Rebull et al. 2018).

We have determined from our UKIDSS GCS–VHS correlation that the proper motions of USco1621 B and USco1556 B are: (−7, −18) ± (10, 10) and (−19, −18) ± (10, 10) mas yr^{-1}, respectively, which are compatible with the USco association. The time baseline of the measurements is nine and seven years, respectively. The errors are obtained from the dispersion of the GCS–VHS correlation of background objects with similar magnitudes and null motions. Figure 2 shows the proper motion diagram of both companions together with *Gaia* DR2 proper motions of the primaries, and the VHS–UKIDSS GCS proper motion of other USco members.

The USco1621 AB and USco1556 AB systems have been previously imaged by several available optical and infrared surveys. There is photometry available for the primaries and the companion candidates in the 2MASS, DENIS, Pan-STARRS,

Table 2. General Data of USco1621 AB and USco1556 AB.

	USco1621 AB		USco1556 AB	
	Primary	Secondary	Primary	Secondary
Astrometry				
R.A. (J2000)	16:21:29.53	16:21:28.31	15:56:24.92	15:56:23.43
DEC (J2000)	−25:29:43.1	−25:29:56.1	−25:41:20.3	−25:41:05.7
Parallax *Gaia* (mas)	7.22±0.05	–	7.08±0.08	–
Distance (pc)	138±1	–	141± 2	–
Separation ($''$)		20.78±0.02		24.78±0.02
Separation (AU)		2880 ± 20		3500 ± 40
($\mu_\alpha$cosδ, μ_δ) *Gaia* DR2 (mas yr^{-1})	(−6.14, −25.62) ± (0.10, 0.07)	–	(−18.45, −22.39) ± (0.13, 0.08)	–
($\mu_\alpha$cosδ, μ_δ) VHS–UKIDSS (mas yr^{-1})	–	(−7, −18) ± (10, 10)	–	(−19, −18) ± (10, 10)
Spectroscopy				
Spectral type	M2.5[a]	M8.5±0.5 (OPT), L0±0.5(NIR)	M3.0[a]	M8.5±0.5 (OPT), L0.5±0.5 (NIR)
Li 6708 EW (Å)	0.29±0.02 [a]	–	0.27±0.02[a]	–
H_α EW (Å)	−4.29±0.06 [a]	–	−5.67±0.04 [a]	–
Photometry				
Gaia G	14.1769±0.0008	21.11±0.03	14.310±0.003	–
Pan-STARRS *g*	16.117±0.003	–	16.15±0.02	–
Pan-STARRS *r*	14.706±0.004	–	14.865±0.013	–
Pan-STARRS *i*	–	20.53±0.06	13.68±0.03	21.05±0.12
Pan-STARRS *z*	–	19.11±0.05	12.986±0.005	19.39±0.06
Pan-STARRS *y*	12.519±0.001	18.02±0.03	12.670±0.002	18.14±0.04
DENIS *I*	12.77±0.02	–	–	–
DENIS *J*	11.11±0.07	15.9±0.2	–	–
GCS *Z*	12.1521±0.0009	18.34±0.04	12.2534±0.0010	18.54±0.04
GCS *Y*	11.7760±0.0008	17.03±0.02	11.9184±0.0008	17.22±0.02
GCS *J*	11.0888±0.0005	15.985±0.010	11.3606±0.0008	16.163±0.012
GCS *H*	–	–	11.1524±0.0007	15.489±0.013
GCS *K*	10.5627±0.0004	14.636±0.006	10.4900±0.0004	14.812±0.007
VHS *J*	–	15.942±0.010	–	16.166±0.010
VHS *Ks*	–	14.704±0.011	–	14.904±0.015
2MASS *J*	11.18±0.02	16.17±0.08	11.37±0.02	16.11±0.08
2MASS *H*	10.43±0.02	15.34±0.10	10.69±0.02	15.39±0.09
2MASS *Ks*	10.19±0.02	14.67±0.09	10.44±0.02	14.85±0.12
WISE *W1*	10.04±0.02	14.09±0.04	10.32±0.02	14.45±0.03
WISE *W2*	9.90±0.02	13.65±0.06	10.18±0.02	14.10±0.05
WISE *W3*	9.55±0.10	>11.3	9.93±0.07	–
Physical parameters				
Rot. period (days)	2.06 [b]	–	4.67 [b]	–
Log ($L_{bol}/L_\odot$)	−1.02±0.03	−3.03±0.11	−1.09±0.04	−3.07±0.11
Effective temp. (K)	3460±100	2270±90	3410±100	2240±100
Mass ($M_\odot$)	0.36±0.08	0.015±0.002	0.33±0.07	0.014±0.002

Notes. [(a)] Spectral type and Lithium and H_α equivalent widths from Rizzuto et al. (2015) [(b)] Rotation period from Rebull et al. (2018)

Gaia, and WISE catalogues (Skrutskie et al. 2006; Epchtein et al. 1997; Chambers et al. 2016; Gaia Collaboration et al. 2016; Wright et al. 2010). All these photometric data are presented in Table 2. The apparent magnitudes and colours of the companion candidates obtained from these surveys are also consistent with young low-mass objects placed at the same heliocentric distance as USco, and these follow the photometric sequences of the association. Figures 3 and 4 show the *J* vs *Z*−*J* and *J* vs *J*−*Ks* colour-magnitude diagrams, respectively. These figures show that both secondaries occupy overluminous locations in the colour-magnitude diagrams with respect to the field dwarfs, which is compatible with a very young age.

3. Follow-up observations and data reduction

3.1. Spectroscopy

We performed low-resolution optical spectroscopy to determine spectral types and to search for signatures of youth to confirm membership to the association.

3.1.1. GTC/OSIRIS optical spectroscopy of USco1621 B

USco1621 B was observed with the Long Slit Spectroscopy mode of the Optical System for Imaging and low-Intermediate-Resolution Integrated Spectroscopy (OSIRIS; Cepa et al. 2000) spectrograph, mounted on the Gran Telescopio Canarias (GTC) at the Observatorio del Roque de Los Muchachos (ORM) in La Palma, Canary Islands, on 29 May 2017. These observations

Table 3. Observations Log

Obs. Date	Telesc/Instrum	Mode	Grating/ Filter	Wavelength Range [μm]	Slit [″]	Pl. Scale [″pix^{-1}]	Disp. [Å pix^{-1}]	Res. Power	Exp. Time	Airmass	Seeing [″]
				USco1621 A							
22 Mar 2019	Keck-I/OSIRIS	AO	K_p	1.96–2.27	–	0.01	–	–	150×1.475s	1.5–1.6	1.0
				USco1621 B							
14 Jun 2005	UKIRT/WFCAM	Img	*Z, Y, J*	–	–	0.4	–	–	20s,20s,5s	1.6	1.8
14 Mar 2011	UKIRT/WFCAM	Img	*K*	–	–	0.4	–	–	10s	1.6	2.0
1 May 2014	VISTA/VIRCAM	Img	*J, Ks*	–	–	0.34	–	–	15s, 7.5s	1.2	1.1
10 Apr 2017	NTT/SofI	Spec	GR	1.53–2.52	1	0.29	10.22	600	4×300s	1.1–1.2	0.8
10 Apr 2017	NTT/SofI	Spec	GB	0.95–1.64	1	0.29	6.96	600	4×300s	1.1–1.2	0.8
29 May 2017	GTC/OSIRIS	Spec	R300R	0.48–1.00	1	0.25	7.74	240	2×600s	1.7–1.8	1.0
22 Mar 2019	Keck-I/OSIRIS	AO	K_p	1.96–2.27	–	0.01	–	–	40×8.851s	1.4–1.5	0.9
				USco1556 A							
22 Mar 2019	Keck-I/OSIRIS	AO	K_p	1.96–2.27	–	0.01	–	–	150×1.475s	1.4	1.0
				USco1556 B							
7 May 2007	UKIRT/WFCAM	Img	*H, K*	–	–	0.4	–	–	10s, 5s	1.5	0.8
15 Jun 2010	UKIRT/WFCAM	Img	*Z*	–	–	0.4	–	–	20s	1.6	0.9
27 Jun 2010	UKIRT/WFCAM	Img	*Y, J*	–	–	0.4	–	–	20s, 10s	1.5	0.7
2 Apr 2011	UKIRT/WFCAM	Img	*K*	–	–	0.4	–	–	10s	1.5	2.0
1 May 2014	VISTA/VIRCAM	Img	*J, Ks*	–	–	0.34	–	–	15s, 7.5s	1.1	0.9
16 Jun 2018	VLT/X-shooter	Spec	VIS	0.55–1.02	1.2	0.158	0.16	6500	5×280s	1.0–1.1	1.0
16 Jun 2018	VLT/X-shooter	Spec	NIR	1.02–2.48	1.2	0.248	0.77	4300	5×300s	1.0–1.1	1.0
22 Mar 2019	Keck-I/OSIRIS	AO	K_p	1.96–2.27	–	0.01	–	–	30×8.851s	1.4	1.0

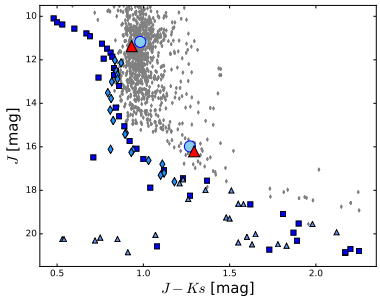

Fig. 4. *J* vs *J-Ks* colour-magnitude diagram. USco1621 A and B are marked with light blue circles, and USco1556 A and B are marked with red triangles. The photometry of both primaries is obtained from 2MASS and the photometry of the secondaries is taken from VHS. Known members of USco are shown as grey diamonds; the photometry of objects with J<14 mag is obtained from the 2MASS catalogue, while the photometry for the fainter ones is determined from VHS data. The VHS photometry has been transformed to the 2MASS photometric system through the colour equations provided by CASU. The photometric sequence of field dwarfs derived by Pecaut & Mamajek (2013) (squares) Dupuy & Liu (2012) (triangles) and Lodieu et al. (2014) (diamonds), displaced to the mean distance of USco, is also shown in blue.

were performed using the 1.0″width long slit in parallactic angle, and the R300R grating (resolving power ∼240, wavelength range of 4800–10 000 Å). The standard configuration includes a 2×2 binning of the OSIRIS detector. Two individual exposures of 600s were taken at two A–B different nodding positions along the slit. The average seeing value was around 1.0″and the airmass of the observations was around 1.7–1.8.

The data reduction was performed using standard routines within the Image Reduction and Analysis Facility (IRAF) environment (Tody 1986, 1993). The raw spectral frames were bias subtracted, divided by flat, combined, and extracted using the `APALL` routine. The instrumental response correction was performed using a spectrum of the white dwarf spectroscopic standard GD153. This standard was also observed using the broad *z*-band filter to correct the OSIRIS R300R grism second order contamination from the emission at wavelengths 4800–4900 Å, which appear at wavelengths between 9600–9800 Å. This contribution is not significant in the case of our secondaries, as these objects barely emit in the bluer wavelengths, but it is noticeable in the white dwarf standard spectrum. The wavelength calibration was performed using HgAr, Ne and Xe arc lamps images. The resulting spectrum is shown in Figures 5 and 6.

3.1.2. NTT/SofI near-infrared spectroscopy of USco1621 B

We also performed near-infrared spectroscopy of USco1621 B to determine its spectral type. The object was observed on 10 April 2017 using the Son Of Isaac (SofI) spectrograph (Moorwood et al. 1998) mounted on the 3.6m New Technology Telescope (NTT) in La Silla Observatory, Chile. The meteorological conditions over the run were good, the airmass value during the exposure was 1.1–1.2 and the average seeing was around 0.8″(FWHM) in the *J* filter. We used the low-resolution red and blue grisms, which provide wavelength ranges of 1.53–2.52 μm and 0.95–1.64 μm, respectively, and a resolving power of 600, with a nominal dispersion of 10.22 and 6.96 Å pix^{-1}, respectively, for a 1.0″wide slit. Four individual exposures of 300s were taken using an ABBA nodding pattern along the slit, for both red and blue configurations. The B6 telluric standard HIP80126 was observed right after the scientific target for telluric correction at similar airmass. We also acquired dome spec-

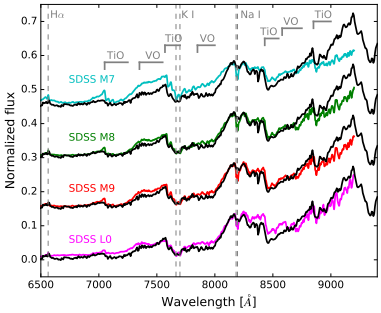

Fig. 5. GTC/OSIRIS optical spectrum of USco1621 B (black) overplotted with SDSS templates (coloured) from Bochanski et al. (2007), degraded to match the OSIRIS resolution, for comparison. The spectra have been normalised at ~8150 Å, and shifted by a constant for clarity. The most prominent spectral features are labelled.

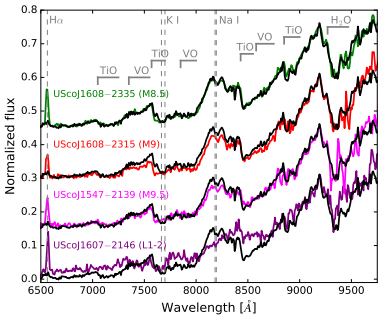

Fig. 6. GTC/OSIRIS optical spectrum of USco1621 B (black) compared to known USco members (coloured) obtained with GTC/OSIRIS using the same instrumental configuration by Lodieu et al. (2018). The spectra have been normalised at ~9200 Å, and shifted by a constant for clarity. The most prominent spectral features are labelled.

tral flat field images and Xe arc-lamp images to perform the flat field correction and the wavelength calibration.

The raw spectroscopic images were flat field corrected, sky subtracted using the A-B and B-A positions to remove the sky emission lines, aligned and combined. Then the spectra were extracted using the IRAF `APALL` routine and wavelength calibrated using the Xe arcs. A similar procedure was used for the telluric standard. We manually removed the intrinsic lines of the B6 telluric star spectra. Then, to correct for the instrumental response, the target spectra were divided by the telluric spectra and multiplied by a black body of 14 500 K. The red and blue spectra were scaled and combined using the overlapping region at ~1.5–1.6 μm. The obtained spectrum is shown in Figures 7 and 8.

Table 4. Spectral indices for spectral type determination.

Index	Value	SpT	Index Ref.[a]
		USco1621 B	
Optical			
TiO-7140	2.66	M6-M8	W05
TiO-8465	1.89	M7.5	S06
TiO5 [b]	0.35	M8.25±0.50	K99, CR02
VO-a [b]	2.51	L0.0±0.75/M9.0±0.5	R95, CR02
PC3	1.97	M8.5±0.25	M99
Infrared [c]			
H_2O	1.13	M9.25±0.5	A07
H_2OD	0.97	L0.75 ±0.75	ML03
H_2O-1	0.69	L0.25±1	S04
H_2O-2	0.89	M9.25±0.5	S04
FeH	0.87	M9.0±0.5	S04
		USco1556 B	
Optical			
TiO-7140	1.72	M9–L0	W05
TiO-8465	2.51	M8–M9	S06
TiO5 [b]	0.52	M9.0±0.5	K99, CR02
VO-a [b]	2.58	L1.0±0.75/M8.5±0.5	R95, CR02
PC3	2.27	M9.5±0.25	M99
Infrared [c]			
H_2O	1.18	L0.5±0.5	A07
H_2OD	1.05	M8.25±0.75	ML03
H_2O-1	0.66	L1.25±1	S04
H_2O-2	0.87	M9.75±0.5	S04
FeH	0.83	L0.0±0.5	S04

Notes. [(a)] References: A07 – Allers et al. (2007), CR02 – Cruz & Reid (2002), K99 – Kirkpatrick et al. (1999), M99 – Martín et al. (1999), ML03 – McLean et al. (2003), R95 – Reid et al. (1995), S04 – Slesnick et al. (2004), S06 – Slesnick et al. (2006), W05 –Wilking et al. (2005) [(b)] Calculated using the relations in Cruz & Reid (2002) [(c)] Results obtained using the Allers & Liu (2013) polynomial fits.

3.1.3. VLT/X-shooter optical and near-infrared spectroscopy of USco1556 B

USco1556 B was observed with the Echelle spectrograph X-shooter (Vernet et al. 2011) mounted on the Very Large Telescope (VLT) at Paranal Observatory (Chile) on 16 June 2018 in service mode. It was observed simultaneously in the three spectroscopic arms (UVB, VIS and NIR, corresponding to ultraviolet, visible, and near-infrared bands; covering 300–560, 560–1024, and 1024–2480 nm regions, respectively). The target is too faint in the UVB band to obtain a spectrum of adequate signal-to-noise-ratio in a reasonable integration time, so we restrict our analysis to the VIS and NIR bands only.

The observations were performed using 1.2″wide slits in both VIS and NIR arms, using an ABBA nodding pattern along

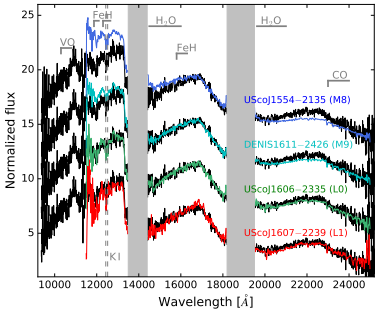

Fig. 7. NTT/SofI near-infrared spectrum of USco1621 B (black) overplotted with USco known members (coloured) obtained with Gemini North/GNIRS by Lodieu et al. (2008), for comparison. GNIRS spectra were convolved with a gaussian function to match the SofI spectral resolution. The spectra have been normalised in the H-band region (wavelength range ∼1.5–1.8 μm), and shifted by a constant for clarity. The regions affected by strong atmospheric telluric absorption bands are marked as grey bands. The most prominent spectral features are labelled.

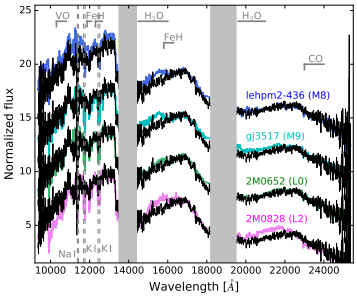

Fig. 8. Same as Fig. 7, but comparing USco1621 B (black) to field dwarf spectra (coloured) observed with NTT/SofI using the same instrumental configuration as the target.

the slits. The measured resolving power is ∼6500 and ∼4300 for VIS and NIR arms, respectively. Five individual exposures of 300s for the near-infrared and 280s for the optical were used. As the readout time is shorter for the NIR arm, it is possible to extend the exposure time in this arm, matching the total observing time in both arms to optimise the observations. The object was near culmination and the average seeing was around 1.0″. The B8V spectrophotometric standard HD148594 was also observed right after the target at a similar airmass to correct for atmospheric telluric absorption.

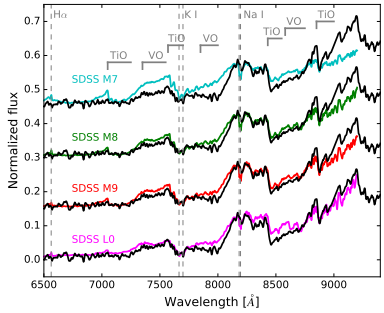

Fig. 9. VLT/X-shooter spectrum of USco1556 B in the VIS band (black) overplotted with SDSS templates (coloured) from Bochanski et al. (2007), for comparison. For a better visualisation, the X-shooter spectrum has been degraded to the resolution of the SDSS spectra using a Gaussian kernel. The spectra have been normalised at ∼8150 Å, and shifted by a constant for clarity. The most prominent spectral features are labelled.

The data reduction was performed using the ESO REFLEX environment (Freudling et al. 2013), which is based on the open source workflow engine Kepler, and IRAF. We used ESO REFLEX to obtain the combined, wavelength calibrated, and flux-calibrated 2D spectra. The X-shooter pipeline (Modigliani et al. 2010) performs bias and dark subtraction; flat-fielding, non-linearity and instrument flexure correction; instrument response and wavelength calibration; and spectral orders combination. Then the spectra were extracted using IRAF `APALL` routine. To perform the telluric correction in the near-infrared, we manually removed the characteristic spectral lines of the telluric star spectrum, divided the spectrum of USco1556 B by the telluric standard spectrum, and then multiplied the result by a black body of 12 500 K. For the optical, we also performed a telluric correction of the spectrum. In this case we also used the IRAF `CONTINUUM` routine to flatten the telluric spectrum before using it to divide the target optical spectrum. The optical and infra-red spectra of USco1556 B are shown in Figures 9 to 12.

3.1.4. Spectral classification in the optical

For the spectral classification in the optical, we have compared the spectrum of USco1621 B and USco1556 B with spectral templates of the Sloan Digital Sky Survey (SDSS; York et al. 2000) obtained by Bochanski et al. (2007). Figures 5 and 9 show the GTC/OSIRIS optical spectrum of USco1621 B and the VLT/X-shooter optical spectrum of USco1556 B together with SDSS standards from M7 to L0. For the comparison, we degraded the resolution of the SDSS and X-shooter spectra by convolving them with a Gaussian kernel, to match the resolution of the OSIRIS spectra. From these comparisons we can see that the depth of the TiO and VO molecular bands match better the M8–M9 spectral types in both cases, but the pseudo-continua follow the spectral energy distribution of the L0 standard. This is probably due to the difference in age of the objects we are trying to

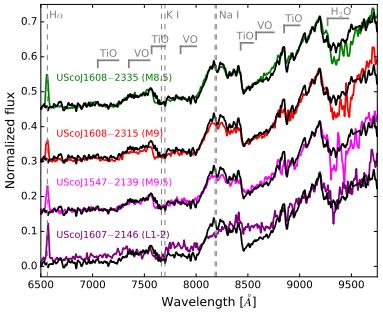

Fig. 10. VLT/X-shooter spectrum of USco1556 B in the VIS band (black) overplotted with USco known members (coloured) obtained with GTC/OSIRIS by Lodieu et al. (2018). X-shooter spectrum has been convolved using a gaussian function to the OSIRIS resolution. The spectra have been normalised at ∼9200 Å, and shifted by a constant for clarity. The most prominent spectral features are labelled.

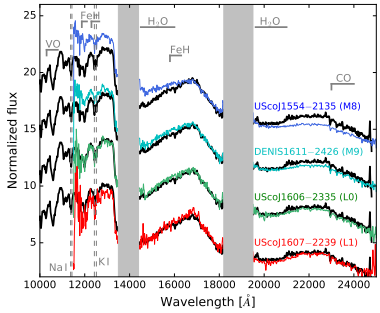

Fig. 11. VLT/X-shooter spectrum of USco1556 B in the NIR band (black) overplotted with USco known members (coloured) obtained with Gemini North GNIRS by Lodieu et al. (2008), for comparison. The X-shooter spectrum has been smoothed using a Gaussian kernel. GNIRS spectra were also degraded by gaussian convolution to match the same spectral resolution. The spectra have been normalised in the *H*-band region (wavelength range ∼1.5–1.8 μm), and shifted by a constant for clarity. Zones affected by atmospheric telluric bands are marked as grey bands. The most prominent spectral features are labelled.

compare. The SDSS standards are built from field-age objects, while our targets are much younger, and oxides are more prominent in low gravity atmospheres (Martin et al. 1996; Zapatero Osorio et al. 1997; Allers & Liu 2013; Zapatero Osorio et al. 2017). This difference in age can also be appreciated in other youth features such as very weak Na I and K I doublets absorption lines (see section 3.1.6 for more details).

We have also compared the optical spectra of USco1621 B and USco1556 B with spectra of known low-mass USco members. Figures 6 and 10 show the optical spectrum of these targets together with 4 USco objects with spectral types M8.5, M9, M9.5 and L1–L2 obtained with GTC/OSIRIS (Lodieu et al. 2018), for comparison. The best fits are obtained with the M8.5 object UScoJ16083049−2335110 for both secondaries.

In addition, we computed a set of typical spectral indices used for spectral classification, whose results are shown in Table 4. The VO-a index (Reid et al. 1995; Cruz & Reid 2002) is right in the frontier of the two polynomial fits provided by Cruz & Reid (2002), so we include the results of the two fits. We caution that oxide bands are gravity-sensitive features, and therefore, these indices may not be suitable for spectral type determination at young ages. As a result of all the visual comparisons and spectral-index determinations, we finally adopted a spectral type of M8.5±0.5 in the optical for both USco1621 B and USco1556 B. We estimated the error bars taking into account that our spectra deviate noticeably from the reference spectra having spectral types 1 subclass earlier or later.

3.1.5. Spectral classification in the near-infrared

To perform the spectral classification in the near-infrared region, we compared the spectra of USco1621 B and USco1556 B with spectra from previously-known USco members observed with the Gemini Near-Infrared Spectrograph GNIRS (Elias et al. 2006) on Gemini North by Lodieu et al. (2008). Figures 7 and 11 show the near-infrared spectrum of USco1621 B and USco1556 B together with spectra of M8, M9, L0 and L1 USco members: UScoJ155419−213543, DENIS161103-242642, UScoJ160606−233513, and UScoJ160727−223904, respectively. We degraded the GNIRS and X-shooter spectra to match the resolution of SofI. The spectral energy distributions of USco1621 B and USco1556 B are both very similar to UScoJ160606−233513, which is classified as an L0 in the infrared, although they are slightly redder in the K band. This dif-

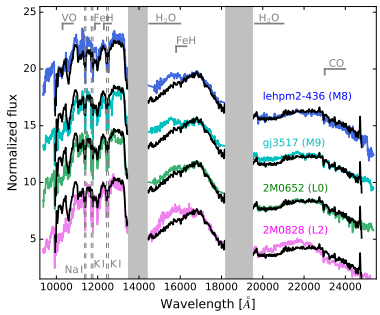

Fig. 12. Same as in Fig. 11, but here comparing USco1556 B (black) to field stars spectra (coloured) obtained with NTT/SofI.

ference is more noticeable for UScо1556 B, and also the peak in the *H* band is more pronounced for this secondary, which may indicate a slightly later spectral type. When comparing with the L1 spectral type UScoJ160727−223904 we find a larger discrepancy in the spectral energy distribution, mostly in the *J* band.

We also compared the near-infrared spectrum of both secondaries with several field-age objects with spectral types M8–L2, observed with NTT/SofI using the same instrumental configuration. These spectra were obtained and reduced following a similar procedure to UScо1621 B. The comparisons are shown in Fig. 8 and Fig. 12. The spectral energy distributions are very similar to the object 2MASS 0652, which is classified as an L0. This typing coincides with that obtained from the young references. We can also distinguish some youth features in our targets, such as weak K I alkali lines and the triangular shape in the *H* band, which are not present in the spectra of the field counterparts (e.g., Lucas et al. 2001; Gorlova et al. 2003; McGovern et al. 2004; Allers & Liu 2013).

We also computed several useful spectral indices in the near-infrared for the spectral classification. We used the water indices H_2O (Allers et al. 2007), H_2OD (McLean et al. 2003), H_2O-1, and H_2O-2 (Slesnick et al. 2004), and the FeH index from Slesnick et al. (2004). The results obtained are shown in Table 4. We used the polynomial fits described in Allers & Liu (2013), which relate the water indices to the corresponding spectral type in the optical for typing our targets. Hydrides like FeH are weak in low-gravity atmospheres. Therefore, this index may not be suitable for spectral type determination as it is atmospheric gravity dependent. Using these comparisons and indices, we finally assigned a spectral type of L0±0.5 to UScо1621 B and of L0.5±0.5 to UScо1556 B in the near-infrared. We estimated the error bars taking into account that our spectra do not resemble the reference spectra with spectral types 1 subclass earlier or later than UScо1621 B and UScо1556 B.

The spectral type determination in the near-infrared does not perfectly coincide with that estimated in the optical. This is not an unusual behaviour for young low-mass objects, and similar discrepancies have been reported earlier in USco and other young clusters and associations (e.g. Luhman & Rieke 1999; Barrado y Navascués et al. 2001; Luhman et al. 2003; Stauffer et al. 2003; Pecaut 2016; Lodieu et al. 2018).

3.1.6. Low-gravity signatures

There are several spectral features from optical and near-infrared observations that can be used as estimators of the surface gravity of an ultra-cool dwarf (T_{eff} typically below 2500 K). In the infrared, we can distinguish weaker alkali lines, particularly 1.169 / 1.177 μm and 1.243/1.252 μm K I doublets, and a triangular shape of the spectrum in the *H* band due to strong water absorption in both sides of the band. Figures 8 and 12 show the comparison of the companions with field objects in the near-infrared where these features can be clearly observed.

In the optical, we can also see weak alkali lines, especially the 8183 / 8195 Å Na I doublet, and also the 7665 / 7699 Å K I doublet. Figures 5 and 9 show the comparison between the young companions and several field dwarf objects in the optical. We note that these doublets may be affected by telluric absorption, and no telluric correction is applied to the GTC/OSIRIS optical spectrum of UScо1621 B. The doublets in this object may therefore be even weaker than they appear.

We did not find H-alpha in emission, which is a common indicator of youth, in any of the two companions. The fraction of objects showing H-alpha emission has its maximum occurrence rate at late-M and early-L spectral types, and declines for mid-L and later spectral types (e.g. Schmidt et al. 2015; Pineda et al. 2016). A similar behaviour is also found in young objects of the USco association, as can be seen in Lodieu et al. (2018). However, the lack of H-alpha emission is not a peculiar feature for these objects, as USco members with similar spectral types may have H-alpha in emission or not (see Figures 6 and 9 in Lodieu et al. 2018). There is also the possibility that the lack of H-alpha emission in some low-mass USco members spectra may be due to variability of the chromospheric activity (Petrus et al. 2019).

Table 5. Gravity-dependent indices.

Index	Value	Gravity[a]	Index Ref.[b]
UScо1621 B			
H-cont	0.95	γ	AL13
CH_4-H	1.07	β	B06
VO_z	1.11	?[c]	AL13
H_2O-K	0.95	γ	B06
UScо1556 B			
H-cont	0.96	γ	AL13
CH_4-H	1.12	γ	B06
VO_z	1.26	γ	AL13
H_2O-K	0.94	γ	B06

Notes. [(a)] Gravity indices as described in Kirkpatrick (2005) and Cruz et al. (2009). Assigned following the plots in Fig. A1 of Appendix A in Lodieu et al. (2018). [(b)] References: AL13 – Allers & Liu (2013), B06 – Burgasser et al. (2006) [(c)] This value is not conclusive for this NIR spectral type, and could indicate either a γ, β or Field gravity subclass.

We also computed gravity-sensitive indices to assess the young nature of our targets and, consequently, their likely membership in the USco association. Lodieu et al. (2018) analysed the most suitable indices for gravity characterisation, and concluded that H-cont, CH_4-H, FeH-H, VO_z , and H_2O-K (Burgasser et al. 2006; Allers & Liu 2013) are the most suitable gravity tracers for low resolution spectra. Table 5 shows the measured indices and the gravity subtype. The gravity subtypes β and γ denote intermediate and very low surface gravity, respectively (Kirkpatrick 2005; Cruz et al. 2009). To estimate these, we followed the positions in the plots presented in Fig. A1 of the Appendix A in Lodieu et al. (2018). Taking into account both the visual comparison and computed indices, we classified both companions as very low-gravity objects compatible with a very young age, like that of USco.

3.2. Keck-I/OSIRIS Adaptive Optics imaging

We observed both the primaries and secondaries of the UScо1621 AB and UScо1556 AB systems at the Keck I Telescope on Maunakea, Hawai'i, using the OH-Suppressing Infra-Red Imaging Spectrograph (OSIRIS) (Larkin et al. 2006) and the Keck Adaptive Optics (AO) system (Wizinowich et al. 2006; van Dam et al. 2006), on 22 March 2019. We used the Laser Guide Star (LGS) mode with the OSIRIS imaging arm (Arriaga et al. 2018). The field of view of the imager is 20″×20″, and the pixel scale is ~0.010″.

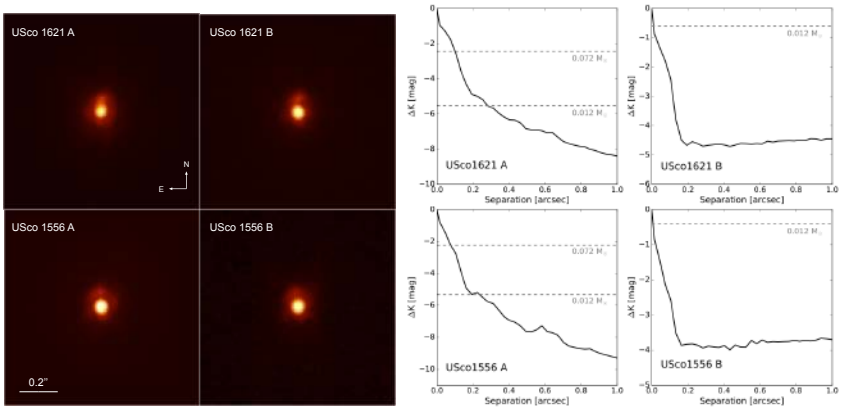

Fig. 13. *Left panels:* Keck-I/OSIRIS Adaptive Optics images of the primaries and secondaries of USco1621 and USco1556 systems, in the K_p filter. The field-of-view of the images is 1″× 1″and the orientation is North up and East to the left. Contrast scale of the images has been adjusted individually. *Right panels:* Contrast curves for the primaries and secondaries of the USco1621 and USco1556 systems for a 3σ detection limit. The expected differential magnitudes for objects at the theoretical mass limits for hydrogen and deuterium burning are marked by dashed lines.

We observed our targets using the K_p filter (λ_c=2.144 μm, $\Delta\lambda$=0.307 μm). The airmass was between 1.4–1.6 and the raw seeing was between 0.9″–1.0″. We used a 5-point dither pattern, with individual exposures of 1.475s for the primaries and 8.851s for the secondaries. Raw images were sky-subtracted, aligned, and combined using IRAF. Figure 13 shows the reduced images of both primaries and secondaries. We also show the contrast curves for the primaries and the secondaries, considering a 3σ detection limit. The contrast curve of the primaries is mostly limited by the contribution of the point spread function (PSF) wings of the bright central object, while for the secondaries it is mostly limited by the background noise.

We do not find any sign of binarity for any of the targets within our contrast limits. For the primaries, we can discard the presence of any low-mass stellar companion at angular separations larger than 0.10″(∼14 AU) and 0.07″(∼10 AU) from USco1621 A and USco1556 A, respectively; and the presence of brown dwarf companions at separations greater than 0.3″(∼40 AU). For the secondaries, we can discard the presence of objects with magnitude differences up to 4.4 and 3.7 mag in K (which correspond to masses higher than ∼5 M_{Jup} for the age of USco) at separations greater than 0.2″(∼28 AU) from USco1621 B and USco1556 B.

4. Luminosity, effective temperature and mass estimations

As a first approach to obtain the luminosity of USco1621 B and USco1556 B, we calculated their absolute bolometric magnitudes from the VHS *Ks*-band photometry, bolometric corrections, and assuming the same heliocentric distances as the primaries, measured by *Gaia* DR2. The bolometric corrections in the *Ks* filter have been derived from the polynomial relations for young objects of the same spectral type from Filippazzo et al. (2015).

For USco1621 B, with an optical spectral type of M8.5±0.5 and a distance of 138±1pc, we obtained a luminosity of $\log(L/L_\odot)$=−2.96±0.08. For USco1556 B, considering an optical spectral type of M8.5±0.5 and a distance of 141±2 pc, we obtained a luminosity of $\log(L/L_\odot) = -3.02\pm0.09$. The errors have been estimated taking into account the photometric error bar from VHS, the parallax error from *Gaia* DR2, the uncertainty in the spectral type determination and the error in the bolometric corrections.

We also computed the luminosity of the primaries in a similar way. We used their 2MASS photometry in the J band and their spectral types from Rizzuto et al. (2015). The distances were obtained from *Gaia* DR2, and the bolometric corrections for the J band from Pecaut & Mamajek (2013). We obtain, for USco1621 A and USco1556 A, luminosities of $\log(L/L_\odot)$=−1.02±0.03 and −1.09±0.04, respectively.

We also derived the luminosity of the secondaries by integrating the total flux from the optical and infrared spectra. We combined the optical and near-infrared spectra by scaling them, using the mean values of the flux in the overlapping region. Then we flux-calibrated our spectra using the UKIDSS GCS photometry in the J band and the integration of the flux of our spectra in this band obtained using the IRAF `SBANDS` routine, as our targets have their maximum emission in this wavelength range. We completed the missing mid-infrared wavelengths and replaced regions of the spectra affected by strong telluric absorption using a BT-Settl model spectrum from Allard et al. (2012); Baraffe et al. (2015). We chose the 2000 K and log(g)=4.0 model, as it better reproduces the spectral energy distribution in the near-infrared and the WISE *W1*, *W2* bands. For wavelengths longer than 100 000 Å, we extrapolated using a Rayleigh-Jeans tail ap-

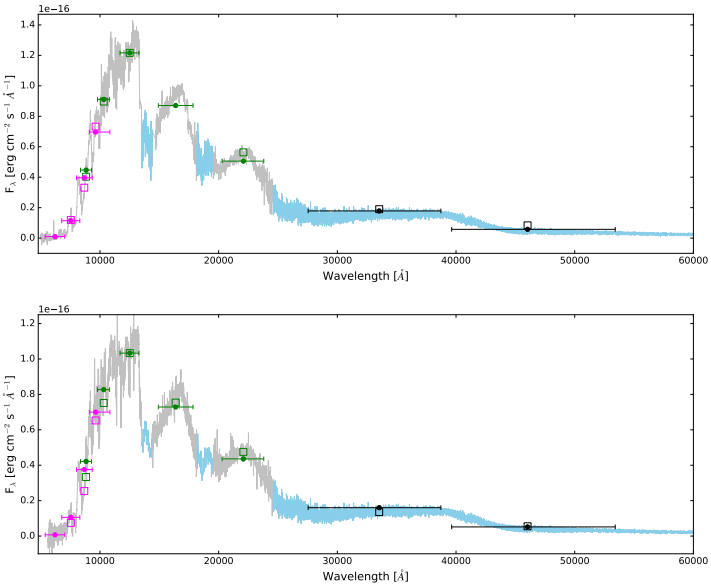

Fig. 14. Optical + Infrared spectra of USco1621 B (upper panel) and USco1556 B (lower panel), in grey, completed with a $T_{\rm eff}$=2000 K and log(g)=4.0 BT-Settl model spectrum from Allard et al. (2012); Baraffe et al. (2015), in light blue. Available photometry from Pan-STARRS (pink open squares), UKIDSS (green open squares), and AllWISE (black open squares) is added. Vertical error bars of the photometry are smaller than the markers. Filled circles correspond to the flux values obtained through direct integration of the spectra in the same filter bands. Horizontal error bars represent the filter bandwidths.

proximation ($f = c{\cdot}\lambda^{-4}$) although its contribution to the total flux is negligible. For wavelengths shorter than ∼5000 Å, the flux is very low (close to zero) and its contribution is also negligible.

Figure 14 shows the spectra for USco1621 B and USco1556 B together with the available photometry from Pan-STARRS, UKIDSS, and AllWISE. We also show the integrated flux in the same bands, obtained using IRAF `SBANDS` routine and convolving with the Pan-STARRS, UKIDSS, and AllWISE filter profiles, which were provided by the Spanish Virtual Observatory Filter Profile Service (Rodrigo et al. 2012). By integrating the full spectra, we calculated the bolometric luminosity using the *Gaia* DR2 distances of the primaries. We obtain a bolometric luminosity of log($L/L_\odot$)=−3.03±0.11 and −3.07±0.11 for USco1621 B and USco1556 B, respectively. These values are in good agreement, at 1σ level, with the ones obtained from the photometry alone. The quoted errors include the spectral noise, the uncertainty in the flux calibration, the error given by the selection of slightly different BT-Settl model-spectra for the mid-IR wavelengths, and the error in the distance.

We estimated the mass and effective temperature of the objects interpolating the BT-Settl theoretical evolutionary models (Allard et al. 2012; Baraffe et al. 2015) for the corresponding bolometric luminosities, and for an age of the USco association of 5–10 Myr. For USco1621 A and USco1556 A, we obtain masses of 0.36±0.08 and 0.33±0.07 $M_\odot$, and effective temperatures of 3460±100 and 3410±100 K, respectively. For USco1621 B and USco1556 B, the combination of luminosity values computed from the direct integration of the spectra with BT-Settl models yields masses and temperatures of 0.015±0.002 and 0.014±0.002 $M_\odot$, and 2270±90 and 2240±100 K for USco1621 B and USco1556 B, respectively, assuming an age between 5–10 Myr.

Figure 15 shows the luminosity vs. age diagram for USco1621 B and USco1556 B and other known wide young substellar companions, together with Ames-COND model (Allard et al. 2001; Baraffe et al. 2003) evolutionary tracks for different masses. Both secondaries are placed slightly above the deuterium-burning mass limit. According to their age, they are entering the deuterium burning phase, where their luminosity will remain with little changes until they reach an age of ∼30 Myr. These two new young wide substellar companions are amongst the least massive at separations wider than 1000 AU discovered up to date.

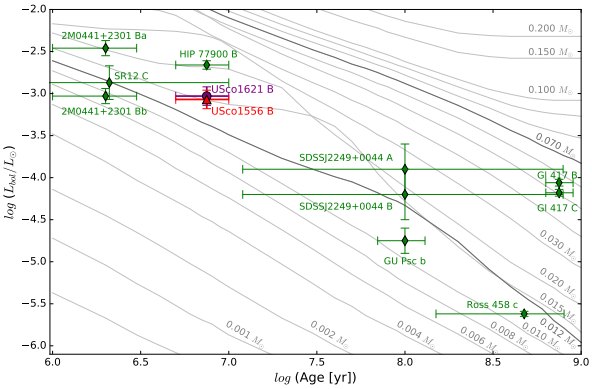

Fig. 15. Log($L/L_\odot$) vs. age diagram for USco1621 B (purple circle) and USco1556 B (red triangle), together with Ames-COND model isomasses from Allard et al. (2001) and Baraffe et al. (2003). Theoretical hydrogen- and deuterium-burning mass limits are marked in dark grey. Other known young wide substellar companions with separations above 1000 AU from Kirkpatrick et al. (2001); Bouy et al. (2003); Allers et al. (2010); Goldman et al. (2010); Todorov et al. (2010); Kuzuhara et al. (2011); Aller et al. (2013); Dupuy et al. (2014); Naud et al. (2014); Bowler & Hillenbrand (2015) (green diamonds) are also included.

5. Discussion

5.1. Companionship of the USco1621 and USco1556 systems

In the previous sections, we determine that USco1621 B and USco1556 B have low-gravity features, which are characteristic of youth. Therefore, both objects belong to the USco star-forming region. However, there is the possibility that both objects belong to USco but are not bound to their primaries and are located at a similar projected position on the sky by chance.

To evaluate whether both systems are physically bound or chance alignments, we estimate the probability of finding isolated USco low-mass brown dwarfs at angular separations closer than 25″of any USco member in our search. Using the survey of similar depth done by Lodieu (2013), we calculated the density of low-mass brown dwarfs and isolated planets in USco. We find a density of 0.84 obj deg^{-2} for USco members with J>15 mag.

Assuming a poissonian distribution, the probability of finding one or more chance alignments is given by

$$P(x > 0) = 1 - P(x = 0) = 1 - e^{-\lambda}\,, \quad (1)$$

and the probability of finding two or more chance alignments is given by:

$$P(x > 1) = 1 - P(x = 1) - P(x = 0) = 1 - e^{-\lambda} - \lambda \cdot e^{-\lambda}, \quad (2)$$

with $\lambda = np$, where P is the poissonian distribution, x is the number of chance alignments found, n is the number of targets in our search (1195) and p is the individual probability of finding a J>15 mag USco member in an area of radius 25″(p=1.27×10^{-4}). We obtain a probability of 14% of finding at least one J>15 mag USco companion candidate by chance alignment. The probability of finding two chance alignments is 1.0%.

In conclusion, the probability that both USco1621 and USco1556 systems are bound is 86%, the probability that at least one of them is bound is 99%, and the probability that none of them is physically related is 1.0%. A precise parallax measurement of the secondaries would help confirming their companionship.

Kraus & Hillenbrand (2008) estimate that for the USco association, true binaries can be distinguished from chance alignments at separations lower than 75″. Candidate companions closer than this limit, although can also be chance alignments, are most likely bound, and the chance alignment probability is progressively lower as we move to closer separations. The components of USco1621 and USco1556 systems are separated 21″and 25″, respectively. Therefore, according to their criteria, these systems are most likely gravitationally bound.

5.2. Origin and evolution of the systems

Although several wide substellar companions with separations above 1000 AU have been found around stars, brown dwarfs, and white dwarfs of different ages, the number of such systems is still very limited. An exhaustive compilation of such wide substellar companions is shown in Table 1.

Several formation scenarios have been proposed to explain the existence of these widely separated systems. It is possible that these very low-mass binaries form in-situ at very wide orbits as a consequence of the fragmentation of the initial molecular cloud, which can result in cores with separations of ~10^3–10^4 AU (e.g. Launhardt et al. 2010; Chen et al. 2013; Goodwin et al. 2007, and references therein). They could also have formed

via disk gravitational instability (e.g. Boss 2001; Whitworth & Stamatellos 2006), which can form substellar objects at separations up to several hundreds of AU (Stamatellos & Whitworth 2009), and later migrated to wider separations. In addition, recent observations indicate that a large fraction of wide, low-mass binaries are in fact triple systems, where the more luminous component is a binary itself (e.g. Elliott & Bayo 2016). One possible explanation of this behaviour is that the three components may form in a compact system, and then one of them, typically the least massive, evolves to wider orbits by three-body dynamical interactions (Delgado-Donate et al. 2004; Reipurth & Mikkola 2012). Another possible mechanism for the existence of very wide binaries is the formation of both components in separate locations and their later gravitational capture (Kouwenhoven et al. 2010). It is not clear which of these mechanisms may be the origin of the USco1621 and USco1556 systems.

To understand the possible future evolution of these systems, we calculated their binding energies and estimated their disruption times. For the binding energies we used the relation

$$U = \frac{-G\, m_1\, m_2}{a}, \tag{3}$$

where G is the gravitational constant, m_1, m_2 are the masses of the binary components and a is the semi-major axis of the orbit. It is important to note that, due to projection effects, the real semi-major axis of the orbit may be larger than the separation we measure here. Fischer & Marcy (1992) made a probabilistic calculation of the average value of the semi-major axis, by performing a Monte Carlo simulation which included all the possible orbital parameters for any elliptical orbits in randomly oriented inclinations. They obtain an average semi-major axis of $\langle a_{rel} \rangle = 1.26 d \langle \alpha \rangle$, where d is the heliocentric distance and $\langle \alpha \rangle$ is the average observed angular separation of the components. Hence, for this average semimajor axis we obtain a binding energy of $(-2.6\pm1.0)\times10^{33}$ J and $(-1.8\pm0.7)\times10^{33}$ J for USco1621 and USco1556 systems, respectively, and an (absolute) upper limit of $(-3.3\pm1.2)\times10^{33}$ J and $(-2.3\pm0.9)\times10^{33}$ J for USco1621 and USco1556 systems, respectively, using the observed separation. This low binding energy is comparable to Oph 16222−2405 (-1.6×10^{33} J; Close et al. 2007), UScoCTIO 108 AB (-1.9×10^{33} J; Béjar et al. 2008), or the ultrawide systems 2MASS J0126AB (-3.0×10^{33} J; Artigau et al. 2007; Caballero 2009) and 2M1258+40 (-2.5×10^{33} J; Radigan et al. 2009).

To estimate the disruption times due to dynamical encounters, we used the soft binary approximation from Binney & Tremaine (1987), given by

$$t_{\rm evap} = \frac{m_1 + m_2}{m_a} \frac{\sigma}{16\sqrt{\pi}\, G\, \rho\, a\, ln\Lambda}, \tag{4}$$

where m_1, m_2 are the masses of the binary components, m_a is the mean mass of the perturbers, σ is the velocity dispersion, G is the gravitational constant, ρ is the mass density of the environment, a is the semimajor axis of the orbit of the binary, and $ln\,\Lambda$ is the Coulomb logarithm, which can be calculated using the expression

$$\Lambda = \frac{b_{\rm max} V_0^2}{G(M+m)}, \tag{5}$$

with $b_{\rm max}$ being the maximum impact parameter that needs to be considered in the perturbations, V_0^2 the relative velocity of the perturber, M the mass of the object (total mass of the binary in our case) and m the mass of the perturber. For $b_{\rm max}$ we used the expression

$$b_{\rm max}(a) = 9.6\ {\rm pc} \left(\frac{v_{\rm rel}}{20\ {\rm km\cdot s^{-1}}}\right)\left(\frac{a}{0.1\ {\rm pc}}\right)^{3/2}\left(\frac{M}{M_\odot}\right)^{-1/2} \tag{6}$$

(Weinberg et al. 1987), where $v_{\rm rel}$ is the relative velocity between the object and the perturber, a is the separation between the binary components, and M is the total mass of the binary.

In addition, we also estimated the disruption time using the approximation in Weinberg et al. (1987), given by

$$t_* = 1.8\cdot10^4\ {\rm Myr}\left(\frac{n_*}{0.05\ {\rm pc^{-3}}}\right)^{-1}\left(\frac{M}{M_\odot}\right)\left(\frac{M_*}{M_\odot}\right)^{-2}\cdot \\ \cdot\left(\frac{<1/v_{\rm rel}>^{-1}}{20\ {\rm km\cdot s^{-1}}}\right)\left(\frac{a_0}{0.1\ {\rm pc}}\right)^{-1}\ln^{-1}\Lambda, \tag{7}$$

where n_* is the density of perturbers, M is the total mass of the binary, M_* is the mean mass of the perturbers, $v_{\rm rel}$ is the relative velocity between the binary and the perturbers, a_0 is the separation of the binary, and $ln\,\Lambda$ is the Coulomb logarithm. We considered a mean perturber mass of $1 M_\odot$ and a mean velocity dispersion of 3.20 km s^{-1} (Wright & Mamajek 2018). Wright & Mamajek (2018) did not find any clear evidence of expansion neither in USco nor in any of the subgroups of Sco-Cen association. This means that it is probable that Sco-Cen was formed during several formation events and not as a single dense cluster that later expanded into a larger region. In this case, we can consider that the actual estimated density in their environments has not significantly changed since their births. To estimate the current density of objects around each of the systems, we used the astrometric and parallactic data from *Gaia* DR2 to select all the targets (belonging to USco or not) located inside a cube of 8 pc side (∼500 pc^3) around each system. We found 259 and 172 objects within these volumes, which correspond to densities of 0.51 and 0.34 obj pc^{-3} around the USco1621 and USco1556 systems, respectively. For the binary separation, we considered the average semimajor axis, $\langle a_{rel} \rangle = 1.26 d \langle \alpha \rangle$, and the measured separation as a lower limit. For these values, the estimated disruption times range between 90–250 and 100–260 Myr, respectively. Therefore, if these systems are really physically bound, they are expected to survive for several Myr in their actual environments. However, at these timescales, the USco association is expected to already be dissipated. In that case, considering a density similar to that of the Solar vicinity in their future environments (0.076–0.084 systems pc^{-3}, calculated using data from The Research Consortium On Nearby Stars, RECONS, in Henry et al. 2018), the systems are expected to survive for ∼0.4–1.7 Gyr.

We have also investigated the possibility that these systems have already suffered a close encounter and are currently in the process of disruption. Using *Gaia* DR2, we have performed a search for nearby objects which could have interacted with the systems in the last thousands of years. Given the minimum escape velocity of the companions at the present location (∼0.4 km s^{-1}), if they are currently in disruption, the perturbation must have happened less than ∼0.1 Myr ago because, otherwise, the companions would have traveled a distance greater than their actual separation. We identified all the nearby objects with heliocentric distances corresponding with those of the primaries ±5 pc, and using their proper motions we traced back their 2-D trajectories over the last 0.3 Myr. The ±5 pc limit implies that we are considering all the possible perturbers (from USco or the field population) with radial velocities differing up to ∼ ±50 km

s^{-1} with respect to the systemic velocity of our systems, because this is the maximum distance the perturber would have travelled in 0.1 Myr. We find several candidates that may have been located within 1 pc of the primaries in the past, but the lack of radial velocity information prevents us from confirming if they were really physically close to the systems in a 3D picture. As a result of this search, we have identified a promising perturber candidate for the USco1621 system. This object is a candidate member of the USco association, 2MASS J16223009−2532319 (Luhman et al. 2018; Damiani et al. 2019), whose distance, 139±2 pc, is compatible with USco1621 A. Their projected separation is 0.88 pc (182 000 AU), and their proper motions are currently diverging, with a maximum approximation just three years ago. The apparent magnitudes and colours of 2MASS J16223009−2532319 indicate an expected spectral type of mid-M. Given the large physical separation of this object to the binary system USco1621 AB, it is difficult to determine if it is part of a triple system or just an USco member located by chance at this separation.

5.3. Adding two new benchmark systems

In USco, several tens of substellar objects with masses around or below the deuterium burning limit mass have been found in isolation (Lodieu et al. 2006, 2007; Dawson et al. 2011; Lodieu 2013; Peña Ramírez et al. 2016; Lodieu et al. 2018). However, only four of these objects have been found as wide companions: UScoCTIO 108 B (Béjar et al. 2008); 1RXS1609b (Lafrenière et al. 2008); GSC 06214-00210 (Ireland et al. 2011); and HIP 77900B (Aller et al. 2013). Two of them (1RXS1609b and GSC 06214-00210) were discovered using adaptive optics and their low angular separations from their brighter primaries make it difficult to fully characterise them, especially at optical wavelengths, allowing only limited spectral characterisation in the infrared. The discovery of USco1621 B and USco1556 B has added two new benchmark objects to this small collection, which are easier to characterise, also in the optical wavelength range.

Other companions in wide orbits have been identified populating distinct young associations and stellar moving groups of similar ages. Some examples are FU Tau B (Luhman et al. 2009) and SCH06 J0359+2009 B (Kraus & Hillenbrand 2012; Martinez & Kraus 2019) in Taurus; SR12 C (Kuzuhara et al. 2011) in Ophiucus; HD 106906 b (Bailey et al. 2014) in Lower Centaurus Crux; or AB Pic B (Chauvin et al. 2005) and 2MASS J2126−8140 (Deacon et al. 2016) in Tucana-Horologium.

6. Summary and final remarks

The main results of this paper are summarised below:

1. Using VHS and UKIDSS GCS data, we found two new wide substellar companions (USco1621 B and USco1556 B) of two previously-known early-M dwarfs in USco. The companions are located at angular separations of 21″and 25″ which, at the distance of their primaries, correspond to projected physical separations of 2880 and 3500 AU, respectively.
2. Using low-resolution spectroscopy, we classified USco1621 B and USco1556 B as M8.5±0.5 in the optical and L0±0.5 and L0.5±0.5 in the near-infrared, respectively.
3. We find later spectral types in the near-infrared than in the optical by 1.5 to 2.0 subclasses. Similar differences have been reported by earlier works on this association.
4. These objects show features of youth in their optical and infrared spectra compatible with the age of USco, which confirms their very young age and their membership to this association.
5. Using high-resolution images from the Keck-I LGS adaptive optics system, we did not find any additional stellar or brown dwarf companion at separations larger than 0.3” (∼40 AU) from the primaries and any additional planetary-mass companion at separations larger than 0.2” from the secondaries (∼28 AU).
6. We derived the bolometric luminosities of USco1621 B and USco1556 B by integrating their spectra and using the distances of the primaries, measured by *Gaia* DR2. We obtain luminosities of $\log(L/L_{\odot})$=−3.03±0.11 and −3.07±0.11 for USco1621 B and USco1556 B, respectively. According to theoretical evolutionary models, we obtain masses of 0.015±0.002 and 0.014±0.002 $M_{\odot}$, and temperatures of 2270±90 and 2240±100 K, for USco1621 B and USco1556 B, respectively. These estimations confirm that they are low-mass brown dwarfs, with masses slightly above the deuterium burning mass limit.
7. We estimated that the probability that both systems are bound systems belonging to USco rather than chance alignments is 86%, the probability that at least one of them is physically bound is 99%, and the probability that none of them are bound is 1.0%.
8. Considering the current densities in the surroundings of each system, we estimated disruption times of few hundreds of Myr for USco1621 and USco1556 systems, which is larger than the current age of USco and its expected dissipation time. Considering a density similar to that of the Solar vicinity after the dissipation of the USco association, the systems are expected to survive for ∼0.4–1.7 Gyr.

Acknowledgements. We thank the anonymous referee for his/her very useful corrections and suggestions, which helped improving this manuscript. P.C., V.J.S.B. and N.L. are partially supported by grant AyA2015-69350-C3-2-P; R.R. by program AyA2014-56359-P; M.R.Z.O. by program AyA2016-79425-C3-2-P and A.P.G by program AyA2015-69350-C3-3-P from the Spanish Ministry of Economy and Competitiveness (MINECO/FEDER). B.G. acknowledges support from the CONICYT through FONDECYT Postdoctoral Fellowship grant No 3170513. This paper is based on observations performed at the European Southern Observatory (ESO) in Chile, under programs 092.C-0874 (PI Gauza), 099.C-0848 (PI Chinchilla) and 0101.C-0389 (PI Chinchilla). This work is based on observations (program 55-GTC30/17A; PI Lodieu) made with the Gran Telescopio Canarias (GTC), operated on the island of La Palma in the Spanish Observatorio del Roque de los Muchachos of the Instituto de Astrofísica de Canarias. Some of the data presented herein were obtained at the W.M. Keck Observatory, which is operated as a scientific partnership among the California Institute of Technology, the University of California and the National Aeronautics and Space Administration. The Observatory was made possible by the generous financial support of the W.M. Keck Foundation. The authors wish to recognise and acknowledge the very significant cultural role and reverence that the summit of Maunakea has always had within the indigenous Hawaiian community. We are most fortunate to have the opportunity to conduct observations from this mountain. This research has made use of the Simbad and Vizier (Ochsenbein et al. 2000) data bases, operated at the Centre de Donneés Astronomiques de Strasbourg (CDS), and NASA's Astrophysics Data System Bibliographic Services (ADS). This work has made use of data from the European Space Agency (ESA) mission Gaia (`https://www.cosmos.esa.int/gaia`), processed by the Gaia Data Processing and Analysis Consortium (DPAC, `https://www.cosmos.esa.int/web/gaia/dpac/consortium`). Funding for the DPAC has been provided by national institutions, in particular the institutions participating in the Gaia Multilateral Agreement. This research has made use of the SVO Filter Profile Service (`http://svo2.cab.inta-csic.es/theory/fps/`) supported from the Spanish MINECO through grant AYA2017-84089. This publication made use of Python programming language (Python Software Foundation, `https://www.python.org`).

References

Allard, F., Hauschildt, P. H., Alexander, D. R., Tamanai, A., & Schweitzer, A. 2001, ApJ, 556, 357
Allard, F., Homeier, D., & Freytag, B. 2012, Philosophical Transactions of the Royal Society of London Series A, 370, 2765
Aller, K. M., Kraus, A. L., Liu, M. C., et al. 2013, ApJ, 773, 63
Allers, K. N., Jaffe, D. T., Luhman, K. L., et al. 2007, ApJ, 657, 511
Allers, K. N. & Liu, M. C. 2013, ApJ, 772, 79
Allers, K. N., Liu, M. C., Dupuy, T. J., & Cushing, M. C. 2010, ApJ, 715, 561
Ardila, D., Martín, E., & Basri, G. 2000, AJ, 120, 479
Arriaga, P., Fitzgerald, M., Johnson, C., Weiss, J., & Lyke, J. E. 2018, in Society of Photo-Optical Instrumentation Engineers (SPIE) Conference Series, Vol. 10702, Ground-based and Airborne Instrumentation for Astronomy VII, 107022U
Artigau, É., Lafrenière, D., Doyon, R., et al. 2007, ApJ, 659, L49
Bailey, V., Meshkat, T., Reiter, M., et al. 2014, ApJ, 780, L4
Baraffe, I., Chabrier, G., Barman, T. S., Allard, F., & Hauschildt, P. H. 2003, A&A, 402, 701
Baraffe, I., Homeier, D., Allard, F., & Chabrier, G. 2015, A&A, 577, A42
Barrado y Navascués, D., Zapatero Osorio, M. R., Béjar, V. J. S., et al. 2001, A&A, 377, L9
Bayo, A., Rodrigo, C., Barrado Y Navascués, D., et al. 2008, A&A, 492, 277
Béjar, V. J. S., Zapatero Osorio, M. R., Pérez-Garrido, A., et al. 2008, ApJ, 673, L185
Best, W. M. J., Liu, M. C., Magnier, E. A., et al. 2017, ApJ, 837, 95
Binney, J. & Tremaine, S. 1987, Galactic dynamics
Bochanski, J. J., West, A. A., Hawley, S. L., & Covey, K. R. 2007, AJ, 133, 531
Boss, A. P. 2001, ApJ, 563, 367
Bouy, H., Brandner, W., Martín, E. L., et al. 2003, AJ, 126, 1526
Bowler, B. P. & Hillenbrand, L. A. 2015, ApJ, 811, L30
Burgasser, A. J., Geballe, T. R., Leggett, S. K., Kirkpatrick, J. D., & Golimowski, D. A. 2006, ApJ, 637, 1067
Burgasser, A. J., Kirkpatrick, J. D., Cutri, R. M., et al. 2000, ApJ, 531, L57
Burningham, B., Cardoso, C. V., Smith, L., et al. 2013, MNRAS, 433, 457
Burrows, A., Hubbard, W. B., Lunine, J. I., & Liebert, J. 2001, Reviews of Modern Physics, 73, 719
Burrows, A., Marley, M., Hubbard, W. B., et al. 1997, ApJ, 491, 856
Caballero, J. A. 2009, A&A, 507, 251
Casali, M., Adamson, A., Alves de Oliveira, C., et al. 2007, A&A, 467, 777
Cepa, J., Aguiar, M., Escalera, V. G., et al. 2000, in Proc. SPIE, Vol. 4008, Optical and IR Telescope Instrumentation and Detectors, ed. M. Iye & A. F. Moorwood, 623–631
Chambers, K. C., Magnier, E. A., Metcalfe, N., et al. 2016, arXiv e-prints, arXiv:1612.05560
Chauvin, G., Lagrange, A.-M., Zuckerman, B., et al. 2005, A&A, 438, L29
Chen, X., Arce, H. G., Zhang, Q., et al. 2013, ApJ, 768, 110
Close, L. M., Zuckerman, B., Song, I., et al. 2007, ApJ, 660, 1492
Cortés-Contreras, M., Béjar, V. J. S., Caballero, J. A., et al. 2017, A&A, 597, A47
Cruz, K. L., Kirkpatrick, J. D., & Burgasser, A. J. 2009, AJ, 137, 3345
Cruz, K. L. & Reid, I. N. 2002, AJ, 123, 2828
Damiani, F., Prisinzano, L., Pillitteri, I., Micela, G., & Sciortino, S. 2019, A&A, 623, A112
David, T. J., Hillenbrand, L. A., Gillen, E., et al. 2019, ApJ, 872, 161
Dawson, P., Scholz, A., & Ray, T. P. 2011, MNRAS, 418, 1231
Dawson, P., Scholz, A., Ray, T. P., et al. 2013, MNRAS, 429, 903
Day-Jones, A. C., Pinfield, D. J., Ruiz, M. T., et al. 2011, MNRAS, 410, 705
Deacon, N. R., Liu, M. C., Magnier, E. A., et al. 2014, ApJ, 792, 119
Deacon, N. R., Liu, M. C., Magnier, E. A., et al. 2012a, ApJ, 757, 100
Deacon, N. R., Liu, M. C., Magnier, E. A., et al. 2012b, ApJ, 755, 94
Deacon, N. R., Schlieder, J. E., & Murphy, S. J. 2016, MNRAS, 457, 3191
Delgado-Donate, E. J., Clarke, C. J., Bate, M. R., & Hodgkin, S. T. 2004, MNRAS, 351, 617
Dupuy, T. J. & Liu, M. C. 2012, ApJS, 201, 19
Dupuy, T. J., Liu, M. C., Allers, K. N., et al. 2018, AJ, 156, 57
Dupuy, T. J., Liu, M. C., & Ireland, M. J. 2014, ApJ, 790, 133
Elias, J. H., Joyce, R. R., Liang, M., et al. 2006, in Proc. SPIE, Vol. 6269, Society of Photo-Optical Instrumentation Engineers (SPIE) Conference Series, 62694C
Elliott, P. & Bayo, A. 2016, MNRAS, 459, 4499
Engle, S. G. & Guinan, E. F. 2011, in Astronomical Society of the Pacific Conference Series, Vol. 451, 9th Pacific Rim Conference on Stellar Astrophysics, ed. S. Qain, K. Leung, L. Zhu, & S. Kwok, 285
Epchtein, N., de Batz, B., Capoani, L., et al. 1997, The Messenger, 87, 27
Faherty, J. K., Burgasser, A. J., West, A. A., et al. 2010, AJ, 139, 176
Fang, Q., Herczeg, G. J., & Rizzuto, A. 2017, ApJ, 842, 123
Feiden, G. A. 2016, A&A, 593, A99
Filippazzo, J. C., Rice, E. L., Faherty, J., et al. 2015, ApJ, 810, 158
Findeisen, K. & Hillenbrand, L. 2010, AJ, 139, 1338
Fischer, D. A. & Marcy, G. W. 1992, ApJ, 396, 178
Freudling, W., Romaniello, M., Bramich, D. M., et al. 2013, A&A, 559, A96
Gaia Collaboration, Brown, A. G. A., Vallenari, A., et al. 2018, A&A, 616, A1
Gaia Collaboration, Prusti, T., de Bruijne, J. H. J., et al. 2016, A&A, 595, A1
Galli, P. A. B., Joncour, I., & Moraux, E. 2018, MNRAS, 477, L50
Gauza, B., Béjar, V. J. S., Pérez-Garrido, A., et al. 2019, MNRAS, 487, 1149
Gauza, B., Béjar, V. J. S., Pérez-Garrido, A., et al. 2015, ApJ, 804, 96
Goldman, B., Marsat, S., Henning, T., Clemens, C., & Greiner, J. 2010, MNRAS, 405, 1140
Goodwin, S. P., Kroupa, P., Goodman, A., & Burkert, A. 2007, Protostars and Planets V, 133
Gorlova, N. I., Meyer, M. R., Rieke, G. H., & Liebert, J. 2003, ApJ, 593, 1074
Hambly, N. C., Collins, R. S., Cross, N. J. G., et al. 2008, MNRAS, 384, 637
Henden, A. & Munari, U. 2014, Contributions of the Astronomical Observatory Skalnate Pleso, 43, 518
Henry, T. J., Jao, W.-C., Winters, J. G., et al. 2018, AJ, 155, 265
Hodgkin, S. T., Irwin, M. J., Hewett, P. C., & Warren, S. J. 2009, MNRAS, 394, 675
Howell, S. B., Sobeck, C., Haas, M., et al. 2014, PASP, 126, 398
Ireland, M. J., Kraus, A., Martinache, F., Law, N., & Hillenbrand, L. A. 2011, ApJ, 726, 113
Irwin, M. J., Lewis, J., Hodgkin, S., et al. 2004, in Proc. SPIE, Vol. 5493, Optimizing Scientific Return for Astronomy through Information Technologies, ed. P. J. Quinn & A. Bridger, 411–422
Kiraga, M. & Stepien, K. 2007, Acta Astron., 57, 149
Kirkpatrick, J. D. 2005, ARA&A, 43, 195
Kirkpatrick, J. D., Dahn, C. C., Monet, D. G., et al. 2001, AJ, 121, 3235
Kirkpatrick, J. D., Reid, I. N., Liebert, J., et al. 1999, ApJ, 519, 802
Kouwenhoven, M. B. N., Goodwin, S. P., Parker, R. J., et al. 2010, MNRAS, 404, 1835
Kraus, A. L. & Hillenbrand, L. A. 2008, ApJ, 686, L111
Kraus, A. L. & Hillenbrand, L. A. 2012, ApJ, 757, 141
Kraus, A. L., Ireland, M. J., Martinache, F., & Hillenbrand, L. A. 2011, ApJ, 731, 8
Kroupa, P. 1995, MNRAS, 277, 1522
Kuzuhara, M., Tamura, M., Ishii, M., et al. 2011, AJ, 141, 119
Lafrenière, D., Jayawardhana, R., & van Kerkwijk, M. H. 2008, ApJ, 689, L153
Larkin, J., Barczys, M., Krabbe, A., et al. 2006, in Proc. SPIE, Vol. 6269, Society of Photo-Optical Instrumentation Engineers (SPIE) Conference Series, 62691A
Launhardt, R., Nutter, D., Ward-Thompson, D., et al. 2010, ApJS, 188, 139
Lawrence, A., Warren, S. J., Almaini, O., et al. 2007, MNRAS, 379, 1599
Lewis, J. R., Irwin, M., & Bunclark, P. 2010, in Astronomical Society of the Pacific Conference Series, Vol. 434, Astronomical Data Analysis Software and Systems XIX, ed. Y. Mizumoto, K.-I. Morita, & M. Ohishi, 91
Lodieu, N. 2013, MNRAS, 431, 3222
Lodieu, N., Dobbie, P. D., & Hambly, N. C. 2011, A&A, 527, A24
Lodieu, N., Hambly, N. C., & Jameson, R. F. 2006, MNRAS, 373, 95
Lodieu, N., Hambly, N. C., Jameson, R. F., & Hodgkin, S. T. 2008, MNRAS, 383, 1385
Lodieu, N., Hambly, N. C., Jameson, R. F., et al. 2007, MNRAS, 374, 372
Lodieu, N., Pérez-Garrido, A., Béjar, V. J. S., et al. 2014, A&A, 569, A120
Lodieu, N., Zapatero Osorio, M. R., Béjar, V. J. S., & Peña Ramírez, K. 2018, MNRAS, 473, 2020
Loutrel, N. P., Luhman, K. L., Lowrance, P. J., & Bochanski, J. J. 2011, ApJ, 739, 81
Lucas, P. W., Roche, P. F., Allard, F., & Hauschildt, P. H. 2001, MNRAS, 326, 695
Luhman, K. L. 2012, ARA&A, 50, 65
Luhman, K. L., Burgasser, A. J., & Bochanski, J. J. 2011, ApJ, 730, L9
Luhman, K. L., Burgasser, A. J., Labbé, I., et al. 2012, ApJ, 744, 135
Luhman, K. L., Herrmann, K. A., Mamajek, E. E., Esplin, T. L., & Pecaut, M. J. 2018, AJ, 156, 76
Luhman, K. L. & Mamajek, E. E. 2012, ApJ, 758, 31
Luhman, K. L., Mamajek, E. E., Allen, P. R., Muench, A. A., & Finkbeiner, D. P. 2009, ApJ, 691, 1265
Luhman, K. L. & Rieke, G. H. 1999, ApJ, 525, 440
Luhman, K. L., Stauffer, J. R., Muench, A. A., et al. 2003, ApJ, 593, 1093
Mace, G. N., Kirkpatrick, J. D., Cushing, M. C., et al. 2013, ApJ, 777, 36
Marcy, G. W. & Chen, G. H. 1992, ApJ, 390, 550
Martín, E. L., Delfosse, X., Basri, G., et al. 1999, AJ, 118, 2466
Martín, E. L., Delfosse, X., & Guieu, S. 2004, AJ, 127, 449
Martin, E. L., Rebolo, R., & Zapatero-Osorio, M. R. 1996, ApJ, 469, 706
Martinez, R. A. & Kraus, A. L. 2019, AJ, 158, 134
McCaughrean, M. J., Close, L. M., Scholz, R.-D., et al. 2004, A&A, 413, 1029
McGovern, M. R., Kirkpatrick, J. D., McLean, I. S., et al. 2004, ApJ, 600, 1020

McLean, I. S., McGovern, M. R., Burgasser, A. J., et al. 2003, ApJ, 596, 561
McMahon, R. G., Banerji, M., Gonzalez, E., et al. 2013, The Messenger, 154, 35
Modigliani, A., Goldoni, P., Royer, F., et al. 2010, in Proc. SPIE, Vol. 7737, Observatory Operations: Strategies, Processes, and Systems III, 773728
Moorwood, A., Cuby, J.-G., & Lidman, C. 1998, The Messenger, 91, 9
Murray, D. N., Burningham, B., Jones, H. R. A., et al. 2011, MNRAS, 414, 575
Mužić, K., Radigan, J., Jayawardhana, R., et al. 2012, AJ, 144, 180
Naud, M.-E., Artigau, É., Malo, L., et al. 2014, ApJ, 787, 5
Ochsenbein, F., Bauer, P., & Marcout, J. 2000, A&AS, 143, 23
Peña Ramírez, K., Béjar, V. J. S., & Zapatero Osorio, M. R. 2016, A&A, 586, A157
Pecaut, M. J. 2016, in IAU Symposium, Vol. 314, Young Stars & Planets Near the Sun, ed. J. H. Kastner, B. Stelzer, & S. A. Metchev, 85–90
Pecaut, M. J. & Mamajek, E. E. 2013, ApJS, 208, 9
Pecaut, M. J. & Mamajek, E. E. 2016, MNRAS, 461, 794
Pecaut, M. J., Mamajek, E. E., & Bubar, E. J. 2012, ApJ, 746, 154
Petrus, S., Bonnefoy, M., Chauvin, G., et al. 2019, arXiv e-prints, arXiv:1910.00347
Pineda, J. S., Hallinan, G., Kirkpatrick, J. D., et al. 2016, ApJ, 826, 73
Pinfield, D. J., Burningham, B., Lodieu, N., et al. 2012, MNRAS, 422, 1922
Preibisch, T., Brown, A. G. A., Bridges, T., Guenther, E., & Zinnecker, H. 2002, AJ, 124, 404
Preibisch, T., Guenther, E., Zinnecker, H., et al. 1998, A&A, 333, 619
Radigan, J., Lafrenière, D., Jayawardhana, R., & Doyon, R. 2009, ApJ, 698, 405
Raghavan, D., McAlister, H. A., Henry, T. J., et al. 2010, ApJS, 190, 1
Rebolo, R., Zapatero Osorio, M. R., Madruga, S., et al. 1998, Science, 282, 1309
Rebull, L. M., Stauffer, J. R., Cody, A. M., et al. 2018, AJ, 155, 196
Reid, I. N., Hawley, S. L., & Gizis, J. E. 1995, AJ, 110, 1838
Reipurth, B. & Mikkola, S. 2012, Nature, 492, 221
Rizzuto, A. C., Ireland, M. J., Dupuy, T. J., & Kraus, A. L. 2016, ApJ, 817, 164
Rizzuto, A. C., Ireland, M. J., & Kraus, A. L. 2015, MNRAS, 448, 2737
Rizzuto, A. C., Ireland, M. J., & Robertson, J. G. 2011, MNRAS, 416, 3108
Rodrigo, C., Solano, E., & Bayo, A. 2012, SVO Filter Profile Service Version 1.0, IVOA Working Draft 15 October 2012
Schmidt, S. J., Hawley, S. L., West, A. A., et al. 2015, AJ, 149, 158
Scholz, R.-D. 2010, A&A, 515, A92
Scholz, R.-D., McCaughrean, M. J., Lodieu, N., & Kuhlbrodt, B. 2003, A&A, 398, L29
Skrutskie, M. F., Cutri, R. M., Stiening, R., et al. 2006, AJ, 131, 1163
Slesnick, C. L., Carpenter, J. M., & Hillenbrand, L. A. 2006, AJ, 131, 3016
Slesnick, C. L., Hillenbrand, L. A., & Carpenter, J. M. 2004, ApJ, 610, 1045
Smith, L. C., Lucas, P. W., Contreras Peña, C., et al. 2015, MNRAS, 454, 4476
Song, I., Zuckerman, B., & Bessell, M. S. 2012, AJ, 144, 8
Stamatellos, D. & Whitworth, A. P. 2009, MNRAS, 392, 413
Stauffer, J. R., Jones, B. F., Backman, D., et al. 2003, AJ, 126, 833
Sutherland, W., Emerson, J., Dalton, G., et al. 2015, A&A, 575, A25
Taylor, M. B. 2005, in Astronomical Society of the Pacific Conference Series, Vol. 347, Astronomical Data Analysis Software and Systems XIV, ed. P. Shopbell, M. Britton, & R. Ebert, 29
Todorov, K., Luhman, K. L., & McLeod, K. K. 2010, ApJ, 714, L84
Tody, D. 1986, in Proc. SPIE, Vol. 627, Instrumentation in astronomy VI, ed. D. L. Crawford, 733
Tody, D. 1993, in Astronomical Society of the Pacific Conference Series, Vol. 52, Astronomical Data Analysis Software and Systems II, ed. R. J. Hanisch, R. J. V. Brissenden, & J. Barnes, 173
Tokovinin, A. & Lépine, S. 2012, AJ, 144, 102
van Dam, M. A., Bouchez, A. H., Le Mignant, D., et al. 2006, PASP, 118, 310
Vernet, J., Dekker, H., D'Odorico, S., et al. 2011, A&A, 536, A105
Walter, F. M., Vrba, F. J., Mathieu, R. D., Brown, A., & Myers, P. C. 1994, AJ, 107, 692
Weinberg, M. D., Shapiro, S. L., & Wasserman, I. 1987, ApJ, 312, 367
Whitworth, A. P. & Stamatellos, D. 2006, A&A, 458, 817
Wilking, B. A., Meyer, M. R., Robinson, J. G., & Greene, T. P. 2005, AJ, 130, 1733
Wizinowich, P. L., Le Mignant, D., Bouchez, A. H., et al. 2006, PASP, 118, 297
Wright, E. L., Eisenhardt, P. R. M., Mainzer, A. K., et al. 2010, AJ, 140, 1868
Wright, E. L., Skrutskie, M. F., Kirkpatrick, J. D., et al. 2013, AJ, 145, 84
Wright, N. J. & Mamajek, E. E. 2018, MNRAS, 476, 381
York, D. G., Adelman, J., Anderson, Jr., J. E., et al. 2000, AJ, 120, 1579
Zacharias, N., Finch, C. T., Girard, T. M., et al. 2013, AJ, 145, 44
Zapatero Osorio, M. R., Béjar, V. J. S., & Peña Ramírez, K. 2017, ApJ, 842, 65
Zapatero Osorio, M. R., Rebolo, R., Martín, E. L., et al. 1997, ApJ, 491, L81

List of Objects

5

Search For Companions in Young Moving Groups

5.1 Introduction

In this chapter, we will present a search for wide substellar companions in four young moving groups (YMGs): β Pictoris (β Pic), Tucana Horologium (THA), TW Hydrae (TWA) and AB Doradus (AB Dor). Figure 5.1 shows the distribution of the members of these YMGs in the sky. These YMGs were selected for several reasons. First of all, they have numerous members ($\gtrsim$100) in the southern hemisphere. They are also close in distance (30–80 pc), which allows us to find very low-mass members within our photometric limiting magnitudes. This close distance also translates into relatively high proper motions for its members, ideal for an astrometric search. Finally, they have different ages, ranging between $\sim$10–150 Myr, allowing us to compare our results between these different stages of their evolution.

5.1.1 AB Doradus

This YMG was named after the young star AB Doradus. It was first proposed by Zuckerman et al. (2004), who identified $\sim$30 candidate members with signs of youth which were moving in the same direction as the star. At the present moment, around 600 members and candidate members have been identified. These members are widely spread in all the sky surface. Their mean heliocentric distance is 30^{+20}_{-10} pc (Gagné & Faherty 2018).

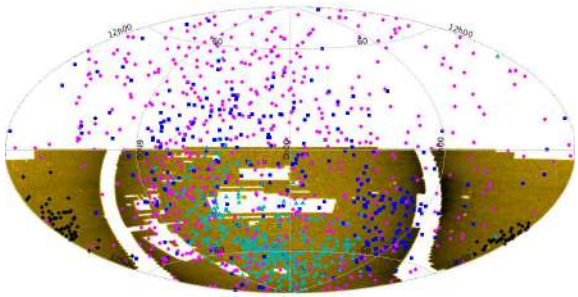

Figure 5.1: Location in the sky of the members of Beta Pictoris (blue squares), Tucana Horologium (light blue triangles), AB Doradus (pink circles) and TW Hydrae (black diamonds). The sky coverage of the VHS is shown in gold colour.

AB Dor is the older YMG in our sample. Its age was proposed to be of ∼50 Myr in its discovery paper by Zuckerman et al. (2004). However, a year later, Luhman et al. (2005) determined that the AB Dor star and also the AB Dor YMG are older than this value, and roughly coeval with the Pleiades (100–125 Myr). Later, Barenfeld et al. (2013) set a lower limit of 110 Myr for its age, based on the contraction times of the K-type members of the association. The more recent work from Bell et al. (2015) obtained an age of 149^{+51}_{-19} Myr based on semi-empirical pre-main-sequence model isochrones fitting.

5.1.2 Tucana-Horologium

The Tucana-Horologium YMG (THA) is formed by two previously independent moving groups: the "Tucanae" moving group, identified by Zuckerman & Webb (2000), and the Horologium moving group, identified by Torres et al. (2000). One year later, Zuckerman et al. (2001b) pointed to the physical association of the two newly-discovered moving groups, as they shared similar space motions, age and heliocentric distance. Around 400 members and candidate members have been identified so far. This YMG is mostly concentrated in the southern hemisphere, and its members are placed at a mean heliocentric distance of 46^{+8}_{-6} pc (Gagné & Faherty 2018).

The ages of the Tucana and Horologium YMGs were proposed to be ∼40 Myr and ∼30 Myr respectively at their discovery. Stelzer & Neuhäuser (2000) determined an age of 10–30 Myr for the Tucanae association based on the X-ray emission of its members. The more recent work by Bell et al. (2015) indicates an age of 45±4 Myr.

5.1.3 β Pictoris

The β Pictoris moving group was named after the star β Pictoris. The first hints of the existence of this moving group were given by Barrado y Navascués et al. (1999), when they discovered two stellar systems which were comoving with the β Pic star. They determined a young age of 20±10 Myr for them. Later, Zuckerman et al. (2001a) identified many more stars which were also moving through space with β Pic, and derived an estimated age of 12^{+8}_{-4} Myr for the YMG, from the location of its members in the H-R diagram. Many later studies have attempted to determine the age of this YMG, obtaining mean age values between 10–40 Myr (see Table 6 in Miret-Roig et al. 2020, and references therein). One of the first ones was performed by Ortega et al. (2002), who estimated a kinematical three-dimensional age of 11.5 Myr, and placed its birthplace in the Scorpius-Centaurus OB association. Much later, Binks & Jeffries (2014) determined an older age of 21±4 Myr, based on the presence of lithium in its members. Bell et al. (2015) also estimated an age of 24±3 Myr from the semi-empirical pre-main-sequence model isochrones fitting. The more recent work by Miret-Roig et al. (2020) based on the dynamical traceback of the β Pic members with *Gaia* obtained a dynamical age of $18.5^{+2.0}_{-2.4}$ Myr. This YMG has more than 300 identified members and candidate members, which are spread on both hemispheres, and placed at a median heliocentric distance of 30^{+20}_{-10} pc (Gagné & Faherty 2018).

5.1.4 TW Hydrae

The TW Hydrae (TWA) association is the youngest YMG in our sample. It was discovered by Kastner et al. (1997), when they identified four stars which were comoving with the T Tauri star TW Hya, and showed signs of youth. They estimated an age of ∼20 Myr for them, as a compromise between their strong X-ray emission that indicated an age roughly or above 20 Myr, and their lithium absorption which indicated an age younger than this. Later, Webb et al. (1999) identified six new members, and proposed a younger age of ∼10 Myr for the YMG, based on the combination of the X-ray emission, the lithium absorption, the Hα emission, the features present in the spectra of the candidate members, and the isochrone fitting of the group. Subsequent studies obtained ages between 8–20 Myr (see Barrado Y Navascués 2006, and references therein) The most recent age estimation from Bell et al. (2015) obtains a value of 10±3 Myr.

At the present moment, almost a hundred candidate members of TWA have been identified. They are concentrated in the southern hemisphere, and their

mean heliocentric distance is 60±10 pc (Gagné & Faherty 2018).

5.2 Search method

The four selected YMGs are widely spread in the sky, some of them having members which entirely cover both hemispheres. For this reason, in this search we decided to cross-match the VHS catalogue with the near-infrared catalogue 2MASS. 2MASS is less deep than VHS or UKIDSS GCS, but its all-sky coverage allows to perform a search in the whole southern hemisphere, where VHS data is available. In the following sub-sections, we will describe in detail the procedure that we followed to perform this search.

5.2.1 YMG members and candidate members compilation

First, we compiled a list of members and candidate members of the four chosen young moving groups, from the literature. The compilation includes objects from López-Santiago et al. (2006); Torres et al. (2006); Messina et al. (2010); Schlieder et al. (2010, 2012a,b); McCarthy & White (2012); Patience et al. (2012); Shkolnik et al. (2012); Moór et al. (2013); Malo et al. (2013, 2014); Ducourant et al. (2014); Kraus et al. (2014); Bell et al. (2015); Best et al. (2015); Gagné et al. (2015b,c); Murphy et al. (2015); Elliott et al. (2016); Messina et al. (2017); Riedel et al. (2017); Schneider et al. (2017); Shkolnik et al. (2017); Gagné et al. (2017); Bardalez Gagliuffi et al. (2018); Gagné & Faherty (2018) Our final compilations include 604 objects in AB Doradus, 344 in Beta Pictoris, 396 in Tucana Horologium, and 95 in TW Hydrae. We also cross-matched the compiled list with *Gaia* DR2 to obtain precise proper motions and parallaxes for those compiled objects with a counterpart in the *Gaia* catalogue.

The compilations include many candidate members whose membership to the associations is uncertain. These objects will be included in the search for companions, but they will not be taken into account for the statistics of the frequency of companions given in Section 5.4.3.

5.2.2 Data download

The first step of the search was to download the data from the VHS catalogue of the corresponding members and candidate members in our compilations. The data download was performed using a webscraper script developed using Python programming language. This script browses the VISTA Science Archive

webpage, logs in using the provided username and password, and performs a list of download queries on it.

Through this script, we required to download the data corresponding to the regions around the positions of each one of the compiled YMG objects, in separate FITS tables. The script also reads the MJD epoch from one of the objects in the region, and adds this information to the name of the downloaded table, as the downloaded tables do not include the epoch information of the observations, and we will need this information for the proper motion calculations.

Wide binaries with separations above 20 000 AU are rare, and a sharp cutoff has been observed at this separation (e.g. Caballero 2009, and references therein). However, some candidate binaries at separations above this cutoff have been found (e.g. Zapatero Osorio & Martín 2004; Caballero 2009; Lodieu et al. 2014; Oelkers et al. 2017; Jiménez-Esteban et al. 2019). In our search, we decided to extend the explored separations up to 50 000 AU to shed light on the very wide population and to avoid a high number of contaminants and chance alignments which may be present for separations above this threshold (Jiménez-Esteban et al. 2019). For the data download, we calculated a maximum radius for the downloaded circular area of the sky corresponding to a physical separation of 50,000 AU for an object placed at a heliocentric distance 2σ closer than the mean distance of each YMG. For all the objects placed further away than this value, which will be the vast majority of the YMG members, the downloaded table will cover larger physical separations than needed. The very few objects which are placed at lower heliocentric distances will not be included in the statistics, as the downloaded area does not completely cover the full 50,000 AU of separations for them.

The mean distances for the selected YMGs were obtained from Gagné & Faherty (2018), and are as follows:

	Mean Dist [pc]	Max downl. area
β Pictoris	30^{+20}_{-10}	$83.4'$
Tucana Horologium	46^{+8}_{-6}	$24.6'$
AB Doradus	30^{+20}_{-10}	$83.4'$
TW Hydrae	60 ± 10	$20.9'$

Table 5.1: Mean distances to the selected YMGs, from Gagné & Faherty (2018), and maximum downloaded area around each member for this work.

Some of the compiled objects were placed in the edges of the VHS coverage

regions, and the circular area of radius 50,000 AU around them is only partially covered in the catalogue. These objects were included in the search, and we looked for companions in the available areas, but they will not be taken into account for the statistics.

5.2.3 Proper motion script

The next step in the procedure is to find all the objects which move with the same apparent movement in the sky as the compiled member at the centre of each downloaded area. For this task, we will cross-correlate the VHS data with the 2MASS catalogue, to compute the proper motion of the sources using the astrometry of the catalogues, and perform the selection. This was achieved using a script based on Python and STILTS.

To estimate the errors in the determination of the proper motions of the VHS–2MASS cross-correlation, we computed the dispersion in the proper motion of the non-moving background objects in each area. We obtained values between 10–20 mas yr^{-1}, depending on the time baseline between the VHS and 2MASS observations in each area (9–19 yr). We adopted twice this value (40 mas yr^{-1}) as a threshold for our proper motion selection of the candidates. In other words, we accepted as candidates all the targets whose VHS–2MASS proper motion measurement differs less than 40 mas yr^{-1} with the primary. This adopted value is conservative, as most of the background objects are very faint sources whose errors in PM are larger than most of our candidates. This conservative threshold prevents us from losing any good candidates, although it will introduce some contaminants (chance alignments with objects with similar but not coincident proper motions) which we will need to filter in following steps.

Most of the YMG members and candidate members in our compilations have relatively high proper motions, as they are close to the Sun. However, some of them have low proper motions, so the astrometric selection of companion candidates is problematic due to the large number of contaminants. We decided to include only members having proper motions of, at least, three times the expected error in the VHS–2MASS proper motion measurements (3×20 mas $yr^{-1} = 60$ mas yr^{-1}). Any YMG member with a proper motion lower than this threshold will not be included in our search.

The step by step procedure of the Proper Motion script is as follows:

1. *Verification of the primary's proper motion.* If the proper motion of the primary is higher than 60 mas yr^{-1}, the search is performed. If the PM is lower than 60 mas yr^{-1}, or there is no PM measurement available, the

search around this object is not performed. The preferred PM taken into account is the *Gaia* measurement. If there is no *Gaia* measurement, the literature PM is used.

2. *Selection of the sky area.* If there is a *Gaia* parallax measurement for the primary, the script calculates the maximum angular separation corresponding to 50,000 AU around the catalogued member. Then, it discards all the objects from the VHS downloaded table whose angular separation is larger than this maximum. If the primary does not have a parallax measurement, the script keeps the whole downloaded sky area around it for the correlation.

3. *Elimination of duplicates.* The VISTA surveys observing strategy implies an overlapping region between the different pawprints. All the sources in these overlapping regions are not blended in the VHS catalogue, and appear as duplicates. In this step, the script performs a STILTS internal match to remove any possible duplicated entries in the VHS tables.

4. *Elimination of faint objects.* The VHS catalogue reaches fainter magnitudes than the 2MASS catalogue. The very faint objects in the VHS catalogue which are not detected in the 2MASS catalogue can lead to mismatches in the cross-correlation. Objects with magnitudes $J > 17$ will not be detected in 2MASS. To avoid this and to optimize the procedure, the scripts selects only the objects with J <17.7 or Ks <17.7 in the VHS downloaded tables, and discards objects fainter than these values. This threshold takes into account possible equal-mass binaries which may be resolved in VHS but not in 2MASS, as the magnitude of the sum of two objects of the same brightness is 0.7 magnitudes below that of each one separately.

5. *First cross-correlation with 2MASS: non-moving objects.* Using STILTS, the script queries the Centre de Données astronomiques de Strasbourg (CDS) X-Match services, which includes all the VizieR and SIMBAD databases, to perform a cross-correlation of the downloaded VHS data with the 2MASS PSC. This first correlation uses a cross-match radius of $0.5''$ to obtain all the non-moving background objects in the area. To avoid possible mismatches, it verifies that the J band photometry of the cross-correlated objects is similar: the difference in the J band photometry between both catalogues must be lower than 0.7 mag for the cross-correlated objects. This difference corresponds to the case of an equal-mass close binary that might be resolved in VHS but not in 2MASS. For

very bright objects (J <12), whose photometry in VHS can be affected by saturation, it just imposes that the object is also bright in 2MASS ($J_{2M} < 12.7$). The objects sucessfully cross-correlated in this step with be set aside.

6. *Computation of the YMG member's expected angular displacement.* The script obtains the VHS epoch from the name of the downloaded table, and the 2MASS epoch from the objects in the first cross-correlation of non-moving objects. Then, using these two epochs and the catalogued YMG member's PM, it calculates the expected total apparent movement of the member in the sky in arcsec. Any possible companion in the area must have moved the same angular distance between the VHS and 2MASS observations. Considering the minimum PM considered and the time baseline between the VHS and 2MASS observations, the minimum angular displacement of the members is $0.5''$–$1.1''$, for an object with a PM of 60 mas yr^{-1}. For a typical PM of the searched members of ∼100–130 mas yr^{-1}, the typical displacement is $0.9''$–$2.5''$.

7. *Second cross-correlation with 2MASS: moving objects.* The script creates a new table with all the objects that were not correlated successfully in the non-moving cross-correlation. Then, it performs a second cross-correlation with the 2MASS PSC through the CDS X-match services. It cross-correlates the objects VHS coordinates against the 2MASS position where the objects should be located if they have moved with the same apparent movement as the central YMG member. The error (cross-match radius) considered in this correlation is 40 mas yr^{-1}, which corresponds to ∼0.4–$0.7''$, depending on the time baseline of each correlation. The cross-matched objects are also required to have a similar J-band photometry in VHS and 2MASS, to discard mismatches and artifacts.

8. *Selection of the PM candidates.* The script creates a final cross-correlation table, linking together the moving and non-moving objects tables. Then, it selects the objects which fulfill the PM selection criteria and creates a table of candidates. This table includes the computed VHS vs. 2MASS proper motions for the selected objects.

9. *Proper Motion diagram creation.* Finally, the script creates a proper motion diagram using the moving and non-moving objects tables. An example of the produced diagrams is shown in Figure 5.2. The script also creates a small text with the main parameters of the cross-correlation and adds it to a log file.

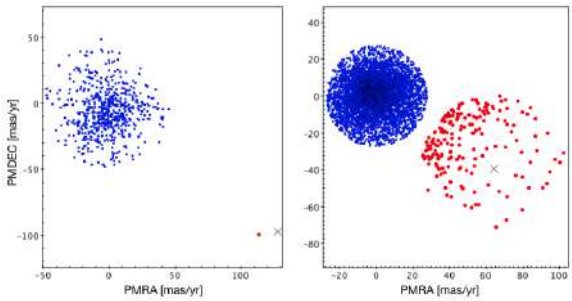

Figure 5.2: Example of the proper motion diagrams obtained through the proper motion script. Left panel shows an example of a β Pic star with a relatively high PM. Right panel shows the result for a β Pic star with lower PM. The catalogued members PM are marked with a cross. PM candidates are shown in red. Non-moving objects are marked in blue.

5.2.4 Photometric selection: Colour selector script

Given that our PM selection was very conservative, this results in a very large number of contaminants in our list of common proper motion companion candidates, as several thousands of candidates were selected. In the next step, we performed a second selection based on the objects J- and K-band photometry, using J versus $J-K$ colour-magnitude diagrams to mark good candidates and reject possible contaminants.

Young objects are usually brighter than their old counterparts, as they are still contracting in their formation following their Hayashi tracks. Some young objects may also appear redder than their old counterparts due to the presence of dust and/or accretion disks surrounding them. Therefore, in this selection, we kept all the objects photometrically brighter and/or redder than this sequence.

Figure 5.3 shows the colour-magnitude selection. In this figure, the photometric field sequence is marked in black, and some known objects from the β Pictoris YMG are shown as red dots, as an example. The grey zones indicate the rejected photometric regions, and the white zones indicate the accepted photometric regions: all the objects in this white zones are considered as candidates and kept for the next steps.

Since many young L-dwarfs are found to be very faint, and red in $J-K$ colour ($J-K > 1.5$), we kept the lower-right region of the diagram, where many already-known young mid-L and late-L objects, as 2M1207 b (Chauvin et al. 2004), VHS1256 b (Gauza et al. 2015), PSO J318 (Liu et al. 2013) or

HR 8799 bcd (Marois et al. 2008), are located. In addition, we decided to keep candidates following the sequence of old field early-T dwarfs, as some young objects as 2M1324+6358 (Looper et al. 2007; Metchev et al. 2008; Gagné et al. 2018), GU Psc b (Naud et al. 2014) and SDSS 1110+0116 (Knapp et al. 2004; Gagné et al. 2015a) are also located in this region. Keeping this zone is problematic, because it is usually highly populated by contaminants (chance alignments with M and earlier-type stars which are placed further away), but we expect to get rid of these contaminants in following steps, through their optical photometry and/or their *Gaia* DR2 astrometry.

To perform the photometric selection, we created a second script using Python. The procedure is as follows:

1. *Computation of the absolute magnitude of the sources.* To obtain the expected absolute magnitudes of the sources, we obtain the heliocentric distance of the central catalogued member through its *Gaia* DR2 parallax, if available. If the member does not have an available parallax measurement, the script uses its spectral type and estimates this distance spectrophotometrically, comparing its J-band magnitude with the theoretical absolute magnitude for its spectral type, using data from Pecaut & Mamajek (2013), Lodieu et al. (2014) and Dupuy & Liu (2012).

2. *Colour selection.* The script performs a colour selection to the candidates selected by proper motion. In this step, we mark those candidates whose M_J versus $J-K$ photometry is compatible with being placed at the same heliocentric distance as the central YMG member. We used the colour cut regions shown in Figure 5.3. They are described as follows:

$$\begin{cases} M_J < 5*(J-K)+2.5, & M_J < 6 \\ (J-K) > 0.73, & 6 < M_J < 10.5 \\ M_J < 5*(J-K)+6.8, & 10.5 < M_J < 13.6 \\ \text{all}, & 13.6 < M_J < 15.6 \\ (J-K) < -0.3 \text{ OR } (J-K) > 1.3, & M_J > 15.6 \end{cases} \tag{5.1}$$

   For bright objects (J <12.5), which may be saturated or within the non-linear regime in VHS, the selection is performed using their 2MASS photometry. For the rest of the objects (J >12.5), it uses the VHS photometry. Objects not having available photometry in any of the J or K bands in their corresponding catalogue are rejected. Objects with adequate photometry are included in a new table and will be kept for the next steps.

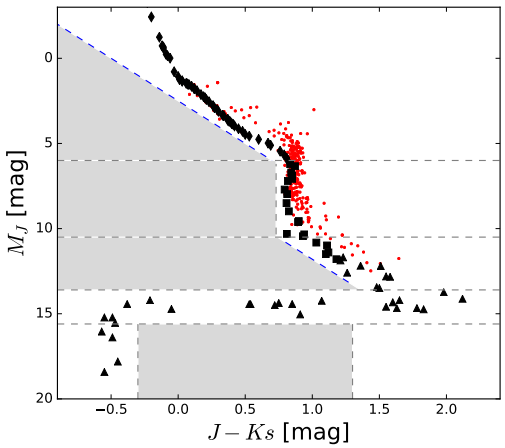

Figure 5.3: Performed colour selection using M_J vs $J-K$ colour-magnitude diagrams. Rejected zones are shaded in grey. The field sequence is marked in black: diamonds from Pecaut & Mamajek (2013), squares from Lodieu et al. (2014), triangles from Dupuy & Liu (2012). Some β Pic compiled members are shown in red, as an example. Their J absolute magnitudes were computed combining their 2MASS J magnitudes and *Gaia* DR2 parallaxes.

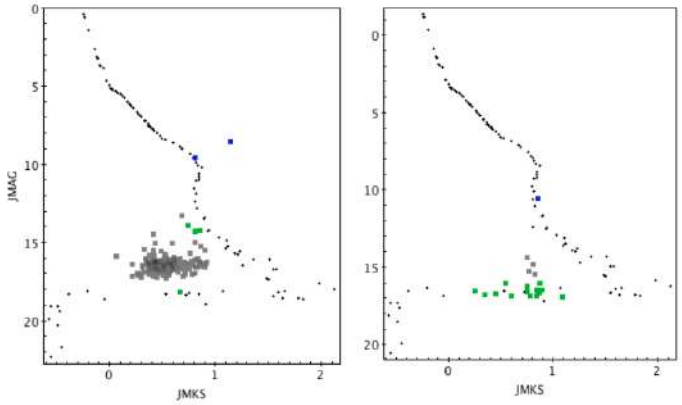

Figure 5.4: Example of the colour-magnitude diagrams obtained through the colour selector script. The field sequence is marked as black dots. Candidates selected using their 2MASS photometry are marked in blue. Candidates selected using their VHS photometry are marked in green. Discarded PM candidates are marked in grey.

3. *Colour-magnitude diagram creation.* Finally, the script creates a colour-magnitude diagram figure showing the field sequence along with the accepted and discarded candidates. Figure 5.4 shows an example of the produced diagrams. The script also creates a small text with the main data of the selection and adds it to a log file.

This step eliminated around two thirds of the candidates that were selected through their PM. However, a few thousands of candidates still remain. Most of these candidates are very faint objects (J >16 mag), which are out of the completitude limits of 2MASS, and whose astrometry in this catalogue is not accurate. Furthermore, as these faint candidates fall in the region corresponding to late-L spectral types in the colour-magnitude selection, the contaminants could not be discriminated in the photometric selection regarding their $J-Ks$ colours.

5.2.5 Gaia DR2 selection

The *Gaia* Data Release 2 provided us with very valuable information to further constrain our candidates easily. Their very precise astrometry (proper motions and parallaxes) helped us to discard many contaminants in our selection. For

this task, we added a new step in our scripts, the *Gaia* selection.

This script cross-correlates the astrometrically and photometrically selected candidates with the *Gaia* DR2 catalogue, and adds their proper motion and parallax information, when available. It also adds the *Gaia* DR2 information of the corresponding YMG central member. Then, it calculates the differences in the proper motion and parallaxes of the pairs (members + candidates), and selects the pairs that are in good agreement with each other, complying with the requirements.

For our selection, we accepted as good candidates all of the pairs whose difference in parallax is lower than 10 times (10σ) the sum of their parallax errors. For the proper motions, we imposed that the difference in both PMRA and PMDEC is lower than 20 mas yr^{-1} each. In addition, those candidates whose primary did not have *Gaia* data but whose *Gaia* parallax was lower than 6.66 (which denote that they are objects placed further than 150 pc and are not YMG members) were also discarded. The conservative thresholds adopted here prevent us from discarding possible companions whose *Gaia* astrometry is not precise (due to binarity or the proximity of other astronomical objects).

In this step, only the pairs having complete and not-matching information in *Gaia* will be discarded. The pairs with matching parallaxes and proper motions, and also the pairs with any component (primary or secondary) lacking proper motion or parallax in *Gaia*, will be kept for the next steps.

In this step, we discarded around 70% of the candidates selected in the previous steps. But a few hundred candidates still remained.

5.2.6 DENIS and AllWISE photometric selections

Those candidates which could not be discriminated using *Gaia* DR2 (including many pairs without available *Gaia* parallax or PM for either the primary or the secondary, and objects with no detection in *Gaia*) were also tested using their optical and mid-IR photometry. For this task, we used DENIS and AllWISE survey data.

The last selector scripts were used to cross-correlate the list of surviving candidates with DENIS and AllWISE databases, and retrieve their I, $w1$ and $w2$ photometry. Then, using the $I - J$ and $w1 - w2$ colours, we discarded the last contaminants. In this step, around 90% of the remaining candidates could be finally discarded. Most of them were very faint objects. Many of these contaminants were extended sources (galaxies) which were faint in the infrared but had a noticeable emission in the optical, and therefore blue $I - J$ colours, and whose not-point-like shape led to uncertain astrometry in the VHS and 2MASS catalogs, simulating a non-existent proper motion. Many others were

very faint objects, whose blue $w1 - w2$ or blue $I - J$ colour pointed towards a much earlier spectral type than expected for them.

However, there were a few tens of objects which passed the Proper Motion and Colour selections, and which could not be discarded either using *Gaia* data or DENIS and AllWISE photometry. These candidates were further investigated. We visually inspected them using available images in VHS, 2MASS, DSS2, WISE or Pan-STARRS; and we retrieved any additional photometric information available in optical and infrared surveys and catalogues. Most of these objects were discarded either by visual inspection (extended sources) or due to having photometric colours which were not compatible with an object placed at the same heliocentric distance as their compiled member. Among these cases, we found several mismatches, objects affected by brighter nearby objects, candidates whose $J - Ks$ colours barely passed the selection but whose photometry from other catalogues indicated a different spectrophotometric distance, and objects with non-reliable astrometry which were not really moving.

As as result, we identified 57 companions candidates in 53 systems in total. The primaries and companion candidates are shown in Tables 5.6 for AB Dor, 5.8 for β Pic, 5.10 for THA, and 5.12 for TWA respectively.

5.3 Spectroscopic follow up observations

The primaries and secondaries without any spectral type measurement in the literature were scheduled for spectroscopic observations, either in the optical or the near-infrared. We observed our targets using the instruments NTT/SofI, WHT/LIRIS, NOT/ALFOSC, duPont/B&C and GTC/OSIRIS. The details on the instrumentation and the data reduction processes can be found in Section **2.3**. The observing log of the targets is shown in Table 5.2.

Similarly to our USco search, the spectral types of the candidates were obtained by comparing their spectra with spectral templates. For the optical spectra, we used the main sequence SDSS templates from Bochanski et al. (2007), for spectral types between M0–L0. For the NIR spectra, we used the IRTF Spectral Library (Cushing et al. 2005; Rayner et al. 2009). The spectral comparisons in low-resolution in the optical are shown in Figures 5.10, 5.11, 5.12 and 5.13 for the AB Dor, β Pic, THA and TWA YMGs respectively. Many of our observed targets show a remarkable Hα emission at 6563Å, which is commonly associated with youth, being a product of chromospheric activity or accretion (Hawley et al. 1996; Gizis et al. 2000; White & Basri 2003; Mohanty & Basri 2003; Muzerolle et al. 2003; Jayawardhana et al. 2003; Mohanty et al. 2005; Caballero et al. 2006). Some of the targets do not show this emission. However, there are reported cases of young objects which do not show any Hα

emission, being this a sufficient but not necessary youth feature (e.g. Martín et al. 2010). The observed targets also show weakened alkali lines, as the KI and NaI doublets (7665 / 7699 Å, and 8183 / 8195 Å, respectively), as a consequence of their low surface gravity. Some of the targets were also observed in high resolution with NOT/ALFOSC, and their comparisons are shown in Figure 5.14. The Li I absorption doublet at 6708 Å can be distinguished only for the target with the latest spectral type in this group, THA368. A close-up display of the Li I wavelength region for this target is shown in the last panel of Figure 5.14.

The spectral comparisons in the NIR are shown in Figures 5.15, 5.16 and 5.17 for the AB Dor, β Pic, and THA YMGs respectively. For the low-resolution comparisons of both optical and NIR, the spectra with the higher resolution, either the targets or the comparison templates, were convolved with gaussians to match the one with the lower resolution. The adopted spectral types for the observed targets are marked and highlighted in boldface in Tables 5.6 for AB Dor, 5.8 for β Pic, 5.10 for THA, and 5.12 for TWA respectively. As in the case of the USco members, the main spectral feature of our later spectral type candidates is ths strong water vapour absorptions at both sides of the H-band wavelength region, which grow in intensity for the latest spectral types. The H-band triangular shape, which is a common feature of youth (e.g. Lucas et al. 2001; Allers & Liu 2013), is not so clearly defined as in the USco members spectra, and can only be remarkably seen in very late spectral type objects, like THA136 and 2MASS 0249−0557 c (see Chapter 6 for this object). A close-up display of the J-band region of the observed NIR targets is shown in Figures 5.18, 5.19 and 5.20 for the AB Dor, β Pic and THA YMGs respectively. For many of our late-M companion candidates, we can distinguish weaker alkali lines in the J-band, as the 1.169 / 1.177 μm and 1.243 / 1.252 μm K I doublets, which is also a sign of youth.

5.4 Results

5.4.1 Explored parameter range and completeness

The distribution of heliocentric distances of the YMG members included in this search are shown in Figure 5.5. The average heliocentric distances for each YMG are shown in Table 5.3. Our search covers separations from $\sim 3''$, corresponding to 120–180 AU for the average heliocentric distances of the YMGs, to 50 000 AU.

Regarding the magnitudes of the candidate companions, our search is complete between magnitudes $J \sim$10–16 mag. Objects brighter than $J \sim$10 mag are

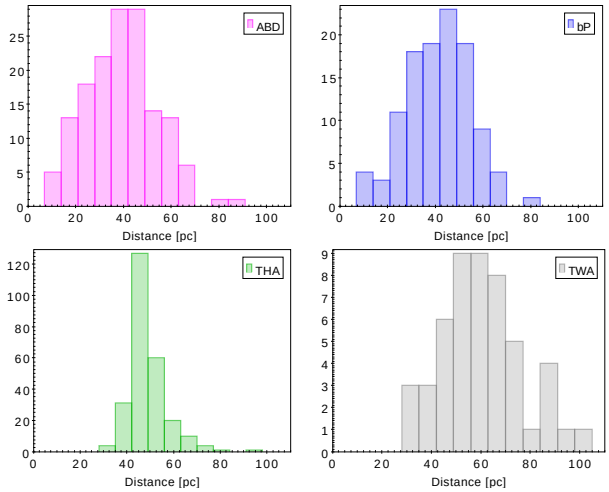

Figure 5.5: Heliocentric distances of the searched compiled members in each YMG, obtained from their *Gaia* DR2 parallaxes.

heavily affected by saturation in VHS, and their astrometry in this catalogue is not reliable, leading to non-reliable PM measurements between VHS–2MASS. Objects fainter than $J \sim$16 mag may have not been detected in our searches because they are out of the completeness range in 2MASS and may not have been detected in the catalogue, or present very high astrometric errors if detected, also leading to non-reliable PM that may prevent their identification as companion candidates. According to the Ames-COND evolutionary models (Allard et al. 2001; Baraffe et al. 2003), for the ages of the four studied YMGs and the average distances of their members, these photometric thresholds imply a similar range of explored masses in the substellar range, although there are greater differences in the explored low-mass stellar range. The mean thresholds for the four studied YMGs are shown in Table 5.3, and they range between 0.008–0.011 $M_{\odot}$ for the low-mass thresholds, and between 0.23–0.45 $M_{\odot}$ for the high-mass ones.

5.4.2 Wide companions in YMGs

The list of the obtained companion candidates for the AB Dor, β Pic, THA and TWA YMGs are presented in Tables 5.6, 5.8, 5.10 and 5.12 respectively, along with some information like their spectral types, parallaxes and PM, and their companionship assessment. More details about the individual candidate systems can be found in Annex B.

Tables 5.7, 5.9, 5.11 and 5.13 show additional parameters of the systems of the four YMGs, like the projected physical separations, masses, effective temperatures and binding energies. We computed the separations in AU for the candidate systems using the *Gaia* parallaxes of the component with the most accurate measurement in each pair. For two of the candidate systems, ABD134 and TWA050, which did not have a parallax measurement in *Gaia* DR2 for any of the components, we used the estimated heliocentric distance of the systems included in the literature. We also computed the luminosities of the components, using their J magnitudes, and the bolometric corrections in the J-band. For objects earlier than M5, we used the bolometric corrections in Pecaut & Mamajek (2013). For the late-M objects, we obtained the bolometric corrections from Lodieu et al. (2011). For the objects later than M9.5, we used the bolometric corrections for young objects in Filippazzo et al. (2015). We also computed the estimated masses and temperatures of the components, using the theoretical evolutionary models from Baraffe et al. (2003) based on the Ames-COND atmospheric models from Allard et al. (2001). The masses and temperatures for the brightest primaries, which were not covered in the Ames-COND models, were obtained using the Pisa pre-main sequence models

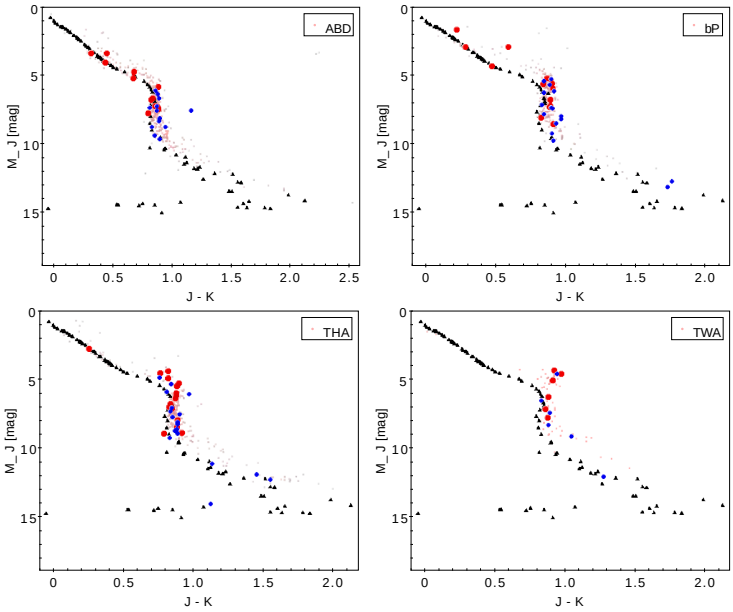

Figure 5.6: M_J vs. $J-K$ colour-magnitude diagrams including the primaries (red) and companions (blue) obtained in each studied YMG. The old-field photometric sequence from Dupuy & Liu (2012), Pecaut & Mamajek (2013) and Lodieu et al. (2014) is shown as black triangles. Some YMG compiled members of each YMG are shown as pink dots. Their colours and absolute magnitudes were obtained combining their 2MASS photometry and their *Gaia* DR2 parallaxes.

(Tognelli et al. 2011). Finally, the tables also include the computed binding energies for the candidate systems.

Figure 5.6 shows the M_J vs. $J-K$ diagrams for the primaries and candidates obtained in the four studied YMGs. Figure 5.7 shows the distribution of the projected physical separation of the candidate companions with J >10 mag. This distribution clearly shows that low-mass candidate companions are more frequently found at shorter separations, and low-mass companions at physical separations larger than a couple of thousands of AU are rare. However, this distribution seems quite flat for wide separations above 5000 AU. This result suggests that this kind of searches can be extended to separations wider than

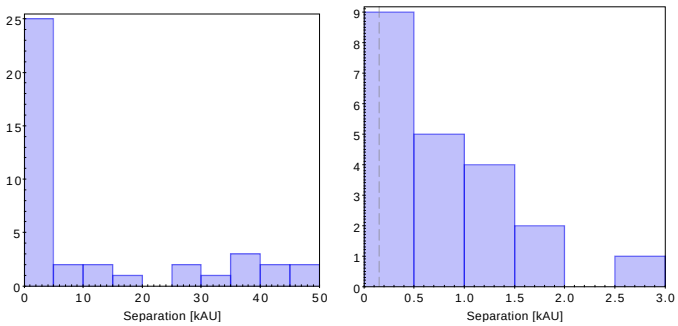

Figure 5.7: Projected physical separations of the companion candidates with J >10 mag. The average completeness lower threshold in separations is shown as a grey dashed line.

50 000 AU, as the number of contaminants does not seem to be very high thanks to the astrometric precision of *Gaia*.

5.4.3 Companion frequencies

In this subsection we compute the companion frequencies for the four studied YMGs separately, and the comparison of these frequencies with the age.

5.4.3.1 AB Dor

From the initial compiled list of 604 members and candidate members of AB Dor, 154 of the objects, in 139 systems, meet the requirements to be included in the statistics. This means, being a confirmed member of AB Dor or having a strong membership probability to the association, having VHS data covering the whole circular sky area of radius 50 000 AU around them, and having proper motions above 60 mas yr^{-1}. Table 5.4 shows the number of compiled members that fulfill the requirements, in AB Dor and the other studied YMGs. Each column in this table indicates the number of compiled objects which fulfill the column requirement in addition to the previous steps. The last two columns indicate the remaining objects and systems which comply with all the requirements.

We found 12 candidate companions with $J > 10$ mag in 11 systems around these AB Dor members which meet the requirements. The candidates range spectral types of M4–M7, and masses between 0.11–0.61 $M_{\odot}$. One of the candidate systems (ABD569) seems to be a chance alignment of two non-bound

objects regarding the astrometry of the components. This results in 11 good candidate companions in 10 systems in this association. Three of them are newly discovered objects, and two more objects were known as candidate members but not related as companions. These numbers translate into **7.2±2.3%** of the AB Dor members having a wide companion in the studied range of magnitudes and separations. This frequency was calculated dividing the number of companion systems by the number of studied systems. The error is estimated considering a poissonian distribution. According to the evolutionary models, all of the found candidates lay in the stellar mass regime, and none of them has a mass of less than 75 M_{Jup}. This translates in lower limit for wide substellar companions of **<1.4%**, with a confident level of 86%. This lower limit is calculated considering also a poissonian distribution.

In addition, we found one wide candidate system with magnitudes J <10 mag (ABD374 + ABD375), and one companion to a catalogued candidate member with dubious membership to the association (ABD080). These two candidates are reported here, but are not included in the companion rate statistics.

5.4.3.2 β Pic

The total number of compiled β Pic members that meet the requirements to be included in the statistics of the search is 109 objects, in 95 systems. We found 9 candidate companions with J>10 mag, in 7 candidate systems, around these catalogued members. Their spectral types range between M4.5–L3, and their masses range between 0.013–0.19 $M_{\odot}$. Three of these candidates were known candidate young object, but they were not previously related as companions. The companion rate in the studied range of magnitudes and separations is **7.4±2.8%** for the β Pic YMG. According to the evolutionary models, 3 of the candidate companions have masses below the stellar/substellar mass boundary. This means a substellar companion rate of **3.2±1.8%**.

In addition, we found 2 candidate companions to two β Pic members which did not have VHS data for the entire circular area of radius 50 000 AU around them. These members (bP040 and bP066) were searched up to ∼27 000 AU and ∼30 000 AU respectively. One of them, bP066, is a planetary mass companion. We also found two candidate wide companion to two β Pic candidate members with ambiguous membership (bP208 and bP288). One of them (bP288) seems to be a chance alignment and not a true companion regarding the astrometry of the components. Furthermore, we found 4 candidate companions with J<10 mag. All these 8 candidates are reported here, but are not included in the companion rate statistics.

5.4.3.3 THA

From the initial compiled list of 396 members and candidate members of THA, 281 members in 267 systems meet the requirements to be included in the statistics. We found 11 good candidate companions with J>10 mag around these catalogued members, and 2 suspected but uncertain candidate companions. The spectral types of the candidate companions range between M3.5–L3, and their masses range between 0.011–0.28 $M_{\odot}$. Six of these objects were known as young candidate members, but they were not related as companions. The two uncertain candidate companions are newly discovered objects. The corresponding companion rate is **4.1±1.2%**, which could increase to 4.9±1.4% if the two uncertain candidate companions are in fact true companions. According to the pre-main sequence evolutionary models, 2 of the good candidate companions are substellar, and also the 2 uncertain companion candidates. This translates to a substellar companion rate of **0.7±0.5%**, which could increase to 1.5±0.7% if the uncertain candidate companions are confirmed.

In addition, we found 2 candidate companions to two ambiguous members of THA (THA051 and THA271). One of them, THA271, is also an uncertain companion, and would also be substellar if it belongs to the THA YMG. We also found 3 candidate companions with J<10 mag. All these 5 candidates are reported here, but are not included in the companion rate statistics.

5.4.3.4 TWA

The total number of compiled TWA members that meet the requirements to be included in the statistics of the search is 55 objects, in 47 systems. We found 5 candidate companions with J>10 mag around these catalogued members. One of the candidate companions (TWA023) seems to be a chance alignment and not a really bound pair. Another of the candidates is affected by a strong extinction, and would be brighter than J=10 mag if corrected. Therefore, we obtained 3 good candidate companions. One of them is a newly discovered object, and another one is a previously known TWA candidate member, but it was not related as a companion. The spectral types of the candidates range between M5.5–M8.5, and their masses range between 0.026–0.11 $M_{\odot}$. The corresponding companion rate in the studied range of magnitudes and separations is **6.4±3.7%**. According to the evolutionary models, 2 of these candidate companions are likely substellar. Hence the substellar companion rate is **4.3±3.0%**.

In addition, we found 2 candidate companions with J<10 mag. These candidates are reported here, but are not included in the companion rate statistics.

5.4.3.5 Comparison of the companion frequencies with the age

Table 5.5 shows the obtained companion rates for the YMGs studied in this work. We find very small companion rates, pointing to the fact that wide low-mass systems are rare, especially for substellar companions, where the obtained rates are lower or similar to 5% for all ages. We find a trend in the frequency of wide substellar companions with the age, and the youngest moving groups present higher companion rates. However, the errors in the frequencies are relatively high, due to the relatively low number of found companions, and this result should be treated with caution.

To compare these results with our search in the Upper Scorpius association, we considered only the substellar candidate companions at separations lower than 9000 AU. To perform the statistics, we included all the catalogued members with available VHS data up to 9000 AU. We obtained 1 companion in TWA, 3 companions in β Pic, 1 companion in THA, and 0 companions in AB Dor. This leads to frequencies of 2.1±2.1% in TWA, 3.0±1.7% in β Pic, 0.4±0.4% in THA, and <0.7% in AB Dor. Our result from the USco search was 1.8±0.4%. We observe that the frequencies are higher for the youngest groups, namely USco, TWA and β Pic, although the errors in the frequencies are very high, as the number of found objects is too low to constitute a statistically significant result.

A previous study by Gauza (2016) obtained a frequency for ultra-cool wide companions to old-field stars at physical projected separations larger than 50–100 AU of 0.5±0.1%, also using VHS data. Another study by Deacon et al. (2014) identified 88 wide M- and L-type companions to a sample of more than 87 000 stars at separations wider than 300 AU, using Pan-STARRS and 2MASS. This translates into a frequency of 0.10±0.01% for the studied range of masses and separations. We find significantly higher companion rates in our young stars sample, showing that the frequency of wide low-mass companions is higher for young stars than in the case of their old counterparts. This can be explained by the dynamical evolution of these systems, which have low binding energies and can be disrupted by stellar encounters during their lifetimes. It may also be due to biases in the detection of substellar companions at older ages, when they become fainter in their evolution. We note that our faintest and less massive companions, which are in the planetary-mass regime, will have temperatures of ∼200–500 K at the Solar age (within the Y dwarf spectral type), and hence they will be very faint to be detected with current facilities. The future operations of JWST and Euclid satellites may shed light on the frequency of these very cold super-Jupiter companions at old ages.

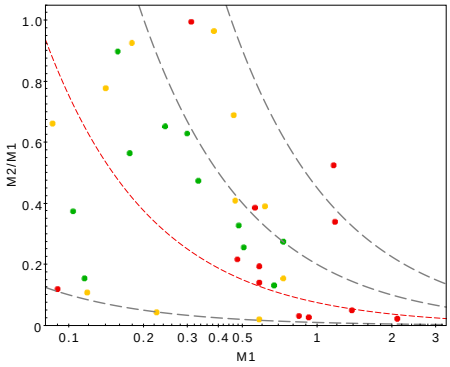

Figure 5.8: Mass-ratio vs. primary mass for the wide companions with J >10 mag. Systems with suspected close-binary components are not included. Wide companions with separations below 1000 AU are marked in green. Companions with separations between 1000–10 000 AU are marked in yellow. Companions with separations wider than 10 000 AU are marked in red. Companion isomasses of 0.010 $M_\odot$, 0.2 $M_\odot$ and 0.45 $M_\odot$ are marked as grey dashed lines, from bottom to top. The substellar mass boundary at 0.075 $M_\odot$ is marked as a red dashed line.

5.4.4 Comparison with theoretical formation scenarios

As we have described in the previous section, we find that low-mass companions at wide separations are rare. This frequency seems to be higher at young ages compared to the field. We also find a decreasing number of companions at larger separations. On the contrary to close binaries (e.g. Cortés-Contreras et al. 2017), we do not find a tendency towards equal-mass binaries for low-mass primaries, and the mass-ratio distribution seems to be uniform. Figure 5.8 shows the mass-ratio of the wide binaries compared to the mass of the primary. This indicates that a companion of any mass may be formed at any of the separations, in the studied range of masses and separations. We find that the mass function of the companions increases towards low masses and can be represented by a power-law ($dN/dm \sim m^{\alpha}$) with index $\alpha = -1$. This distribution does not show any noticeable change in the substellar mass boundary. These results are compatible with a core or disk fragmentation scenario for the formation of wide binaries. However, in the core fragmentation scenario we would not expect binaries to form with separations wider than ∼10 000 AU, which corresponds to the typical size of star-forming cores (Ward-Thompson et al. 2007). One possibility for these very wide systems above 10 000

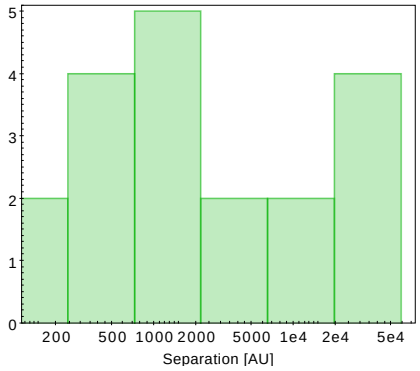

Figure 5.9: Separation distribution for the wide systems including at least one known or suspected close-binary component.

AU is the formation during cluster dissolution, in which objects that are initially unbound at birth may form a binary as their primordial star cluster dissipates, if they are close in space and their velocities are similar (Kouwenhoven et al. 2010). Another possibility is the dynamical interaction with other members of the star-forming region (e.g. Weinberg et al. 1987; Close et al. 2007), in which wide companions would have formed in a more compact configuration and would have been pushed later to wider separations or even ejected.

Many wide companions are found to be part of triple systems, in which two of the components form a close binary and the third component is placed at a wide separation from them (Law et al. 2010; Allen et al. 2012). Reipurth & Mikkola (2012) proposed that these systems are formed at shorter separations, and the wide component migrates to a wider orbit due to dynamical interactions between the three bodies. Their simulations found that many of these triple systems do not reach a stable configuration with time and are eventually disrupted. Most of the stable configurations have a close binary with a separation between 10–100 AU, and a wide companion with a separation between 200–10 000 AU, with a peak at 1000–2000 AU. Stable triple systems with wide companions at separations above 10 000 AU (up to $2{\cdot}10^6$ AU) are also found, although they are rare. We selected the wide systems found in our search in which one of the components is a known or suspected close binary, to compare the distribution of separations with the results from Reipurth & Mikkola (2012). Figure 5.9 shows the obtained distribution, which is compatible with

their results, and which shows a peak at ∼1000 AU. Our distribution shows a high number of systems with separations wider than 20 000 AU. These systems may be unstable systems in the process of disruption according to the results in Reipurth & Mikkola (2012) for ages between 10–100 Myr.

Name	RA	DEC	Range	Instrument	Date	Grating	Slit	Expt
THA023c	00:30:25.18	−62:36:03.8	NIR	NTT/SofI	02 Nov 2018	GB, GR	1″	4x30s, 4x30s
THA23	00:30:25.72	−62:36:01.5	NIR	NTT/SofI	02 Nov 2018	GB, GR	1″	4x30s, 4x30s
bP40	02:01:46.70	+01:17:16.2	OPT	NOT/ALFOSC	02 Oct 2018	gr5, gr17	1″	2x30s, 2x300s
bP41	02:01:46.90	+01:17:06.0	OPT	NOT/ALFOSC	02 Oct 2018	gr5, gr17	1″	2x30s, 2x300s
THA99	02:07:01.76	−44:06:38.0	NIR	NTT/SofI	22 Jun 2018	GB, GR	1″	4x120s, 4x120s
THA99c	02:07:01.98	−44:06:44.4	NIR	NTT/SofI	22 Jun 2018	GB, GR	1″	4x120s, 4x120s
ABD49	02:10:53.46	−46:03:51.2	NIR	NTT/SofI	02 Nov 2018	GB, GR	1″	4x120s, 4x120s
ABD50	02:10:55.38	−46:03:58.7	NIR	NTT/SofI	02 Nov 2018	GB, GR	1″	4x60s, 4x60s
bP61	02:39:48.33	−42:53:05.2	NIR	NTT/SofI	02 Nov 2018	GB, GR	1″	4x30s, 4x30s
bP61	02:39:48.33	−42:53:05.2	OPT	DuPont/B&C	02 Oct 2019	600/7500	1″	1800s
THA136	02:40:12.09	−53:05:52.7	NIR	NTT/SofI	21 Jun 2018	GB, GR	1″	4x300s, 4x300s
bP066c	02:49:54.36	−05:58:01.5	NIR	NTT/SofI	04 Nov 2018	GB, GR	1″	4x600s, 4x300s
bP066c	02:49:54.36	−05:58:01.5	OPT	GTC/OSIRIS	27 Jan 2019	R500R	0.8″	4x1600s
THA158	02:54:34.77	−51:08:28.8	NIR	NTT/SofI	22 Jun 2018	GB, GR	1″	4x150s, 4x150s
ABD072c	02:54:52.21	−07:09:24.2	NIR	NTT/SofI	04 Nov 2018	GB, GR	1″	4x60s, 4x60s
ABD072c	02:54:52.21	−07:09:24.2	OPT	NOT/ALFOSC	02 Oct 2018	gr5, gr17	1″	2x120s, 2x900s
ABD72	02:54:52.47	−07:09:25.6	NIR	NTT/SofI	04 Nov 2018	GB, GR	1″	4x60s, 4x60s
ABD72	02:54:52.47	−07:09:25.6	OPT	NOT/ALFOSC	02 Oct 2018	gr5, gr17	1″	4x150s, 4x150s
ABD80	03:11:42.40	−15:37:18.4	OPT	NOT/ALFOSC	02 Oct 2018	gr17	1″	2x900s
ABD080c	03:11:42.69	−15:37:32.7	OPT	NOT/ALFOSC	02 Oct 2018	gr5, gr17	1″	2x30s, 2x900s
THA362	03:29:03.801	−48:03:36.59	NIR	NTT/SofI	02 Nov 2018	GB, GR	1″	4x150s, 4x150s
THA362	03:29:03.801	−48:03:36.59	OPT	DuPont/B&C	24 Mar 2019	600/7500	1″	600s
THA363	03:29:04.353	−48:03:33.98	NIR	NTT/SofI	02 Nov 2018	GB, GR	1″	4x120s, 4x120s
THA363	03:29:04.353	−48:03:33.98	OPT	DuPont/B&C	24 Mar 2019	600/7500	1″	600s
THA364	03:48:40.509	−37:38:19.98	NIR	NTT/SofI	02 Nov 2018	GB, GR	1″	4x30s, 4x30s
THA367	04:08:22.26	−27:44:39.9	OPT	NOT/ALFOSC	02 Oct 2018	gr5, gr17	1″	2x120s, 2x600s
THA368	04:08:22.37	−27:44:34.4	OPT	NOT/ALFOSC	02 Oct 2018	gr5, gr17	1″	2x120s, 2x600s
ABD510	06:02:21.074	−13:55:17.47	NIR	NTT/SofI	03 Nov 2018	GB, GR	1″	4x120s, 4x120s
ABD510	06:02:21.074	−13:55:17.47	OPT	DuPont/B&C	25 Mar 2019	600/7500	1″	2x300s
ABD168	06:02:21.90	−13:55:32.5	NIR	NTT/SofI	03 Nov 2018	GB, GR	1″	4x12s, 4x12s
ABD511	06:02:25.913	−13:56:39.99	NIR	NTT/SofI	04 Nov 2018	GB, GR	1″	4x150s, 4x150s
ABD511	06:02:25.913	−13:56:39.99	OPT	NOT/ALFOSC	02 Oct 2018	gr5	1″	2x120s
bP141	08:22:47.40	−57:26:53.0	NIR	NTT/SofI	03 Nov 2018	GB, GR	1″	4x30s, 4x120s
bP141c	08:22:47.87	−57:26:45.1	NIR	NTT/SofI	03 Nov 2018	GB, GR	1″	4x30s, 4x120s
bP141c	08:22:47.87	−57:26:45.1	OPT	DuPont/B&C	24 Mar 2019	600/7500	1″	900s
TWA23	11:03:51.66	−37:11:48.3	OPT	DuPont/B&C	24 Mar 2019	600/7500	1″	2x1200
TWA023c	11:04:07.27	−37:06:12.0	OPT	DuPont/B&C	24 Mar 2019	600/7500	1″	2x1800s
ABD548	11:21:59.825	−74:27:48.45	NIR	NTT/SofI	03 Nov 2018	GB, GR	1″	4x150s, 4x150s
ABD548	11:21:59.825	−74:27:48.45	OPT	DuPont/B&C	25 Mar 2019	600/7500	1″	2x900s
ABD548c	11:22:00.37	−74:28:10.5	NIR	NTT/SofI	03 Nov 2018	GB, GR	1″	4x150s, 4x150s
ABD548c	11:22:00.37	−74:28:10.5	OPT	DuPont/B&C	25 Mar 2019	600/7500	1″	600s
ABD556	14:15:41.498	−77:43:06.56	OPT	DuPont/B&C	24 Mar 2019	600/7500	1″	2x600s
ABD557	14:15:42.072	−77:42:46.73	OPT	DuPont/B&C	24 Mar 2019	600/7500	1″	2x600s
ABD559	14:41:07.109	−43:57:01.40	OPT	DuPont/B&C	24 Mar 2019	600/7500	1″	600s
ABD560	14:41:07.502	−43:57:01.67	OPT	DuPont/B&C	24 Mar 2019	600/7500	1″	600s
ABD569	16:06:07.018	−72:00:47.62	OPT	DuPont/B&C	25 Mar 2019	600/7500	1″	2x300s
ABD569c	16:07:10.09	−71:51:01.7	OPT	DuPont/B&C	25 Mar 2019	600/7500	1″	3x1200s
bP314	17:02:09.319	−67:34:46.27	NIR	NTT/SofI	02 Nov 2018	GB, GR	1″	4x120s, 4x120s
bP314	17:02:09.319	−67:34:46.27	OPT	DuPont/B&C	24 Mar 2019	600/7500	1″	2x600s
bP315	17:02:09.818	−67:34:33.84	NIR	NTT/SofI	02 Nov 2018	GB, GR	1″	4x120s, 4x120s
bP315	17:02:09.818	−67:34:33.84	OPT	DuPont/B&C	24 Mar 2019	600/7500	1″	2x600s
ABD316c	19:00:16.32	−28:37:53.1	NIR	NTT/SofI	04 Nov 2018	GB, GR	1″	4x120s, 4x120s
ABD587c	19:18:44.38	−68:59:53.4	OPT	DuPont/B&C	24 Mar 2019	600/7500	1″	2x600s
ABD587c	19:18:44.38	−68:59:53.4	OPT	DuPont/B&C	25 Mar 2019	600/7500	1″	2x600s
ABD587A	19:18:48.816	−69:10:22.45	OPT	DuPont/B&C	24 Mar 2019	600/7500	1″	600s
ABD587B	19:18:48.816	−69:10:22.45	OPT	DuPont/B&C	24 Mar 2019	600/7500	1″	600s
bP208	19:22:34.09	−54:29:18.1	NIR	NTT/SofI	03 Nov 2018	GB, GR	1″	4x120s, 4x120s
bP208	19:22:34.09	−54:29:18.1	OPT	DuPont/B&C	25 Mar 2019	600/7500	1″	900s
bP208c	19:22:34.14	−54:29:21.6	NIR	NTT/SofI	03 Nov 2018	GB, GR	1″	4x120s, 4x120s
bP208c	19:22:34.14	−54:29:21.6	OPT	DuPont/B&C	25 Mar 2019	600/7500	1″	900s
THA273c	20:42:16.24	−55:52:07.4	NIR	NTT/SofI	21 Jun 2018	GB, GR	1″	4x120s, 4x120s
THA273	20:43:04.52	−55:47:11.5	NIR	NTT/SofI	21 Jun 2018	GB, GR	1″	4x150s, 4x150s
THA281	21:12:15.99	−81:28:45.3	NIR	NTT/SofI	02 Nov 2018	GB, GR	1″	4x120s, 4x120s
bP257c2	21:19:20.28	−81:45:44.7	NIR	NTT/SofI	02 Nov 2018	GB, GR	1″	4x120s, 4x120s
ABD344c	21:47:15.90	−48:02:38.9	NIR	NTT/SofI	22 Jun 2018	GB, GR	1″	4x120s, 4x120s
ABD344c	21:47:15.90	−48:02:38.9	OPT	DuPont/B&C	25 Mar 2019	600/7500	1″	300s
bP264c	21:55:17.38	−00:46:23.1	NIR	NTT/SofI	22 Jun 2018	GB, GR	1″	4x120s, 4x120s
bP264c	21:55:17.38	−00:46:23.1	OPT	NOT/ALFOSC	02 Oct 2018	gr5, gr17	1″	2x60s, 2x900s
bP264	21:55:17.41	−00:45:47.8	OPT	NOT/ALFOSC	02 Oct 2018	gr5, gr17	1″	2x60s, 2x900s
THA333	23:27:09.60	−85:15:21.0	NIR	NTT/SofI	22 Jun 2018	GB, GR	1″	4x120s, 4x120s

Table 5.2: Observations log for YMGs candidate systems.

	Av. Dist. [pc]	SD	Av. mass range [$M_\odot$]
TW Hydrae	60	16	$\sim$ 0.250–0.008
β Pictoris	41	13	$\sim$ 0.230–0.009
Tucana Horologium	49	8	$\sim$ 0.400–0.011
AB Doradus	40	16	$\sim$ 0.450–0.020
USco*	146	23	$\sim$ 0.200–0.010

Table 5.3: Average heliocentric distances of the studied YMGs, and explored mass range for the average distance. Heliocentric distances are obtained from the *Gaia* DR2 parallaxes of the searched members. Mass ranges for the YMGs are obtained using the Ames-COND evolutionary models (Allard et al. 2001; Baraffe et al. 2003). (*)The data from the search in the USco association are also included for comparison.

YMG	Compil.	Available in VHS	PM>60 mas yr^{-1}	Strong memb.	50k coverage	Systems
AB Dor	604	240	182	168	**154**	**139**
THA	396	353	313	285	**281**	**267**
β Pic	344	191	147	122	**109**	**95**
TWA	95	92	66	61	**55**	**47**

Table 5.4: Compiled members in each YMG which fulfill the requirements for the statistics. Each column indicates the number of objects fulfilling the column requirement plus the previous columns requirements. The last columns indicate the number of objects and systems which fulfill all the requirements.

	Age [Myr][a]	Total comp.	Substellar comp.	n[b]
TW Hydrae	10±3	6.4±3.7%	4.3±3.0%	47
β Pictoris	24±3	7.4±2.8%	3.2±1.8%	95
Tucana Horologium	45±4	4.1±1.2%	0.7±0.5%	267
AB Doradus	149^{+51}_{-19}	7.2±2.3%	<1.4%	139
USco*	5–10 [c]	3.2±0.5%*	1.8±0.4%*	1195

Table 5.5: Wide companion rates for the 4 studied YMGs. The results from the search in the USco association in Chapter 3 are also included for comparison. *(a)* Ages from Bell et al. (2015). *(b)* Number of searched compiled systems in the statistics. *(c)* Age range from David et al. (2019). *(*)* These results correspond to the search up to a separation of 9000 AU only.

ID	RA	DEC	Jmag[a]	Sep ['/]	SpT OPT	Ref[b]	SpT NIR	Ref[b]	Parallax [mas][c]	pmra [mas yr^{-1}][c]	pmdec [mas yr^{-1}][c]	Comp?
ABD50	02:10:55.38	−46:03:58.7	9.288 ±0.021	21.4	K3	2	**K5–K7**	1	12.2275 ±0.0905	56.249 ±0.123	−26.663 ±0.124	y
ABD49	02:10:53.46	−46:03:51.2	11.228 ±0.021	–	–		**M5**	1	11.1389 ±0.5377*	50.897 ±0.668*	−15.872 ±0.683*	y
ABD72	02:54:52.47	−07:09:25.6	9.999 ±0.025	4.1	**M3**	1	**M4**	1	21.5234 ±0.0666	38.938 ±0.149	−55.285 ±0.13	y
ABD072c	02:54:52.21	−07:09:24.2	12.072 ±0.045		**M5**	1	**M5.5**	1	21.3807 ±0.0896	34.261 ±0.194	−64.692 ±0.165	y
ABD080c	03:11:42.69	−15:37:32.7	9.127 ±0.026	15.0	**M3**	1	–	–	42.5635 ±0.0417	103.102 ±0.07	−182.07 ±0.081	y ABD?
ABD80	03:11:42.40	−15:37:18.4	11.448 ±0.027		**M5**	1	–	–	42.4888 ±0.0786	103.732 ±0.121	−177.256 ±0.133	y ABD?
ABD134	05:11:09.68	−04:10:54.4	7.807 ±0.021	218.9	G0	3	–	–	–	15.0±1.6[†]	−55.3±1.6[†]	y?
ABD134c2	05:10:55.05	−04:10:56.3	11.649 ±0.023		–		–	–	–	19.3±4.1[†]	−52.8±4.2[†]	y?
ABD168	06:02:21.90	−13:55:32.5	8.439 ±0.021	19.1	K4	5	**M0**	1	22.1507 ±0.0406	−6.383 ±0.074	−92.849 ±0.081	y
ABD510	06:02:21.074	−13:55:17.47	11.560 ±0.023		**M5**	1	**M6**	1	21.3539 ±0.1806	−5.704 ±0.348	−91.182 ±0.34	y
ABD511	06:02:25.913	−13:56:39.99	12.6273 ±0.0009	108.6	**M6.5**	1	**M6.5**	1	22.2525 ±0.1106	−8.153 ±0.222	−83.786 ±0.227	y
ABD548c	11:22:00.37	−74:28:10.5	9.817 ±0.026	22.4	**M3**	1	–	–	–	−70.9±7.8[†]	−2.7±7.8[†]	y?
ABD548	11:21:59.825	−74:27:48.45	12.087 ±0.043		**M4.5**	1	**M4**	1	15.8176 ±0.0528	−65.613 ±0.1	−4.005 ±0.087	y?
ABD556	14:15:41.498	−77:43:06.56	11.067 ±0.022	19.9	**M4**	1	–	–	17.2777 ±0.0437	−66.183 ±0.068	−61.653 ±0.065	y
ABD557	14:15:42.072	−77:42:46.73	11.135 ±0.021		**M4**	1	–	–	17.1374 ±0.0429	−66.013 ±0.063	−63.294 ±0.062	y
ABD559	14:41:07.109	−43:57:01.40	9.721 ±0.039	4.1	**M5**	1	–	–	33.6184 ±0.1807	−131.499 ±0.398	−201.809 ±0.26	y
ABD560	14:41:07.502	−43:57:01.67	11.018 ±0.032		**M7**	1	–	–	34.7144 ±0.1538	−120.846 ±0.264	−190.405 ±0.182	y
ABD569	16:06:07.018	−72:00:47.62	10.744 ±0.024	652.9	**M4**	1	–	–	17.0387 ±0.0303	−43.685 ±0.04	−80.904 ±0.051	n?
ABD569c	16:07:10.09	−71:51:01.7	14.100 ±0.002		**M5**	1	–	–	–	−34.3±8.7[†]	−38.1±8.7[†]	n?
ABD316	19:01:06.04	−28:42:50.4	7.463 ±0.018	718.6	G1	2	–	–	15.2679 ±0.042	5.327 ±0.083	−95.094 ±0.076	y??
ABD316c	19:00:16.32	−28:37:53.1	10.134 ±0.023		–		**K5–K7**	1	16.1232 ±0.0533	−5.146 ±0.09	−107.219 ±0.078	y??
ABD587c	19:18:44.38	−68:59:53.4	11.679 ±0.023	626.0	**M3**	1	–	–	–	22.3±14.1[†]	−83.6±14.1[†]	y?
ABD587	19:18:48.816	−69:10:22.45	11.495 ±0.033*	–	**M6**	1	–	–	16.1574 ±0.0598	14.955 ±0.066	−92.226 ±0.089	y?
ABD587	–	–	–		**M6**	1	–	–	16.3541 ±0.0653	11.445 ±0.073	−91.968 ±0.096	y?
ABD344	21:47:19.65	−48:03:16.7	10.734 ±0.022	53.1	M4	4	–	–	15.7704 ±0.1229	54.193 ±0.151	−89.707 ±0.215	y
ABD344c	21:47:15.90	−48:02:38.9	11.497 ±0.024		**M6**	1	**M5**	1	15.9461 ±0.0552	49.848 ±0.07	−84.906 ±0.096	y
ABD374	23:11:52.05	−45:08:10.6	7.467 ±0.026	19.6	G8	2	–	–	20.8274 ±0.0683	87.469 ±0.05	−93.499 ±0.091	y
ABD375	23:11:53.62	−45:08:00.4	9.724 ±0.024		M3	2	–	–	21.1338 ±0.1211*	74.896 ±0.105*	−94.183 ±0.172*	y

Table 5.6: AB Dor companion candidates. *(a)* J magnitudes from VHS for targets fainter than J=12.5, and from 2MASS for targets brighter than J=12.5. *(b)* References: (1) This work, (2) Torres et al. (2006); (3) Nesterov et al. (1995), (4) Riaz et al. (2006), (5) Torres et al. (2008). *(c)* Values from the *Gaia* DR2 catalogue. Values marked with an asterisk (*) may be affected by close binarity and not be reliable. Values marked with a dagger ([†]) are obtained from the PPMXL catalogue.

ID	RA	DEC	Jmag	sep [″]	sep [AU]	log (L/L$_\odot$)	M [M$_\odot$][a]	T [K][a]	U$_{bind}$ [J]
ABD50	02:10:55.38	−46:03:58.7	9.288 ± 0.021			−0.570 ± 0.041	$0.831\ ^{+0.016}_{-0.020}$	$4708\ ^{+65}_{-54}$	
ABD49	02:10:53.46	−46:03:51.2	11.228 ± 0.021	21.4	1750 ± 10	−1.574 ± 0.049*	$0.456\ ^{+0.023*}_{-0.019}$	$3620\ ^{+28*}_{-30}$	$-3.82\mathrm{E}35\ ^{+3.2E34*}_{-2.9E34}$
ABD72	02:54:52.47	−07:09:25.6	9.999 ± 0.025			−1.505 ± 0.039*	$0.45 + 0.18$ *(1)	$3615 + 3262$ *(1)	
ABD072c	02:54:52.21	−07:09:24.2	12.072 ± 0.045	4.1	190 ± 5	−2.403 ± 0.059	$0.158\ ^{+0.024}_{-0.023}$	$3205\ ^{+57}_{-69}$	$-9.32\mathrm{E}35$*
ABD080c	03:11:42.69	−15:37:32.7	9.127 ± 0.026			−1.749 ± 0.040	$0.387\ ^{+0.026}_{-0.022}$	$3523\ ^{+29}_{-41}$	
ABD80	03:11:42.40	−15:37:18.4	11.448 ± 0.027	15.0	352 ± 3	−2.749 ± 0.036	$0.099\ ^{+0.018}_{-0.013}$	$2927\ ^{+97}_{-57}$	$-1.91\mathrm{E}35\ ^{+4.1E34}_{-5.2E34}$
ABD134	05:11:09.68	−04:10:54.4	7.807 ± 0.021			0.153†*	1.17†*	5774†*	
ABD134c2	05:10:55.05	−04:10:56.3	11.649 ± 0.023	218.9	16830†	−1.728†	0.40†	3534†	$-4.81\mathrm{E}34$†
ABD168	06:02:21.90	−13:55:32.5	8.439 ± 0.021			−0.846 ± 0.029	$0.726\ ^{+0.010}_{-0.020}$	$4326\ ^{+46}_{-46}$	
ABD510	06:02:21.074	−13:55:17.47	11.56 ± 0.023	19.1	862 ± 5	−2.227 ± 0.034	$0.201\ ^{+0.021}_{-0.014}$	$3300\ ^{+36}_{-38}$	$-2.99\mathrm{E}35\ ^{+3.6E34}_{-4.3E34}$
ABD511	06:02:25.913	−13:56:39.99	12.6273 ± 0.0009	108.6	4903 ± 9	−2.662 ± 0.009	$0.113\ ^{+0.014}_{-0.009}$	$3028\ ^{+38}_{-30}$	$-2.95\mathrm{E}34\ ^{+3.8E33}_{-4.1E33}$
ABD548c	11:22:00.37	−74:28:10.5	9.817 ± 0.026			−1.165 ± 0.039*	$0.612\ ^{+0.013*}_{-0.031}$	$3945\ ^{+66*}_{-82}$	
ABD548	11:21:59.825	−74:27:48.45	12.087 ± 0.043	22.4	1416 ± 8	−2.101 ± 0.046*	$0.240\ ^{+0.022*}_{-0.027}$	$3359\ ^{+31*}_{-41}$	$-1.83\mathrm{E}35\ ^{+3.0E34*}_{-2.7E34}$
ABD556	14:15:41.498	−77:43:06.56	11.067 ± 0.022			−1.763 ± 0.037	$0.381\ ^{+0.026}_{-0.021}$	$3516\ ^{+29}_{-30}$	
ABD557	14:15:42.072	−77:42:46.73	11.135 ± 0.021	19.9	1161 ± 7	−1.790 ± 0.037	$0.368\ ^{+0.026}_{-0.030}$	$3502\ ^{+30}_{-39}$	$-2.13\mathrm{E}35\ ^{+3.5E34}_{-3.2E34}$
ABD559	14:41:07.109	−43:57:01.40	9.721 ± 0.039			−1.877 ± 0.060	$0.330\ ^{+0.039}_{-0.043}$	$3462\ ^{+40}_{-46}$	
ABD560	14:41:07.502	−43:57:01.67	11.018 ± 0.032	4.1	118 ± 4	−2.408 ± 0.029	$0.157\ ^{+0.018}_{-0.018}$	$3202\ ^{+40}_{-40}$	$-7.75\mathrm{E}35\ ^{+1.99E35}_{-2.15E35}$
ABD316	19:01:06.04	−28:42:50.4	7.463 ± 0.018			0.143 ± 0.020	$1.157\ ^{+0.011}_{-0.011}$	$5757\ ^{+40}_{-35}$	
ABD316c	19:00:16.32	−28:37:53.1	10.134 ± 0.023	718.6	47066 ± 37	−1.177 ± 0.018	$0.608\ ^{+0.006}_{-0.022}$	$3933\ ^{+29}_{-29}$	$-2.636\mathrm{E}34\ ^{+1.13E33}_{-5.3E32}$
ABD587c	19:18:44.38	−68:59:53.4	11.679 ± 0.023			−1.928 ± 0.038	$0.309\ ^{+0.033}_{-0.033}$	$3441\ ^{+29}_{-38}$	
ABD587	19:18:48.816	−69:10:22.45	11.495 ± 0.033*	626.0	38744 ± 44	−1.931 ± 0.022*	$0.21 + 0.19$ *(2)	$3317 + 3274$ *(2)	$-5.63\mathrm{E}33$*
ABD344	21:47:19.65	−48:03:16.7	10.734 ± 0.022			−1.567 ± 0.038	$0.458\ ^{+0.019}_{-0.023}$	$3624\ ^{+21}_{-38}$	
ABD344c	21:47:15.90	−48:02:38.9	11.497 ± 0.024	53.1	3330 ± 9	−1.912 ± 0.050	$0.316\ ^{+0.033}_{-0.038}$	$3447\ ^{+35}_{-43}$	$-7.67\mathrm{E}34\ ^{+1.27E34}_{-1.17E34}$
ABD374	23:11:52.05	−45:08:10.6	7.467 ± 0.026			−0.228 ± 0.020	$0.978\ ^{+0.009}_{-0.009}$	$5206\ ^{+37}_{-31}$	
ABD375	23:11:53.62	−45:08:00.4	9.724 ± 0.024	19.6	941 ± 6	−1.367 ± 0.039*	$0.532\ ^{+0.020*}_{-0.021}$	$3764\ ^{+33*}_{-50}$	$-9.76\mathrm{E}35\ ^{+5.3E34*}_{-5.2E34}$

Table 5.7: Luminosities, masses, effective temperature and binding energies of the candidate companions in AB Dor. Values marked with an asterisk (*) may not be reliable due to suspected binarity. Values marked with a dagger (†) were calculated using the estimated heliocentric distance for the components from Elliott et al. (2016). *(a) Notes:* (1) Masses of the SB estimated from the luminosity ratio L_A/L_B=0.19 from Torres et al. (2002). (2) Masses of the VB estimated from the flux ratio in the *Gaia G*-band photometry.

ID	RA	DEC	Jmag[a]	Sep [']	SpT OPT	Ref[b]	SpT NIR	Ref[b]	Parallax [mas][c]	pmra [mas yr^{-1}][c]	pmdec [mas yr^{-1}][c]	Comp?
bP36	01:37:35.40	−06:45:38.0	6.225 ± 0.024		G9	9	–	–	41.5902 ± 0.0433	171.758 ± 0.081	−98.054 ± 0.062	y
bP35	01:36:55.10	−06:47:37.9	9.707 ± 0.022	612.1	M3.5	10	–	–	41.715 ± 0.1137	173.469 ± 0.255	−100.143 ± 0.15	y
bP41	02:01:46.90	+01:17:06.0	9.095 ± 0.019		**M3**	1	–	–	20.2511 ± 0.0572	74.746 ± 0.092	−49.096 ± 0.079	y
bP40	02:01:46.70	+01:17:16.2	9.147 ± 0.024	10.4	**M3.5**	1	–	–	20.1683 ± 0.0491	75.838 ± 0.079	−46.704 ± 0.073	y
bP60	02:39:47.99	−42:53:30.0	4.678 ± 0.266		A1	4	–	–	24.7076 ± 0.393	125.808 ± 0.574	−11.612 ± 0.628	y
bP61	02:39:48.33	−42:53:05.2	9.237 ± 0.034	25.6	**M5**	1	**M5.5**	1	25.2573 ± 0.1472	105.724 ± 0.198	−23.317 ± 0.215	y
bP61c	02:40:47.59	−42:53:37.7	12.199 ± 0.024	654.8	M6	5	–	–	24.8430 ± 0.0795	102.764 ± 0.125	−24.931 ± 0.127	y
bP66	02:49:56.39	−05:57:35.2	11.963 ± 0.027		M6	6	–	–	15.1097 ± 0.1026	48.657 ± 0.193	−36.174 ± 0.173	y
bP066c	02:49:54.36	−05:58:01.5	16.531 ± 0.008	40.0	L2.5	2	L3	2	–	46.0±2.3[‡]	−32.0±2.1[‡]	y
bP141	08:22:47.40	−57:26:53.0	8.626 ± 0.024		M3	7	–	–	77.4877 ± 0.0716	−372.239 ± 0.157	481.326 ± 0.157	y
bP141c	08:22:47.87	−57:26:45.1	10.256 ± 0.029	8.7	**M7**	1	**M6**	1	77.4495 ± 0.0706	−371.155 ± 0.165	437.05 ± 0.158	y
bP314	17:02:09.319	−67:34:46.27	9.839 ± 0.023		**M5**	1	**M6**	1	24.2245 ± 0.0386	−20.274 ± 0.044	−99.483 ± 0.063	y
bP315	17:02:09.818	−67:34:33.84	10.460 ± 0.023	12.7	**M6.5**	1	**M7**	1	24.1766 ± 0.0501	−20.461 ± 0.052	−99.239 ± 0.081	y
bP171	17:17:25.50	−66:57:04.0	5.288 ± 0.032		G5+K0	11	–	–	32.7801 ± 0.0267	−21.213 ± 0.029	−137.125 ± 0.039	y
bP172	17:17:31.20	−66:57:05.4	8.542 ± 0.027	34.0	M3	12	–	–	32.9529 ± 0.0574	−14.759 ± 0.066	−145.104 ± 0.091	y
bP191	18:42:06.90	−55:54:25.5	9.488 ± 0.024		M3	7	–	–	19.4722 ± 0.0499	12.137 ± 0.064	−78.933 ± 0.05	y
bP191c	18:42:04.83	−55:54:12.6	10.677 ± 0.023	21.9	M4.5	8	–	–	19.3333 ± 0.0602	11.093 ± 0.073	−77.915 ± 0.058	y
bP197	18:48:06.30	−62:13:47.0	6.416 ± 0.030		P5	13	–	–	19.7597 ± 0.0373	13.056 ± 0.051	−80.028 ± 0.047	y
bP195	18:46:52.55	−62:10:36.6	8.746 ± 0.019	550.3	M1	12	–	–	19.7766 ± 0.0491	13.369 ± 0.065	−80.141 ± 0.06	y
bP208	19:22:34.09	−54:29:18.1	11.534 ± 0.057		**M2**	1	**M3**	1	7.7466 ± 0.1083	37.894 ± 0.135	−122.298 ± 0.106	y-nbP
bP208c	19:22:34.14	−54:29:21.6	11.985 ± 0.028	3.6	**M3**	1	**M3**	1	7.8815 ± 0.0422	39.319 ± 0.055	−124.689 ± 0.042	y-nbP
bP222	19:56:04.30	−32:07:37.7	8.710 ± 0.029		K9	14	–	–	19.5153 ± 0.0459	33.449 ± 0.092	−68.395 ± 0.053	y
bP221	19:56:02.90	−32:07:18.7	8.959 ± 0.027	26.3	N4	8	–	–	18.0279 ± 0.9677*	36.143 ± 1.547*	−65.725 ± 1.322*	y
bP252	21:10:31.40	−27:10:57.8	10.296 ± 0.023		M4.5	8	–	–	24.7683 ± 0.107	67.836 ± 0.133	−75.457 ± 0.092	y
bP251	21:10:30.90	−27:10:51.3	11.200 ± 0.026	9.4	M5	8	–	–	24.8489 ± 0.1408	70.047 ± 0.174	−76.061 ± 0.122	y
bP257	21:25:27.40	−81:38:27.6	8.239 ± 0.030		M2	3	–	–	29.2836 ± 0.069	59.843 ± 0.111	−107.723 ± 0.114	y
bP257c	21:26:50.40	−81:40:29.3	15.352 ± 0.007	217.4	L3	3	–	–	29.2463 ± 0.9205	56.511 ± 1.656	−115.369 ± 2.441	y
bP257c2	21:19:20.28	−81:45:44.6	11.143 ± 0.026	907.1	–	–	**M6.5**	1	29.0306 ± 0.0775	56.595 ± 0.114	−112.591 ± 0.117	y
THA281	21:12:15.99	−81:28:45.3	10.668 ± 0.023	1836.7	M5.5	5	**M5.5**	1	28.5728 ± 0.0594	52.297 ± 0.096	−112.228 ± 0.136	y
bP264c	21:55:17.38	−00:46:23.1	10.977 ± 0.024		**M5**	1	**M5**	1	17.7966 ± 0.0782	63.695 ± 0.126	−55.297 ± 0.135	y
bP264	21:55:17.41	−00:45:47.8	11.092 ± 0.024	35.4	**M5**	1	–	–	17.6637 ± 0.0847	63.816 ± 0.129	−54.775 ± 0.132	y
bP288	23:41:51.98	−02:56:29.7	10.500 ± 0.024		–	–	–	–	–	101.6±5.4[†]	−74.1±5.4[†]	n?
bP288c	23:40:24.40	−03:06:46.2	12.5894 ± 0.0012	1449.7	–	–	–	–	–	98.8±4.1[†]	−115.9±4.1[†]	n?

Table 5.8: β Pic companion candidates. *(a)* J magnitudes from VHS for targets fainter than J=12.5, and from 2MASS for targets brighter than J=12.5. *(b)* References: (1) This work, (2) ?, (3) Deacon et al. (2016), (4) Gagné et al. (2016), (5) Gagné et al. (2015c), (6) Shkolnik et al. (2017), (7) Riedel et al. (2017), (8) Riaz et al. (2006), (9) Gray et al. (2003), (10) Shkolnik et al. (2009), (11) Barstow (1987), (12) Torres et al. (2006), (13) Houk & Cowley (1975), (14) Pecaut & Mamajek (2013). *(c)* Values from the *Gaia* DR2 catalogue. Values marked with an asterisk (*) may be affected by close binarity and not be reliable. Values marked with a dagger ([†]) are obtained from the PPMXL catalogue. Values marked with a double dagger ([‡]), from Dupuy et al. (2018).

ID	RA	DEC	Jmag	sep ['/]	sep [AU] [a]	log $(L/L_{\odot})$ [a]	M [$M_{\odot}$]	T [K]	U_{bind} [J]
bP36	01:37:35.40	−06:45:38.0	6.225 ± 0.024	612.1	14717 ± 29	−0.340 ± 0.023	0.991 ± 0.046	4483 ± 147	−1.57E34 ± 2.1E33
bP35	01:36:55.10	−06:47:37.9	9.707 ± 0.022			−1.089 ± 0.038	0.133 ± 0.022	3176 ± 52	
bP41	02:01:46.90	+01:17:06.0	9.095 ± 0.019	10.4	516 ± 5	−1.087 ± 0.036	0.557 ± 0.067	3612 ± 68	−1.00E36 ± 2.7E35
bP40	02:01:46.70	+01:17:16.2	9.147 ± 0.024			−1.136 ± 0.038	0.523 ± 0.072	3580 ± 70	
bP60	02:39:47.99	−42:53:30.0	4.678 ± 0.266	25.6	1014 ± 8	1.258 ± 0.164*	2.09 ± 0.21*	9257 ± 701*	−1.22E36 ± 3.4E35*
bP61	02:39:48.33	−42:53:05.2	9.237 ± 0.034			−1.412 ± 0.041	0.336 ± 0.057	3425 ± 60	
bP61c	02:40:47.59	−42:53:37.7	12.199 ± 0.024	654.8	26358 ± 56	−2.586 ± 0.019	0.053 ± 0.008	2765 ± 50	−7.43E33 ± 1.88E33*
bP66A	02:49:56.39	−05:57:35.2	11.963 ± 0.027			−2.59±0.09 [1]	0.053±0.014	2762 ± 103	
bP66B	02:49:56.39	−05:57:35.2	-		2.17 ± 0.22 [1]	−2.64±0.09 [1]	0.050±0.013	2728 ± 100	
bP066c	02:49:54.36	−05:58:01.5	16.531 ± 0.0076	40.0	1950 ± 200 [1]	−4.00 ± 0.09 [1]	0.011 ± 0.001	1544 ± 76	−1.02E33 ± 4.7E32
bP141	08:22:47.40	−57:26:53.0	8.626 ± 0.024	8.7	112 ± 2	−2.140 ± 0.038	0.104 ± 0.017	3059 ± 89	−6.42E34 ± 2.37E34
bP141c	08:22:47.87	−57:26:45.1	10.256 ± 0.029			−2.800 ± 0.028	0.039 ± 0.007	2599 ± 71	
bP314	17:02:09.319	−67:34:46.27	9.839 ± 0.023	12.7	524 ± 5	−1.612 ± 0.050	0.243 ± 0.043	3340 ± 60	−1.32E35 ± 4.2E34
bP315	17:02:09.818	−67:34:33.84	10.46 ± 0.023			−1.873 ± 0.018	0.159 ± 0.020	3230 ± 40	
bP171	17:17:25.50	−66:57:04.0	5.288 ± 0.032	34.0	1037 ± 4	0.286 ± 0.030*	1.10 + 1.00 [2]	5400 + 5050 [2]	−1.48E36 ± 2.6E35
bP172	17:17:31.20	−66:57:05.4	8.542 ± 0.027			−1.288 ± 0.040	0.414 ± 0.066	3485 ± 62	
bP191	18:42:06.90	−55:54:25.5	9.488 ± 0.024	21.9	1125 ± 6	−1.214 ± 0.038	0.465 ± 0.069	3527 ± 67	−1.40E35 ± 5.1E34
bP191c	18:42:04.83	−55:54:12.6	10.677 ± 0.023			−1.758 ± 0.050	0.191 ± 0.037	3275 ± 58	
bP197	18:48:06.30	−62:13:47.0	6.416 ± 0.03	550.3	27850 ± 26	0.398 ± 0.037	1.292 ± 0.046	5927 ± 405	−5.74E34± 5.8E33
bP195	18:46:52.55	−62:10:36.6	8.746 ± 0.019			−0.890 ± 0.032	0.701 ± 0.050	3779 ± 89	
bP208	19:22:34.09	−54:29:18.1	11.534 ± 0.057	3.6	458 ± 13	−1.245 ± 0.051	0.443 ± 0.076	3508 ± 74	−5.66E35 ± 2.17E35
bP208c	19:22:34.14	−54:29:21.6	11.985 ± 0.028			−1.425 ± 0.039	0.329 ± 0.056	3419 ± 59	
bP222	19:56:04.30	−32:07:37.7	8.71 ± 0.029	26.3	1348 ± 6	−0.833 ± 0.024	0.741 ± 0.038	3834 ± 88	−5.79E35 ± 9.5E34*
bP221	19:56:02.90	−32:07:18.7	8.959 ± 0.027			−1.032 ± 0.040*	0.596 ± 0.066*	3653 ± 80*	
bP252	21:10:31.40	−27:10:57.8	10.296 ± 0.023	9.4	380 ± 5	−1.814 ± 0.052	0.175 ± 0.030	3253 ± 52	−8.13E34 ± 2.87E34
bP251	21:10:30.90	−27:10:51.3	11.2 ± 0.026			−2.176 ± 0.053	0.099 ± 0.015	3033 ± 137	
bP257	21:25:27.40	−81:38:27.6	8.239 ± 0.03	217.4	7424 ± 18	−1.053 ± 0.038	0.581 ± 0.066	3636 ± 69	−1.77E33 ± 3.1E32
bP257c	21:26:50.40	−81:40:29.3	15.352 ± 0.0073			−3.667 ± 0.093	0.013 ± 0.001	1795 ± 74	
bP257c2	21:19:20.28	−81:45:44.6	11.143 ± 0.026	907.1	30976 ± 66	−2.310 ± 0.020	0.082 ± 0.011	2935 ± 38	−2.72E33 ± 6.7E32
THA281	21:12:15.99	−81:28:45.3	10.668 ± 0.023	1836.7	64279 ± 113	−2.091 ± 0.035	0.113 ± 0.018	3091 ± 126	−1.86E33 ± 5.0E32
bP264c	21:55:17.38	−00:46:23.1	10.977 ± 0.024	35.4	1989 ± 8	−1.799 ± 0.051	0.179 ± 0.030	3258 ± 52	−2.66E34 ± 9.6E33
bP264	21:55:17.41	−00:45:47.8	11.092 ± 0.024			−1.845 ± 0.051	0.166 ± 0.029	3241 ± 51	

Table 5.9: Luminosities, masses, effective temperature and binding energies of the candidate companions in β Pic. The age range considered for the M, T and $U_{\rm bin}$ computation is 20–30 Myr. Values marked with an asterisk (*) may not be reliable due to suspected binarity. Values marked with a dagger (†) are calculated using the PISA pre-main sequence models (Tognelli et al. 2011). *(a) Notes:* (1) Values from Dupuy et al. (2018). (2) Values for the SB from Strassmeier & Rice (2000).

ID	RA	DEC	Jmag[a]	Sep ['/]	SpT OPT	Ref[b]	SpT NIR	Ref[b]	Parallax [mas][c]	pmra [mas yr^{-1}][c]	pmdec [mas yr^{-1}][c]	Comp?
THA023	00:30:25.72	−62:36:01.5	8.445 ± 0.024	4.6	M2.2	2	**M3**	1	22.2753 ± 0.2785*	87.488 ± 0.503*	−54.685 ± 0.421*	y
THA023c	00:30:25.18	−62:36:03.8	9.273 ± 0.120		–	–	**M5**	1	22.5766 ± 0.055	96.589 ± 0.099	−52.711 ± 0.082	y
THA051	01:13:15.34	−64:11:35.1	8.615 ± 0.021	178.6	K1	3	–	–	15.2916 ± 0.021	72.486 ± 0.037	0.24 ± 0.032	y? n-TH?
THA051c	01:13:06.98	−64:08:45.1	10.018 ± 0.021		–	–	–	–	–	73.1±10.1†	10.0±10.1†	y? n-TH?
THA359	01:56:30.75	−74:57:27.6	12.004 ± 0.027	307.8	–	–	–	–	23.2063 ± 0.0906	96.784 ± 0.15	−11.298 ± 0.15	?
THA359c	01:57:08.82	−74:52:58.0	17.141 ± 0.026		–	–	–	–	–	–	–	?
THA99	02:07:01.76	−44:06:38.0	9.270 ± 0.027	6.8	M3.5	4	**M3.5**	1	23.3925 ± 0.0428	98.55 ± 0.063	−33.44 ± 0.06	y
THA099c	02:07:01.98	−44:06:44.4	11.361 ± 0.030		M5.5	4	**M5.5**	1	23.4263 ± 0.0868	104.665 ± 0.117	−32.788 ± 0.114	y
THA141	02:41:46.83	−52:59:52.3	7.582 ± 0.023	22.0	K6	5	–	–	22.825 ± 0.0373	96.765 ± 0.061	−14.16 ± 0.068	y
THA142	02:41:47.30	−52:59:30.6	8.481 ± 0.027		M2	5	–	–	23.0277 ± 0.0837	93.521 ± 0.135	−11.58 ± 0.166	y
THA136	02:40:12.09	−53:05:52.7	14.270 ± 0.002	927.1	M9.5	6	**M9.5**	1	23.1591 ± 0.3199	95.65 ± 0.52	−15.647 ± 0.562	y
THA144	02:42:04.04	−53:59:00.0	10.110 ± 0.023	23.0	M4.3	2	–	–	23.3932 ± 0.1179	95.965 ± 0.181	−14.918 ± 0.201	y
THA143	02:42:02.04	−53:59:14.7	10.833 ± 0.022		M4.3	2	–	–	23.6594 ± 0.0513	97.749 ± 0.083	−13.531 ± 0.09	y
THA157	02:54:33.16	−51:08:31.3	8.668 ± 0.027	15.3	M2+M3	12	–	–	22.8539 ± 0.1105	93.484 ± 0.188	−11.806 ± 0.187	y
THA158	02:54:34.77	−51:08:28.8	12.074 ± 0.024		–	–	**M5**	1	22.7894 ± 0.0718	93.58 ± 0.117	−9.168 ± 0.113	y
THA363	03:29:04.35	−48:03:34.0	10.988 ± 0.029	6.2	**M5.5**	1	**M5**	1	23.9415 ± 0.0442	90.926 ± 0.076	−3.257 ± 0.105	y
THA362	03:29:03.80	−48:03:36.6	11.167 ± 0.022		**M5.5**	1	**M5**	1	23.9712 ± 0.0468	93.94 ± 0.08	−4.358 ± 0.11	y
THA207A	03:48:35.88	−37:37:12.5	3.900 ± 1.054	7.9	B9.5	13	–	–	18.9755 ± 0.1726*	80.678 ± 0.266*	−5.007 ± 0.317*	y
THA207B	03:48:35.48	−37:37:19.0	**6.936** ± –		A1	13	–	–	18.9081 ± 0.1200*	63.251 ± 0.190*	−8.658 ± 0.219*	y
THA364	03:48:40.51	−37:38:20.0	9.511 ± 0.022	86.3	–	–	**M4**	1	18.7547 ± 0.0297	74.238 ± 0.041	−4.652 ± 0.065	y
THA212	04:00:03.82	−29:02:16.5	7.964 ± 0.026	11.5	K4.1	2	–	–	20.2513 ± 0.1017	72.522 ± 0.182	−12.476 ± 0.177	y
THA213	04:00:03.95	−29:02:28.0	8.280 ± 0.029		K4.6	2	–	–	20.484 ± 0.0295	74.549 ± 0.049	−17.849 ± 0.061	y
THA367	04:08:22.26	−27:44:39.9	10.382 ± 0.026	5.7	**M4.5**	1	–	–	18.421 ± 0.2793*	67.305 ± 0.378*	−18.84 ± 0.501*	y
THA368	04:08:22.37	−27:44:34.4	12.299 ± 0.035		**M6.5**	1	–	–	18.8477 ± 0.0885	69.007 ± 0.119	−15.541 ± 0.161	y
THA239	04:48:00.66	−50:41:25.5	8.741 ± 0.026	367.1	K7	5	–	–	16.7787 ± 0.0759	56.89 ± 0.152	19.24 ± 0.198	y?
THA238	04:47:57.79	−50:35:20.0	10.868 ± 0.024		M4	2	–	–	–	56.4±8.0†	16.7±8.0†	y?
THA251	06:46:13.54	−83:59:29.5	6.553 ± 0.029	655.4	F5	7	–	–	17.2797 ± 0.0255	18.322 ± 0.046	62.517 ± 0.049	?
THA251c	06:52:20.29	−84:04:50.4	13.0316 ± 0.0012		–	–	–	–	4.7066 ± 0.2102	7.87 ± 0.517	55.714 ± 0.265	?
THA251c	06:52:20.29	−84:04:50.4	–		–	–	–	–	–	1.8±11.5†	52.6±11.5†	–
THA271c	20:33:04.19	−56:46:50.1	12.9017 ± 0.0012	754.2	–	–	–	–	15.8151 ± 0.1067	30.742 ± 0.139	−93.338 ± 0.133	?
THA271	20:33:44.74	−56:35:33.8	15.836 ± 0.006		L0	8	–	–	–	16.0±6.1‡	−73.1±12.5‡	? TH?
THA273c	20:42:16.24	−55:52:07.4	10.045 ± 0.023	503.1	M2.3	2	**M4.5**	1	17.5668 ± 0.0812	16.759 ± 0.12	−81.615 ± 0.118	y
THA273	20:43:04.52	−55:47:11.5	12.296 ± 0.023		–	–	**M5.5**	1	18.136 ± 0.0802	14.395 ± 0.114	−83.902 ± 0.125	y
THA330	23:22:52.41	−61:51:11.5	11.534 ± 0.023	16.5	M5	9	–	–	23.5643 ± 0.0652	77.774 ± 0.096	−78.195 ± 0.102	y
THA331	23:22:52.99	−61:51:27.5	15.350 ± 0.003		L2	10	L3	11	23.2405 ± 1.0493	80.092 ± 1.447	−81.969 ± 1.621	y
THA335	23:27:34.47	−85:12:36.4	10.850 ± 0.022	167.2	M3.8	2	–	–	19.3391 ± 0.054	64.913 ± 0.134	−50.072 ± 0.09	y
THA333	23:27:09.60	−85:15:21.0	10.647 ± 0.022		–	–	**M6**	1	20.3514 ± 0.1417*	62.623 ± 0.398*	−50.203 ± 0.248*	y
THA336	23:28:57.63	−68:02:33.8	9.257 ± 0.023	762.2	M2.5	4	–	–	21.7164 ± 0.0235	73.503 ± 0.041	−68.137 ± 0.042	y
THA337	23:29:17.52	−67:49:59.8	10.793 ± 0.025		M3.5	2	–	–	21.7647 ± 0.045	73.624 ± 0.071	−68.011 ± 0.071	y

Table 5.10: THA companion candidates. *(a)* J magnitudes from VHS for targets fainter than J=12.5, and from 2MASS for targets brighter than J=12.5. *(b)* References: (1) This work, (2) Kraus et al. (2014), (3) Torres et al. (2000), (4) Riaz et al. (2006), (5) Torres et al. (2006), (6) Martín et al. (2010), (7) Houk & Cowley (1975), (8) Gagné et al. (2015c), (9) Gagné et al. (2015b), (10) Cruz et al. (2009), (11) Faherty et al. (2016), (12) Flagg et al. (2020), (13) Gray & Garrison (1987). *(c)* Values from the *Gaia* DR2 catalogue. Values marked with an asterisk may be affected by close binarity and not be reliable. Values marked with a dagger (†) are obtained from the PPMXL catalogue. Values marked with a double dagger (‡) obtained from Gagné et al. (2015b).

ID	RA	DEC	Jmag	sep [']	sep [AU]	log (L/L$_\odot$)	M [M$_\odot$][a]	T [K]	U$_{bind}$ [J]
THA23	00:30:25.72	−62:36:01.5	8.445 ± 0.024	4.6	204 ± 5	−0.909 ± 0.035*	0.54 + 0.49[1]	–	−4.42E36*
THA023c	00:30:25.18	−62:36:03.8	9.273 ± 0.12			−1.325 ± 0.089	0.496 ± 0.077	3572 ± 84	
THA51	01:13:15.34	−64:11:35.1	8.615 ± 0.021	178.6	11680 ± 10	−0.455 ± 0.033	0.849 ± 0.026	4641 ± 129	−7.80E34 ± 3.1E33
THA051c	01:13:06.98	−64:08:46.1	10.018 ± 0.021			−1.132 ± 0.021	0.609 ± 0.015	3718 ± 54	
THA359	01:56:30.754	−74:57:27.63	12.004 ± 0.027	307.8	13264 ± 32	−2.441 ± 0.053	0.090 ± 0.012	2949 ± 47	−1.35E32 ± 2.6E31
THA359c	01:57:08.82	−74:52:58.0	17.1413 ± 0.026			−4.181 ± 0.100	0.011 ± 0.001	1431 ± 72	
THA99	02:07:01.76	−44:06:38.0	9.27 ± 0.027	6.8	291 ± 5	−1.314 ± 0.040*	0.84[2]	–	−6.57E35*
THA099c	02:07:01.98	−44:06:44.4	11.361 ± 0.03			−2.195 ± 0.037	0.129 ± 0.015	3157 ± 38	
THA141	02:41:46.83	−52:59:52.3	7.582 ± 0.023	22.0	964 ± 5	−0.498 ± 0.022*	0.7 + 0.7[1]	–	−2.82E36*
THA142	02:41:47.30	−52:59:30.6	8.481 ± 0.027	927.1	40618 ± 39	−0.933 ± 0.036*	0.56 + 0.54[1]	–	−1.76E33*
THA136	02:40:12.09	−53:05:52.7	14.2697 ± 0.002			−3.293 ± 0.066	0.029 ± 0.005	2241 ± 89	
THA144	02:42:04.04	−53:59:00.0	10.11 ± 0.023	23.0	972 ± 5	−1.660 ± 0.038	0.298 ± 0.036	3411 ± 35	−1.02E35 ± 2.4E34
THA143	02:42:02.04	−53:59:14.7	10.833 ± 0.022			−1.949 ± 0.038	0.188 ± 0.020	3283 ± 34	
THA157	02:54:33.16	−51:08:31.3	8.668 ± 0.027	15.3	671 ± 5	−1.007 ± 0.036*	0.40 + 0.27[3]	–	−1.54E35*
THA158	02:54:34.77	−51:08:28.8	12.074 ± 0.024			−2.453 ± 0.051	0.088 ± 0.012	2942 ± 46	
THA363	03:29:04.353	−48:03:33.98	10.988 ± 0.029	6.2	259 ± 4	−2.066 ± 0.037	0.157 ± 0.018	3227 ± 36	−1.51E35 ± 3.7E34
THA362	03:29:03.801	−48:03:36.59	11.167 ± 0.022			−2.137 ± 0.034	0.141 ± 0.015	3189 ± 37	
THA207A	03:48:35.88	−37:37:12.5	3.9 ± 1.054	7.9	416 ± 6	1.935 ± 0.552	3.08 ± 1.15[1]	12001 ± 2566[1]	−6.60E35 ± 2.87E35
THA207B	03:48:35.48	−37:37:19.0	6.936 ± –			0.588 ± –	–	–	
THA364	03:48:40.509	−37:38:19.98	9.511 ± 0.022	86.3	4602 ± 8	−1.219 ± 0.037	0.559 ± 0.033	3644 ± 58	
THA212	04:00:03.82	−29:02:16.5	7.964 ± 0.026	11.5	561 ± 5	−0.520 ± 0.043	0.830 ± 0.029	4531 ± 143	−3.56E36*
THA213	04:00:03.95	−29:02:28.0	8.28 ± 0.029			−0.671 ± 0.036*	0.70 + 0.67[4]	3913 + 3846[4]	
THA367	04:08:22.26	−27:44:39.9	10.382 ± 0.026	5.7	302 ± 6	−1.611 ± 0.052*	0.322 ± 0.043*	3433 ± 38*	−1.82E35 ± 4.5E34*
THA368	04:08:22.37	−27:44:34.4	12.299 ± 0.035			−2.390 ± 0.023	0.096 ± 0.008	2982 ± 57	
THA239	04:48:00.66	−50:41:25.5	8.741 ± 0.026	367.1	21879 ± 34	−0.702 ± 0.020*	0.7 + 0.35[5]	–	−4.74E34*
THA238	04:47:57.79	−50:35:20.0	10.868 ± 0.024			−1.665 ± 0.039*	0.28 + 0.28[1]	–	
THA251	06:46:13.54	−83:59:29.5	6.553 ± 0.029	655.4	37929 ± 22	0.460 ± 0.036	1.370 ± 0.025[1]	6535 ± 64[1]	−4.53E33 ± 5.3E32
THA251c	06:52:20.29	−84:04:50.4	13.0316 ± 0.0012			−2.596 ± 0.041	0.071 ± 0.007	2853 ± 42	
THA271c	20:33:04.19	−56:46:50.1	12.9017 ± 0.0012	754.2	47689 ± 87	−2.467 ± 0.042	0.086 ± 0.010	2934 ± 40	−4.63E31 ± 8.8E30
THA271	20:33:44.74	−56:35:33.8	15.8362 ± 0.0057			−3.573 ± 0.076	0.015 ± 0.001	1892 ± 69	
THA273c	20:42:16.24	−55:52:07.4	10.045 ± 0.023	503.1	27740 ± 46	−1.359 ± 0.034	0.473 ± 0.040	3552 ± 36	−3.09E33 ± 5.5E32
THA273	20:43:04.52	−55:47:11.5	12.296 ± 0.023			−2.347 ± 0.034	0.103 ± 0.010	3026 ± 94	
THA330	23:22:52.41	−61:51:11.5	11.534 ± 0.023	16.5	700 ± 5	−2.266 ± 0.051	0.115 ± 0.015	3114 ± 99	−5.35E33 ± 2.88E33
THA331	23:22:52.99	−61:51:27.5	15.3496 ± 0.0034			−3.565 ± 0.091	0.018 ± 0.007	1938 ± 140	
THA333	23:27:09.60	−85:15:21.0	10.647 ± 0.022	167.2	8646 ± 14	−1.748 ± 0.018*	0.259 ± 0.023*	3369 ± 25*	−1.30E34 ± 2.9E33*
THA335	23:27:34.47	−85:12:36.4	10.85 ± 0.022			−1.781 ± 0.038	0.245 ± 0.031	3354 ± 34	
THA336	23:28:57.63	−68:02:33.8	9.257 ± 0.023	762.2	35098 ± 23	−1.216 ± 0.038	0.560 ± 0.033	3645 ± 58	−6.10E33 ± 1.09E33
THA337	23:29:17.52	−67:49:59.8	10.793 ± 0.025			−1.859 ± 0.038	0.217 ± 0.026	3321 ± 32	

Table 5.11: Luminosities, masses, effective temperature and binding energies of the candidate companions in THA. The age range considered for the M, T and $U_{\rm bin}$ computation is 40–50 Myr. Values marked with an asterisk (*) may not be reliable due to suspected binarity. Values marked with a dagger (†) are calculated using the PISA pre-main sequence models (Tognelli et al. 2011). *(a) Notes:* (1) Masses for the close binary from Shan et al. (2017). (2) Mass of the SB1 from Baron et al. (2019). (3) Masses for the SB2 components from Flagg et al. (2020). (4) Masses estimated from the V-band magnitude difference of the components in the Tycho Double Star Catalogue (Fabricius et al. 2002). (5) Masses for the components of the close binary from Elliott et al. (2015).

ID[a]	RA	DEC	Jmag[b]	Sep ['/]	SpT OPT	Ref[c]	SpT NIR	Ref[c]	Parallax [mas][d]	pmra [mas yr^{-1}][d]	pmdec [mas yr^{-1}][d]	Comp?
TWA20	11:01:51.91	−34:42:17.0	8.217 ± 0.024		K6	2	–	–	16.6428 ± 0.0416	−68.389 ± 0.054	−14.016 ± 0.059	y
TWA21	11:02:09.83	−34:30:35.5	13.0084 ± 0.0011	735.6	M8.5	3	–	–	16.731 ± 0.2121	−68.979 ± 0.328	−13.805 ± 0.285	y
TWA23	11:03:51.66	−37:11:48.3	12.421 ± 0.024		**M5.5**	1	–	–	11.7733 ± 0.0931	−62.848 ± 0.109	6.923 ± 0.122	n?
TWA0023c	11:04:07.27	−37:06:12.0	14.832 ± 0.004	384.8	**M5.5**	1	–	–	–	−34.1 ±8.9[†]	7.1 ±8.9[†]	n?
TWA39	11:21:17.45	−34:46:49.8	8.429 ± 0.037		M1	2	–	–	16.6732 ± 0.0409	−68.997 ± 0.058	−16.866 ± 0.052	y
TWA38	11:21:17.24	−34:46:45.5	8.431 ± 0.043	5.1	M1	2	–	–	16.7004 ± 0.0318	−69.096 ± 0.041	−18.131 ± 0.036	y
TWA46c	11:32:18.22	−30:18:31.6	15.411 ± 0.005		M4	5	M4	5	21.5846 ± 0.2988	−88.979 ± 0.515	−23.956 ± 0.332	y
TWA46	11:32:18.31	−30:19:51.8	9.641 ± 0.024	80.2	M5	4	M5	4	20.85 ± 0.1122	−88.577 ± 0.155	−25.066 ± 0.115	y
TWA48	11:32:41.25	−26:51:55.9	8.337 ± 0.024		M2	6	–	–	21.6101 ± 0.086	−90.645 ± 0.14	−27.41 ± 0.091	y
TWA47	11:32:41.16	−26:52:09.0	9.837 ± 0.024	13.2	M5	6	–	–	21.5244 ± 0.1148	−90.756 ± 0.172	−23.973 ± 0.113	y
TWA0049c	11:35:30.11	−19:46:50.1	11.926 ± 0.024		–	–	–	–	10.8304 ± 0.0522	−124.838 ± 0.093	−54.145 ± 0.053	y
TWA49	11:35:30.03	−19:47:06.2	12.213 ± 0.024	16.2	–	–	–	–	10.9771 ± 0.0754	−124.346 ± 0.136	−52.87 ± 0.078	y
TWA50	11:38:25.38	−38:41:52.5	11.644 ± 0.024		–	–	–	–	–	−68.7±9.4[†]	−1.9±9.4[†]	y?
TWA050c	11:38:26.93	−38:43:13.8	12.125 ± 0.023	83.1	M5	7	–	–	–	−71.5±9.4[†]	−4.0±9.4[†]	y?

Table 5.12: TWA companion candidates. *(a)* These IDs relate to the entries of the candidate members compilation, and are not the official names of the TWA objects. *(b)* J magnitudes from VHS for targets fainter than J=12.5, and from 2MASS for targets brighter than J=12.5. *(c)* References: (1) This work, (2) Torres et al. (2006), (3) Scholz et al. (2005), (4) Looper et al. (2010b), (5) Looper et al. (2010a), (6) Webb et al. (1999), (7) Gagné et al. (2017) *(d)* Values from the *Gaia* DR2 catalogue. Values marked with a dagger ([†]) are obtained from the PPMXL catalogue.

ID[a]	RA	DEC	Jmag	sep ['']	sep [AU]	log ($L/L_\odot$)	M [$M_\odot$]	T [K]	U_{bind} [J]
TWA20	11:01:51.91	−34:42:17.0	8.217 ± 0.024			-0.477 ± 0.022	$0.919\ ^{+0.018}_{-0.118}$	$3904\ ^{+384}_{-130}$	
TWA21	11:02:09.83	−34:30:35.5	13.0084 ± 0.0011	735.6	44199 ± 37	-2.550 ± 0.037	$0.026\ ^{+0.011}_{-0.011}$	$2545\ ^{+166}_{-165}$	$-9.43\mathrm{E}32\ ^{+2.28E32}_{-2.27E32}$
TWA39	11:21:17.45	−34:46:49.8	8.429 ± 0.037			-0.617 ± 0.039	$0.773\ ^{+0.063}_{-0.149}$	$3775\ ^{+334}_{-128}$	
TWA38	11:21:17.24	−34:46:45.5	8.431 ± 0.043	5.1	305 ± 6	-0.618 ± 0.042	$0.772\ ^{+0.065}_{-0.152}$	$3774\ ^{+337}_{-130}$	$-3.45\mathrm{E}36\ ^{+1.27E36}_{-6.7E35}$
TWA46c	11:32:18.22	−30:18:31.6	15.4109 ± 0.0046			-3.671 ± 0.032	−	−	
TWA46	11:32:18.31	−30:19:51.8	9.641 ± 0.024	80.2	3847 ± 14	-1.403 ± 0.052	$0.224\ ^{+0.056}_{-0.068}$	$3276\ ^{+68}_{-71}$	−
TWA48	11:32:41.25	−26:51:55.9	8.337 ± 0.024			-0.828 ± 0.035	$0.563\ ^{+0.027}_{-0.108}$	$3613\ ^{+227}_{-106}$	
TWA47	11:32:41.16	−26:52:09.0	9.837 ± 0.024	13.2	611 ± 6	-1.512 ± 0.051	$0.186\ ^{+0.048}_{-0.048}$	$3234\ ^{+64}_{-60}$	$-3.02\mathrm{E}35\ ^{+1.23E35}_{-1.44E35}$
TWA049c	11:35:30.11	−19:46:50.1	11.926 ± 0.024			-1.680 ± 0.038	$0.140\ ^{+0.027}_{-0.034}$	$3168\ ^{+30}_{-68}$	
TWA49	11:35:30.03	−19:47:06.2	12.213 ± 0.024	16.2	1496 ± 10	-1.822 ± 0.038	$0.109\ ^{+0.023}_{-0.026}$	$3105\ ^{+26}_{-127}$	$-1.80\mathrm{E}34\ ^{+7.7E33}_{-8.2E33}$
TWA50	11:38:25.38	−38:41:52.5	11.644 ± 0.024			$-1.969^{\dagger *}$	$0.086^{\dagger *}$	$2980^{\dagger *}$	
TWA050c	11:38:26.93	−38:43:13.8	12.125 ± 0.023	83.1	$4986^{\dagger}$	$-2.202^{\dagger *}$	$0.057^{\dagger *}$	$2856^{\dagger *}$	$-1.73\mathrm{E}33^{\dagger *}$

Table 5.13: Luminosities, masses, effective temperature and binding energies of the candidate companions in TWA. The age range considered for the M, T and $U_{\rm bin}$ computation is 7–13 Myr. Values marked with an asterisk (*) may not be reliable due to suspected binarity. Values marked with a dagger (†) are calculated using the estimated heliocentric distance in Gagné et al. (2017). *(a)* These IDs relate to the entries of the candidate members compilation, and are not the official names of the TWA objects.

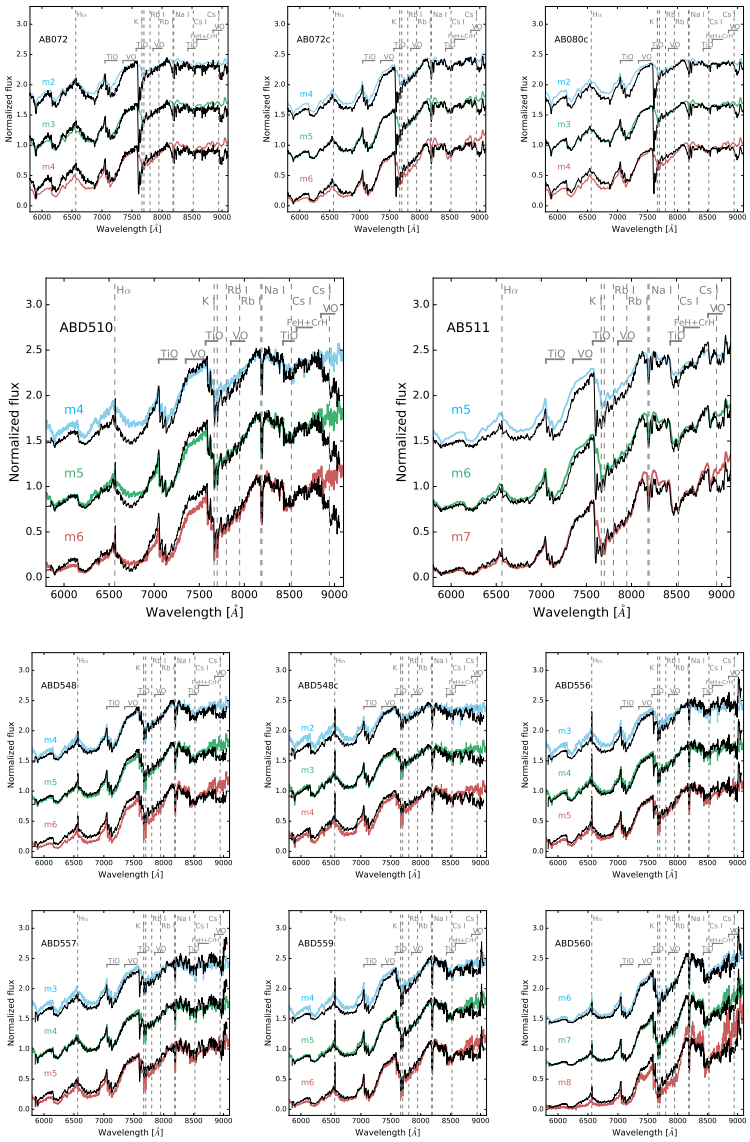

Figure 5.10: Optical spectra of the observed candidate companions from AB Dor. The candidate spectra are shown in black. Template spectra are shown in colours, for comparison. The spectra were normalised at ∼8080 Å and shifted by a constant for clarity. Some remarkable spectral features are marked in grey.

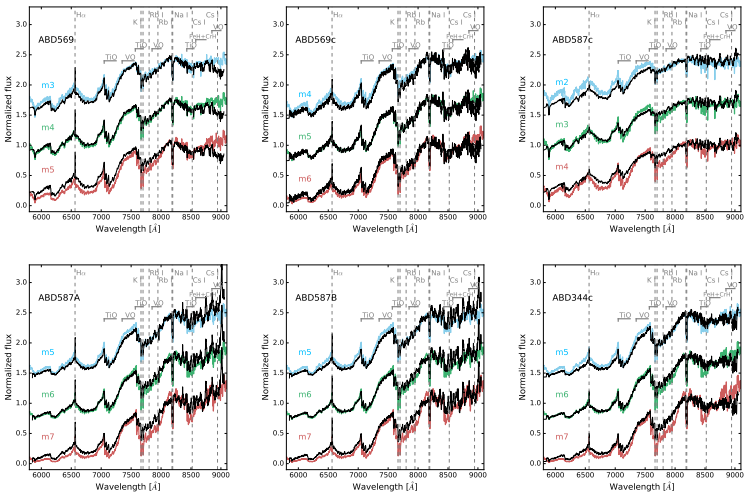

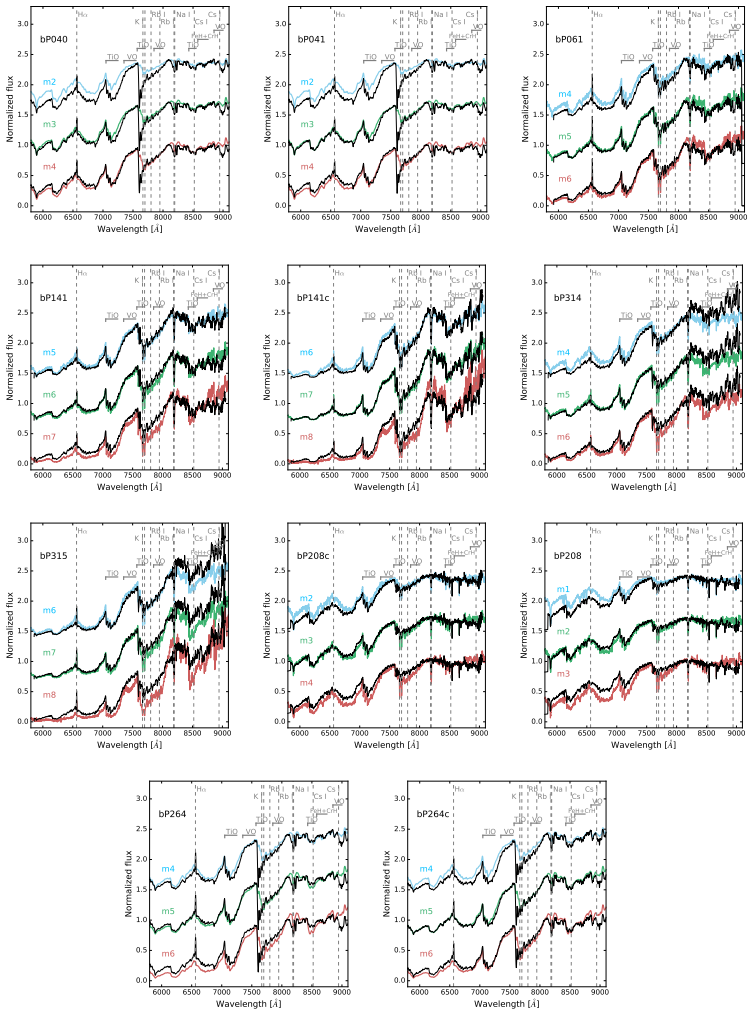

Figure 5.11: Optical spectra of the observed candidate companions from β Pic. The candidate spectra are shown in black. Template spectra are shown in colours, for comparison. The spectra were normalised at ∼8080 Å and shifted by a constant for clarity. Some remarkable spectral features are marked in grey.

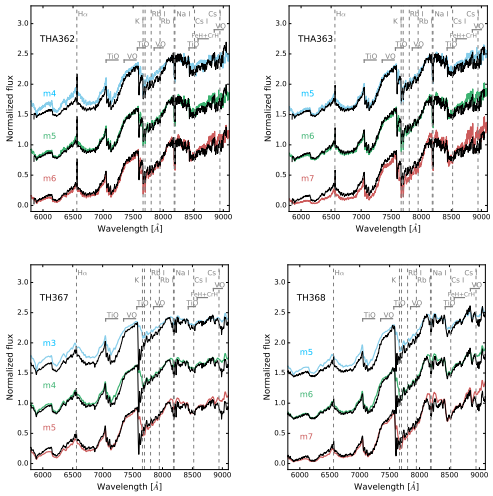

Figure 5.12: Optical spectra of the observed candidate companions from THA. The candidate spectra are shown in black. Template spectra are shown in colours, for comparison. The spectra were normalised at ∼8080 Å and shifted by a constant for clarity. Some remarkable spectral features are marked in grey.

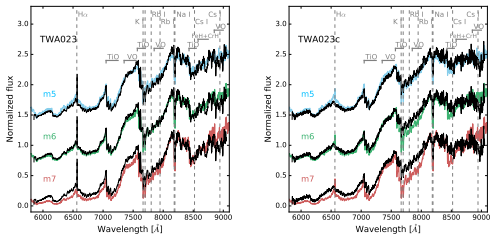

Figure 5.13: Optical spectra of the observed candidate companions from TWA. The candidate spectra are shown in black. Template spectra are shown in colours, for comparison. The spectra were normalised at ∼8080 Å and shifted by a constant for clarity. Some remarkable spectral features are marked in grey.

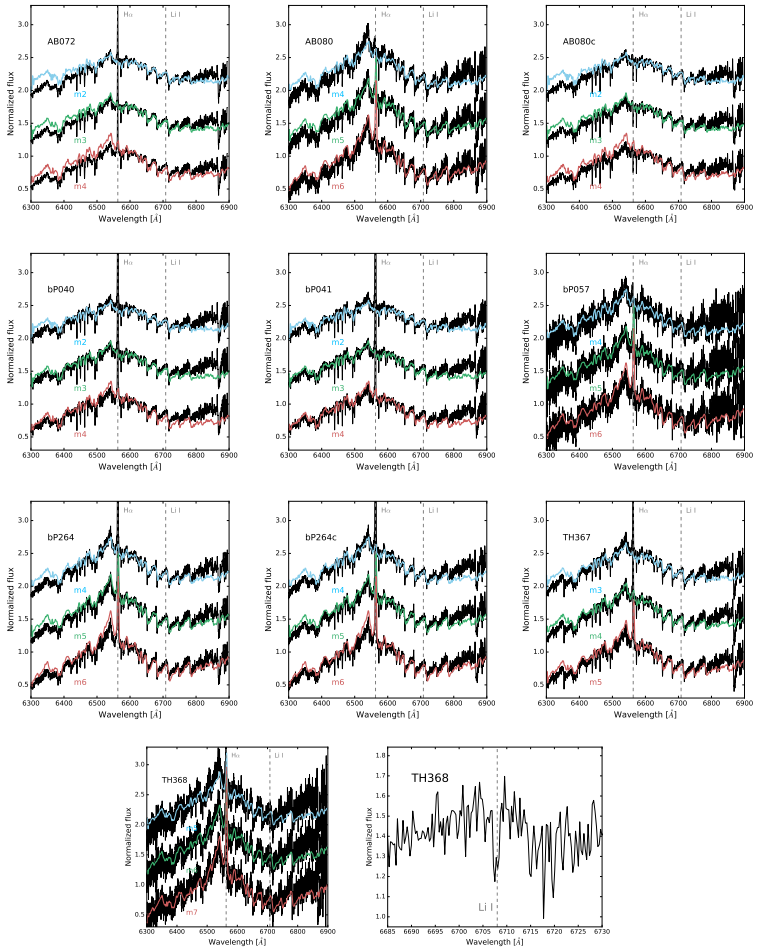

Figure 5.14: High-resolution optical spectra of some candidate companions observed with NOT/ALFOSC. The candidate spectra are shown in black. Template spectra are shown in colours, for comparison. The spectra were normalised at ∼6600 Å and shifted by a constant for clarity. The last panel shows a close-up figure of the Li I doublet region of the target THA368. Some remarkable spectral features are marked in grey.

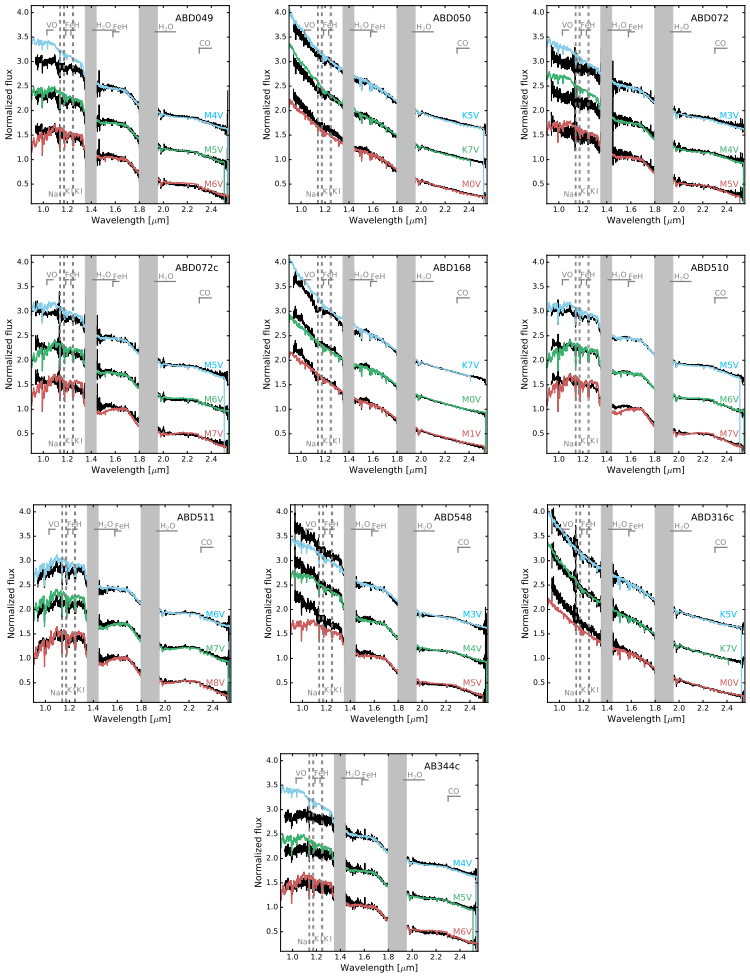

Figure 5.15: NIR spectra of the observed candidate companions from AB Dor. The candidate spectra are shown in black. Template spectra are shown in colours, for comparison. The spectra were normalised at 1.68 μm and shifted by a constant for clarity. Regions strongly affected by atmospheric telluric absorption are covered with grey bands. Some remarkable spectral features are marked in grey.

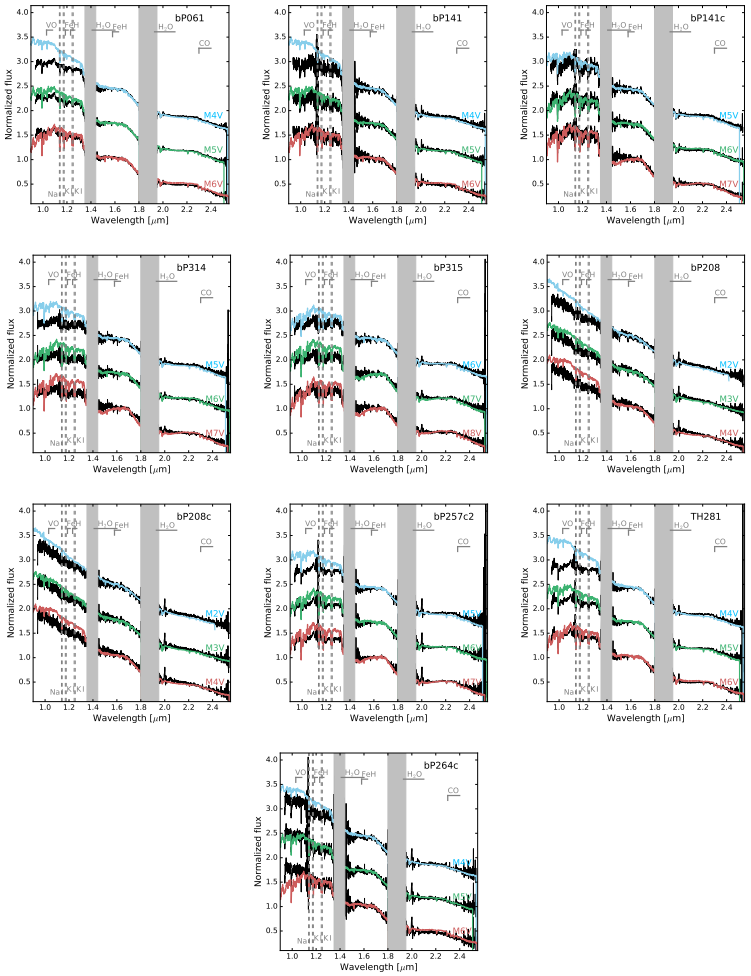

Figure 5.16: NIR spectra of the observed candidate companions from β Pic. The candidate spectra are shown in black. Template spectra are shown in colours, for comparison. The spectra were normalised at 1.68 μm and shifted by a constant for clarity. Regions strongly affected by atmospheric telluric absorption are covered with grey bands. Some remarkable spectral features are marked in grey.

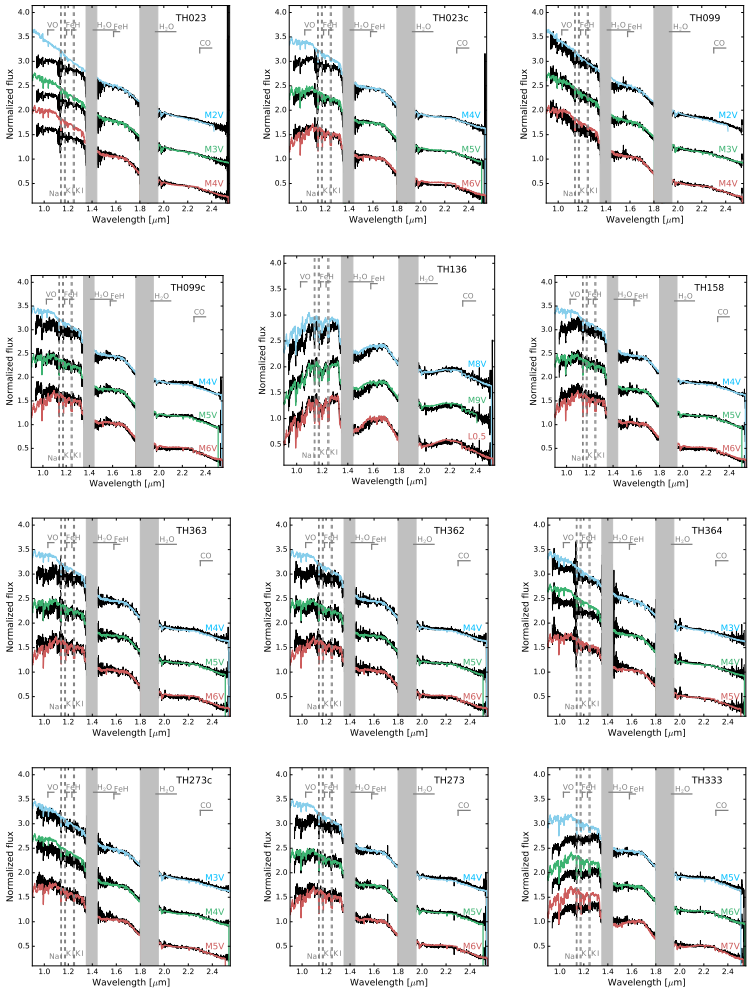

Figure 5.17: NIR spectra of the observed candidate companions from THA. The candidate spectra are shown in black. Template spectra are shown in colours, for comparison. The spectra were normalised at 1.68 μm and shifted by a constant for clarity. Regions strongly affected by atmospheric telluric absorption are covered with grey bands. Some remarkable spectral features are marked in grey.

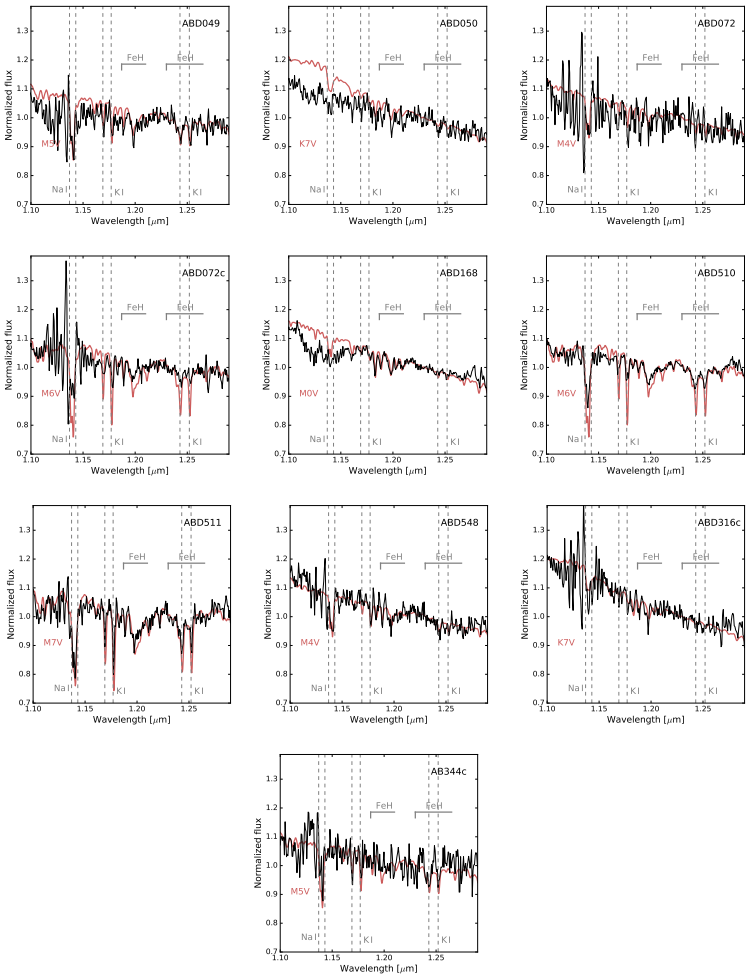

Figure 5.18: J-band display for the AB Dor targets. The candidate spectra are shown in black. Template spectra are shown in red, for comparison. The spectra were normalised at 1.23 μm. Some remarkable spectral features are marked in grey.

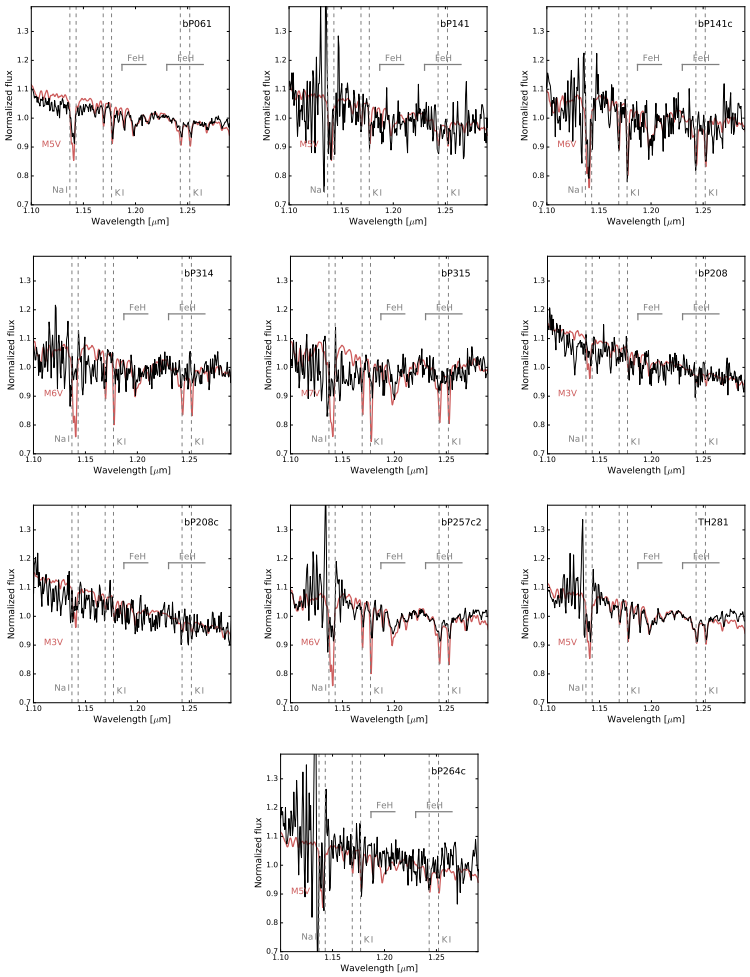

Figure 5.19: J-band display for the β Pic targets. The candidate spectra are shown in black. Template spectra are shown in red, for comparison. The spectra were normalised at 1.23 μm. Some remarkable spectral features are marked in grey.

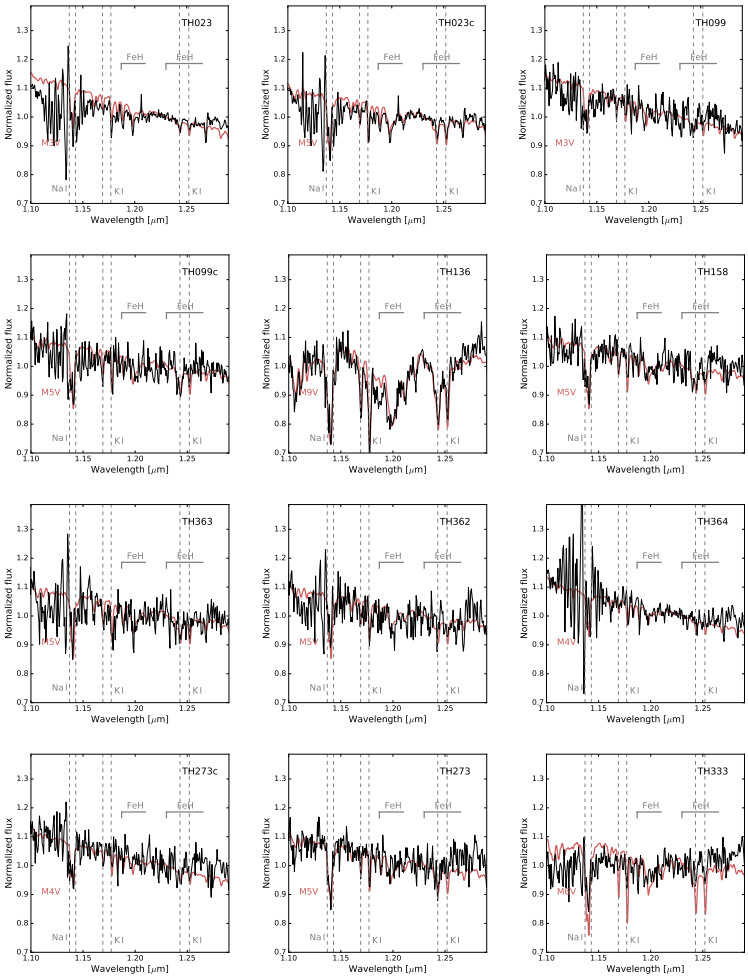

Figure 5.20: *J*-band display for the THA targets. The candidate spectra are shown in black. Template spectra are shown in red, for comparison. The spectra were normalised at 1.23 μm. Some remarkable spectral features are marked in grey.

6

Strong Hα emission in the young planetary-mass companion 2MASS J0249−0557 c

In this chapter we present the characterization of one of the most interesting objects found in the YMGs search: 2MASS J0249−0557 c. These results have been accepted for publication with the title "Strong Hα emission in the young planetary mass companion 2MASS J0249−0557 c" in the peer-reviewed journal "Astronomy & Astrophysics" (Chinchilla et al. 2020a). The article is included here in the original format of the journal.

Astronomy & Astrophysics manuscript no. 38731corr
December 9, 2020

Strong Hα emission in the young planetary mass companion 2MASS J0249−0557 c

P. Chinchilla[1,2], V. J. S. Béjar[1,2], N. Lodieu[1,2], M. R. Zapatero Osorio[3], and B. Gauza[4,5]

[1] Instituto de Astrofísica de Canarias (IAC), Calle Vía Láctea s/n, 38200 La Laguna, Tenerife, Spain.
e-mail: pchinchilla.astro@gmail.com
[2] Departamento de Astrofísica, Universidad de La Laguna (ULL), 38205 La Laguna, Tenerife, Spain.
[3] Centro de Astrobiología (CSIC-INTA), Ctra. de Ajalvir km 4, 28850 Torrejón de Ardoz, Madrid, Spain.
[4] Centre for Astrophysics Research, University of Hertfordshire, College Lane, Hatfield AL10 9AB, UK.
[5] Janusz Gil Institute of Astronomy, University of Zielona Góra, Lubuska 2, 65-265 Zielona Góra, Poland.

Received 24 June 2020; accepted 10 November 2020

ABSTRACT

Aims. Our objective is the optical and near-infrared spectroscopic characterisation of 2MASS J0249−0557 c, a recently discovered young planetary mass companion to the β Pictoris (∼25 Myr) member 2MASS J0249−0557.
Methods. Using the Visible and Infrared Survey Telescope for Astronomy (VISTA) Hemisphere Survey (VHS) and the Two Micron All Sky Survey (2MASS) data, we independently identified the companion 2MASS J0249−0557 c. We also obtained low-resolution optical spectroscopy of this object using the Optical System for Imaging and low-intermediate-Resolution Integrated Spectroscopy (OSIRIS) spectrograph at the Gran Telescopio Canarias (GTC), and near-infrared spectroscopy using the Son of Isaac (SofI) spectrograph on the New Technology Telescope (NTT).
Results. We classified 2MASS J0249−0557 c with a spectral type of L2.5±0.5 in the optical and L3±1 in the near-infrared. We identified several spectroscopic indicators of youth both in the optical and in the near-infrared that are compatible with the age of the β Pictoris moving group: strong absorption due to oxides, weak alkaline atomic lines, and a triangular shape of the H-band pseudo-continuum. We also detect a strong Hα emission, with a pseudo-equivalent width (pEW) of -90^{+20}_{-40} Å, which seems persistent at timescales from several days to a few years. This indicates strong chromospheric activity or disk accretion. Although many M-type brown dwarfs have strong Hα emission, this target is one of the very few L-type planetary mass objects in which this strong Hα emission has been detected. Lithium absorption at 6708 Å is observed with pEW $\lesssim$ 5 Å. We also computed the binding energy of 2MASS J0249−0557 c and obtained an (absolute) upper limit of $U = (-8.8 \pm 4.4)10^{32}$ J.
Conclusions. Similarly to other young brown dwarfs and isolated planetary mass objects, strong Hα emission due to accretion or chromospheric activity is also present in young planetary mass companions at ages of some dozen million years. We also found that 2MASS J0249−0557 c is one of the wide substellar companions with the lowest binding energy known to date.

Key words. brown dwarfs – planetary systems – binaries:visual – open clusters and associations: individual: β Pictoris – Stars: pre-main sequence

1. Introduction

One of the main challenges in astronomy today is understanding the formation and evolution of planetary systems. The characterisation of planets of different ages is key to providing a more accurate picture of the different stages of their formation. However, this characterisation is very difficult because planets are frequently too close to their parent stars and are too faint compared to them to be directly imaged. One possible solution for this issue is finding wide (>50–100 AU) planetary mass companions, which can serve as analogues to the close-orbit giant planets. Because these objects have a wide separation from their primary star, they can be fully characterised using spectroscopy (e.g. Aller et al. 2013; Bowler et al. 2014; Deacon et al. 2014; Gauza et al. 2015; Dupuy et al. 2018; Chinchilla et al. 2020).

β Pictoris is a young moving group (YMG) named after its brightest and most famous member, the A-type star β Pictoris. The group was first discovered by Zuckerman et al. (2001), who identified 17 young stellar systems moving through space together with the main representative of the group. With an age of ∼20–25 Myr (Barrado y Navascués et al. 1999; Mentuch et al. 2008; Binks & Jeffries 2014; Malo et al. 2014; Mamajek & Bell 2014; Bell et al. 2015; Shkolnik et al. 2017) and a mean heliocentric distance of ∼40 pc (Miret-Roig et al. 2018), its youth and proximity make the β Pictoris YMG one of the best laboratories for the search and characterisation of young substellar companions.

One of the most recently discovered wide planetary mass companions is 2MASS J02495436−0558015 (hereafter 2MASS J0249−0557 c; Dupuy et al. 2018). This is a $11.6^{+1.3}_{-1.0}\,M_{\rm Jup}$ object orbiting at a separation of ∼1950 AU from the M6 member of β Pictoris YMG 2MASS J02495639−0557352. The primary itself has been resolved by the Keck Laser Guide Star (LGS) adaptive optics into a close (2.17±0.22 AU, 0.04″) brown dwarf pair (hereafter 2MASS J0249−0557 AB), with estimated masses of $48^{+13}_{-12.0}\,M_{\rm Jup}$ and $44^{+14}_{-11.0}\,M_{\rm Jup}$, respectively (Dupuy et al. 2018).

We present the independent discovery and new optical and near-infrared characterisation of 2MASS J0249−0557 c. Section 2 describes the main characteristics of the system. In Section 3 we present the independent identification of this object. Section 4 describes the optical and near-infrared spectroscopic observations obtained for the planetary mass companion, and section 5

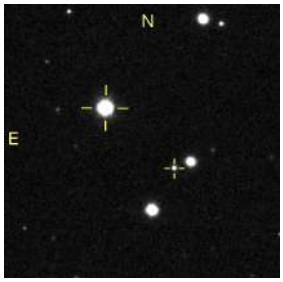

Fig. 1. J-band VHS finding chart for the 2MASS J0249−0557 system. The system components are marked with crosses. The field of view is 2′× 2′and the orientation is north up and east to the left. The angular separation between the components is 40.0″.

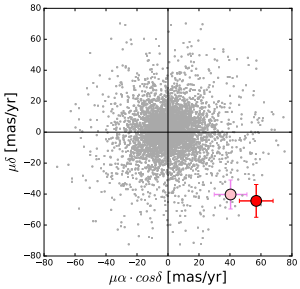

Fig. 2. Proper motion diagram for 2MASS J0249−0557 AB (light pink) and 2MASS J0249−0557 c (red) from the VHS–2MASS cross correlation. Other cross-correlated objects in the same field of view are marked in grey.

presents the main results. Finally, Section 6 provides the summary and final remarks.

2. 2MASS J0249−0557 system

The primary, 2MASS J0249−0557, was included in Shkolnik et al. (2017) as a new confirmed member of β Pic moving group. They determined a spectral type of M6 and found very low gravity signs in its near-infrared spectrum. They measured a radial velocity of 14.42 ± 0.44 km s^{-1}, a lithium pseudo-equivalent width (pEW) of 0.59±0.05 Å and a strong Hα emission line with a pEW of −11.6±0.1 Å.

Dupuy et al. (2018) recently published the discovery of 2MASS J0249−0557 c as a wide (39.959±0.005″, 1950±200 AU) companion to 2MASS J0249−0557, one of the targets from the Hawaii Infrared Parallax Program. They also found that the primary is a tight brown dwarf binary, revealing that 2MASS J0249−0557ABc is a bound triple system. Using the Keck/NIRC2 instrument and the laser guide star adaptive optic system (LGS AO), they resolved the primary into two similar magnitude objects located at an angular separation of 44.4±2 mas (equivalent to 2.17±0.22 AU). They determined a near-infrared spectral type of L2 VL-G for the wide companion and masses of 48^{+13}_{-12} and 44^{+14}_{-11} M_{Jup} for the tight binary and $11.6^{+1.3}_{-1.0}$ M_{Jup} for the wide companion. They measured the parallax and proper motions, and confirmed the membership of this system in the β Pic moving group. They showed that the companion 2MASS J0249−0557 c is physically bound, which means that this is one of the few triple substellar systems known to date.

3. Independent identification of 2MASS J0249−0557 c

As part of our efforts to characterise the frequency of wide substellar companions around young nearby stars, we performed a search for common proper motion companions to known members and candidate members of the β Pictoris YMG, among other young stellar kinematic groups, using data from the Visible and Infrared Survey Telescope for Astronomy (VISTA) Hemisphere Survey (VHS, McMahon et al. 2013) catalogue in combination

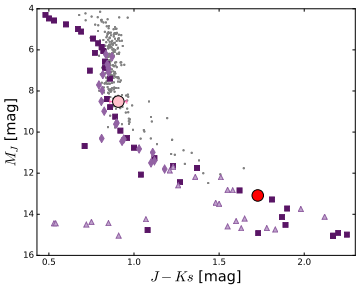

Fig. 3. M_J vs. J−Ks colour-magnitude diagram for 2MASS J0249−0557 AB (light pink) and 2MASS J0249−0557 c (red). Other known β Pic members are plotted as grey dots. The photometric sequence of field dwarfs derived by Pecaut & Mamajek (2013, squares), Dupuy & Liu (2012, triangles), and Lodieu et al. (2014, diamonds) is also shown in purple.

with the Two Micron All-Sky Survey (2MASS, Skrutskie et al. 2006) catalogue.

For this purpose, we first compiled a list of 348 known members and candidate members of β Pictoris, which we obtained from Schlieder et al. (2010, 2012), Malo et al. (2013), Bell et al. (2015), Best et al. (2015), Gagné et al. (2015a), Gagné et al. (2015b), Elliott et al. (2016), Messina et al. (2017), Schneider et al. (2017), Shkolnik et al. (2017) and Gagné & Faherty (2018). One of the members in this list is 2MASS J0249−0557.

Secondly, we queried the VHS database to download all the available data in a circular area corresponding to 50 000 AU around each β Pic candidate member in the compilation. The angular area corresponding to this radius was calculated in most of the cases using the available parallaxes from *Gaia* DR2. For the objects without parallaxes, we downloaded all the data in

a 83.4′ radius, which corresponds to a physical separation of 50 000 AU for an object placed at 10 pc distance, considering this as a lower limit for the heliocentric distance of β Pic members.

Then, we cross-matched the VHS data with the 2MASS catalogue to identify nearby objects whose proper motions matched those of the primaries within an error of 40 mas yr^{-1} in total. This value is at least twice the typical dispersion in the measured proper motions of non-moving background objects, which is 10–20 mas yr^{-1}, depending on the time baseline between the VHS and 2MASS observations (9–19 years). To the targets with compatible proper motions, we later applied photometric selection criteria using VHS and 2MASS (Skrutskie et al. 2006) photometry and also DENIS and/or AllWISE data (Epchtein et al. 1997; Wright et al. 2010) when available. We selected as good candidate companions those objects whose magnitudes and colours followed a well-defined photometric sequence with their primaries in different colour-magnitude diagrams, and which therefore can be placed at the same heliocentric distance. We also used *Gaia* DR2 (Gaia Collaboration et al. 2016, 2018) astrometry for the brightest candidates to discard chance alignments.

As a result of this search, we found 2MASS J0249−0557 c, placed at a distance of 39.947±0.014 arcsec from 2MASS J0249−0557, with a position angle of 228.°644 ± 0.°020. These measured separation and position angles are compatible with those published in Dupuy et al. (2018). This is the faintest candidate companion identified in our search. However, because we are limited to the completeness of 2MASS (J∼16) in this search, other candidate companions with similar masses and spectral types may have remained undetected. Figure 1 shows the finding chart for the 2MASS J0249−0557 system. The proper motion of the candidate companion agreed well with the motion of the primary, and its magnitude and colours were consistent with an L-type object located at the same heliocentric distance as the primary brown dwarf pair. Figures 2 and 3 show the proper motion diagram and J–J-Ks colour magnitude diagram for the system.

2MASS J0249−0557 was imaged by VHS, 2MASS, Pan-STARRS (Chambers et al. 2016), the Sloan Digital Sky Survey (SDSS; York et al. 2000), WISE, and Gaia. The available photometric data for the system are presented in Table 1.

Table 1. General data of 2MASS J0249−0557 AB and c.

Astrometry	AB	c
R.A. (J2000)	02 : 49 : 56.39	02 : 49 : 54.36
DEC (J2000)	−05 : 57 : 35.2	−05 : 58 : 01.5
Parallax (mas) [a]	20.5 ± 2.1	20.1 ± 3.5
Distance (pc) [a]		$48.9^{+4.4}_{-5.4}$
Separation (arcsec) [a]	0.0444 ± 0.0002″	39.959 ± 0.005″
Separation (AU) [a]	2.17 ± 0.22	1950 ± 200
P.M. (mas yr^{-1}) [a]	(42.9, −30.2) ±(2.0, 1.8)	(46.0, −32.0) ±(2.3, 2.1)
Spectroscopy		
Spectral type	M6 [b]	L2.5 ± 0.5 OPT, L3 ± 1 NIR [c]
Li pEW (Å)	0.59 ± 0.05 [b]	≲ 5
Hα pEW (Å)	−11.61 ± 0.1 [b]	-90^{+20}_{-40} [c]
Photometry		
Gaia g	15.6894 ± 0.0012	–
SDSS *u*	21.47 ± 0.14	–
SDSS *g*	18.721 ± 0.008	–
SDSS *r*	17.197 ± 0.006	–
SDSS *i*	14.977 ± 0.005	20.76 ± 0.13
SDSS *z*	13.754 ± 0.005	19.28 ± 0.15
Pan-STARRS *g*	18.419 ± 0.008	–
Pan-STARRS *r*	17.145 ± 0.005	–
Pan-STARRS *i*	14.992 ± 0.004	21.36 ± 0.06
Pan-STARRS *z*	13.984 ± 0.004	19.92 ± 0.03
Pan-STARRS *y*	13.409 ± 0.004	18.93 ± 0.03
VHS *J*	11.9667 ± 0.0007	16.531 ± 0.008
VHS *Ks*	11.2535 ± 0.0009	14.804 ± 0.009
2MASS *J*	11.96 ± 0.03	16.55 ± 0.11
2MASS *H*	11.36 ± 0.03	15.48 ± 0.13
2MASS *K*	11.06 ± 0.02	14.88 ± 0.12
WISE *w1*	10.84 ± 0.02	14.13 ± 0.03
WISE *w2*	10.60 ± 0.02	13.59 ± 0.04
WISE *w3*	10.39 ± 0.06	–

Notes. [a] Data from Dupuy et al. (2018). [b] Data from Shkolnik et al. (2017). [c] Data from this work.

4. Follow-up observations and data reduction

4.1. GTC/OSIRIS optical spectroscopy

2MASS J0249−0557 c was observed on 27 January 2019 with the Optical System for Imaging and low-intermediate-Resolution Integrated Spectroscopy (OSIRIS; Cepa et al. 2000) spectrograph at the 10.4 m Gran Telescopio Canarias (GTC) in La Palma, Canary Islands. The observations were performed in long-slit spectroscopy mode, using the R500R grism (wavelength coverage 0.48–1.00 μm) and the 0.8″wide slit placed in parallactic angle, providing a resolution of ∼440 at 7200 Å. Four exposures of 1600s were obtained using an ABBA nodding pattern with a 14″offset along the slit. The object acquisition was performed using the Sloan z filter. The seeing value was 0.7″. The spectrophotometric standard G191-B2B (DA white dwarf, V=11.7) was also observed with the same instrumental configuration to correct for the instrumental response. The observation log is shown in Table 2.

The data reduction was performed using standard routines within the Image Reduction and Analysis Facility (IRAF) environment (Tody 1986, 1993). The images were corrected for bias and were flat-fielded. Then, the 2D images of the four individual exposures of the target were corrected for bad pixels and cosmic rays using IMEDIT. The four target spectra and the spectrophotometric standard spectrum were extracted using the APALL routine. The spectra were wavelength calibrated at each nodding position using HgAr, Ne, and Xe arc images. The spectrum of the standard was corrected for second-order contamination of the light at wavelengths 4800–4900 Å using a spectrum taken with the z-band filter, following the procedure explained in Zapatero Osorio et al. (2014). We obtained the sensitivity function from the standard star spectrum. Then, the spectra of the target were corrected for instrumental response using this sensitivity function. Finally, for an optimal combination of the four spectra, the data were aligned in wavelength with respect to the first exposure by cross-correlating the observations (the regions with strong telluric absorption were excluded from the cross correlation). The final combined spectrum is shown in Figures 4 and 5.

4.2. NTT/SofI infrared spectroscopy

We obtained near-infrared low-resolution spectroscopy of 2MASS J0249−0557 c on 21 June 2018 and 4 November 2018

Table 2. Observation log for 2MASS J0249−0557 c

Obs. Date	Telesc/Instrum	Mode	Grating/ Filter	Wavelength Range [μm]	Slit [″]	Pl. Scale [″/pix]	Disp. [Å/*pix*]	Res. Power	Exp. Time [s]	Airmass	Seeing [″]
11 Sep 2016	VISTA/VIRCAM	Img	J, Ks	–	–	0.34	–	–	8×15, 8×7.5	1.1	0.9
21 Jun 2018	NTT/SofI	Spec	GR	1.53–2.52	1	0.29	10.22	600	4×300	1.4–1.5	0.9
21 Jun 2018	NTT/SofI	Spec	GB	0.95–1.64	1	0.29	6.96	600	4×600	1.6–1.8	0.9
4 Nov 2018	NTT/SofI	Spec	GR	1.53–2.52	1	0.29	10.22	600	4×300	1.2–1.3	0.6
4 Nov 2018	NTT/SofI	Spec	GB	0.95–1.64	1	0.29	6.96	600	4×600	1.1–1.2	0.6
27 Jan 2019	GTC/OSIRIS	Spec	R500R	0.48–1.00	0.8	0.25	4.88	440	4×1600	1.2–1.4	0.7

using the Son of Isaac (SofI) spectrograph (Moorwood et al. 1998) mounted on the 3.6 m New Technology Telescope (NTT) at the La Silla Observatory, Chile, to determine the spectral type of the candidate companion and search for features of youth. We used long-slit spectroscopy mode with the 1.0″ wide slit, and the low-resolution blue and red grisms (wavelength ranges 0.95–1.64 μm and 1.53–2.52 μm, respectively, resolving power 600, and nominal dispersion 6.96 and 10.22 Å pix^{-1}, respectively). The exposures were taken using an ABBA nodding pattern along the slit, with 600s and 300s individual exposure times in each position for blue and red grisms, respectively. We also observed the B7 telluric standards HIP14143 and HIP17457 after the exposures and at similar airmasses to correct for telluric absorption. To perform the flat-field correction and wavelength calibration, we also acquired continuum-lamp images and Xe arc-lamp images. A log of these observations is included in Table 2.

The data reduction was performed using the SofI pipeline by ESO within the Gasgano environment (Gebbinck & Sforna 2007) and standard IRAF routines for both the target and telluric standards. The raw spectroscopic images were flat-field and dark corrected, aligned, and combined using Gasgano. We then used the IRAF APALL routine to extract the spectra from these 2D combined images, and wavelength calibrated them using the Xe arcs. We manually removed the intrinsic lines of the spectrum of the telluric star. Finally, to correct for the instrumental response, the target spectra were divided by the telluric spectra and multiplied by a black body of 14 500 K, which is the corresponding temperature for the telluric star spectral type (Pecaut & Mamajek 2013). For a better result in the signal-to-noise ratio, we combined the resulting spectra from the two observations. The final spectrum is shown in Figures 6 and 7.

5. Results and discussion

5.1. Optical characterisation and spectral classification

We have compared the optical spectrum of 2MASS J0249−0557 c with several young and old L-dwarf templates to determine the optical spectral type and analyse its spectral features. Figure 4 shows the comparison between the GTC/OSIRIS optical spectrum of 2MASS J0249−0557 c and some old field L-type standards from Kirkpatrick et al. (1999) and Kirkpatrick et al. (2000), observed with the Low Resolution Imaging Spectrometer (LRIS) and the 400/8500 grism (R∼1100) on the Keck-I Telescope. LRIS spectra were convolved with a Gaussian to match the GTC/OSIRIS spectral resolution.

From this comparison, we find that the general spectral energy distribution of 2MASS J0249−0557 c in the optical fits that of the early and intermediate old-field L dwarfs. When we focus on the pseudo-continuum, the overall shape of the spectrum, particularly above 8000 Å, coincides with that of the intermediate old field dwarf of L5 spectral type. However, the depth of the VO, TiO, FeH, and CrH absorption bands in the optical spectrum of the target are better reproduced by early old field L dwarfs. These differences in the spectral features can be explained by the effect of the low gravity of the young object, which is still contracting. These discrepancies are frequent when young objects are compared with old counterparts, and can be misinterpreted as a difference in spectral type. For example, the shapes of the VO bands at 7300–7600 Å and 7800–8000 Å are closer in depth to the L1–L2 spectral templates. TiO at 8400–8600 Å is weakened and closer to later spectral types. This can also be seen at the 7000–7400 Å TiO band. Alkali lines are also weakened, as can be seen in the NaI doublet at 8183–8195 Å or in the CsI line at 8521 Å.

We also observed a tentative detection of the absorption line of Li I at 6708 Å, with a pEW of $\lesssim$ 5 Å. Nevertheless, the feature is barely distinguishable from the spectral noise at a 2σ level. The obtained value is compatible with a total preservation of lithium, as expected for a β Pictoris L2–3 member (Kirkpatrick et al. 2000).

For a more accurate spectral type classification, we also compared the optical spectrum of 2MASS J0249−0557 c to the spectra of some known young objects with spectral types L1–L5. Figure 5 shows these comparisons. This figure shows the strong resemblance of the spectrum of 2MASS J0249−0557 c to the optical spectra of 2MASS J00452143+1634446 (2MASS 0045+1634), which is classified as an L2, and G 196–3B (Rebolo et al. 1998), which is classified as an L3. 2MASS 0045+1634 is a young substellar object, with an estimated age of 10–100 Myr (Zapatero Osorio et al. 2014). It has been claimed as a likely member of the Argus moving group (40–50 Myr; Torres et al. 2008; Zuckerman 2019) by Gagné et al. (2014). G 196–3B is a young object, with an estimated age of 20–300 Myr, and it is also likely younger than 100 Myr (Zapatero Osorio et al. 2010, 2014). Gagné et al. (2014) indicated a moderate probability that G196–3B belongs to the AB Doradus moving group (∼125 Myr; Zuckerman et al. 2004; Luhman et al. 2005; Barenfeld et al. 2013). The spectra coincide in the overall shapes and in the depth of the oxide bands, suggesting that they may have similar temperatures and gravities. The most remarkable difference between our target and these comparison spectra in the optical is the Hα emission line, which is strong in 2MASS J0249−0557 c but it is not detected in either 2MASS 0045+1634 or G 196–3B (Mohanty & Basri 2003). We discuss this in more detail in section 5.4.

We have also computed spectral indices from Martín et al. (1999) to assess the spectral classification of this target. They are listed in Table 3. We excluded other commonly used indices related to the oxides because these features are strongly affected by gravity and are not adequate for spectral type determination

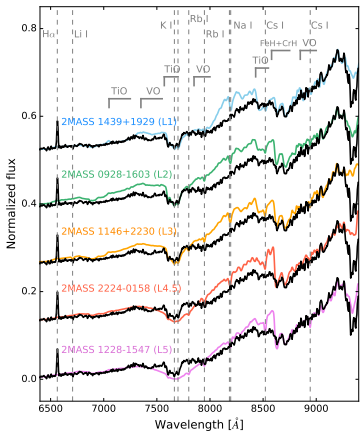

Fig. 4. GTC/OSIRIS optical spectrum of 2MASS J0249−0557 c (black) compared to old field optical L standards from Kirkpatrick et al. (1999) and Kirkpatrick et al. (2000) observed with Keck-I/LRIS (coloured). LRIS spectra were convolved with a Gaussian to match the OSIRIS spectrum resolution. Spectra were normalised at wavelength ∼9200 Å and shifted by a constant for clarity. Several spectral features are marked in grey.

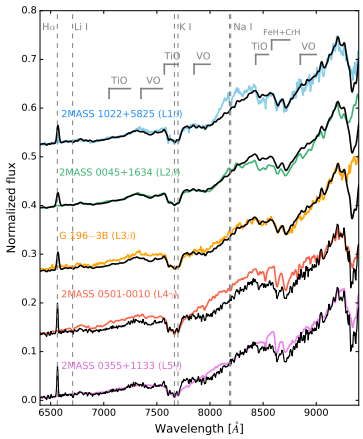

Fig. 5. GTC/OSIRIS optical spectrum of 2MASS J0249−0557 c (black) compared to other known young L objects (coloured) from Cruz et al. (2009, 2MASS 1022+5825, 2MASS 0501−0010 and 2MASS 0355+1133) and Zapatero Osorio et al. (2014, 2MASS 0045+1634 and G196–3B). The GTC/OSIRIS spectrum was convolved with Gaussians to match the young L1–L3 template spectra resolutions. For the L4–L5 comparisons, the template spectra were convolved to match the target spectral resolution. Spectra were normalised at wavelength ∼9200 Å and shifted by a constant for clarity. Some spectral features are marked in grey.

Table 3. Spectral indices for spectral type determination.

Index	Value	SpT	Index Ref.[a]
Optical			
PC3	2.78	L1.5±0.5	M99
PC6	21.9	M8–L4	M99
Infrared			
H_2O [b]	1.35	L4±0.5	A07
H_2OD [b]	0.99	L0.25±0.75	ML03
H_2O-1 [b]	0.59	L3.25±1.00	S04
H_2O-2 [b]	0.82	L1.25±0.50	S04

Notes. [(a)] References: A07 – Allers et al. (2007), M99 – Martín et al. (1999), ML03 – McLean et al. (2003), S04 – Slesnick et al. (2004). [(b)] Results obtained using the Allers & Liu (2013) polynomial fits.

in young objects. Based on our comparison with young and field L dwarfs and the spectral indices, we finally adopted a classification in the optical of L2.5±0.5.

5.2. Infrared spectral classification

To determine the near-infrared spectral type, we compared our NTT/SofI spectrum with infrared spectra of known young and field objects. Figure 6 shows a comparison of our 2MASS J0249−0557 c near-infrared spectrum with several old field L dwarfs from Kirkpatrick et al. (1999) and Kirkpatrick et al. (2000). This figure shows that the spectral energy distribution of our target in the near-infrared bands resembles that of the L3 and L4.5 spectral types, except for the different shapes of the *H* band and the depth of some molecular bands such as VO and FeH, which are more intense in 2MASS J0249−0557 c. The triangular shape of the *H* band (e.g., Lucas et al. 2001; Allers & Liu 2013) is a remarkable feature that reveals the young nature of this object.

Figure 7 shows the near-infrared spectrum of 2MASS J0249−0557 c compared to very low gravity L spectral templates from Cruz et al. (2018). The spectrum fits the L2γ, L3γ, and L4γ templates in each of the individual near-infrared bands rather well. This is clearly visible in the slopes of the H_2O absorption bands at either side of the *H* band, and also at the red side of the *J* band. However, there are some discrepancies. For example, the VO band at 1.06 μm is stronger in 2MASS J0249−0557 c than

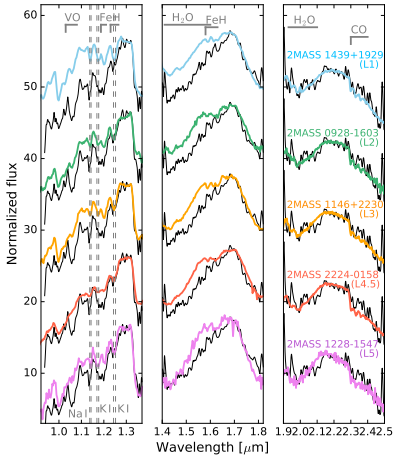

Fig. 6. NTT/SofI spectrum of 2MASS J0249−0557 c (black) compared to old field L standards from Kirkpatrick et al. (1999) and Kirkpatrick et al. (2000) observed with IRTF/SpeX (coloured) by Burgasser et al. (2004), Burgasser et al. (2010), and Cruz et al. (2018). The NTT/SofI spectrum was convolved with a Gaussian to match the resolution of SpeX spectra. *J*, *H*, and *K* bands are displayed and normalised separately. Some spectral features, such as the VO, FeH, H_2O, and CO bands or the NaI and KI doublets, are marked in grey.

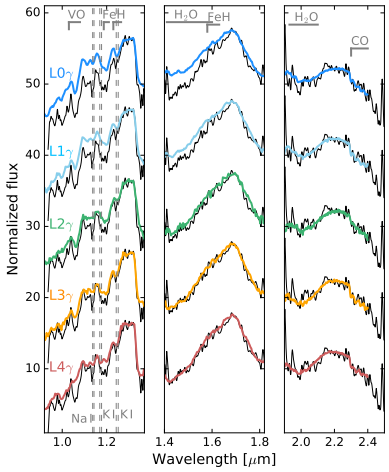

Fig. 7. Same as Fig. 6, but comparing the NTT/SofI spectrum of 2MASS J0249−0557 c (black) to near-infrared very low gravity L dwarf templates from Cruz et al. (2018) (coloured). The NTT/SofI spectrum was convolved with a Gaussian to match the spectral resolution of the templates.

in the templates. For an old object this would imply an earlier spectral type, but in this case, it may indicate a lower gravity, and hence a younger age for 2MASS J0249−0557 c compared to the templates. Although all the objects used to produce these template spectra show very low gravity features, and at least one of the three objects used to produce the L3γ template is probably a member of β Pic (see Cruz et al. 2018), they may have a wider range of ages and many of them may be older than this young moving group.

To confirm this spectral type classification, we also estimated the near-infrared spectral indices based on H_2O absorption bands from Allers et al. (2007), McLean et al. (2003) and Slesnick et al. (2004) and the best gravity-dependent indices defined by Lodieu et al. (2018) for the gravity type. These indices are shown in Table 3 and Table 4. Based on these comparisons and the spectral indices, we finally adopted a spectral type of L3±1 γ in the near-infrared for 2MASS J0249−0557 c, where the γ suffix is an indication of very low gravity features. This classification is compatible with the spectral type determination of L2±1 VL-G assigned by Dupuy et al. (2018), where VL-G also indicates a very low gravity. This is consistent with the signs of youth we have found in the optical and near-infrared spectra and with the expected age for a member of β Pic.

Table 4. Gravity-dependent indices.

Index	Value	Gravity[a]	Index Ref.[b]
H-cont	0.99	γ	AL13
CH_4-H	1.16	β–γ	B06
VO_z	1.50	γ	AL13
H_2O-K	0.86	β–γ	B06

Notes. [a] Gravity indices as described in Kirkpatrick (2005) and Cruz et al. (2009). Assigned following the plots in Fig. A1 of Lodieu et al. (2018). [b] References: AL13 – Allers & Liu (2013), B06 – Burgasser et al. (2006)

5.3. Comparison between optical and near-infrared spectral classification

We adopted a spectral type of L3±1 in the near-infrared, which agrees well with previous determination by Dupuy et al. (2018), and L2.5±0.5 in the optical. This is the first classification of this object in this wavelength range. Although the uncertainty in the spectral type determination of young objects is larger than in older field L dwarfs because the low-gravity templates do not constitute a homogeneous sample of targets with the same age and hence evolutionary state, our classification in the optical and in the near-infrared is compatible.

Previous studies in very young open clusters and associations with ages younger than ~ 10 Myr have shown that L dwarfs may have a slightly earlier spectral type in the optical than in the near-infrared (Zapatero Osorio et al. 2017; Lodieu et al. 2018). However, this does not seem to be the case for L dwarfs belonging to YMGs and associations at ages >10 Myr (Cruz et al. 2018). The β Pic group is close to the frontier between the two age groups and therefore is a favourable place to investigate this issue in more detail.

5.4. Hα emission in 2MASS J0249−0557 c

As pointed out in previous sections, the strong Hα emission line at 6563 Å is a remarkable feature of this object. To investigate the chromospheric activity and its variability, we measured the Hα pEW in the final combined GTC/OSIRIS spectrum by fitting a Gaussian profile to the line using the SPLOT task within the IRAF environment. We repeated this procedure several times, selecting a wide range of acceptable continuum levels. The average measured pEW is -90^{+20}_{-40}Å. The quoted error takes the spread of the measured pEWs with the different choices of the continuum level into account.

This object was also observed by the Extended Baryon Oscillation Spectroscopic Survey (eBOSS; Dawson et al. 2016) from the SDSS on 3 December 2015. This survey is carried out using the BOSS spectrographs (Smee et al. 2013) mounted on the SDSS 2.5m telescope (Gunn et al. 2006) at the Apache Point Observatory, New Mexico. The eBOSS optical spectral coverage is 3600–10400 Å, and the spectral resolution is 1300–2500 (Alam et al. 2015). The eBOSS spectra are publicly available in the SDSS Sky Server.[1] Due to the faintness of the object in the bluer range, the signal-to-noise ratio of the spectrum is rather poor in the Hα region, and the pseudo-continuum level is nearly zero. Nevertheless, the Hα emission line can be recognised. We measured a lower limit in the Hα emission of 20 Å from the eBOSS spectrum (pEW < −20Å).

The left panel of Figure 8 shows the comparison between the Hα lines of the eBOSS and the GTC/OSIRIS spectra of 2MASS J0249−0557 c. The time baseline between the observations is three years. This figure shows that the emission of Hα appears at both epochs. Although it is possible that we have observed the object during two isolated flare episodes by chance, it is therefore more likely that the Hα emission in 2MASS J0249−0557 c is persistent on timescales of years and is not related to episodic events.

We have also analysed the variations in the Hα emission within the individual exposures of the GTC/OSIRIS observations. Four exposures of 1600s (~27 min) were taken. We extracted the individual spectra and measured the Hα pEW in each one of them separately. Table 5 shows the Hα measurements of the individual exposures and of the combined spectrum. The right panel of Figure 8 shows the comparison between the four individual exposures. We find consistent values of the Hα pEW in them, with some variations that do not seem to be significant within the errors. Because the pseudo-continuum flux of the target in the wavelength region around Hα is low, the measured errors of the pEW in the individual spectra are relatively large.

[1] http://skyserver.sdss.org/dr15/en/home.aspx

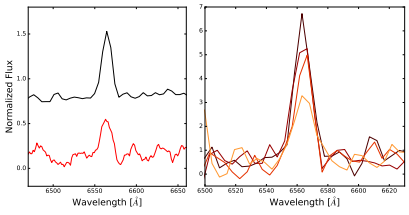

Fig. 8. Variation in the Hα emission line. The left panel shows the Hα line in our GTC/OSIRIS spectrum (black) compared with the eBOSS spectrum (red). The eBOSS spectrum has been smoothed for a better visualisation. The right panel shows the Hα line extracted from the four GTC/OSIRIS individual exposures separately.

Table 5. Hα measurements for 2MASS J0249−0557 c.

	MJD	Hα pEW (Å)
eBOSS	57359	< −20 [a]
OSIRIS Indiv. 1	58510.841	-110^{+40}_{-100}
OSIRIS Indiv. 2	58510.859	-110^{+40}_{-80}
OSIRIS Indiv. 3	58510.878	-130^{+70}_{-60} [b]
OSIRIS Indiv. 4	58510.897	-80^{+40}_{-70}
OSIRIS Comb.	58510.87	-90^{+20}_{-40}

Notes. [a] The pseudo-continuum emission in the Hα region is too close to zero in this spectrum. [b] Very low continuum level in the Hα region.

5.5. Hα emission in ultra-cool dwarfs

The Hα line found in emission in ultra-cool dwarfs is usually associated with chromospheric activity and/or accretion (Hawley et al. 1996; Gizis et al. 2000; White & Basri 2003; Mohanty & Basri 2003; Muzerolle et al. 2003; Jayawardhana et al. 2003; Mohanty et al. 2005; Caballero et al. 2006). It is a common feature in late-M and early-L objects and occurs most frequently at ~M7 spectral type. It decreases dramatically for mid-L and later spectral types (Gizis et al. 2000; Schmidt et al. 2015; Pineda et al. 2016). In addition, although some old L-type objects may present Hα emission lines due to flares and close binarity, a strong and stable Hα emission is commonly associated with youth (Liebert et al. 2003). However, many known young objects lack Hα emission (e.g. Martín et al. 2010; Lodieu et al. 2018; Chinchilla et al. 2020). Stable and strong Hα emission therefore is a sufficient but not necessary indicator of youth.

We can find many examples of young late-M brown dwarfs with strong Hα in emission in open clusters and associations of different ages (e.g. Luhman et al. 1997; Béjar et al. 1999; Luhman 1999; Ardila et al. 2000; Comerón et al. 2000; Martín et al. 2001; Briceño et al. 2002; Zapatero Osorio et al. 2002b; Barrado y Navascués & Martín 2003; White & Basri 2003; Mohanty et al. 2005; Lodieu et al. 2006; Slesnick et al. 2006; Barrado y Navascués et al. 2007; Lodieu et al. 2011). However, there are very few young L-dwarfs with a pronounced Hα emis-

sion. Two outstanding cases are 2MASS J11151597+1937266, an L2γ in the planetary mass regime with a strong Hα emission (pEW=560±82 Å, Theissen et al. 2017, 2018); and Delorme 1 (AB)b, an L0 substellar companion to the young binary star 2MASS J01033563−5515561 (Hα pEW=135±5 Å, Delorme et al. 2013; Eriksson et al. 2020). In Sigma Orionis (1–8 Myr; Zapatero Osorio et al. 2002b), S Ori 71, a young L0 brown dwarf was reported to have an Hα pEW of around −700 Å (Barrado y Navascués et al. 2002). A similar case in this open cluster is S Ori 55, a substellar M9 object at the deuterium-burning mass limit with a variable Hα with pEW of 180–410 Å (Zapatero Osorio et al. 2002a). In these two cases the presence of strong Hα emission is attributed to the presence of an accretion disk, mass transfer in a binary system, or flare activity. Finally, although many late-M dwarfs in the Upper Scorpius (∼5–10 Myr) association have strong Hα emission, only a few of the early L-type objects of this region also present noticeable Hα emission, such as VISTA J1607−2146, VISTA J1611−2215, and VISTA 1615−2229 (Lodieu et al. 2018).

In addition, some candidate young exoplanets still in their formation stage have been found to present strong Hα emission, probably caused by accretion. This is the case of PDS 70 b and c (Wagner et al. 2018; Haffert et al. 2019), and LkCa15 (Kraus & Ireland 2012; Sallum et al. 2015), although recent studies showed that the Hα emission in this last object may come from an inner disk structure and not from a planet (Thalmann et al. 2016; Mendigutía et al. 2018; Currie et al. 2019). Some techniques have been proposed for using this Hα emission as a resource to detect new young exoplanets, such as spectro-astrometry (Mendigutía et al. 2018), or adaptive optics imaging in the Hα band (e.g. Close et al. 2014; Huélamo et al. 2018; Cugno et al. 2019; Zurlo et al. 2020).

2MASS J0249−0557 c is very similar in age, mass, and temperature to the planet β Pic b (Lagrange et al. 2010). This object may therefore show a similarly strong Hα emission. On the other hand, another similar wide companion in the β Pic moving group is 2MASS J21265040−8140293. This object has a spectral type of L3 and orbits the β Pic candidate member TYC 9486-927-1 at a separation of > 4500 AU (Deacon et al. 2016).[2] However, 2MASS J21265040−8140293 does not show any remarkable Hα emission (pEW > −15Å) in its optical spectrum (Cruz et al. 2007)[3]. The planet β Pic b has only been spectroscopically observed in the near-infrared (Chilcote et al. 2017), and no optical spectrum has been obtained so far. The possibility of an Hα emission in this planetary mass object therefore has not been tested yet.

In conclusion, strong Hα emission such as is observed in 2MASS J0249−0557 c is uncommon among old field L dwarfs, but several cases of young L-type objects exhibiting Hα emission at similar strength are known. However, in most of these examples, the objects are younger than 10 Myr, and this may be related to the presence of accretion disks. At the age of the β Pic (∼20–25 Myr), the gas in the disks is expected to have dissipated (Haisch et al. 2001). Nevertheless, this may not be the case for lower mass substellar objects, which may have longer disk-decay timescales (Riaz & Gizis 2008). Some cases of β Pic brown dwarf members show signs of the presence of a disk and ongoing accretion (e.g. 2M0335+23, 2M1935−28; Shkolnik et al. 2009, 2012; Liu et al. 2016), therefore this possibility cannot be ruled out. The lack of IR excess in the *WISE* $w1$ and $w2$ photometry of the object (see Table 1) indicates the absence of a warm disk around it. However, although the origin of the Hα emission may be chromospheric, we cannot rule out a colder disk of material or the possibility of gas accretion in the object. As an example, some of the planetary mass objects with signs of accretion in Sigma Orionis, such as S Ori 55, only show infrared excesses at wavelengths longer than 5 microns (Zapatero Osorio et al. 2007a).

[2] As pointed out in Deacon et al. (2016), this system is also compatible with the Tucana-Horologium association. However, it most likely belongs to the β Pic association.

[3] Spectrum available at the BDNYC database in `http://database.bdnyc.org/browse`

5.6. Binding energy and tidal disruption

Widely separated systems, especially those with low binding energies, are prone to disruption by external perturbations, such as close encounters with other stars (Kroupa 1995; Close et al. 2007). This is the case of the 2MASS J0249−0557 c component.

We calculated the binding energy of the system, as described in Chinchilla et al. (2020). Masses and separations were obtained from Dupuy et al. (2018). We infer an (absolute) upper limit for the binding energy of 2MASS J0249−0557 c of $U = (-8.8 \pm 4.4)10^{32}$ J. This result considers an orbital semi-major axis equal to the current observed separation. However, the actual semi-major axis may be larger due to projection effects. When we consider an average semi-major axis of $\langle a_{rel} \rangle = 1.26\, d\, \langle \alpha \rangle$ (Fischer & Marcy 1992), where d is the heliocentric distance and $\langle \alpha \rangle$ is the average observed angular separation of the components, the binding energy would become $U \sim (-7.0 \pm 3.4)10^{32}$ J. This binding energy is surprisingly low and makes this system one of the most fragile wide systems discovered up to date. Figure 9 shows the binding energy of 2MASS J0249−0557 AB(c) in comparison with other very wide (>1000 AU) binaries, exoplanets, and the planets of our Solar System. This figure shows that 2MASS J0249−0557 AB(c) is one of the substellar companions with the lowest binding energy known to date.

In order to estimate the time that this system is expected to survive in its actual environment, we calculated the expected disruption time using the relations from Binney & Tremaine (1987) and Weinberg et al. (1987), also as described in Chinchilla et al. (2020). We considered a similar mean velocity dispersion as the solar neighbourhood, calculated using the data in Zapatero Osorio et al. (2007b); we obtain a value of 52.8 km s^{-1}. To obtain the density of stars around the system, we used *Gaia* DR2 to select all the objects in a sphere of 8 pc radius around the system. We found 138 objects in this volume, which corresponds to a density of 0.064 obj pc^{-3}. Using these values, we obtain an estimated disruption time of 4–14 Gyr. We must consider that this system may have formed in a denser environment, similar to young forming regions and associations. Considering a higher density of objects (∼10 obj pc^{-3}), we obtain a disruption time of 30–60 Myr for this system. These two results combined indicate that the system may have been formed in the outskirts of a young open cluster or stellar association, being physically bound since then, and that it will probably survive to ages similar to that of our Solar System. It is interesting to note that 2MASS J0249−0557 c, with an estimated mass of ∼12 M_{Jup}, will have a temperature of ∼ 500 K at the age of the Sun, within the Y dwarf spectral type range, which makes the detection of similar systems at these old ages very difficult with current means. The James Webb Space Telescope (JWST), with its near. and mid-infrared capabilities, may be able to identify these types of objects.

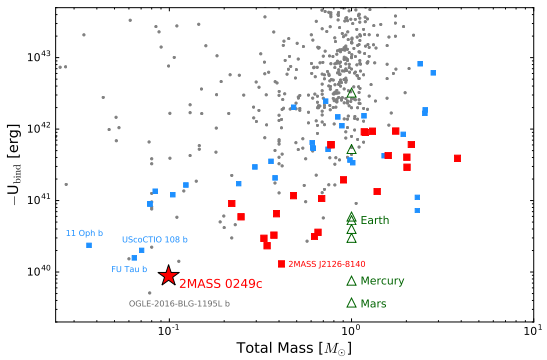

Fig. 9. Binding energy compared to the total mass of the system for known substellar companions, including planets and brown dwarfs. The binding energy of 2MASS J0249−0557 c is marked with a red star. Other substellar companions with separations >1000 AU are marked as red squares (masses and separations from Chinchilla et al. (2020) and references therein). Objects with orbital separations <100 AU are marked as grey dots, and objects with separations between 100–1000 AU are marked as small blue squares (masses and separations from The Extrasolar Planets Encyclopaedia[4]; Schneider et al. (2011)). The binding energies of the Solar System planets are also included, marked as green triangles.

6. Summary and final remarks

We presented the independent identification of 2MASS J0249−0557 c: a wide (1950±200 AU) substellar companion of the binary brown dwarfs 2MASS J0249−0557 AB, recently discovered by Dupuy et al. (2018). We found this candidate companion in our proper motion search around YMG members by combining the astrometry and photometry of the VHS and 2MASS catalogues, and using photometry from other catalogues such as DENIS and/or AllWise, and astrometry from *Gaia* DR2, when available.

We acquired optical and near-infrared spectroscopy of 2MASS J0249−0557 c to characterise its spectral energy distribution and atmospheric properties. We assigned a spectral type of L2.5±0.5 in the optical and L3±1 in the near-infrared. This spectral classification is consistent with that of Dupuy et al. (2018).

We found spectral features characteristic of youth, such as strong Hα emission in the optical, a peaked shape in the *H* band, weak alkaline lines, and strong VO, TiO, and FeH bands both in the optical and near-infrared. We observe a tentative Li I detection with a pEW of $\lesssim 5$ Å. These features are consistent with the very low gravity classification by Dupuy et al. (2018) and with the expected membership in β Pic.

2MASS J0249−0557 c shows a strong Hα emission line, with a pEW of -90^{+20}_{-40}, which is likely stable on timescales of hours and years. This emission is not very common among old field L dwarfs, but it may be present in some of the young early-L dwarfs, especially those located in regions of ages younger than 10 Myr. This reinforces the young age of 2MASS J0249−0557 c.

With an (absolute) upper limit of $U = (-8.8 \pm 4.4)10^{32}$J, 2MASS J0249−0557 AB(c) is one of the widest low-mass systems with the lowest binding energy known to date. It may have been formed in the outskirts of a young star formation region and it is expected to survive at ages similar to our Solar System. The solar vicinity may be populated by similar systems, but they may have remained unnoticed with current facilities.

[4] `http://exoplanet.eu`

Acknowledgements. We thank the anonymous referee for his/her very useful corrections and suggestions, which helped improving this manuscript. This paper is based on observations performed at the European Southern Observatory (ESO) in Chile, under programme 0101.C-0389, PI: P. Chinchilla. This work is based on observations (program GTC06-18BDDT, PI: P. Chinchilla) made with the Gran Telescopio Canarias (GTC), operated on the island of La Palma in the Spanish Observatorio del Roque de los Muchachos of the Instituto de Astrofísica de Canarias. The authors want to thank Dr. Antonio Cabrera for performing the DDT GTC/OSIRIS observations, and Prof. Rafael Rebolo and Prof. Eduardo Martín for their useful comments and discussions. P.C., V.J.S.B. and N.L. were financially supported by the program PID2019-109522GB-C53, and M.R.Z.O. by the program PID2019-109522GB-C51 of the Ministerio de Ciencia e Innovación. This research has made use of the Simbad and Vizier databases, operated at the centre de Données Astronomiques de Strasbourg (CDS), and of NASA's Astrophysics Data System Bibliographic Services (ADS). This research has also made use of some of the tools developed as part of the Virtual Observatory. This work has made use of data from the European Space Agency (ESA) mission *Gaia* (`https://www.cosmos.esa.int/gaia`), processed by the *Gaia* Data Processing and Analysis Consortium (DPAC, `https://www.cosmos.esa.int/web/gaia/dpac/consortium`). Funding for the DPAC has been provided by national institutions, in particular the institutions participating in the *Gaia* Multilateral Agreement. This publication makes use of data products from the Two Micron All Sky Survey, which is a joint project of the University of Massachusetts and the Infrared Processing and Analysis Center/California Institute of Technology, funded by the National Aeronautics and Space Administration and the National Science Foundation. This publication has made use of the Young Brown Dwarf Compilation maintained by the BDNYC collaboration led by Kelle Cruz, Emily Rice, and Jackie Faherty. This publication made use of Python programming language (Python Software Foundation, `https://www.python.org`).

References

Alam, S., Albareti, F. D., Allende Prieto, C., et al. 2015, ApJS, 219, 12
Aller, K. M., Kraus, A. L., Liu, M. C., et al. 2013, ApJ, 773, 63
Allers, K. N., Jaffe, D. T., Luhman, K. L., et al. 2007, ApJ, 657, 511
Allers, K. N. & Liu, M. C. 2013, ApJ, 772, 79
Ardila, D., Martín, E., & Basri, G. 2000, AJ, 120, 479
Barenfeld, S. A., Bubar, E. J., Mamajek, E. E., & Young, P. A. 2013, ApJ, 766, 6
Barrado y Navascués, D. & Martín, E. L. 2003, AJ, 126, 2997
Barrado y Navascués, D., Stauffer, J. R., Morales-Calderón, M., et al. 2007, ApJ, 664, 481
Barrado y Navascués, D., Stauffer, J. R., Song, I., & Caillault, J. P. 1999, ApJ, 520, L123
Barrado y Navascués, D., Zapatero Osorio, M. R., Martín, E. L., et al. 2002, A&A, 393, L85
Béjar, V. J. S., Zapatero Osorio, M. R., & Rebolo, R. 1999, ApJ, 521, 671
Bell, C. P. M., Mamajek, E. E., & Naylor, T. 2015, MNRAS, 454, 593
Best, W. M. J., Liu, M. C., Magnier, E. A., et al. 2015, ApJ, 814, 118
Binks, A. S. & Jeffries, R. D. 2014, MNRAS, 438, L11
Binney, J. & Tremaine, S. 1987, Galactic dynamics
Bowler, B. P., Liu, M. C., Kraus, A. L., & Mann, A. W. 2014, ApJ, 784, 65
Briceño, C., Luhman, K. L., Hartmann, L., Stauffer, J. R., & Kirkpatrick, J. D. 2002, ApJ, 580, 317
Burgasser, A. J., Cruz, K. L., Cushing, M., et al. 2010, ApJ, 710, 1142
Burgasser, A. J., Geballe, T. R., Leggett, S. K., Kirkpatrick, J. D., & Golimowski, D. A. 2006, ApJ, 637, 1067
Burgasser, A. J., McElwain, M. W., Kirkpatrick, J. D., et al. 2004, AJ, 127, 2856
Caballero, J. A., Martín, E. L., Zapatero Osorio, M. R., et al. 2006, A&A, 445, 143
Cepa, J., Aguiar, M., Escalera, V. G., et al. 2000, in Proc. SPIE, Vol. 4008, Optical and IR Telescope Instrumentation and Detectors, ed. M. Iye & A. F. Moorwood, 623–631
Chambers, K. C., Magnier, E. A., Metcalfe, N., et al. 2016, arXiv e-prints, arXiv:1612.05560
Chilcote, J., Pueyo, L., De Rosa, R. J., et al. 2017, AJ, 153, 182
Chinchilla, P., Béjar, V. J. S., Lodieu, N., et al. 2020, A&A, 633, A152
Close, L. M., Follette, K. B., Males, J. R., et al. 2014, ApJ, 781, L30
Close, L. M., Zuckerman, B., Song, I., et al. 2007, ApJ, 660, 1492
Comerón, F., Neuhäuser, R., & Kaas, A. A. 2000, A&A, 359, 269
Cruz, K. L., Kirkpatrick, J. D., & Burgasser, A. J. 2009, AJ, 137, 3345
Cruz, K. L., Núñez, A., Burgasser, A. J., et al. 2018, AJ, 155, 34
Cruz, K. L., Reid, I. N., Kirkpatrick, J. D., et al. 2007, AJ, 133, 439
Cugno, G., Quanz, S. P., Hunziker, S., et al. 2019, A&A, 622, A156
Currie, T., Marois, C., Cieza, L., et al. 2019, ApJ, 877, L3
Dawson, K. S., Kneib, J.-P., Percival, W. J., et al. 2016, AJ, 151, 44
Deacon, N. R., Liu, M. C., Magnier, E. A., et al. 2014, ApJ, 792, 119
Deacon, N. R., Schlieder, J. E., & Murphy, S. J. 2016, MNRAS, 457, 3191
Delorme, P., Gagné, J., Girard, J. H., et al. 2013, A&A, 553, L5
Dupuy, T. J. & Liu, M. C. 2012, ApJS, 201, 19
Dupuy, T. J., Liu, M. C., Allers, K. N., et al. 2018, AJ, 156, 57
Elliott, P., Bayo, A., Melo, C. H. F., et al. 2016, A&A, 590, A13
Epchtein, N., de Batz, B., Capoani, L., et al. 1997, The Messenger, 87, 27
Eriksson, S. C., Asensio Torres, R., Janson, M., et al. 2020, A&A, 638, L6
Fischer, D. A. & Marcy, G. W. 1992, ApJ, 396, 178
Gagné, J. & Faherty, J. K. 2018, ApJ, 862, 138
Gagné, J., Faherty, J. K., Cruz, K. L., et al. 2015a, ApJS, 219, 33
Gagné, J., Lafrenière, D., Doyon, R., Malo, L., & Artigau, É. 2014, ApJ, 783, 121
Gagné, J., Lafrenière, D., Doyon, R., Malo, L., & Artigau, É. 2015b, ApJ, 798, 73
Gaia Collaboration, Brown, A. G. A., Vallenari, A., et al. 2018, A&A, 616, A1
Gaia Collaboration, Prusti, T., de Bruijne, J. H. J., et al. 2016, A&A, 595, A1
Gauza, B., Béjar, V. J. S., Pérez-Garrido, A., et al. 2015, ApJ, 804, 96
Gebbinck, M. K. & Sforna, D. 2007, Gasgano Users Manual, 66
Gizis, J. E., Monet, D. G., Reid, I. N., et al. 2000, AJ, 120, 1085
Gunn, J. E., Siegmund, W. A., Mannery, E. J., et al. 2006, AJ, 131, 2332
Haffert, S. Y., Bohn, A. J., de Boer, J., et al. 2019, Nature Astronomy, 3, 749
Haisch, Karl E., J., Lada, E. A., & Lada, C. J. 2001, ApJ, 553, L153
Hawley, S. L., Gizis, J. E., & Reid, I. N. 1996, AJ, 112, 2799
Huélamo, N., Chauvin, G., Schmid, H. M., et al. 2018, A&A, 613, L5
Jayawardhana, R., Mohanty, S., & Basri, G. 2003, ApJ, 592, 282
Kirkpatrick, J. D. 2005, ARA&A, 43, 195
Kirkpatrick, J. D., Reid, I. N., Liebert, J., et al. 1999, ApJ, 519, 802
Kirkpatrick, J. D., Reid, I. N., Liebert, J., et al. 2000, AJ, 120, 447
Kraus, A. L. & Ireland, M. J. 2012, ApJ, 745, 5
Kroupa, P. 1995, MNRAS, 277, 1522
Lagrange, A. M., Bonnefoy, M., Chauvin, G., et al. 2010, Science, 329, 57
Liebert, J., Kirkpatrick, J. D., Cruz, K. L., et al. 2003, AJ, 125, 343
Liu, M. C., Dupuy, T. J., & Allers, K. N. 2016, ApJ, 833, 96
Lodieu, N., Dobbie, P. D., & Hambly, N. C. 2011, A&A, 527, A24
Lodieu, N., Hambly, N. C., & Jameson, R. F. 2006, MNRAS, 373, 95
Lodieu, N., Pérez-Garrido, A., Béjar, V. J. S., et al. 2014, A&A, 569, A120
Lodieu, N., Zapatero Osorio, M. R., Béjar, V. J. S., & Peña Ramírez, K. 2018, MNRAS, 473, 2020
Lucas, P. W., Roche, P. F., Allard, F., & Hauschildt, P. H. 2001, MNRAS, 326, 695
Luhman, K. L. 1999, ApJ, 525, 466
Luhman, K. L., Liebert, J., & Rieke, G. H. 1997, ApJ, 489, L165
Luhman, K. L., Stauffer, J. R., & Mamajek, E. E. 2005, ApJ, 628, L69
Malo, L., Doyon, R., Feiden, G. A., et al. 2014, ApJ, 792, 37
Malo, L., Doyon, R., Lafrenière, D., et al. 2013, ApJ, 762, 88
Mamajek, E. E. & Bell, C. P. M. 2014, MNRAS, 445, 2169
Martín, E. L., Delfosse, X., Basri, G., et al. 1999, AJ, 118, 2466
Martín, E. L., Dougados, C., Magnier, E., et al. 2001, ApJ, 561, L195
Martín, E. L., Phan-Bao, N., Bessell, M., et al. 2010, A&A, 517, A53
McLean, I. S., McGovern, M. R., Burgasser, A. J., et al. 2003, ApJ, 596, 561
McMahon, R. G., Banerji, M., Gonzalez, E., et al. 2013, The Messenger, 154, 35
Mendigutía, I., Oudmaijer, R. D., Schneider, P. C., et al. 2018, A&A, 618, L9
Mentuch, E., Brandeker, A., van Kerkwijk, M. H., Jayawardhana, R., & Hauschildt, P. H. 2008, ApJ, 689, 1127
Messina, S., Lanzafame, A. C., Malo, L., et al. 2017, A&A, 607, A3
Miret-Roig, N., Antoja, T., Romero-Gómez, M., & Figueras, F. 2018, A&A, 615, A51
Mohanty, S. & Basri, G. 2003, ApJ, 583, 451
Mohanty, S., Jayawardhana, R., & Basri, G. 2005, ApJ, 626, 498
Moorwood, A., Cuby, J.-G., & Lidman, C. 1998, The Messenger, 91, 9
Muzerolle, J., Hillenbrand, L., Calvet, N., Briceño, C., & Hartmann, L. 2003, ApJ, 592, 266
Pecaut, M. J. & Mamajek, E. E. 2013, ApJS, 208, 9
Pineda, J. S., Hallinan, G., Kirkpatrick, J. D., et al. 2016, ApJ, 826, 73
Rebolo, R., Zapatero Osorio, M. R., Madruga, S., et al. 1998, Science, 282, 1309
Riaz, B. & Gizis, J. E. 2008, ApJ, 681, 1584
Sallum, S., Follette, K. B., Eisner, J. A., et al. 2015, Nature, 527, 342
Schlieder, J. E., Lépine, S., & Simon, M. 2010, AJ, 140, 119
Schlieder, J. E., Lépine, S., & Simon, M. 2012, AJ, 144, 109
Schmidt, S. J., Hawley, S. L., West, A. A., et al. 2015, AJ, 149, 158
Schneider, A. C., Windsor, J., Cushing, M. C., Kirkpatrick, J. D., & Shkolnik, E. L. 2017, AJ, 153, 196
Schneider, J., Dedieu, C., Le Sidaner, P., Savalle, R., & Zolotukhin, I. 2011, A&A, 532, A79
Shkolnik, E., Liu, M. C., & Reid, I. N. 2009, ApJ, 699, 649
Shkolnik, E. L., Allers, K. N., Kraus, A. L., Liu, M. C., & Flagg, L. 2017, AJ, 154, 69
Shkolnik, E. L., Anglada-Escudé, G., Liu, M. C., et al. 2012, ApJ, 758, 56
Skrutskie, M. F., Cutri, R. M., Stiening, R., et al. 2006, AJ, 131, 1163
Slesnick, C. L., Carpenter, J. M., & Hillenbrand, L. A. 2006, AJ, 131, 3016
Slesnick, C. L., Hillenbrand, L. A., & Carpenter, J. M. 2004, ApJ, 610, 1045
Smee, S. A., Gunn, J. E., Uomoto, A., et al. 2013, AJ, 146, 32
Thalmann, C., Janson, M., Garufi, A., et al. 2016, ApJ, 828, L17
Theissen, C. A., Burgasser, A. J., Bardalez Gagliuffi, D. C., et al. 2018, ApJ, 853, 75
Theissen, C. A., West, A. A., Shippee, G., Burgasser, A. J., & Schmidt, S. J. 2017, AJ, 153, 92
Tody, D. 1986, in Proc. SPIE, Vol. 627, Instrumentation in astronomy VI, ed. D. L. Crawford, 733
Tody, D. 1993, in Astronomical Society of the Pacific Conference Series, Vol. 52, Astronomical Data Analysis Software and Systems II, ed. R. J. Hanisch, R. J. V. Brissenden, & J. Barnes, 173
Torres, C. A. O., Quast, G. R., Melo, C. H. F., & Sterzik, M. F. 2008, Young Nearby Loose Associations, ed. B. Reipurth, Vol. 5, 757
Wagner, K., Follete, K. B., Close, L. M., et al. 2018, ApJ, 863, L8
Weinberg, M. D., Shapiro, S. L., & Wasserman, I. 1987, ApJ, 312, 367
White, R. J. & Basri, G. 2003, ApJ, 582, 1109
Wright, E. L., Eisenhardt, P. R. M., Mainzer, A. K., et al. 2010, AJ, 140, 1868
York, D. G., Adelman, J., Anderson, Jr., J. E., et al. 2000, AJ, 120, 1579
Zapatero Osorio, M. R., Béjar, V. J. S., Martín, E. L., Barrado y Navascués, D., & Rebolo, R. 2002a, ApJ, 569, L99
Zapatero Osorio, M. R., Béjar, V. J. S., Miles-Páez, P. A., et al. 2014, A&A, 568, A6
Zapatero Osorio, M. R., Béjar, V. J. S., Pavlenko, Y., et al. 2002b, A&A, 384, 937
Zapatero Osorio, M. R., Béjar, V. J. S., & Peña Ramírez, K. 2017, ApJ, 842, 65
Zapatero Osorio, M. R., Caballero, J. A., Béjar, V. J. S., et al. 2007a, A&A, 472, L9
Zapatero Osorio, M. R., Martín, E. L., Béjar, V. J. S., et al. 2007b, ApJ, 666,

1205
Zapatero Osorio, M. R., Rebolo, R., Bihain, G., et al. 2010, ApJ, 715, 1408
Zuckerman, B. 2019, ApJ, 870, 27
Zuckerman, B., Song, I., & Bessell, M. S. 2004, ApJ, 613, L65
Zuckerman, B., Song, I., Bessell, M. S., & Webb, R. A. 2001, ApJ, 562, L87
Zurlo, A., Cugno, G., Montesinos, M., et al. 2020, A&A, 633, A119

7

Conclusions

We have performed an astrometric and photometric search for low-mass companions to young nearby stars using VHS data in combination with other optical and near-infrared surveys.

In the USco region, we have combined the VHS data with UKIDSS GCS and Pan-STARRS in a search around 1195 known members. We identified 39 bona fide companions in 38 systems. 21 of these objects were already reported as candidate companions in the literature, 16 objects were reported as USco members but not related as companions, and 2 objects are new discoveries. We find that 3.2±0.5% of the USco members have a wide companion in the range of masses between 0.010 $M_\odot < M < 0.2\ M_\odot$ and separations between 400–8700 AU. Regarding substellar companions, we obtain a companion frequency of 1.8±0.4%. One of the candidates has a planetary mass (below the deuterium-burning mass limit), but our search is not complete below 11 M_{Jup} and we can only impose a lower limit of 0.08% in the frequency of very wide planetary mass companions.

Two of the most interesting identified wide companions in USco are USco1621 B and USco1556 B, which are very low-mass brown dwarfs with masses close to the deuterium-burning minimum mass, orbiting two early-M USco stars at separations of 2880 and 3500 AU respectively. We determined masses of 16±2 and 15±2 M_{Jup} for USco1621 B and USco1556 B respectively, a spectral type of M8.5±0.5 for both in the optical, and a spectral type of L0±0.5 and L0.5±0.5 respectively in the near-infrared.

We have performed another search in four YMGs (AB Dor, β Pic, THA and TWA) using VHS and 2MASS, up to physical separations of 50 000 AU. In

TWA we found 3 companions around 55 members, with spectral types M5.5–M8.5 and masses between 0.026–0.11 $M_{\odot}$. In β Pic, we identified 9 companions in 7 systems around 109 members, with spectral types between M4.5–L3 and masses between 0.013–0.19 $M_{\odot}$. In THA, we found 11 companions around 281 members, with spectral types between M3.5–L3 and masses between 0.011–0.28 $M_{\odot}$. Finally, in AB Dor, we found 11 wide companions in 10 systems around 154 members, with spectral types between M4–M7 and masses between 0.11–0.61 $M_{\odot}$..

The frequencies of wide companions in the studied ranges of masses are 6.4±3.7% in TWA, 7.4±2.8% in β Pic, 4.1±1.2% in THA and 7.2±2.3% in AB Dor. Considering substellar companions only, the frequencies are 4.3±3.0% for TWA, 3.2±1.8% for β Pic, 0.7±0.5% for THA and a lower limit of <1.4% for AB Dor.

We obtained low-resolution spectroscopy in the optical and the near-infrared for most of the components (primaries and companions) which were not spectroscopically characterised in the literature. The spectral types of the candidate companions range between early-M and early-L. We identified youth features such as a strong Hα emission, weaker alkali lines, and a triangular shape in the H-band pseudo-continuum in the near-infrared for the latest spectral types.

Among the wide substellar companions in the β Pic YMG, we independently identified the planetary mass companion 2MASS J0249-0557 c, also reported by Dupuy et al. (2018). This object shows a very strong Hα emission, which is not common among L-type objects, due to either a strong chromospheric activity or ongoing accretion. It is also one of the wide substellar companions with the lowest binding energy found to date.

In summary, our main conclusions are that the substellar companions in very wide orbits around young stars are rare, with a frequency around 1–4% for the young studied populations. We find higher frequencies for younger ages, although the number of companions is relatively low to conclude that this trend is statistically significant. These observational results indicate that the formation mechanism for very wide substellar binaries may be similar to that of low-mass stars.

Wide substellar companions allow for their full spectroscopic characterisation, which is otherwise very difficult to do for close-orbit giant planets and brown dwarfs. The identification and spectral characterisation of objects like USco1621 B, USco1556 B or 2MASS J0249−0557 c provide a unique opportunity to investigate the atmospheric properties of exoplanets, such as alkaline absorption, dust and cloud formation, rotation, chromospheric activity or accretion, and lithium abundance.

7.1 Final conclusions

- We have performed a search for wide substellar companions to members of Upper Scorpius and four young moving groups of different ages, using astrometry and photometry of the VHS in combination with other surveys (UKIDSS GCS, Pan-STARRS, 2MASS, *Gaia*, and more).
- We identified 39 very low-mass wide companions in USco, 3 companions in TWA, 9 companions in β Pic, 11 companions in THA and 11 companions in AB Dor. We determined companion frequencies of 6.4±3.7% in TWA, 7.4±2.8% in β Pic, 4.1±1.2% in THA and 7.2±2.3% in AB Dor. Considering substellar companions only, the frequencies are 4.3±3.0% for TWA, 3.2±1.8% for β Pic, 0.7±0.5% for THA and a lower limit of <1.4% for AB Dor.
- We obtained low-resolution spectroscopy of most of the components that were not characterised previously in the literature, either in the optical or the near-infrared wavelength range, in several observing campaigns. The spectral type of the companions range between early-M and early-L, and they show youth features in their spectra.
- We conclude that substellar companions in very wide orbits are rare, with frequencies around 1–4% for the studied young populations. We find a higher frequency of wide substellar companions with younger ages, but the large errors in the frequency determinations prevent from obtaining a statistically significant trend. The observational results indicate that the formation mechanism for very wide substellar binaries may be similar to that of low-mass stars.
- We identified some very interesting wide companions with masses around the deuterium burning minimum mass, like USco1621 B, USco1556 B and 2MASS J0249−0557 c. These objects are young giant-planet analogues, which can be fully characterised through spectroscopy.

Bibliography

Adams, F. C., Ruden, S. P., & Shu, F. H. 1989, ApJ, 347, 959

Alcock, C., Allsman, R. A., Alves, D., et al. 1996, ApJ, 471, 774

—. 1998, ApJ, 499, L9

Allard, F., Hauschildt, P. H., Alexander, D. R., Tamanai, A., & Schweitzer, A. 2001, ApJ, 556, 357

Allard, F., Homeier, D., & Freytag, B. 2012, Philosophical Transactions of the Royal Society of London Series A, 370, 2765

Allen, P. R., Burgasser, A. J., Faherty, J. K., & Kirkpatrick, J. D. 2012, AJ, 144, 62

Allen, P. R., Koerner, D. W., McElwain, M. W., Cruz, K. L., & Reid, I. N. 2007, AJ, 133, 971

Aller, K. M., Kraus, A. L., Liu, M. C., et al. 2013, ApJ, 773, 63

Allers, K. N., & Liu, M. C. 2013, ApJ, 772, 79

Allers, K. N., Liu, M. C., Dupuy, T. J., & Cushing, M. C. 2010, ApJ, 715, 561

Alonso, R., Brown, T. M., Torres, G., et al. 2004, ApJ, 613, L153

Alonso-Floriano, F. J., Caballero, J. A., Cortés-Contreras, M., Solano, E., & Montes, D. 2015, A&A, 583, A85

Alonso-Floriano, F. J., Caballero, J. A., & Montes, D. 2011, in Stellar Clusters & Associations: A RIA Workshop on Gaia, 344–347

Ardila, D., Martín, E., & Basri, G. 2000, AJ, 120, 479

Artigau, É., Kouach, D., Donati, J.-F., et al. 2014, in Society of Photo-Optical Instrumentation Engineers (SPIE) Conference Series, Vol. 9147, Ground-based and Airborne Instrumentation for Astronomy V, ed. S. K. Ramsay, I. S. McLean, & H. Takami, 914715

Arzoumanian, D., André, P., Didelon, P., et al. 2011, A&A, 529, L6

Auvergne, M., Bodin, P., Boisnard, L., et al. 2009, A&A, 506, 411

Baglin, A., Auvergne, M., Barge, P., et al. 2006, in ESA Special Publication, Vol. 1306, The CoRoT Mission Pre-Launch Status - Stellar Seismology and Planet Finding, ed. M. Fridlund, A. Baglin, J. Lochard, & L. Conroy, 33

Bakos, G., Noyes, R. W., Kovács, G., et al. 2004, PASP, 116, 266

Baraffe, I., Chabrier, G., Barman, T. S., Allard, F., & Hauschildt, P. H. 2003, A&A, 402, 701

Baraffe, I., Homeier, D., Allard, F., & Chabrier, G. 2015, A&A, 577, A42

Bardalez Gagliuffi, D. C., Gagné, J., Faherty, J. K., & Burgasser, A. J. 2018, ApJ, 854, 101

Barenfeld, S. A., Bubar, E. J., Mamajek, E. E., & Young, P. A. 2013, ApJ, 766, 6

Barenfeld, S. A., Carpenter, J. M., Sargent, A. I., et al. 2019, ApJ, 878, 45

Baron, F., Lafrenière, D., Artigau, É., et al. 2019, AJ, 158, 187

Barrado Y Navascués, D. 2006, A&A, 459, 511

Barrado y Navascués, D., & Martín, E. L. 2003, AJ, 126, 2997

Barrado y Navascués, D., Stauffer, J. R., Song, I., & Caillault, J. P. 1999, ApJ, 520, L123

Barstow, M. A. 1987, MNRAS, 228, 251

Basri, G. 2000, ARA&A, 38, 485

Basu, S., & Vorobyov, E. I. 2012, ApJ, 750, 30

Bate, M. R. 2009, MNRAS, 392, 590

—. 2012, MNRAS, 419, 3115

Bate, M. R., Bonnell, I. A., & Bromm, V. 2002, MNRAS, 332, L65

—. 2003, MNRAS, 339, 577

Batygin, K., & Brown, M. E. 2016, AJ, 151, 22

Beaulieu, J. P., Bennett, D. P., Fouqué, P., et al. 2006, Nature, 439, 437

Béjar, V. J. S., Zapatero Osorio, M. R., Pérez-Garrido, A., et al. 2008, ApJ, 673, L185

Bell, C. P. M., Mamajek, E. E., & Naylor, T. 2015, MNRAS, 454, 593

Benavides, R., Rica, F., Reina, E., et al. 2010, Journal of Double Star Observations, 6, 30

Bennett, N. W. W., Laing, J. D., & Evans, D. S. 1962, Royal Greenwich Observatory Bulletins, 61, 91

Bertiau, F. C. 1958, ApJ, 128, 533

Best, W. M. J., Liu, M. C., Magnier, E. A., et al. 2015, ApJ, 814, 118

Best, W. M. J., Liu, M. C., Magnier, E. A., et al. 2017, ApJ, 837, 95

Biller, B., Allers, K., Liu, M., Close, L. M., & Dupuy, T. 2011, ApJ, 730, 39

Biller, B. A., Liu, M. C., Wahhaj, Z., et al. 2013, ApJ, 777, 160

Binks, A. S., & Jeffries, R. D. 2014, MNRAS, 438, L11

Binks, A. S., Jeffries, R. D., & Wright, N. J. 2020, MNRAS, 494, 2429

Binney, J., & Tremaine, S. 1987, Galactic dynamics

Blaauw, A. 1964, ARA&A, 2, 213

—. 1978, Internal Motions and Age of the Sub-Association Upper Scorpio, ed. L. V. Mirzoyan, 101

Bochanski, J. J., West, A. A., Hawley, S. L., & Covey, K. R. 2007, AJ, 133, 531

Bond, I. A., Udalski, A., Jaroszyński, M., et al. 2004, ApJ, 606, L155

Bonnell, I. A. 1994, MNRAS, 269, 837

Bonnell, I. A., & Bate, M. R. 1994, MNRAS, 271, 999

Borucki, W. J., Koch, D., Basri, G., et al. 2010, Science, 327, 977

Boss, A. P. 1987, ApJ, 319, 149

—. 1988, ApJ, 331, 370

—. 1997, Science, 276, 1836

—. 2001, ApJ, 563, 367

—. 2006, ApJ, 641, 1148

Bouchy, F., & Sophie Team. 2006, in Tenth Anniversary of 51 Peg-b: Status of and prospects for hot Jupiter studies, ed. L. Arnold, F. Bouchy, & C. Moutou, 319–325

Bouy, H., Brandner, W., Martín, E. L., et al. 2003, AJ, 126, 1526

Bowler, B. P., & Hillenbrand, L. A. 2015, ApJ, 811, L30

Bowler, B. P., Liu, M. C., Shkolnik, E. L., & Dupuy, T. J. 2013, ApJ, 774, 55

Bowler, B. P., Liu, M. C., Shkolnik, E. L., & Tamura, M. 2015, ApJS, 216, 7

Bracewell, R. N. 1978, Nature, 274, 780

Brandeker, A., Jayawardhana, R., Khavari, P., Haisch, Karl E., J., & Mardones, D. 2006, ApJ, 652, 1572

Burgasser, A. J., Kirkpatrick, J. D., Reid, I. N., et al. 2003, ApJ, 586, 512

Burgasser, A. J., Kirkpatrick, J. D., Cutri, R. M., et al. 2000, ApJ, 531, L57

Burgasser, A. J., Kirkpatrick, J. D., Brown, M. E., et al. 2002, ApJ, 564, 421

Burningham, B., Cardoso, C. V., Smith, L., et al. 2013, MNRAS, 433, 457

Burrows, A., & Liebert, J. 1993, Reviews of Modern Physics, 65, 301

Burrows, A., Marley, M., Hubbard, W. B., et al. 1997, ApJ, 491, 856

Butler, R. P., Marcy, G. W., Fischer, D. A., et al. 1999, ApJ, 526, 916

Caballero, J. A. 2009, A&A, 507, 251

Caballero, J. A., Martín, E. L., Zapatero Osorio, M. R., et al. 2006, A&A, 445, 143

Cannon, A. J., & Pickering, E. C. 1901, Annals of Harvard College Observatory, 28, 129

—. 1993, VizieR Online Data Catalog, III/135A

Carson, J., Thalmann, C., Janson, M., et al. 2013, ApJ, 763, L32

Carson, J. C., Marengo, M., Patten, B. M., et al. 2011, ApJ, 743, 141

Casali, M., Adamson, A., Alves de Oliveira, C., et al. 2007, A&A, 467, 777

Chabrier, G., & Baraffe, I. 1997, A&A, 327, 1039

—. 2000, ARA&A, 38, 337

Chabrier, G., Baraffe, I., Allard, F., & Hauschildt, P. 2000, ApJ, 542, 464

Chabrier, G., Baraffe, I., Allard, F., & Hauschildt, P. H. 2005, arXiv Astrophysics e-prints, astro-ph/0509798

Chabrier, G., Baraffe, I., & Plez, B. 1996, ApJ, 459, L91

Charbonneau, D., Brown, T. M., Latham, D. W., & Mayor, M. 2000, ApJ, 529, L45

Chauvin, G., Lagrange, A. M., Dumas, C., et al. 2004, A&A, 425, L29

—. 2005a, A&A, 438, L25

Chauvin, G., Lagrange, A. M., Zuckerman, B., et al. 2005b, A&A, 438, L29

Chauvin, G., Lagrange, A. M., Bonavita, M., et al. 2010, A&A, 509, A52

Chauvin, G., Faherty, J., Boccaletti, A., et al. 2012, A&A, 548, A33

Chauvin, G., Vigan, A., Bonnefoy, M., et al. 2015, A&A, 573, A127

Chen, X., Arce, H. G., Zhang, Q., et al. 2013, ApJ, 768, 110

Chilcote, J., Pueyo, L., De Rosa, R. J., et al. 2017, AJ, 153, 182

Chinchilla, P., Béjar, V. J. S., Lodieu, N., Zapatero Osorio, M. R., & Gauza, B. 2020a, arXiv e-prints, arXiv:2011.10002

Chinchilla, P., Béjar, V. J. S., Lodieu, N., et al. 2020b, A&A, 633, A152

Close, L. M., Siegler, N., Freed, M., & Biller, B. 2003, ApJ, 587, 407

Close, L. M., Zuckerman, B., Song, I., et al. 2007, ApJ, 660, 1492

Cody, A. M., Hillenbrand, L. A., David, T. J., et al. 2017, ApJ, 836, 41

Colavita, M. M., Serabyn, E., Millan-Gabet, R., et al. 2009, PASP, 121, 1120

Cortés-Contreras, M., Béjar, V. J. S., Caballero, J. A., et al. 2017, A&A, 597, A47

Cruz, K. L., Kirkpatrick, J. D., & Burgasser, A. J. 2009, AJ, 137, 3345

Curiel, S., Ortiz-León, G. N., Mioduszewski, A. J., & Torres, R. M. 2020, AJ, 160, 97

Cushing, M. C. 2014, in Astrophysics and Space Science Library, Vol. 401, 50 Years of Brown Dwarfs, ed. V. Joergens, 113

Cushing, M. C., Rayner, J. T., & Vacca, W. D. 2005, ApJ, 623, 1115

Cushing, M. C., Kirkpatrick, J. D., Gelino, C. R., et al. 2011, ApJ, 743, 50

Daemgen, S., Bonavita, M., Jayawardhana, R., Lafrenière, D., & Janson, M. 2015, ApJ, 799, 155

Daly, R. A., & McLaughlin, G. C. 1992, ApJ, 390, 423

David, T. J., Hillenbrand, L. A., Cody, A. M., Carpenter, J. M., & Howard, A. W. 2016, ApJ, 816, 21

David, T. J., Hillenbrand, L. A., Gillen, E., et al. 2019, ApJ, 872, 161

Davidson, K. 1975, , 26, 99

Dawson, P., Scholz, A., & Ray, T. P. 2011, MNRAS, 418, 1231

Dawson, P., Scholz, A., Ray, T. P., et al. 2013, MNRAS, 429, 903

Day-Jones, A. C., Pinfield, D. J., Ruiz, M. T., et al. 2011, MNRAS, 410, 705

de Geus, E. J., de Zeeuw, P. T., & Lub, J. 1989, A&A, 216, 44

de La Fuente Marcos, C., & de La Fuente Marcos, R. 2014, MNRAS, 443, L59

de Zeeuw, P. T., Hoogerwerf, R., de Bruijne, J. H. J., Brown, A. G. A., & Blaauw, A. 1999, AJ, 117, 354

de Zeeuw, T., & Brand, J. 1985, Photometric age determination of OB-associations (I), ed. W. Boland & H. van Woerden, Vol. 120, 95

Deacon, N. R., Schlieder, J. E., & Murphy, S. J. 2016, MNRAS, 457, 3191

Deacon, N. R., Liu, M. C., Magnier, E. A., et al. 2012a, ApJ, 755, 94

—. 2012b, ApJ, 757, 100

—. 2014, ApJ, 792, 119

Delfosse, X., Beuzit, J. L., Marchal, L., et al. 2004, in Astronomical Society of the Pacific Conference Series, Vol. 318, Spectroscopically and Spatially Resolving the Components of the Close Binary Stars, ed. R. W. Hilditch, H. Hensberge, & K. Pavlovski, 166–174

Delorme, P., Gagné, J., Girard, J. H., et al. 2013, A&A, 553, L5

Delrez, L., Gillon, M., Queloz, D., et al. 2018, in Society of Photo-Optical Instrumentation Engineers (SPIE) Conference Series, Vol. 10700, Ground-based and Airborne Telescopes VII, ed. H. K. Marshall & J. Spyromilio, 107001I

Desrochers, M.-E., Artigau, É., Gagné, J., et al. 2018, ApJ, 852, 55

Dieterich, S. B., Henry, T. J., Golimowski, D. A., Krist, J. E., & Tanner, A. M. 2012, AJ, 144, 64

Dobashi, K., Uehara, H., Kandori, R., et al. 2005, PASJ, 57, S1

Ducourant, C., Teixeira, R., Galli, P. A. B., et al. 2014, A&A, 563, A121

Dumusque, X., Pepe, F., Lovis, C., et al. 2012, Nature, 491, 207

Dupuy, T. J., & Liu, M. C. 2012, ApJS, 201, 19

Dupuy, T. J., Liu, M. C., & Ireland, M. J. 2014, ApJ, 790, 133

Dupuy, T. J., Liu, M. C., Allers, K. N., et al. 2018, AJ, 156, 57

Duquennoy, A., & Mayor, M. 1991, A&A, 500, 337

Elias, J. H., Joyce, R. R., Liang, M., et al. 2006a, in Society of Photo-Optical Instrumentation Engineers (SPIE) Conference Series, Vol. 6269, Society of Photo-Optical Instrumentation Engineers (SPIE) Conference Series, 62694C

Elias, J. H., Rodgers, B., Joyce, R. R., et al. 2006b, in Society of Photo-Optical Instrumentation Engineers (SPIE) Conference Series, Vol. 6269, Society of Photo-Optical Instrumentation Engineers (SPIE) Conference Series, 626914

Elliott, P., & Bayo, A. 2016, MNRAS, 459, 4499

Elliott, P., Bayo, A., Melo, C. H. F., et al. 2014, A&A, 568, A26

—. 2016, A&A, 590, A13

Elliott, P., Huélamo, N., Bouy, H., et al. 2015, A&A, 580, A88

Epchtein, N., de Batz, B., Capoani, L., et al. 1997, The Messenger, 87, 27

Esplin, T. L., & Luhman, K. L. 2020, AJ, 159, 282

Esplin, T. L., Luhman, K. L., Miller, E. B., & Mamajek, E. E. 2018, AJ, 156, 75

Fabricius, C., Høg, E., Makarov, V. V., et al. 2002, A&A, 384, 180

Faherty, J. K., Burgasser, A. J., West, A. A., et al. 2010, AJ, 139, 176

Faherty, J. K., Riedel, A. R., Cruz, K. L., et al. 2016, ApJS, 225, 10

Fang, Q., Herczeg, G. J., & Rizzuto, A. 2017, ApJ, 842, 123

Farihi, J., Becklin, E. E., & Zuckerman, B. 2005, ApJS, 161, 394

Feiden, G. A. 2016, A&A, 593, A99

Filippazzo, J. C., Rice, E. L., Faherty, J., et al. 2015, ApJ, 810, 158

Findeisen, K., & Hillenbrand, L. 2010, AJ, 139, 1338

Fisher, R. T. 2004, ApJ, 600, 769

Flagg, L., Shkolnik, E. L., Weinberger, A., et al. 2020, ApJ, 896, 153

Fontanive, C., Biller, B., Bonavita, M., & Allers, K. 2018, MNRAS, 479, 2702

Freudling, W., Romaniello, M., Bramich, D. M., et al. 2013, A&A, 559, A96

Gagné, J., Allers, K. N., Theissen, C. A., et al. 2018, ApJ, 854, L27

Gagné, J., Burgasser, A. J., Faherty, J. K., et al. 2015a, ApJ, 808, L20

Gagné, J., & Faherty, J. K. 2018, ApJ, 862, 138

Gagné, J., Lafrenière, D., Doyon, R., Malo, L., & Artigau, É. 2014, ApJ, 783, 121

—. 2015b, ApJ, 798, 73

Gagné, J., Faherty, J. K., Cruz, K. L., et al. 2015c, ApJS, 219, 33

Gagné, J., Faherty, J. K., Mamajek, E. E., et al. 2017, ApJS, 228, 18

Galli, P. A. B., Joncour, I., & Moraux, E. 2018, MNRAS, 477, L50

Garrison, R. F. 1967, ApJ, 147, 1003

Gaudi, B. S., Bennett, D. P., Udalski, A., et al. 2008, Science, 319, 927

Gauza, B. 2016, PhD thesis, -

Gauza, B., Béjar, V. J. S., Pérez-Garrido, A., et al. 2015, ApJ, 804, 96

Gauza, B., Béjar, V. J. S., Pérez-Garrido, A., et al. 2019, MNRAS, 487, 1149

Gebbinck, M. K., & Sforna, D. 2007, Gasgano User's Manual, 66

Ghez, A. M., Neugebauer, G., & Matthews, K. 1993, AJ, 106, 2005

Gizis, J. E., Monet, D. G., Reid, I. N., et al. 2000, AJ, 120, 1085

Gizis, J. E., Reid, I. N., Knapp, G. R., et al. 2003, AJ, 125, 3302

Goldman, B., Marsat, S., Henning, T., Clemens, C., & Greiner, J. 2010, MNRAS, 405, 1140

González-Fernández, C., Hodgkin, S. T., Irwin, M. J., et al. 2018, MNRAS, 474, 5459

Goodwin, S. P., Whitworth, A. P., & Ward-Thompson, D. 2004, A&A, 414, 633

Gray, R. O., Corbally, C. J., Garrison, R. F., et al. 2006, AJ, 132, 161

Gray, R. O., Corbally, C. J., Garrison, R. F., McFadden, M. T., & Robinson, P. E. 2003, AJ, 126, 2048

Gray, R. O., & Garrison, R. F. 1987, ApJS, 65, 581

Hambly, N. C., Collins, R. S., Cross, N. J. G., et al. 2008, MNRAS, 384, 637

Han, C., Udalski, A., Choi, J. Y., et al. 2013, ApJ, 762, L28

Hawkins, M. R. S. 1986, MNRAS, 223, 845

Hawley, S. L., Gizis, J. E., & Reid, I. N. 1996, AJ, 112, 2799

Hayashi, C., & Nakano, T. 1963, Progress of Theoretical Physics, 30, 460

Hennebelle, P., & Chabrier, G. 2008, ApJ, 684, 395

Henry, T. J., Jao, W.-C., Winters, J. G., et al. 2018, AJ, 155, 265

Herczeg, G. J., & Hillenbrand, L. A. 2015, ApJ, 808, 23

Hester, J. J., Scowen, P. A., Sankrit, R., et al. 1996, AJ, 111, 2349

Hodgkin, S. T., Irwin, M. J., Hewett, P. C., & Warren, S. J. 2009, MNRAS, 394, 675

Høg, E., Fabricius, C., Makarov, V. V., et al. 2000, A&A, 355, L27

Houk, N., & Cowley, A. P. 1975, University of Michigan Catalogue of two-dimensional spectral types for the HD stars. Volume I. Declinations -90_ to -53_f0.

Houk, N., & Smith-Moore, M. 1988, Michigan Catalogue of Two-dimensional Spectral Types for the HD Stars. Volume 4, Declinations -26°.0 to -12°.0., Vol. 4

Houk, N., & Swift, C. 1999, Michigan Spectral Survey, 5, 0

Ireland, M. J., Kraus, A., Martinache, F., Law, N., & Hillenbrand, L. A. 2011, ApJ, 726, 113

Irwin, J., Charbonneau, D., Nutzman, P., & Falco, E. 2009, in Transiting Planets, ed. F. Pont, D. Sasselov, & M. J. Holman, Vol. 253, 37–43

Irwin, M. J., Lewis, J., Hodgkin, S., et al. 2004, in Proc. SPIE, Vol. 5493, Optimizing Scientific Return for Astronomy through Information Technologies, ed. P. J. Quinn & A. Bridger, 411–422

Itoh, Y., Hayashi, M., Tamura, M., et al. 2005, ApJ, 620, 984

Janson, M., Bergfors, C., Goto, M., Brandner, W., & Lafrenière, D. 2010, ApJ, 710, L35

Janson, M., Durkan, S., Hippler, S., et al. 2017, A&A, 599, A70

Janson, M., Bergfors, C., Brandner, W., et al. 2014, ApJS, 214, 17

Jappsen, A. K., Klessen, R. S., Larson, R. B., Li, Y., & Mac Low, M. M. 2005, A&A, 435, 611

Jayawardhana, R., Mohanty, S., & Basri, G. 2003, ApJ, 592, 282

Jehin, E., Gillon, M., Queloz, D., et al. 2011, The Messenger, 145, 2

Jiménez-Esteban, F. M., Solano, E., & Rodrigo, C. 2019, AJ, 157, 78

Jones, M. O., & Bate, M. R. 2018, MNRAS, 478, 2650

Kalas, P., Graham, J. R., Chiang, E., et al. 2008, Science, 322, 1345

Kasper, M., Apai, D., Janson, M., & Brandner, W. 2007, A&A, 472, 321

Kastner, J. H., Zuckerman, B., Weintraub, D. A., & Forveille, T. 1997, Science, 277, 67

Kerins, E. J., & Carr, B. J. 1994, MNRAS, 266, 775

Kirkpatrick, J. D. 2005, ARA&A, 43, 195

Kirkpatrick, J. D., Dahn, C. C., Monet, D. G., et al. 2001, AJ, 121, 3235

Kirkpatrick, J. D., Henry, T. J., & McCarthy, Jr., D. W. 1991, ApJS, 77, 417

Kirkpatrick, J. D., Reid, I. N., Liebert, J., et al. 1999, ApJ, 519, 802

Kirkpatrick, J. D., Gelino, C. R., Cushing, M. C., et al. 2012, ApJ, 753, 156

Knapp, G. R., Leggett, S. K., Fan, X., et al. 2004, AJ, 127, 3553

Koerner, D. W., Kirkpatrick, J. D., McElwain, M. W., & Bonaventura, N. R. 1999, ApJ, 526, L25

Köhler, R., Kunkel, M., Leinert, C., & Zinnecker, H. 2000, A&A, 356, 541

Konacki, M., Torres, G., Jha, S., & Sasselov, D. D. 2003, Nature, 421, 507

Könyves, V., André, P., Men'shchikov, A., et al. 2015, A&A, 584, A91

Könyves, V., André, P., Arzoumanian, D., et al. 2020, A&A, 635, A34

Kotani, T., Tamura, M., Suto, H., et al. 2014, in Society of Photo-Optical Instrumentation Engineers (SPIE) Conference Series, Vol. 9147, Ground-based and Airborne Instrumentation for Astronomy V, ed. S. K. Ramsay, I. S. McLean, & H. Takami, 914714

Kouwenhoven, M. B. N., Goodwin, S. P., Parker, R. J., et al. 2010, MNRAS, 404, 1835

Kratter, K. M., Matzner, C. D., & Krumholz, M. R. 2008, ApJ, 681, 375

Kratter, K. M., Matzner, C. D., Krumholz, M. R., & Klein, R. I. 2010, ApJ, 708, 1585

Kraus, A. L., & Hillenbrand, L. A. 2007a, ApJ, 662, 413

—. 2007b, ApJ, 664, 1167

—. 2009, ApJ, 703, 1511

—. 2012, ApJ, 757, 141

Kraus, A. L., Ireland, M. J., Martinache, F., & Hillenbrand, L. A. 2011, ApJ, 731, 8

Kraus, A. L., Ireland, M. J., Martinache, F., & Lloyd, J. P. 2008, ApJ, 679, 762

Kraus, A. L., Shkolnik, E. L., Allers, K. N., & Liu, M. C. 2014, AJ, 147, 146

Kraus, A. L., White, R. J., & Hillenbrand, L. A. 2005, ApJ, 633, 452

Kumar, S. S. 1963, ApJ, 137, 1121

Kunkel, M. 1996, PhD thesis, -

Kuzuhara, M., Tamura, M., Ishii, M., et al. 2011, AJ, 141, 119

Kuzuhara, M., Tamura, M., Kudo, T., et al. 2013, ApJ, 774, 11

Lada, C. J. 2006, ApJ, 640, L63

Lafrenière, D., Jayawardhana, R., Janson, M., et al. 2011, ApJ, 730, 42

Lafrenière, D., Jayawardhana, R., & van Kerkwijk, M. H. 2008, ApJ, 689, L153

Lafrenière, D., Jayawardhana, R., van Kerkwijk, M. H., Brandeker, A., & Janson, M. 2014, ApJ, 785, 47

Lafrenière, D., Doyon, R., Marois, C., et al. 2007, ApJ, 670, 1367

Lagrange, A. M., Bonnefoy, M., Chauvin, G., et al. 2010, Science, 329, 57

Lannier, J., Delorme, P., Lagrange, A. M., et al. 2016, A&A, 596, A83

Larson, R. B. 1985, MNRAS, 214, 379

Law, N. M., Dhital, S., Kraus, A., Stassun, K. G., & West, A. A. 2010, ApJ, 720, 1727

Leinert, C., Henry, T., Glindemann, A., & McCarthy, D. W., J. 1997, A&A, 325, 159

Leinert, C., Zinnecker, H., Weitzel, N., et al. 1993, A&A, 278, 129

Lépine, S., & Simon, M. 2009, AJ, 137, 3632

Lewis, J. R., Irwin, M., & Bunclark, P. 2010, in Astronomical Society of the Pacific Conference Series, Vol. 434, Astronomical Data Analysis Software and Systems XIX, ed. Y. Mizumoto, K.-I. Morita, & M. Ohishi, 91

Linder, E. F., & Mordasini, C. 2016, A&A, 589, A134

Liu, M. C., Wahhaj, Z., Biller, B. A., et al. 2010, in Society of Photo-Optical Instrumentation Engineers (SPIE) Conference Series, Vol. 7736, Adaptive Optics Systems II, ed. B. L. Ellerbroek, M. Hart, N. Hubin, & P. L. Wizinowich, 77361K

Liu, M. C., Delorme, P., Dupuy, T. J., et al. 2011, ApJ, 740, 108

Liu, M. C., Magnier, E. A., Deacon, N. R., et al. 2013, ApJ, 777, L20

Lodato, G., Meru, F., Clarke, C. J., & Rice, W. K. M. 2007, MNRAS, 374, 590

Lodieu, N. 2013, MNRAS, 431, 3222

Lodieu, N., Dobbie, P. D., & Hambly, N. C. 2011, A&A, 527, A24

Lodieu, N., Hambly, N. C., & Jameson, R. F. 2006, MNRAS, 373, 95

Lodieu, N., Hambly, N. C., Jameson, R. F., & Hodgkin, S. T. 2008, MNRAS, 383, 1385

Lodieu, N., Hambly, N. C., Jameson, R. F., et al. 2007, MNRAS, 374, 372

Lodieu, N., Pérez-Garrido, A., Béjar, V. J. S., et al. 2014, A&A, 569, A120

Lodieu, N., Zapatero Osorio, M. R., Béjar, V. J. S., & Peña Ramírez, K. 2018, MNRAS, 473, 2020

Looper, D. L., Bochanski, J. J., Burgasser, A. J., et al. 2010a, AJ, 140, 1486

Looper, D. L., Kirkpatrick, J. D., & Burgasser, A. J. 2007, AJ, 134, 1162

Looper, D. L., Mohanty, S., Bochanski, J. J., et al. 2010b, ApJ, 714, 45

López-Santiago, J., Montes, D., Crespo-Chacón, I., & Fernández-Figueroa, M. J. 2006, ApJ, 643, 1160

Loutrel, N. P., Luhman, K. L., Lowrance, P. J., & Bochanski, J. J. 2011, ApJ, 739, 81

Lovis, C., Ségransan, D., Mayor, M., et al. 2011, A&A, 528, A112

Low, C., & Lynden-Bell, D. 1976, MNRAS, 176, 367

Lucas, P. W., Roche, P. F., Allard, F., & Hauschildt, P. H. 2001, MNRAS, 326, 695

Luhman, K. L., Burgasser, A. J., & Bochanski, J. J. 2011, ApJ, 730, L9

Luhman, K. L., Burgasser, A. J., Labbé, I., et al. 2012, ApJ, 744, 135

Luhman, K. L., Herrmann, K. A., Mamajek, E. E., Esplin, T. L., & Pecaut, M. J. 2018, AJ, 156, 76

Luhman, K. L., & Mamajek, E. E. 2012, ApJ, 758, 31

Luhman, K. L., Mamajek, E. E., Allen, P. R., Muench, A. A., & Finkbeiner, D. P. 2009, ApJ, 691, 1265

Luhman, K. L., Stauffer, J. R., & Mamajek, E. E. 2005, ApJ, 628, L69

Luhman, K. L., Wilson, J. C., Brandner, W., et al. 2006, ApJ, 649, 894

Luyten, W. J., & Hughes, H. S. 1980, Proper Motion Survey, University of Minnesota, 55, 1

Mace, G. N., Kirkpatrick, J. D., Cushing, M. C., et al. 2013, ApJ, 777, 36

Magazzu, A., Martin, E. L., & Rebolo, R. 1993, ApJ, 404, L17

Malo, L., Artigau, É., Doyon, R., et al. 2014, ApJ, 788, 81

Malo, L., Doyon, R., Lafrenière, D., et al. 2013, ApJ, 762, 88

Manchado, A., Fuentes, F. J., Prada, F., et al. 1998, Society of Photo-Optical Instrumentation Engineers (SPIE) Conference Series, Vol. 3354, LIRIS: a long-slit intermediate-resolution infrared spectrograph for the WHT, ed. A. M. Fowler, 448–455

Marois, C., Macintosh, B., Barman, T., et al. 2008, Science, 322, 1348

Marois, C., Zuckerman, B., Konopacky, Q. M., Macintosh, B., & Barman, T. 2010, Nature, 468, 1080

Marsh, K. A., Kirk, J. M., André, P., et al. 2016, MNRAS, 459, 342

Martin, E. L., Basri, G., Delfosse, X., & Forveille, T. 1997, A&A, 327, L29

Martín, E. L., Delfosse, X., Basri, G., et al. 1999, AJ, 118, 2466

Martín, E. L., Delfosse, X., & Guieu, S. 2004, AJ, 127, 449

Martin, E. L., Montmerle, T., Gregorio-Hetem, J., & Casanova, S. 1998, MNRAS, 300, 733

Martin, E. L., Rebolo, R., Magazzu, A., & Pavlenko, Y. V. 1994, A&A, 282, 503

Martín, E. L., Phan-Bao, N., Bessell, M., et al. 2010, A&A, 517, A53

Mathieu, R. D., Walter, F. M., & Myers, P. C. 1989, AJ, 98, 987

Matsumoto, T., & Hanawa, T. 2003, ApJ, 595, 913

Matzner, C. D., & Levin, Y. 2005, ApJ, 628, 817

Mayer, L., Wadsley, J., Quinn, T., & Stadel, J. 2005, MNRAS, 363, 641

Mayor, M., & Queloz, D. 1995, Nature, 378, 355

Mayor, M., Pepe, F., Queloz, D., et al. 2003, The Messenger, 114, 20

McCarthy, C., & Zuckerman, B. 2004, AJ, 127, 2871

McCarthy, K., & White, R. J. 2012, AJ, 143, 134

McCaughrean, M. J., Close, L. M., Scholz, R.-D., et al. 2004, A&A, 413, 1029

McMahon, R. G., Banerji, M., Gonzalez, E., et al. 2013, The Messenger, 154, 35

Messina, S., Desidera, S., Turatto, M., Lanzafame, A. C., & Guinan, E. F. 2010, A&A, 520, A15

Messina, S., Millward, M., Buccino, A., et al. 2017, A&A, 600, A83

Mestel, L., & Ruderman, M. A. 1967, MNRAS, 136, 27

Metchev, S. A., & Hillenbrand, L. A. 2009, ApJS, 181, 62

Metchev, S. A., Kirkpatrick, J. D., Berriman, G. B., & Looper, D. 2008, ApJ, 676, 1281

Michell, J. 1767, Philosophical Transactions of the Royal Society of London Series I, 57, 234

Miret-Roig, N., Galli, P. A. B., Brandner, W., et al. 2020, A&A, 642, A179

Modigliani, A., Goldoni, P., Royer, F., et al. 2010, in Proc. SPIE, Vol. 7737, Observatory Operations: Strategies, Processes, and Systems III, 773728

Moe, M., & Di Stefano, R. 2017, ApJS, 230, 15

Mohanty, S., & Basri, G. 2003, ApJ, 583, 451

Mohanty, S., Jayawardhana, R., & Basri, G. 2005, ApJ, 626, 498

Moór, A., Szabó, G. M., Kiss, L. L., et al. 2013, MNRAS, 435, 1376

Moorwood, A., Cuby, J.-G., & Lidman, C. 1998, The Messenger, 91, 9

Murphy, S. J., Lawson, W. A., & Bento, J. 2015, MNRAS, 453, 2220

Murray, D. N., Burningham, B., Jones, H. R. A., et al. 2011, MNRAS, 414, 575

Muterspaugh, M. W., Lane, B. F., Kulkarni, S. R., et al. 2010, AJ, 140, 1657

Mužić, K., Radigan, J., Jayawardhana, R., et al. 2012, AJ, 144, 180

Muzerolle, J., Hillenbrand, L., Calvet, N., Briceño, C., & Hartmann, L. 2003, ApJ, 592, 266

Nakajima, T., Oppenheimer, B. R., Kulkarni, S. R., et al. 1995, Nature, 378, 463

Naud, M.-E., Artigau, É., Doyon, R., et al. 2017, AJ, 154, 129

Naud, M.-E., Artigau, É., Malo, L., et al. 2014, ApJ, 787, 5

Nayakshin, S. 2010, MNRAS, 408, L36

Nelson, A. F. 2000, ApJ, 537, L65

Nesterov, V. V., Kuzmin, A. V., Ashimbaeva, N. T., et al. 1995, A&AS, 110, 367

Neuhaeuser, R., Torres, G., Sterzik, M. F., & Randich, S. 1997, A&A, 325, 647

Neuhäuser, R., Brandner, W., Alves, J., Joergens, V., & Comerón, F. 2002, A&A, 384, 999

Neuhäuser, R., Guenther, E. W., Alves, J., et al. 2003, Astronomische Nachrichten, 324, 535

Nielsen, E. L., Liu, M. C., Wahhaj, Z., et al. 2013, ApJ, 776, 4

Nutzman, P., & Charbonneau, D. 2008, PASP, 120, 317

Oelkers, R. J., Stassun, K. G., & Dhital, S. 2017, AJ, 153, 259

Offner, S. S. R., Dunham, M. M., Lee, K. I., Arce, H. G., & Fielding, D. B. 2016, ApJ, 827, L11

Offner, S. S. R., Kratter, K. M., Matzner, C. D., Krumholz, M. R., & Klein, R. I. 2010, ApJ, 725, 1485

Oke, J. B., & Gunn, J. E. 1982, PASP, 94, 586

Oppenheimer, B. R., Golimowski, D. A., Kulkarni, S. R., et al. 2001, AJ, 121, 2189

Ortega, V. G., de la Reza, R., Jilinski, E., & Bazzanella, B. 2002, ApJ, 575, L75

Padoan, P., Jones, B. J. T., & Nordlund, Å. P. 1997, ApJ, 474, 730

Padoan, P., & Nordlund, Å. 2002, ApJ, 576, 870

—. 2004, ApJ, 617, 559

Patience, J., Ghez, A. M., Reid, I. N., & Matthews, K. 2002, AJ, 123, 1570

Patience, J., King, R. R., De Rosa, R. J., et al. 2012, A&A, 540, A85

Pecaut, M. J., & Mamajek, E. E. 2013, ApJS, 208, 9

—. 2016, MNRAS, 461, 794

Pecaut, M. J., Mamajek, E. E., & Bubar, E. J. 2012, ApJ, 746, 154

Pepe, F. A., Cristiani, S., Rebolo Lopez, R., et al. 2010, in Society of Photo-Optical Instrumentation Engineers (SPIE) Conference Series, Vol. 7735, Ground-based and Airborne Instrumentation for Astronomy III, ed. I. S. McLean, S. K. Ramsay, & H. Takami, 77350F

Perryman, M., Hartman, J., Bakos, G. Á., & Lindegren, L. 2014, ApJ, 797, 14

Persson, S. E., Murphy, D. C., Krzeminski, W., Roth, M., & Rieke, M. J. 1998, AJ, 116, 2475

Pinfield, D. J., Burningham, B., Lodieu, N., et al. 2012, MNRAS, 422, 1922

Pollacco, D. L., Skillen, I., Collier Cameron, A., et al. 2006, PASP, 118, 1407

Pollack, J. B., Hubickyj, O., Bodenheimer, P., et al. 1996, , 124, 62

Preibisch, T., Brown, A. G. A., Bridges, T., Guenther, E., & Zinnecker, H. 2002, AJ, 124, 404

Preibisch, T., Guenther, E., & Zinnecker, H. 2001, AJ, 121, 1040

Preibisch, T., Guenther, E., Zinnecker, H., et al. 1998, A&A, 333, 619

Preibisch, T., & Zinnecker, H. 1999, AJ, 117, 2381

Pringle, J. E. 1989, MNRAS, 239, 361

Quirrenbach, A., Amado, P. J., Mandel, H., et al. 2010, in Society of Photo-Optical Instrumentation Engineers (SPIE) Conference Series, Vol. 7735, Ground-based and Airborne Instrumentation for Astronomy III, ed. I. S. McLean, S. K. Ramsay, & H. Takami, 773513

Rafikov, R. R. 2005, ApJ, 621, L69

Raghavan, D., McAlister, H. A., Henry, T. J., et al. 2010, ApJS, 190, 1

Rameau, J., Chauvin, G., Lagrange, A. M., et al. 2013a, A&A, 553, A60

—. 2013b, ApJ, 772, L15

Rauer, H., Catala, C., Aerts, C., et al. 2014, Experimental Astronomy, 38, 249

Rayner, J. T., Cushing, M. C., & Vacca, W. D. 2009, ApJS, 185, 289

Rayner, J. T., Toomey, D. W., Onaka, P. M., et al. 2003, PASP, 115, 362

Rebolo, R., Martin, E. L., & Magazzu, A. 1992, ApJ, 389, L83

Rebolo, R., Zapatero Osorio, M. R., & Martín, E. L. 1995, Nature, 377, 129

Rebull, L. M., Stauffer, J. R., Cody, A. M., et al. 2018, AJ, 155, 196

Rees, M. J. 1976, MNRAS, 176, 483

Reid, I. N., & Gizis, J. E. 1997, AJ, 113, 2246

Reid, I. N., Gizis, J. E., Kirkpatrick, J. D., & Koerner, D. W. 2001, AJ, 121, 489

Reipurth, B., & Clarke, C. 2001, AJ, 122, 432

Reipurth, B., & Mikkola, S. 2012, Nature, 492, 221

Riaz, B., Gizis, J. E., & Harvin, J. 2006, AJ, 132, 866

Ricker, G. R., Winn, J. N., Vanderspek, R., et al. 2014, in Society of Photo-Optical Instrumentation Engineers (SPIE) Conference Series, Vol. 9143, Space Telescopes and Instrumentation 2014: Optical, Infrared, and Millimeter Wave, ed. J. Oschmann, Jacobus M., M. Clampin, G. G. Fazio, & H. A. MacEwen, 914320

Riedel, A. R., Alam, M. K., Rice, E. L., Cruz, K. L., & Henry, T. J. 2017, ApJ, 840, 87

Rizzuto, A. C., Ireland, M. J., Dupuy, T. J., & Kraus, A. L. 2016, ApJ, 817, 164

Rizzuto, A. C., Ireland, M. J., & Kraus, A. L. 2015, MNRAS, 448, 2737

Rodriguez, D. R., Zuckerman, B., Kastner, J. H., et al. 2013, ApJ, 774, 101

Sahlmann, J., Lazorenko, P. F., Ségransan, D., et al. 2014, A&A, 565, A20

—. 2013, A&A, 556, A133

Salpeter, E. E. 1955, ApJ, 121, 161

Sartori, M. J., Lépine, J. R. D., & Dias, W. S. 2003, A&A, 404, 913

Saumon, D., Hubbard, W. B., Burrows, A., et al. 1996, ApJ, 460, 993

Saumon, D., Marley, M. S., Abel, M., Frommhold, L., & Freedman, R. S. 2012, ApJ, 750, 74

Schlieder, J. E., Lépine, S., & Simon, M. 2010, AJ, 140, 119

—. 2012a, AJ, 143, 80

—. 2012b, AJ, 144, 109

Schneider, A. C., Shkolnik, E. L., Allers, K. N., et al. 2019, AJ, 157, 234

Schneider, A. C., Windsor, J., Cushing, M. C., Kirkpatrick, J. D., & Shkolnik, E. L. 2017, AJ, 153, 196

Scholz, R.-D. 2010, A&A, 515, A92

Scholz, R.-D., McCaughrean, M. J., Lodieu, N., & Kuhlbrodt, B. 2003, A&A, 398, L29

Scholz, R. D., McCaughrean, M. J., Zinnecker, H., & Lodieu, N. 2005, A&A, 430, L49

Schroeder, D. J., Golimowski, D. A., Brukardt, R. A., et al. 2000, AJ, 119, 906

Seager, S., & Sasselov, D. D. 2000, ApJ, 537, 916

Seifahrt, A., Stürmer, J., Bean, J. L., & Schwab, C. 2018, in Society of Photo-Optical Instrumentation Engineers (SPIE) Conference Series, Vol. 10702, Ground-based and Airborne Instrumentation for Astronomy VII, ed. C. J. Evans, L. Simard, & H. Takami, 107026D

Shan, Y., Yee, J. C., Bowler, B. P., et al. 2017, ApJ, 846, 93

Shapley, H. 1958, Of stars and men. The human response to an expanding universe

Shkolnik, E., Liu, M. C., & Reid, I. N. 2009, ApJ, 699, 649

Shkolnik, E. L., Allers, K. N., Kraus, A. L., Liu, M. C., & Flagg, L. 2017, AJ, 154, 69

Shkolnik, E. L., Anglada-Escudé, G., Liu, M. C., et al. 2012, ApJ, 758, 56

Shu, F. H., Adams, F. C., & Lizano, S. 1987, ARA&A, 25, 23

Siegler, N., Close, L. M., Cruz, K. L., Martín, E. L., & Reid, I. N. 2005, ApJ, 621, 1023

Siegler, N., Close, L. M., Mamajek, E. E., & Freed, M. 2003, ApJ, 598, 1265

Silk, J. 1977, ApJ, 214, 152

Skrutskie, M. F., Cutri, R. M., Stiening, R., et al. 2006, AJ, 131, 1163

Slesnick, C. L., Carpenter, J. M., & Hillenbrand, L. A. 2006, AJ, 131, 3016

Slesnick, C. L., Hillenbrand, L. A., & Carpenter, J. M. 2008, ApJ, 688, 377

Smith, L. C., Lucas, P. W., Contreras Peña, C., et al. 2015, MNRAS, 454, 4476

Stamatellos, D., Hubber, D. A., & Whitworth, A. P. 2007, MNRAS, 382, L30

Stamatellos, D., & Whitworth, A. P. 2009, MNRAS, 392, 413

Stelzer, B., & Neuhäuser, R. 2000, A&A, 361, 581

Sterzik, M. F., Alcalá, J. M., Covino, E., & Petr, M. G. 1999, A&A, 346, L41

Stevenson, D. J. 1978, Proceedings of the Astronomical Society of Australia, 3, 227

Strassmeier, K. G., & Rice, J. B. 2000, A&A, 360, 1019

Sutherland, W., Emerson, J., Dalton, G., et al. 2015, A&A, 575, A25

Tamura, M. 2009, in American Institute of Physics Conference Series, Vol. 1158, Exoplanets and Disks: Their Formation and Diversity, ed. T. Usuda, M. Tamura, & M. Ishii, 11–16

Tarter, J. C. 1975, PhD thesis, California Univ., Berkeley.

Thalmann, C., Carson, J., Janson, M., et al. 2009, ApJ, 707, L123

Tobin, J. J., Looney, L. W., Li, Z.-Y., et al. 2016, ApJ, 818, 73

Todorov, K., Luhman, K. L., & McLeod, K. K. 2010, ApJ, 714, L84

Tognelli, E., Prada Moroni, P. G., & Degl'Innocenti, S. 2011, A&A, 533, A109

Tohline, J. E. 2002, ARA&A, 40, 349

Tokovinin, A. 2014, AJ, 147, 86

Tokovinin, A., & Briceño, C. 2018, AJ, 156, 138

—. 2020, AJ, 159, 15

Toomre, A. 1964, ApJ, 139, 1217

Torres, C. A. O., da Silva, L., Quast, G. R., de la Reza, R., & Jilinski, E. 2000, AJ, 120, 1410

Torres, C. A. O., Quast, G. R., da Silva, L., et al. 2006, A&A, 460, 695

Torres, C. A. O., Quast, G. R., Melo, C. H. F., & Sterzik, M. F. 2008, Young Nearby Loose Associations, ed. B. Reipurth, Vol. 5, 757

Torres, G., Neuhäuser, R., & Guenther, E. W. 2002, AJ, 123, 1701

Trujillo, C. A., & Sheppard, S. S. 2014, Nature, 507, 471

Tuomi, M. 2012, A&A, 543, A52

Vernet, J., Dekker, H., D'Odorico, S., et al. 2011, A&A, 536, A105

Vigan, A., Patience, J., Marois, C., et al. 2012, A&A, 544, A9

Vogt, S. S., Allen, S. L., Bigelow, B. C., et al. 1994, in Society of Photo-Optical Instrumentation Engineers (SPIE) Conference Series, Vol. 2198, Instrumentation in Astronomy VIII, ed. D. L. Crawford & E. R. Craine, 362

Wahhaj, Z., Liu, M. C., Nielsen, E. L., et al. 2013, ApJ, 773, 179

Walter, F. M. 1986, ApJ, 306, 573

Walter, F. M., Vrba, F. J., Mathieu, R. D., Brown, A., & Myers, P. C. 1994, AJ, 107, 692

Ward-Duong, K., Patience, J., De Rosa, R. J., et al. 2015, MNRAS, 449, 2618

Ward-Thompson, D., André, P., Crutcher, R., et al. 2007, in Protostars and Planets V, ed. B. Reipurth, D. Jewitt, & K. Keil, 33

Watkins, S. J., Bhattal, A. S., Boffin, H. M. J., Francis, N., & Whitworth, A. P. 1998a, MNRAS, 300, 1205

—. 1998b, MNRAS, 300, 1214

Webb, R. A., Zuckerman, B., Platais, I., et al. 1999, ApJ, 512, L63

Weinberg, M. D., Shapiro, S. L., & Wasserman, I. 1987, ApJ, 312, 367

White, R. J., & Basri, G. 2003, ApJ, 582, 1109

Whitworth, A. P. 2018, Brown Dwarf Formation: Theory, ed. H. J. Deeg & J. A. Belmonte, 95

Whitworth, A. P., Chapman, S. J., Bhattal, A. S., et al. 1995, MNRAS, 277, 727

Whitworth, A. P., & Stamatellos, D. 2006, A&A, 458, 817

Whitworth, A. P., & Zinnecker, H. 2004, A&A, 427, 299

Wilking, B. A., Gagné, M., & Allen, L. E. 2008, Star Formation in the ρ Ophiuchi Molecular Cloud, ed. B. Reipurth, Vol. 5, 351

Wolszczan, A. 1994, Science, 264, 538

Wolszczan, A., & Frail, D. A. 1992, Nature, 355, 145

Wright, E. L., Eisenhardt, P. R. M., Mainzer, A. K., et al. 2010, AJ, 140, 1868

Wright, E. L., Skrutskie, M. F., Kirkpatrick, J. D., et al. 2013, AJ, 145, 84

Wright, N. J., & Mamajek, E. E. 2018, MNRAS, 476, 381

Zapatero Osorio, M. R., & Martín, E. L. 2004, A&A, 419, 167

Zapatero Osorio, M. R., Martín, E. L., Béjar, V. J. S., et al. 2007, ApJ, 666, 1205

Zhu, Z., Hartmann, L., Nelson, R. P., & Gammie, C. F. 2012, ApJ, 746, 110

Zúñiga-Fernández, S., Bayo, A., Elliott, P., et al. 2020, arXiv e-prints, arXiv:2010.08575

Zuckerman, B., Rhee, J. H., Song, I., & Bessell, M. S. 2011, ApJ, 732, 61

Zuckerman, B., & Song, I. 2004, ARA&A, 42, 685

Zuckerman, B., Song, I., & Bessell, M. S. 2004, ApJ, 613, L65

Zuckerman, B., Song, I., Bessell, M. S., & Webb, R. A. 2001a, ApJ, 562, L87

Zuckerman, B., Song, I., & Webb, R. A. 2001b, ApJ, 559, 388

Zuckerman, B., & Webb, R. A. 2000, ApJ, 535, 959

A

Appendix A

A.1 Information about the individual systems in the USco search

A.1.1 USco 154925.08−284352.7 and USco 15:49:24.85−28:43:51.6 (M2+M4)

The primary in this system was identified by Dawson et al. (2011) in their search for brown dwarfs in USco using UKIDSS and 2MASS data. It was later observed by Rizzuto et al. (2015) using WiFeS optical spectrograph on the Australian National University 2.3m telescope, and they determined a spectral type of M2.

We found the secondary placed at a separation of only 3″. This object was reported as a candidate companion in Tokovinin & Briceño (2020). We observed both objects using NTT/SofI and found spectral types of M2 and M4.

Both components of this system have available parallax and proper motion measurements in the *Gaia* DR2, and their values are in good agreement with being placed at the same heliocentric distance and be moving with the same velocities. Therefore, we confirm that these objects are most likely bound.

A.1.2 155318.82−230639.5 and 155318.63−230631.3

The primary of this system was proposed to be a USco member by Ardila et al. (2000). We found a companion candidate placed at 11″ of it. According to *Gaia* DR2, their parallaxes and PM are in very good agreement. However, their parallactic distance indicates that they are closer in distance than USco,

and their PM are not in good agreement with the association. Therefore, we consider that, although this may be a truly bound pair, they are not likely members of USco.

A.1.3 USco 155430.11−272019.1 and USco 155430.47−271957.5 (B6+M9)

This pair was discovered by Aller et al. (2013). The primary (also called HIP 77900) is a well known Usco member, with a spectral type of B6 (Garrison 1967). The secondary (HIP 77900B) is placed at a distance of 22″, which corresponds to a physical separation of 3200 AU. It was observed by Aller et al. (2013) using SpeX NIR spectrograph on the 3m NASA IRTF Telescope on Mauna Kea, they found a spectral type of M9, and estimate a mass of 19^{+7}_{-4} M_{Jup} considering an age of 5 Myr, or 20^{+7}_{-3} M_{Jup} considering 10 Myr.

Gaia DR2 includes a parallax and PM measurement for both components in this system. They are both in good agreement with the USco association. However, the secondary's measurements have very large errors, so we cannot use this data to further assess the companionship of these two objects.

A.1.4 USco 155548.82−251224.1, USco 155548.40−251217.4 and USco 155547.88−251217.3 (G3+M2.5+M5)

We found USco 155547.88−251217.3 close to two catalogued members of USco: USco 155548.82−251224.1 (HD 142506) and USco 155548.40−251217.4. HD 142506 is a G3 star proposed as an USco member in the PhD Thesis of Kunkel (1996) and later included in Preibisch & Zinnecker (1999). USco 155548.40−251217.4 was found by Kraus & Hillenbrand (2009) as a possible companion of HD 142506. They estimate a spectral type of M2.5 for it. The three components are included in Barenfeld et al. (2019) as candidate companions, detected using *Gaia* DR2 data.

The faintest object, USco 155547.88−251217.3, was also found by Kraus & Hillenbrand (2009) as another possible companion of HD 142506. They discarded their companionship regarding the astrometry of the objects, as they measure a discrepancy between their proper motions higher than 3σ. However, the recent *Gaia* DR2 data show very similar PM and parallaxes for this pair.

We observed the faintest component using NTT/SofI, and we determine a spectral type of M5.

The three objects are compatible, photometrically and astrometrically, with the USco association. However, according to the *Gaia* DR2 parallaxes, the M2.5 dwarf USco 155548.40−251217.4 is closer in our line of sight. Nevertheless, the astrometric noise of this source is very high for such a bright object,

and may be affected for example by the object being a close binary. Therefore, on the contrary of what Kraus & Hillenbrand (2009) presents, we propose HD 142506 and USco 155547.88−251217.3 to be real companions, and we consider that the M2.5 USco 155548.40−251217.4 may be another member of USco in a casual visual alignment with the system, or may be also a true companion with an anomalous *Gaia* DR2 astrometry.

A.1.5 USco 155624.92−254120.3 and USco 155623.44−254105.6 (M3+M8.5)

This system was published in Chinchilla et al. (2020b). The details can be found in the attached paper in Chapter 4.

A.1.6 USco 155836.21−234802.0 and USco 155835.98−234813.6 (M3+M4)

These two objects are USco known members, and previously proposed as candidate companions in the literature. The secondary, USco 155835.98−234813.6 (named UScoCTIO 80) was classified as an M4 by Ardila et al. (2000), and they found a moderate Hα emission in its spectrum of −8.7Å. USco 155836.21−234802.0 (named UCAC3 133-1777729) was proposed as a wide candidate companion to UScoCTIO 80 by Kraus & Hillenbrand (2009). Their separation is 12″. They determined a spectral type of M3, and found also an Hα emission in its spectrum of −9.9Å. They found that the primary is, in fact, a close visual binary itself, with a physical separation of 7.8 AU and masses of 0.35 and 0.36 $M_\odot$ (Kraus & Hillenbrand 2012). As UCAC3 133-1777729 is the primary in the system, it was named as UScoCTIO 80 A, and the originally named UScoCTIO 80 was renamed as UScoCTIO 80 B.

The *Gaia* DR2 proper motions and parallaxes of both components are in very good agreement with USco, and also between each other. *Gaia* DR2 does not identify the primary as a duplicated source, and its astrometric error is not higher than the expected for an individual source, although it is a close binary itself. Considering the separation and the astrometry of the components, we confirm this system as a likely truly bound system.

A.1.7 USco 155853.51−251233.4 and USco 155853.97−251151.8 (M1+M4.5)

The primary is an M1 dwarf, reported as an USco member in the PhD Thesis of M. Kunkel (1996).

We found the secondary at a distance of 42″from it. It does not have an entry in *Gaia* DR2, despite being bright enough for *Gaia* to detect it. This object is also included in Luhman et al. (2018) as a candidate USco member, but it is not confirmed through spectroscopy. We observed it using WHT/LIRIS

and found a spectral type of M4.5. Considering the large separation and the lack of more precise parallax measurement from *Gaia*, we cannot discard that this object is a chance alignment.

We found an additional faint object close to this system when visual inspecting the system with *Gaia* DR2: 15585552−2512041. It has a *Gaia* PM and parallax compatible with the USco association, but with a very high astrometric error. However, this object was discarded in our search due to its bluer $J - K$ colour ($J - Ks = 0.69$), which does not follow the USco photometric sequence. The $G - J$ colour of this object indicates a spectral type of ∼M5, and it is detected in DSS2, so it seems to be a low-mass object which is placed further away than the USco association.

Kraus & Hillenbrand (2009) found a closer candidate companion for this primary, placed at $11''$ from the primary, 2M15585415−2512407, but they discard it regarding its astrometry. In addition, *Gaia* DR2 data indicate very different parallaxes and PM for the two objects. Therefore, we also agree that this object is a chance alignment and not a real companion.

A.1.8 USco 155958.99−243815.3 and USco 155957.94−243813.3 (M4+M4)

The two components of this system were discovered by Ardila et al. (2000) in their photometric search for low-mass stars and brown dwarfs in USco using the 60 cm Michigan Curtis Schmidt Telescope at Cerro Tololo Inter-American Observatory (CTIO, Chile). They were named as UScoCTIO 89 and UScoCTIO 91. Both are very similar in magnitude. The slighty fainter one (secondary; UScoCTIO 91) was observed by Luhman et al. (2018) using the Hydra multi-object optical spectrograph on the 4m Blanco Telescope at CTIO in Chile; they estimate a spectral type of M4.5. These objects were not previously related as candidate companions.

We observed both components using WHT/LIRIS. We estimate spectral types of M4 and M4.

The *Gaia* DR2 data indicates that these two objects are placed at the same heliocentric distance and have nearly the same PM. Therefore, we consider that they are likely true companions.

A.1.9 USco 160015.68−223158.0 and USco 160015.33−223157.5 (M4+??)

The primary of this system was originally found by Luhman & Mamajek (2012) in their photometric search for USco members using Spitzer Space Telescope and WISE data. Luhman et al. (2018) observed it using Hydra, they obtained a spectral type of M4 and observed spectral features that indicated a membership

to the USco association.

We found the secondary placed at a distance of 5″ from the primary. This object was not previously reported in the literature. We observed both primary and secondary using WHT/LIRIS, but unfortunately, the spectra from that night were affected by a configuration error in the spectral filters and could not be used for spectral classification. We expected a spectral type between M7–M8 for it, according to its magnitudes and colours.

The secondary does not have a parallax and PM measurement in *Gaia* DR2, probably due to its faintness. Neither it nor the primary have a Duplicate Source flag. Despite the lack of a parallactic distance for the secondary, as the components are very close in the sky (5″), we estimate a high probability that they are truly bound.

A.1.10 USco 160017.66−225653.7 and USco 160019.44−225629.0 (M7+M8)

The components of this system were previously known, but they were not identified as companions. Both primary and secondary were discovered by Ardila et al. (2000). They were named as UScoCTIO 119 and UScoCTIO 131. The secondary was observed by Martín et al. (2004), they determined an optical spectral type of M8 and a clear membership to USco. Later, Luhman et al. (2018) observed it and determined a spectral type of M7. The primary did not have any available spectrum in the literature, so we observed it using WHT/LIRIS, and found a spectral type of M7.

Both components have a complete astrometric solution in *Gaia* DR2. Their parallaxes and proper motions are in very good agreement with the USco association, and they are compatible with each other in parallax, although there are slight differences in their proper motion. However, due to their relative faintness, the astrometric errors of their measurements are very high. We consider that this pair is most likely truly bound.

A.1.11 USco 160049.89−192800.4 and USco 160050.65−192750.4 (M1.5+M6.5)

These objects were known as USco members, but not related as companions. The primary was discovered by Rizzuto et al. (2015), they estimated a spectral type of M1.5. The secondary was found by Martín et al. (2010), they estimate a spectral type of M6.5 and identify low-gravity features in the spectrum. The two objects are placed at a 15″ separation from each other.

The primary has a parallax and proper motion measurement in *Gaia* DR2, which is compatible with the USco association. *Gaia* DR2 presents two entries for the secondary, and is not able to provide a parallax or PM measurement for

them. Therefore, we cannot use this astrometric data to confirm their companionship. But regarding the short angular separation between the components, we consider that they are likely bound.

A.1.12 USco 160052.84−244038.0 and USco 160052.79−244035.5 (M3+M4)

The primary of this system was discovered by Luhman & Mamajek (2012). Luhman et al. (2018) observed it using Hydra spectrograph, and found a spectral type of M3.25 and clear indicators of youth.

We found the secondary placed at only 3″ from the primary. This pair was reported as candidate companions in Tokovinin & Briceño (2020). We observed both components using WHT/LIRIS, and found spectral types of M3 and M4 for them.

The *Gaia* DR2 astrometric data of both components is in perfect agreement, both in the parallaxes and PM. We consider that this pair is truly bound.

A.1.13 USco 160210.45−224128.3 and USco 160209.63−224058.0 (K5+M5)

The primary in this candidate system (also called ScoPMS 23) is a K5 spectroscopic binary identified by Mathieu et al. (1989), with a period of 2.4 days. It was included as an USco candidate member by Walter et al. (1994). It also has a close stellar companion, 0.6 magnitudes fainter in K, placed at a 0.3″ distance (Lafrenière et al. 2014).

We found a wide companion placed at a distance of 32″ from it. This object was proposed as an USco candidate member by Lodieu (2013), and also by Luhman et al. (2018), but they did not confirm is spectroscopically. We observed it using WHT/LIRIS and found a spectral type of M5.

The primary does not have available parallax and PM measurements in *Gaia* DR2, probably due to its binarity. Therefore, we cannot use *Gaia* data to further assess their companionship and discard a possible chance alignment. However, regarding the angular separation, we consider that this system is likely truly bound.

A.1.14 USco 160234.18−220035.4 and USco 160232.27−220048.7 (M6+M5.75)

The two components of this system were discovered by Luhman & Mamajek (2012), but they were not related as companions. Their angular separation in the sky is 30″. Luhman et al. (2018) estimate a spectral type of M6 for the brightest one using Hydra spectrograph, and M5.75 for the faintest using SpeX spectrograph.

The parallaxes and PM of the two components are in very good agreement according to *Gaia* DR2 data. We propose this system as true companions.

A.1.15 USco 160301.78−262621.9 and USco 160302.35−262616.5 (M0+M5)

The primary in this system was found by Rizzuto et al. (2015). They estimated a spectral type of M0.

We found the secondary placed at 10″from the primary. It is also a known USco candidate member, discovered by Dawson et al. (2013), and also included as a candidate USco member in Luhman et al. (2018), but they did not confirm it spectroscopically. It was reported as a candidate companion in Tokovinin & Briceño (2020). We observed it using WHT/LIRIS, and found a spectral type of M5.

Their *Gaia* DR2 parallaxes and PM are in very good agreement with each other, and with the USco association. Therefore, we consider that these objects form a truly bound system.

A.1.16 USco 160417.41−194228.8 and USco 160417.92−194150.8 (M3.5+M5)

Both components of this system were separately discovered by Luhman & Mamajek (2012). Their separation is 39″. These objects were proposed as candidate wide companions by Barenfeld et al. (2019), who found them using *Gaia* DR2 data. Luhman et al. (2018) determine a spectral type of M3.5 and M5 for the primary and secondary, respectively, using Hydra spectrograph, and a clear USco membership for both. Barenfeld et al. (2019) also find another closer object with coincident parallax and PM placed at 5.5″of the primary. This object was not detected in our search because it is brighter than J=12.5. We propose this system as a truly bound triple system.

A.1.17 USco 160442.70−225452.8 and USco 160440.26−225432.5 (??+M6)

Both components in this pair, USco 160442.70−225452.8 (named UScoCTIO 83) and USco 160440.26−225432.5 (named UScoCTIO 127) were found by Ardila et al. (2000), but they did not determine their spectral types. The separation between them is 40″. The secondary was later observed by Luhman et al. (2018), they determined a spectral type of M6 for it.

The *Gaia* DR2 astrometry of this pair shows very different values for both the proper motions and parallaxes of the two components. According to it, the faintest component (UScoCTIO 127) is placed at a heliocentric distance of 159 pc and has a proper motion which is in very good agreement with USco. However, the brightest component (UScoCTIO 83) is placed at a higher

heliocentric distance of 215 pc, and its proper motion is quite different to UScoCTIO 127. Their astrometric errors are not higher than the expected for their brightness, and they are not marked either as duplicated sources. Therefore, we consider that this pair is a chance alignment and are not truly bound companions.

A.1.18 USco 160553.94−181842.7 and USco 160554.09−181849.1 (M7+M9.5)

This pair (also called UScoCTIO 108 and UScoCTIO 108B) was found by Béjar et al. (2008) in their search for faint companions using 2MASS, DENIS and UKST. The primary is an M7 brown dwarf originally found by Ardila et al. (2000). The secondary is an M9.5 low mass brown dwarf, very close to the deuterium-burning mass-limit. Their separation is 670 AU. The estimated masses are $60\pm20 M_{Jup}$ and 14^{+2}_{-8} M_{Jup} for the primary and secondary, respectively, assuming an age range of 1–8 Myr for USco.

The *Gaia* DR2 astrometry of the primary is in good agreement with the USco association. The secondary is too faint for *Gaia* DR2 to detect it. We also identified this pair in our search, and confirm this system as likely true companions.

A.1.19 USco 160611.99−193533.1 and USco 160611.44−193540.7 (M5+M5+M5)

The primary in this system was discovered by Preibisch et al. (2002) as a candidate USco member. They determined a spectral type of M5 and measured a moderate emission in Hα, compatible with a young age. The secondary, which is placed at $11''$, was discovered as a candidate companion by Kraus & Hillenbrand (2007b). They determined a spectral type of M5 also for the wide companion, and found youth features in its spectrum. They also discovered that the primary is a close binary itself, with nearly equal components, and assigned a spectral type of M5+M5 to it. Hence, this would be a triple system formed by three M5 components, two of them forming a tighter binary, and the third one as a wide companion. They estimate masses of 0.14 + 0.12 $M_\odot$ for the tight binary, and 0.14 $M_\odot$ for the wide companion.

The *Gaia* DR2 astrometry for this "pair" is in very good agreement with the USco association, and also between each other. *Gaia* DR2 does not identify the primary as a duplicated source, and its astrometric errors are not above the usual for its brightness, despite being a close binary. Considering this good astrometric agreement and their separation, we confirm this objects as true companions, forming a hierarchical triple system.

A.1.20 USco 160647.94−184143.7 and USco 160647.98−184148.1 (M0+??)

The primary of this system was found by Rizzuto et al. (2015), they observed it using the Wide-Field Spectrograph (WiFeS) at the Australian National University 2.3 m Telescope. They determine a spectral type of M0, and find youth features in the spectrum that indicate its membership to the association.

We found the secondary placed at a distance of $4''$. This object was reported as a candidate companion in Tokovinin & Briceño (2020). We observed both the primary and the secondary using WHT/LIRIS, but unfortunately the data were not correctly obtained and could not be used for spectral type classification.

According to *Gaia* DR2, the parallaxes and PM of both objects are in agreement, although the secondary has a high error in its parallax measurement, possibly due to its faintness and the close bright primary. But due to their closeness and their compatible *Gaia* DR2 astrometry we propose this system as a truly bound pair.

A.1.21 USco 16075796−2040087, USco 160800.51−204028.9, USco 160757.13−204017.6 and USco 160758.50−203948.8 (M1+M5+M5.5+M6)

The brightest and faintest components in this group of candidates were proposed as a wide binary by Kraus & Hillenbrand (2009). The "secondary" is an M6 dwarf discovered by Slesnick et al. (2006) in their photometric search for low-mass objects in USco, using data from 2MASS and data taken with the Quest-2 camera on the 1.2m Oschin Schmidt Telescope at Palomar Observatory, in USA. The optical spectroscopy was acquired using the Double Spectrograph on the 200 inch Palomar telescope. Kraus & Hillenbrand (2009) discovered the "primary" placed at $21''$(3120 AU) from the secondary. They estimate a spectral type of M1. They estimate masses of 0.70 $M_\odot$ and 0.074 $M_\odot$ for the "primary" and "secondary", respectively. This object has a very strong Hα emission, of −357 Å(Kraus & Hillenbrand 2009). Cody et al. (2017) indicate that the primary star of this system may be in fact earlier than M1, and estimate a spectral type between G6–K5. Barenfeld et al. (2019) presents that the star is in fact a stellar tight binary, with a separation of only 6.3 AU, and which presents a dust and gas circumbinary disk that extends to 46^{+6}_{-2} AU, wider than the binary separation.

The *Gaia* parallaxes and PM of these two objects are compatible with the USco association. However, there are discrepancies between them. Therefore, altough these objects may be USco members which are close in the sky by chance, and whose heliocentric distances are different, we suspect that the M1's astrometry may be highly affected by its close binarity, and, hence, it may be

actually placed at the same heliocentric distance as the M6 "secondary".

We found a third object close to these two, USco 160757.13−204017.6. This object is included as an USco candidate in Rebull et al. (2018), and is also presented as a candidate companion in this system by Barenfeld et al. (2019). Its *Gaia* parallax and PM are in agreement with USco and with the M6 object. We observed this third object using NTT/SofI and found a spectral type of M5.5. We conclude that this object has a high probability of being a companion of the M6 dwarf USco 160758.50−203948.8 and the M1 binary star USco 16075796−2040087.

Furthermore, we found another additional object, placed at a distance of 49″ from each of the bound components: 2MASS J16080051-2040289. This object was proposed as an USco member by Preibisch et al. (2001), who determined a spectral type of M5 and found youth features in it. It is also presented as a candidate companion in the system by Barenfeld et al. (2019). The *Gaia* PM and parallax of this object is also compatible with being another component in the multiple system.

A.1.22 USco 160843.40−260216.8 and USco 160844.38−260214.0 (G9+M8.25)

This pair was proposed as candidate companions by Kraus & Hillenbrand (2009). The primary was identified as an USco member by Preibisch et al. (1998) in their spectroscopic survey for PMS stars in USco, using FLAIR II spectrograph on the UK Schmidt Telescope, at the Anglo-Australian Observatory in Australia. They assigned a spectral type of G7. Later, Torres et al. (2006) assigned a spectral type of G9. The secondary was found by Kraus & Hillenbrand (2009), and later observed by Luhman et al. (2018) using SpeX spectrograph. They estimate a spectral type of M8.25. Their separation is 13.5″.

We also observed this candidate companion, using NTT/SofI. We obtained a spectral type of M7.5. Their *Gaia* DR2 proper motions and parallaxes are more or less in good agreement, although the error in the secondary's measurements is high, probably due to the faintness of the source. We consider that this system is most likely truly bound.

A.1.23 USco 160920.89−192725.9 and USco 160920.54−192632.1 (A0+M5.5)

USco 160920.89−192725.9 (also named HD 144981) is a well known USco member with a spectral type of A0. The candidate companion, USco 160920.54−192632.1, was discovered by Luhman & Mamajek (2012) in their search for members of the association. It has a spectral type of M5.5 (Luhman et al. 2018). The

angular separation between these objects is 49″.

The primary star is flagged as a duplicated source in *Gaia* DR2. Nevertheless, the *Gaia* DR2 astrometric data of these objects is in agreement with the USco association, and also between each other. We consider that, despite the high angular separation between the components, this system is most likely truly bound.

A.1.24 USco 161020.87−233155.6 and USco 161019.42−233109.3 (M5.5+M5.75)

These two objects were found by Lodieu et al. (2007) in their search for brown dwarfs in USco using UKIDSS GCS data. Both objects were later observed by Lodieu et al. (2011) using the AAOmega spectrograph at the 3.9m Anglo-Australian Telescope (AAT), in Australia. They determined spectral types of M5.5 and M5.75 for the primary and secondary, respectively, and a mass of 0.182 $M_\odot$ for the primary. They measure a PM for the secondary of (−5.10, −2.45) mas yr^{-1}, and therefore, they classify it as a proper-motion non-member of USco. However, *Gaia* DR2 measures a PM of (−10.07, −22.68) mas yr^{-1} for the object, which is perfectly compatible with the association.

The parallaxes and proper motions from *Gaia* are compatible with belonging to the USco association for both objects. However, the discrepancies among these values and the high angular separation of this system suggests that these objects may not be real companions, and that they are most likely a chance alignment between unrelated USco members.

A.1.25 USco 161021.74−190406.6 and USco 161021.78−190402.4 (M3+M5)

This pair was identified by Kraus & Hillenbrand (2009). The primary is an M3 dwarf identified as an USco member by Walter et al. (1994). They obtained its spectral type using the IIDS spectrograph on the 2.1m telescope at the Kitt Peak National Observatory, in USA. The secondary was discovered by Kraus & Hillenbrand (2009), but they did not determine its spectral type. The angular separation of the components is 5″.

We observed both primary and secondary using WHT/LIRIS, and determined spectral types of M2–3 and M5.

Walter et al. (1994) named this primary ScoPMS 042b, as they find another component, an M1 USco member which they name ScoPMS 042a, placed at a distance of 1.9′ from it. *Gaia* DR2 indicates that this source is duplicated, and does not provide a PM and parallax measurement. Considering the high angular separation from the system, and the lack of more precise astrometric measurements, we cannot confirm whether ScoPMS 042a is also a

part of the system, but we confirm that USco 161021.74−190406.6 and USco 161021.78−190402.4 are most likely true companions.

A.1.26 USco 161031.95−191306.1 and USco 161032.33−191308.7 (K7+M9).

This pair was found by Kraus & Hillenbrand (2009) in their search for candidate wide companions in Taurus and USco, using 2MASS data; and were later confirmed spectroscopically by Aller et al. (2013). The primary is a K7 dwarf found by Preibisch et al. (2002). For the secondary, Aller et al. (2013) obtained a spectral type of M9±0.5 through spectroscopic observations using SpeX spectrograph at the 3m NASA IRTF Telescope in Mauna Kea (Hawai'i). The angular separation between the components is around 6″, which corresponds to a physical projected separation of 840±90 AU. They estimate masses of $0.88^{+0.14}_{-0.17}$ $M_\odot$ (5 Myr) or $0.87^{+0.11}_{-0.18}$ $M_\odot$ (10 Myr) for the primary, and 19^{+7}_{-4} M_{Jup} (5 Myr) or 20^{+7}_{-3} M_{Jup} (10 Myr) for the secondary.

We also identified this pair in our search. Their *Gaia* DR2 parallaxes and proper motions are also in good agreement, although the secondary has a relatively high error in its astrometry measurements, due to its faintness. We confirm this system as companions.

A.1.27 USco 161123.05−190523.2 and USco 161119.35−190508.2 (M3+M6.5)

The brightest component in this system was discovered by Preibisch et al. (2001) as an USco member. They determined a spectral type of M3, and measured an Hα emission of −6.9Å. The faintest component was included in Luhman & Mamajek (2012) as a candidate member. Its spectral type is M6.5 (Luhman et al. 2018). The separation between these objects is 55″.

The high angular separation of this system indicates a high probability of being a chance alignment. However, the *Gaia* DR2 astrometry of the components is in good agreement, both in parallaxes and proper motions. Hence, we propose this system as truly bound.

A.1.28 USco 161159.27−190653.4, USco 161159.23−190656.2 and USco 161156.90−190647.0 (K2+M4+M1+M9.25)

This is one of the most interesting systems in our results. The primary, also called ScoPMS 048, is a K star observed by Walter (1986) and proposed as an USco member by Walter et al. (1994). Mathieu et al. (1989) discovered that the K star is a double-lined spectroscopic binary, with a period of 10.4 days, and masses of 1.2 $M_\odot$ and 0.22 $M_\odot$ (mass ratio of 0.18) for the components.

It has a wide companion, named as ScoPMS 048 B, at a separation of 3.4″, presented together with ScoPMS 048 as a visual binary by Martin et al. (1998). They estimated spectral types of K3+M1:, through spectroscopy obtained with the IDS spectrograph on the 2.5m Isaac Newton Telescope (INT) in La Palma, Spain.

We found an additional companion, placed at a distance of 34″ from ScoPMS 048AB. This object is too faint for *Gaia* DR2 to detect it. It was proposed as an USco candidate member by Luhman et al. (2018), but it was not confirmed spectroscopically. We observed it using VLT/X-Shooter, and also in the optical with FORS2 at the VLT. We obtained a spectral type of M9.25 in the optical, and L1 in the near-infrared. Regarding its apparent magnitude and its spectral type, this object would be slightly below the deuterium burning mass limit if it is placed at the same distance as the primaries, with an estimated mass of 9–13 M_{Jup} considering an age between 5–10 Myr.

Despite the lack of *Gaia* astrometric data for this companion, and regarding the angular separation, we consider that this candidate is likely truly bound, being a fourth component in this system.

A.1.29 USco 161248.93−180052.5 and USco 161248.97−180049.6 (M3+M8.5).

This pair, separated by only 3″, was found by Aller et al. (2013) in their search for wide planetary mass companions in USco, using Pan-STARRS and UKIDSS data. The primary is an M3 dwarf found by Preibisch et al. (2002). For the secondary, Aller et al. (2013) obtained a spectral type of M8.5±0.5 through spectroscopic observations using SpeX spectrograph at the 3m NASA IRTF Telescope in Mauna Kea (Hawai'i). The estimated separation of the components is 430±40 AU. They estimate masses of $0.36^{+0.14}_{-0.15}$ $M_{\odot}$ for the primary, and 23^{+12}_{-6} M_{Jup} (5 Myr) or 26^{+16}_{-7} M_{Jup} (10 Myr) for the secondary.

We also identified this pair in our search. Their *Gaia* DR2 parallaxes and proper motions are also in good agreement. We confirm this system as true companions.

A.1.30 USco 16130234−2501460 and USco 161301.89−250141.3 (M2+M3)

This primary was proposed as an USco member by Luhman & Mamajek (2012). It was observed by Luhman et al. (2018) using Hydra spectrograph, they determined a spectral type of M2, and identified clear signs of youth in its spectrum.

We found the secondary placed at 8″ from the primary. This object was included in Luhman et al. (2018) as a candidate member of USco, but they did not confirm it or determine its spectral type. It was also reported as a

candidate companion in Tokovinin & Briceño (2020). We observed it using WHT/LIRIS and obtained a spectral type of M3.

The *Gaia* DR2 parallaxes and PM of the components are in good agreement with the USco association. However, there is a small discrepancy between their parallaxes. Furthermore, the *Gaia* DR2 astrometric error for the primary is unusually high for a bright object. This high error could be due to the primary being a close binary, and, in that case, its astrometry could be affected by this issue, and could be not reliable. We consider that this is most likely a truly bound system with a binary primary presenting anomalous *Gaia* astrometry.

A.1.31 USco 161336.89−232729.8, USco 161336.48−232735.3 and USco 161334.77−232815.8 (M4.5+M5.75+M5.75)

The three components in this system were discovered by Lodieu et al. (2007), and later observed spectroscopically by Lodieu et al. (2011). They obtain spectral types of M4.5, M5.75 and M5.75 for them. For the faintest objects, they also measure a moderate Hα emission of -10.2 Å and -9.7 Å for USco 161336.48−232735.3 and USco 161334.77−232815.8 respectively.

The primary's *Gaia* DR2 astrometry is in very good agreement with the USco association. USco 161336.48−232735.3 is placed at only $8''$ from it, but it does not have a proper motion nor parallax measurement in *Gaia* DR2. It is not marked either as a duplicated source. Therefore, although its close separation indicates a low probability of chance alignment, we cannot use *Gaia* DR2 data to further assess its companionship.

The faintest component, found in our search, USco 161334.77−232815.8, is placed further away from the primary, at $54''$ from it. It does have a *Gaia* DR2 measurement in both proper motion and parallax. Its astrometry is compatible with the USco association, however, there are discrepancies with the primary's proper motion and parallax. We cannot establish either the companionship with USco 161336.48−232735.3, due to its lack of *Gaia* precise proper motion and parallax. Consequently, due to the high separation of this component and the astrometric discrepancies with the primary, we consider that this object is most likely not bound to the brighter close pair.

A.1.32 USco 161340.45−223315.6 and USco 161340.26−223319.4 (M5.5+M6.5)

The primary in this candidate system was proposed as an USco candidate member by Luhman & Mamajek (2012), and was later observed by Luhman et al. (2018) using COSMOS and SpeX spectrographs. They determine a spectral type of M5.5

We found the secondary at a distance of 4″ from the primary. This object was proposed as an USco member by Luhman et al. (2018). They observed it using SpeX spectrograph and determined a spectral type of M6.5. We observed both the primary and the secondary using NTT/SofI, and we obtained spectral types of M6.5 and M7.

Both parallaxes and PM from *Gaia* DR2 of the two components are in very good agreement. We consider that this pair is most likely truly bound.

A.1.33 USco 161412.59−245428.7 and Usco 161415.73−245501.4 (M0.5+??)

The primary of this candidate system was proposed as an Usco member by Rizzuto et al. (2015). They determined a spectral type of M0.5 for it.

We found a second object placed at a distance of 54″ from this member. Its *Gaia* DR2 parallax and PM are in good agreement with the USco association. However, there are high discrepancies with the primary's astrometric data. Furthermore, none of the components show any unusually high astrometric errors for their brightness. Regarding this, we consider that these objects are not truly bound, but casual alignments among USco members.

A.1.34 USco 161452.69−230802.6 and USco 161451.31−230851.7 (M3.5+M5)

The primary in this system (also called RIK-139) was discovered by Rizzuto et al. (2015). They determined a spectral type of M3.5. Tokovinin & Briceño (2018) resolved this object into a close binary, separated by only 0.7″. The candidate wide companion, placed at 52″ from it, was included in the search for candidate members having circumstellar disks by Esplin et al. (2018). They determined a spectral type of M5 and measured some spectral features such as the lithium absorption, with a pEW of 0.6Å. They determined that this object presents a transitional disk, with an excess in WISE $w3$ and $w4$ filters.

The *Gaia* DR2 astrometry for these objects have a large discrepancy in the parallax, and also in the right ascension proper motion. However, the primary is marked as a duplicated source in *Gaia* DR2, and presents astrometric errors that are higher than expected for its brightness. This is probably due to its binarity. However, the discrepancy is significantly higher than the errors.

There is a possibility that the *Gaia* parallax and proper motion of the primary is in a greater manner affected by its binarity, but, on the other hand, the very high angular separation of the targets indicate a very high probability of chance alignment. Therefore, we conclude that this system is most likely not bound.

A.1.35 USco 161512.39−242009.3 and USco 161511.16−242015.3 (M4+M6)

This pair was found by Kraus & Hillenbrand (2009). The secondary is an M6 previously found by Slesnick et al. (2006). Then Kraus & Hillenbrand (2009) discovered the primary, placed at 18″ from it. They determined its optical spectral type using Double Spectrograph (DBSP Oke & Gunn 1982) on the 5m Hale telescope at Palomar Observatory – the same spectrograph used in the discovery of the secondary – and obtained a spectral type of M4. They estimated masses of 0.24 $M_\odot$ and 0.074 $M_\odot$ (78 M_{Jup}) for the primary and secondary, respectively.

We also identified this pair in our search. Their *Gaia* DR2 parallaxes and proper motions are also in good agreement between each other. We confirm this system as most likely true companions.

A.1.36 USco 161520.24−233358.8 and USco 161520.09−233354.5 (M4+M5.75)

These two objects were found by Lodieu et al. (2007). Their angular separation is 5″. The primary was observed by Luhman et al. (2018) using SpeX spectrograph in the NASA Infrared Telescope Facility (IRTF) on Mauna Kea; they determine an M4 spectral type. The secondary was observed by Lodieu et al. (2011) using AAT/AAOmega. They determined a spectral type of M5.75 and a mass of 0.085 $M_\odot$.

We also identified this pair in our search. Their *Gaia* DR2 parallaxes and proper motions are also in perfect agreement. We can confirm this system as true companions.

A.1.37 USco 161730.32−243839.0 and USco 161730.57−243837.3 (M0+M4)

The primary of this system was found by Rizzuto et al. (2015). They estimated a spectral type of M0 through observations using WiFeS at the Australian National University 2.3 m Telescope.

We found the secondary at an angular separation of only 4″ from it. It was also proposed as an USco candidate by Luhman et al. (2018), but they did not confirm it spectroscopically. It was reported as a candidate companion in Tokovinin & Briceño (2020). We observed it using WHT/LIRIS, and found a spectral type of M4.

Both objects have available parallax and PM measurements in *Gaia* DR2, and their values are in perfect agreement. We confirm that these objects are likely true companions.

A.1.38 USco 16181568−2347084 and USco 161811.69−234726.5 (M5.5+M6)

The primary in this system was discovered by Slesnick et al. (2008). They found a spectral type of M5.5, and estimated a mass of 0.10 $M_{\odot}$ for it.

We found the secondary at a distance of 58″ from the primary. This is one of the widest systems found in our search. This object does not have any previous reference in the literature. We observed it using WHT/LIRIS, and found a spectral type of M6.

Despite the very high angular separation of this system, their *Gaia* DR2 parallaxes and PMs are in very good agreement. Therefore, we suggest that this system is likely bound.

A.1.39 USco 161843.23−220934.5 and USco 161840.74−220948.2 (M5.5+M6)

The secondary in this candidate system is a known USco brown dwarf found by Martín et al. (2004). They estimated a spectral type of M7 and found youth features in its spectrum. Luhman et al. (2018) later estimated a spectral type of M6.

We found a brighter target at a distance of 37″ from this object. Its photometry and astrometry are compatible with the USco association. It was observed by Luhman et al. (2018) using SpeX spectrograph, and they found a spectral type of M5.5.

The *Gaia* DR2 astrometry of this pair is slightly discrepant, but compatible. The angular separation between them is moderate. Therefore, we consider that although there is a non-negligible probability that these objects may form a chance alignment between USco members, and are not real companions, they are most likely truly bound.

A.1.40 USco 161951.41−224126.8 and USco 161951.44−224133.3 (M5.5+M6.75)

The primary of this system was identified by Cody et al. (2017) as an USco candidate, they also report that it has periodic bursts, with a periodicity of 6.9 days. It was later observed spectroscopically by Esplin et al. (2018) using SpeX spectrograph, and they find a spectral type of M5.5 and clear youth features. The secondary was discovered earlier, by Luhman & Mamajek (2012). Luhman et al. (2018) observed it using SpeX spectrograph and found a spectral type of M6.75, and clear youth features too. Their separation is 7″.

We also observed the primary using WHT/LIRIS, and found a spectral type of M7.

Their *Gaia* parallaxes and proper motion are compatible, although the errors of the secondary's astrometry are quite high due to its faintness. Taking

into account this, and their short separation, we consider that this pair is most likely truly bound.

A.1.41 USco 162050.23−223538.79 and USco 162049.26−223513.3 (A9+M5.5)

The primary, also called HD 147137, is a well known USco member (de Zeeuw et al. 1999), with a spectral type of A9.

We discovered the secondary placed at 29″ from the primary. This object was also identified as an USco member by Luhman et al. (2018), they determined a spectral type of M5.5 in the optical. We observed it using NTT/SofI and obtained a spectral type of M7 in the near-infrared.

The *Gaia* DR2 parallax and PM of both components in this candidate system are in agreement with the USco association, and also between each other. We consider that this pair is most likely truly bound.

A.1.42 USco 1621−2529 and USco 1621−2529 B (M2.5+M8.5)

This system was published in Chinchilla et al. (2020b). The details can be found in the attached paper in Chapter 4.

A.1.43 USco 162357.24−262024.5 and USco 162401.19−262036.0

The primary in this system is a M4.5 USco member found by Rizzuto et al. (2015).

The candidate secondary is placed at a distance of 54″, which is one of the widest candidate systems found in this work. This object was proposed as a candidate member of USco by Lodieu (2013) and also by Luhman et al. (2018), but they did not determine its spectral type. We observed it using NTT/SofI, and we found a spectral type of M7.

Gaia DR2 does not provide a parallax nor PM for the primary, and it indicates that it is a duplicated source. The secondary has a parallax and PM measurement, which is in agreement with the USco association. Due to the high separation of these objects, and the lack of precise *Gaia* astrometric data to determine if they are really placed at the same heliocentric distance, we consider that these objects are most likely not bound.

A.1.44 USco 162359.02−273603.8 and USco 162358.53−273552.9 (M3.5+?)

The primary of this system is an M3.5 USco member found by Rizzuto et al. (2015). Tokovinin & Briceño (2018) discovered that this object is in fact a tight

triple system, with the B and C components forming a close pair separated by only 0.14″ that orbits the central primary star at a separation of 0.44″.

We found an additional companion placed at 13″ from the "triple primary". This object was proposed as a candidate USco member by Lodieu (2013) and also by Luhman et al. (2018), but they did not determine its spectral type.

The primary of this system does not have a parallax and PM measurement in *Gaia* DR2, due to its multiplicity. The secondary has parallax and PM measurements, but its astrometric errors are high. This could be due to binarity, or to the faintness of the source. Its parallactic measurement places it at almost 300 pc distance, which would compromise its USco membership, but this measurement has a very large error. However, its PM is in good agreement with the USco association. Regarding the close separation, we consider that this system is most likely truly bound.

A.1.45 USco 162415.52−254434.5 and USco 162416.15−254427.3 (M0+?)

The primary of this system was discovered by Rizzuto et al. (2015). They found a spectral type for it of M0.

The secondary is an USco candidate member proposed by Lodieu (2013), and also by Luhman et al. (2018), but they did not determine its spectral type. The separation between the components is 11″. This object was also reported as a candidate companion in Tokovinin & Briceño (2020).

The *Gaia* DR2 data for both objects is in good agreement with the USco association, but it is discrepant with each other. However, the errors in the measurements of the secondary are very high due to its faintness, and the primary is flagged as a duplicated source, and hence its parallax may not be correct. Regarding this, and the short angular separation, we consider that this system is most likely truly bound.

A.1.46 USco 162557.91−260037.5 and USco 162602.36−260036.4

The primary in this candidate system was identified as an USco member by Rizzuto et al. (2015), with a spectral type of G8. It was discovered to be an eclipsing binary by David et al. (2016), composed by a 1.4 $M_\odot$ primary and a 0.84 $M_\odot$ (likely mid-K or early-M type) secondary.

We found the secondary placed at a separation of almost 60″ from the primary. This object has not been proposed as a candidate member in the literature. We observed this object using NTT/SofI and obtained a spectral type of M6.

The secondary has a *Gaia* DR2 parallax and PM compatible with belonging to the USco association. The parallax is also in good agreement with the primary. However, the *Gaia* PM is highly discrepant. We do not expect the binarity of the primary to affect its astrometry, as the components are too close to each other. Regarding this and the high separation of this system, we suspect that these objects are not truly bound.

A.1.47 USco 162712.74−250401.8 and USco 162715.86−250404.7

The primary in this system is an M1 USco member discovered by Rizzuto et al. (2015).

We found the secondary at a separation of 43″. This object was also found as an USco candidate member by Luhman et al. (2018), but they did not determine its spectral type. We observed it using NTT/SofI and found a spectral type of M5.5.

The *Gaia* parallax and PM astrometry for both objects is in good agreement with the USco association. However, they are discrepant with each other, and their astrometric errors are not unusually high. Therefore, we consider that these objects form a casual alignment and are not true companions.

A.1.48 USco 163334.96−183254.0 and USco 163334.73−183254.8 (M3.5+M6)

The primary of this system was found by Rizzuto et al. (2015), they obtained a spectral type of M3.5 and found youth features in its spectrum.

We found the companion candidate placed at only 3″ from this primary. This object was reported as a candidate companion in Tokovinin & Briceño (2020). We observed both components using NTT/SofI, and found spectral types of M3 and M6 for them.

The *Gaia* DR2 parallaxes and PM of the components are in very good agreement, with low astrometric errors. Therefore, we conclude that this system is most likely truly bound.

A.2 Finding charts of the USco systems

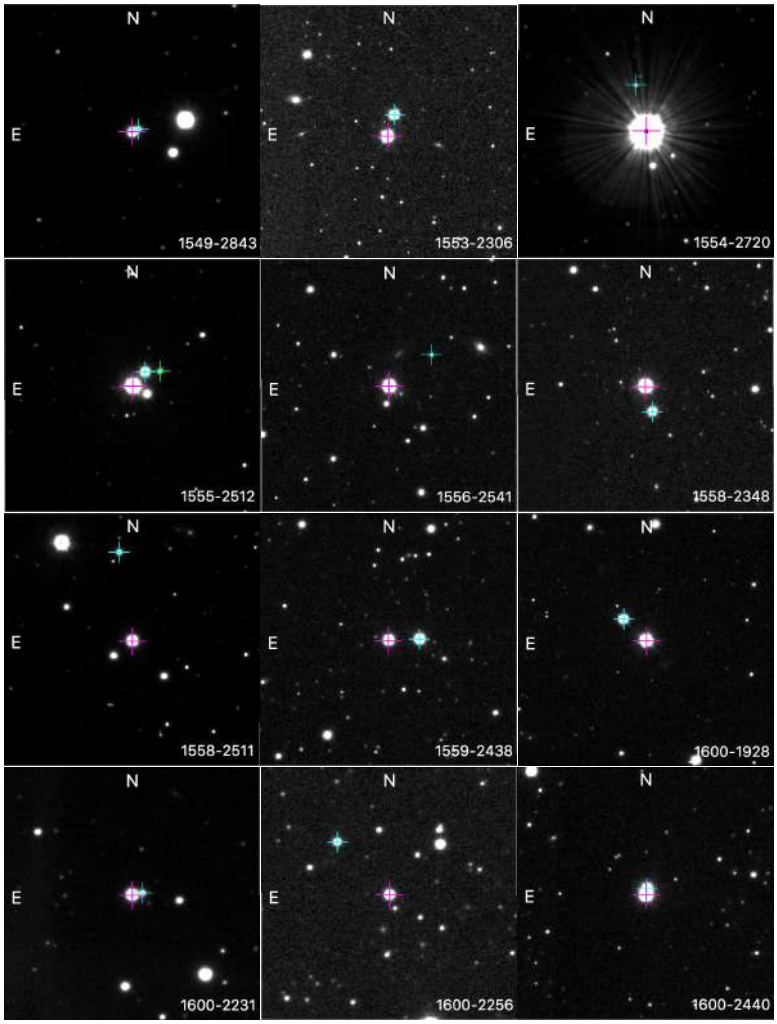

Figure A.1: VHS J-band finding charts of the candidate systems. Primaries and candidate companions are marked with coloured crosses. The orientation is North up and East to the left. The field of view is $2' \times 2'$.

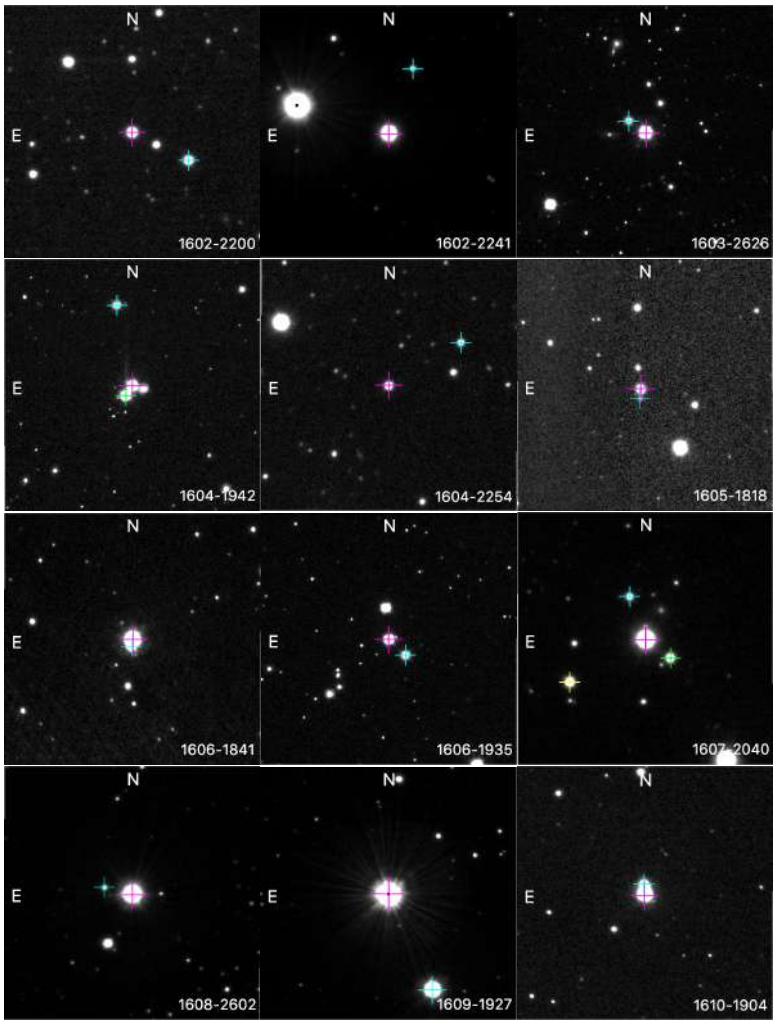

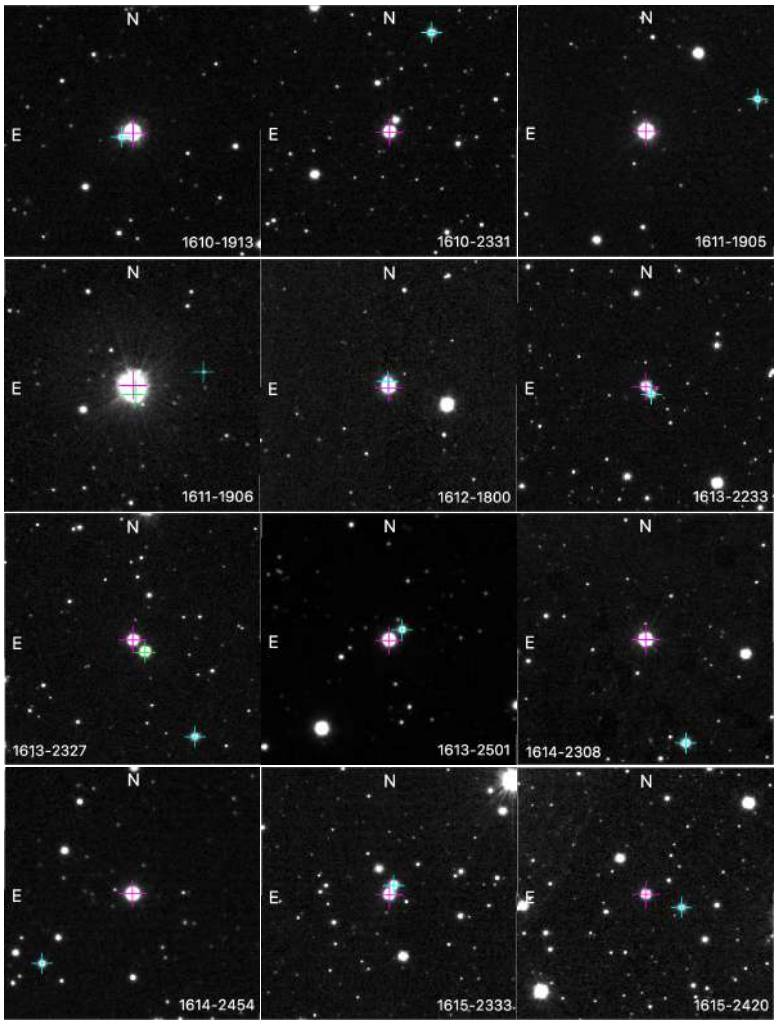

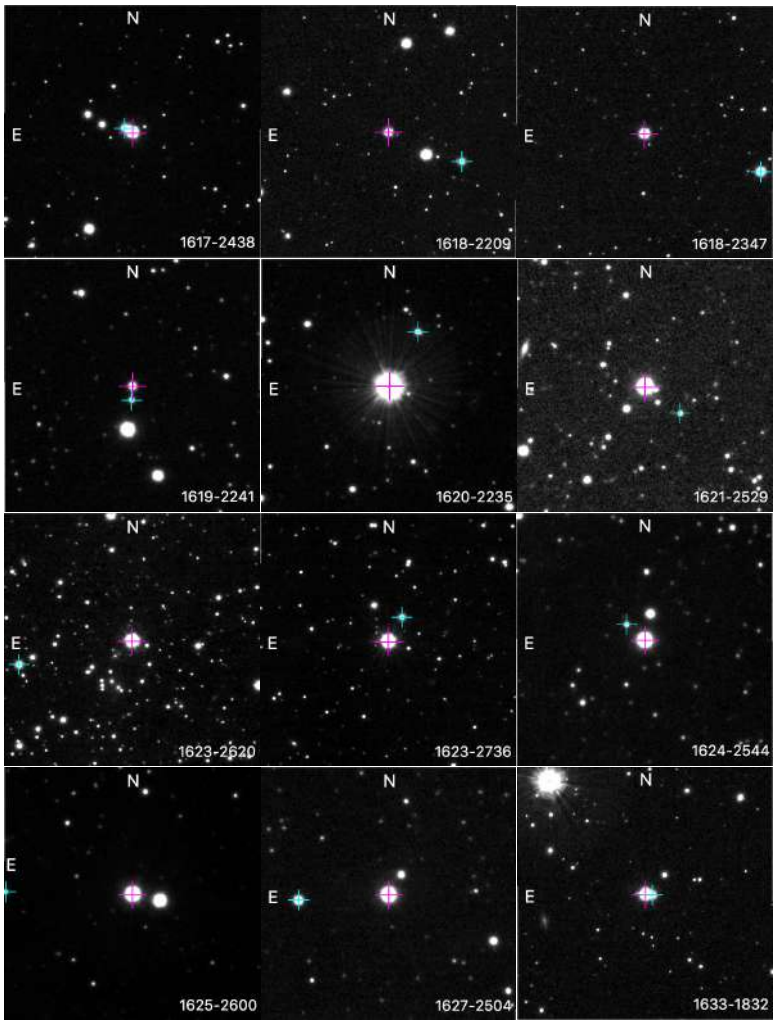

B

Appendix B

B.1 Details on the individual AB Dor candidate systems

B.1.0.1 ABD 049 and ABD 050

The primary in this candidate system (ABD 050) is called CD-46 644. Torres et al. (2006) determined a spectral type of K3 for it. It has been claimed as an AB Dor and THA member in the literature. It was proposed as an Horologium member by Torres et al. (2000). Kraus et al. (2014) also confirmed it as a THA member, and Bell et al. (2015) included it as a THA member. However, Torres et al. (2008) included it as a high probability AB Dor member, estimating a 70% probability of belonging to this YMG. McCarthy & White (2012) and Elliott et al. (2016) also proposed it as an AB Dor member. Recently, Binks et al. (2020) used the BANYANΣ code and determined that the most likely YMG for this object is AB Dor.

We found the secondary placed at only 21″ from the primary. It is also a compiled candidate member to AB Dor. Its name is UCAC2 11911537. This object was proposed as a candidate companion to the primary by Torres et al. (2008). It was proposed as an AB Dor member by McCarthy & White (2012) and also by Elliott et al. (2016), but it does not have a spectral type measurement in the literature. The *Gaia* DR2 astrometric error of the secondary is too high for its brightness, although it is not marked as a duplicated source.

We obtained near-infrared spectroscopy of the primary and secondary using NTT/SofI, and obtained a spectral type of late-K for the primary, and M5 for the secondary.

B.1.0.2 ABD 072c

The primary in this system is called 2MASS J02545247−0709255. It is a spectroscopic binary, with an orbital period of 12 days (Torres et al. 2002), and a luminosity ratio of L_B/L_A=0.19. Its spectral type is M3 (Neuhaeuser et al. 1997). We found the candidate companion at a separation of only 4″. This companion was also reported by Torres et al. (2002) as a visual binary. Hence, this system is in fact triple.

Both the primary and companion have entries in the *Gaia* DR2 catalogue. Their *Gaia* parallaxes are in perfect agreement, although their PMs have slight discrepancies.

We observed the primary and the candidate companion both in the optical and the near-infrared, using NOT/ALFOSC and NTT/SofI, respectively. We obtained spectral types of M3 and M5 in the optical, and M4 and M5.5 in the NIR.

B.1.0.3 ABD 080c

The catalogued member in this system is a high proper motion star. Its name is LP 772-14. It is placed at only 24 pc according to its *Gaia* DR parallax. It was proposed as an AB Dor candidate member by Gagné et al. (2015b), with a membership probability of only 27%. Therefore, the membership of this catalogued object is dubious. They estimated an expected spectral type of ∼M5.7 from its photometry.

We found a candidate companion, which is brighter than the compiled member, placed at 15″ from this object. The candidate companion is also known as LP 772-15. This companion candidate was previously known in the literature, with an estimated expected spectral type of ∼M2.2 (Luyten & Hughes 1980; Gagné et al. 2015b). The *Gaia* DR2 astrometry of both objects is in very good agreement, both in PM and parallax.

We observed both the primary and the candidate companion in the optical, using NOT/ALFOSC, and obtained spectral types of M3 and M5 for them.

B.1.0.4 ABD 134c2

The primary in this system is HD 293857, a G0 star proposed as an AB Dor member by Torres et al. (2008). We found a candidate companion placed at a distance of 3.6′ from it. The candidate companion was proposed as an AB Dor member by Elliott et al. (2016), but it does not have a spectral type measurement in the literature. We expect a spectral type of ∼M2.5. Both

objects have an estimated heliocentric distance of 76.9 pc (Elliott et al. 2016), which corresponds to an estimated physical separation of ∼17 000 AU.

The companion does not have an entry in *Gaia* DR2 despite being bright enough for *Gaia* to detect it. The primary does have an entry in *Gaia*, but does not have a parallax and PM measurement, and is marked as a duplicated source. Both objects have an entry in the PPMXL catalogue, and their PMs are in good agreement.

B.1.0.5 ABD 168, ABD 510 and ABD 511

The primary in this system is called BD-13 1328, and it is a K4 star, proposed as an AB Dor member by Torres et al. (2008). It is placed at a heliocentric distance of 45 pc according to its *Gaia* DR2 parallax. We found two candidate companions to this primary. One of them (ABD 510) is placed at only 19″ from the primary, which corresponds to a projected physical separation of 900 AU. The other one (ABD 511) is placed at 1.8′, which corresponds to 4900 AU. Both candidates were included as AB Dor candidate members in Gagné & Faherty (2018), with estimated spectral types from their photometry of ∼M5 and ∼M6, respectively. They also identified the objects as candidate companions to BD-13 1328 using *Gaia* DR2 astrometry.

The *Gaia* parallaxes and PMs of the three components in this candidate system are in good agreement.

We acquired optical spectroscopy of ABD 511 using NOT/ALFOSC, and optical spectroscopy of ABD 510 using DuPont/B&C. We also obtained near-infrared spectroscopy of ABD 168, ABD 510 and ABD 511 using NTT/SofI. We obtained spectral types of M5 and M6.5 in the optical for ABD 510 and ABD 511 respectively, confirming the expected spectral types in Gagné & Faherty (2018). In the NIR, we obtained spectral types of M0, M6 and M6.5 for the three components.

B.1.0.6 ABD 548c

The compiled member in this system was proposed as an AB Dor member by Gagné & Faherty (2018). It is visually double in 2MASS, but it has only one entry in this catalogue. Gaia detects two objects, one of them has a parallax that corresponds to a distance of 63 pc, and the other one has a parallax that places it at ∼3 kpc, and, hence, would not be a part of the system. We found a brighter object placed at only 22″ from this AB Dor member.

The companion candidate (candidate to primary) has an entry in *Gaia* DR2, but does not have a parallax and PM measurement. It is neither marked

as a duplicated source. If it is placed at the same heliocentric distance as the AB Dor member, we would expect a spectral type of late-K. Its $G-J$ colour indicates a spectral type of ∼M4, which is not in good agreement with the expected, and it would indicate that this object is placed much closer in our line of sight. However, its PPMXL proper motion is in perfect agreement with the *Gaia* PM of the compiled member.

The fainter compiled member has an expected spectral type of ∼M3.5, according to its brightness and its parallax. Its $G-J$ colour indicates a slightly later spectral type, of ∼M4.5.

We observed both the primary and the candidate in the optical using DuPont/B&C, and in the near-infrared using NTT/SofI. We obtained a spectral type of M3 and M4.5 in the optical for the brightest and faintest object, respectively, and a spectral type of M4 in the near-infrared for the faintest. According to the difference in magnitude of these objects, this implies that the brightest M3 candidate companion could be placed at the same heliocentric distance as the faint one if it is formed by an equal-mass binary of M3+M3.

B.1.0.7 ABD 556 and ABD 557

The two components in this candidate system were proposed as AB Dor candidate members in Gagné & Faherty (2018), using *Gaia* DR2 astrometry and photometry. They are placed at a heliocentric distance of 58 pc, and they have a separation of 20″, which corresponds to a projected physical separation of 1200 AU. Gagné & Faherty (2018) estimated an expected spectral type of ∼M4 for both from their photometry, and proposed them as candidate companions regarding their PM and parallax.

The *Gaia* DR2 astrometry of the components is in very good agreement with each other.

We acquired optical spectroscopy of both components using DuPont/B&C, and obtained spectral types of M4 for both of them, confirming the expected spectral types predicted by Gagné & Faherty (2018).

B.1.0.8 ABD 559 and ABD 560

The primary in this system is also known as UCAC4 231-078764. The two components in this candidate system were proposed as AB Dor candidate members by Gagné & Faherty (2018). They are placed at a heliocentric distance of only 29 pc. The separation between them is only 4″, which corresponds to a projected physical separation of 120 AU. Gagné & Faherty (2018) estimated a spectral type of ∼M5 for both according to their photometry.

The *Gaia* DR2 PM and parallax of the components is in very good agreement, although with slight discrepancies. However, although none of them is marked as a duplicated source, the primary has slightly high errors for an object of its brightness. This could be due to the proximity of the companion.

We acquired optical spectroscopy of both components using DuPont/B&C, and obtained spectral types of M5 and M7 for them.

B.1.0.9 ABD 569c

The primary in this system was proposed as an AB Dor candidate member by Gagné & Faherty (2018). They estimated a spectral type of ∼M4 from its photometry. Its parallax indicates a heliocentric distance of 59 pc. We found a candidate companion placed at a distance of 11′ from it, which corresponds to a projected physical separation of 38 300 AU at the distance of the primary.

The candidate companion is detected in *Gaia* DR2, but does not have a complete 5-parameter astrometric solution. According to its brightness, if it is placed at the same heliocentric distance as the primary we would expect a spectral type of ∼M6. Its $G-J$ colour indicates a spectral type of ∼M5–M5.5. The candidate companion has two PM measurements in the PPMXL catalogue. Both of them have significant discrepancies in the pmdec value, compromising their companionship.

We observed both the primary and the candidate companion using DuPont/B&C, and obtained spectral types of M4 and M5, which is a very small difference in spectral type considering a difference in J magnitude of more than 3 mag. We consider that these objects are most likely a casual alignment.

B.1.0.10 ABD 316c

The primary in this system is also known as HD 176367. It is a G1 star, proposed as an AB Dor member by Torres et al. (2008). According to its *Gaia* DR2 parallax, it is placed at a heliocentric distance of 65 pc. We found a candidate companion at an angular separation of 12′, which corresponds to 47 100 AU for the heliocentric distance of the primary.

The *Gaia* DR2 parallaxes and proper motions of the components are similar but have some discrepancies. Their astrometric errors are not very high either, and they are not marked as duplicated sources.

We observed the candidate companion in the near-infrared using NTT/SofI, and obtained a spectral type of late-K.

B.1.0.11 ABD 587c

The compiled member in this system was proposed as an AB Dor candidate member by Gagné & Faherty (2018). It has only one entry in the 2MASS catalogue, but it is visually elongated in the images. It has two entries in *Gaia* DR2, with similar brightness, which are compatible in parallax and PM and are separated 2.7″. According to the parallax, they are placed at a heliocentric distance of 62 pc, which implies a separation of 170 AU for the two components. Using the fluxes in the *Gaia* G band, we estimate a luminosity relation of $L_B/L_A \approx 0.82$. We found a companion candidate placed at a wider distance of 10.4′ from this pair, which corresponds to a projected physical separation of 38 600 AU.

The companion has an entry in *Gaia* DR2, but does not have a parallax and PM measurement. It is not marked as a duplicated source either. According to its brightness, we expect a spectral type of ∼M3 if it is placed at the same heliocentric distance as the binary catalogued member. Its $G - J$ colour also indicates a spectral type of ∼M2.5–M3. It has a proper motion measurement in the PPMXL catalogue which is in agreement with the *Gaia* PM of the binary member, within its errors.

Considering that the compiled member is resolved by *Gaia* but not by 2MASS, and that the two components have similar brightness according to *Gaia*, their $G - J$ colours indicate a spectral type of ∼M4+M4. This would imply two objects with lower masses than the companion candidate, and hence the companion candidate would be the primary of the system.

We obtained optical spectroscopy of the three components of this candidate system using DuPont/B&C, and obtained spectral types of M6+M6 for the binary, and M3 for the companion candidate, confirming that the wide companion candidate is in fact the primary in the system.

B.1.0.12 ABD 344c

The primary in this system is also known as 2MASS J21471964−4803166, its spectral type is M4 (Riaz et al. 2006). It was first proposed as a THA member by Malo et al. (2013). Later, Malo et al. (2014) gave a membership probability of 98.2% to the AB Dor moving group. Bell et al. (2015) also included it as a bona fide AB Dor member. It is placed at a heliocentric distance of 63 pc according to its *Gaia* DR2 parallax.

We found a companion candidate at an angular separation of 53″ from this primary, which corresponds to a projected angular separation of 3400 AU. This candidate companion was also reported by Schneider et al. (2019). The *Gaia*

DR2 astrometry of both components is in very good agreement between each other.

We obtained optical spectroscopy of the candidate companion using DuPont/B&C, and near-infrared spectroscopy using NTT/SofI. We obtained spectral types of M6 in the optical, and M5 in the NIR.

B.1.0.13 ABD 374 and ABD 375

The primary in this candidate system is also known as HD 218860. It is a G8 star, included as an AB Dor bona fide member in Zuckerman et al. (2004). It is placed at a heliocentric distance of 48 pc according to *Gaia* DR2. We found a candidate companion placed at a distance of 20″, which corresponds to a projected physical separation of 940 AU. This object is already known as a companion, and it is known as HD 218860B. It has a spectral type of M3 (Torres et al. 2006).

The *Gaia* DR2 astrometry of both components in this system is in good agreement. The astrometric error of the secondary is unusually high for its brightness, and it is marked as a duplicated source.

B.2 Details on the individual β Pic candidate systems

B.2.0.1 bP 035 and bP 036

The primary in this system is the star Ex Cet. Its spectral type has been classified as G5 (Cannon & Pickering 1993), G9 (Gray et al. 2003) and K0/1 (Houk & Swift 1999). It is placed at a heliocentric distance of 24 pc according to its *Gaia* DR2 parallax. Although previous references proposed it as an Hercules-Lyra member, it was proposed as a β Pic candidate member by Elliott et al. (2016). Gagné & Faherty (2018) also reclassified this object from Hercules-Lyra member to β Pic member.

The companion candidate is known as Ex Cet B. It is placed at an angular separation of 10′ from the primary, corresponding to a projected physical separation of 14 700 AU. It was identified as a wide common proper motion companion by Alonso-Floriano et al. (2011) and Alonso-Floriano et al. (2015). Its spectral type is M3.5 (Shkolnik et al. 2009).

The *Gaia* DR2 astrometry of these two objects is in very good agreement with each other.

B.2.0.2 bP 040 and bP 041

The two components in this candidate system were proposed as a β Pic candidate members by Schlieder et al. (2010). They were identified as proper motion candidate companions by Alonso-Floriano et al. (2015). Their heliocentric distance is 50 pc according to their *Gaia* DR2 parallax. Their separation is 10″, corresponding to a projected physical separation of 520 AU. They do not have an available spectral type estimation in the literature. Their *Gaia* DR2 astrometry is in very good agreement with each other.

We obtained optical spectroscopy of the two components in this system using NOT/ALFOSC. We obtained spectral types of M3 and M3.5 for them. These objects did not have available VHS data in the complete sky circular area with a radius of 50 000 AU around them, and were searched up to only ∼27 000 AU. Therefore, we report them here as candidate companions, but they are not included in the companion statistics.

B.2.0.3 bP 060 and bP 061

The primary in this system is the A1 star s Eri, also known as HIP 12413. It was proposed as a Columba member by Zuckerman et al. (2011). Later, Malo et al. (2013) obtained a membership probability of 96% to β Pic for it, but indicated that its astrometry fits in both associations. Bell et al. (2015) also included it as a bona fide β Pic member. Its heliocentric distance is 40 pc, according to its *Gaia* DR2 parallax. This object is in fact a tight unresolved binary (named HIP 12413 AB) with a third component (HIP 12413 C) placed at an angular separation of 26″, which corresponds to a physical projected separation of 1000 AU.

We found an additional wide companion in this system at an angular separation of 11′ from the primary. This object, also known as 2MASS J02404759−4253377 (now HIP 12413 D), was proposed as a THA candidate member by Gagné et al. (2015b), they assign a membership probability of 99.4% to this association. Later, Gagné et al. (2015c) obtained a spectral type of M6, and found signs of a low gravity for it. They assigned an estimated age of 20–40 Myr.

According to *Gaia* DR2, this wider companion is astrometrically in good agreement with HIP 12413 ABC. All the objects have similar parallaxes and proper motions. The primary has a slightly discrepant proper motion, but its astrometric errors are higher than expected for its brightness, and it is also marked as a duplicated source, so its *Gaia* DR2 astrometry may be affected by its binarity.

The component HIP 12413 C did not have a spectral type measurement

in the literature, so we observed it in the optical and the near-infrared, using DuPont/B&C and NTT/SofI, respectively, we obtained a spectral type of M5 in the optical, and M5.5 in the NIR.

B.2.0.4 bP066c (2MASS J0249 c)

The name of the catalogued member in this system is 2MASS J0249−0557. The details of this system can be found in the attached article in Chapter 6. This catalogued member did not have available VHS data in the complete sky circular area with radius 50 000 AU around it, but only up to a radius of ∼29 800 AU. Therefore, this candidate companion is reported here, but was not considered in the companion frequency statistics.

B.2.0.5 bP 141c

The primary in this candidate system is known as L 186-67. It is an M4.5 star (Riaz et al. 2006) with a very high proper motion. It is placed at a distance of 13 pc according to its *Gaia* DR2 parallax. It was proposed as an ambiguous candidate of either β Pic or AB Dor by Malo et al. (2013), and later it was proposed as a β Pic member by Malo et al. (2014), with a membership probability of 91.9%.

We found a candidate companion at only 9″from the primary, which translates into a projected physical separation of 112 AU. This system was presented in Alonso-Floriano et al. (2015) as a bound system, but they did not determine the spectral type of the companion. The *Gaia* DR2 astrometry of the two components is in very good agreement.

We observed both the primary and the candidate companion in the optical and the near-infrared, using DuPont/B&C and NTT/SofI, and obtained spectral types of M5.5 and M7 in the optical, and M5.5 and M6 in the NIR.

B.2.0.6 bP 314 and bP 315

Both components in this system were proposed as β Pic candidate members by Gagné & Faherty (2018). They assigned an expected spectral type of ∼M4 and ∼M5 for them. They are placed at a heliocentric distance of 41 pc, according to their *Gaia* DR2 parallaxes. Their angular separation is 13″, corresponding to a projected physical separation of 520 AU. Gagné & Faherty (2018) also identified these objects as a comoving pair. The *Gaia* astrometry of the components is in very good agreement with each other.

We observed both components in the optical and the near-infrared, using DuPont/B&C and NTT/SofI, and obtained spectral types of M5 and M6.5 in

the optical, and M6 and M7 in the NIR. These spectral types make this system incredibly interesting, as a precise measurement of their lithium absorptions would give a precise constraint on their age.

B.2.0.7 bP 171 and bP 172

The primary in this candidate system is known as HD 155555, or V824 Ara. It is a short period spectroscopic binary, with a G5+K0 spectral type (Bennett et al. 1962; Barstow 1987). It is placed at a heliocentric distance of 31 pc, according to its *Gaia* DR2 parallax. It was proposed as a β Pic candidate member by Zuckerman et al. (2001a).

The candidate companion is known as HD 155555C, or V824 Ara C. It is placed at an angular separation of $34''$ from the binary primary, which corresponds to a projected physical separation of 1000 AU. Its spectral type is M3 (Torres et al. 2006). The *Gaia* DR2 astrometry of this object is in good agreement with the primary, although there is a small discrepancy in the PM.

B.2.0.8 bP 191c

The primary in this candidate system is known as 2MASS J18420694-5554254. It is an M3 star (Riedel et al. 2017), proposed as a β Pic candidate member by Malo et al. (2013). It is placed at a heliocentric distance of 51 pc according to its *Gaia* DR2 parallax. The candidate companion is placed at $22''$, which corresponds to a projected physical separation of 1100 AU. Its spectral type is M4.5 (Riaz et al. 2006). This pair was proposed as a wide binary by Alonso-Floriano et al. (2015). The *Gaia* DR2 astrometry of both components is in very good agreement with each other.

B.2.0.9 bP 195 + bP 197

The primary in this candidate system is known as HD 173167. It is an F5 star (Houk & Cowley 1975), proposed as a candidate member of β Pic by Moór et al. (2013). It is placed at a heliocentric distance of 51 pc, according to its *Gaia* DR2 parallax.

The candidate companion is placed at an angular separation of $9'$, which corresponds to a projected physical separation of 27 800 AU. Its spectral type is M1 (Torres et al. 2006). It was originally identified as a companion by Alonso-Floriano et al. (2011), Alonso-Floriano et al. (2015). Its *Gaia* DR2 parallax and PM are in perfect agreement with the primary.

B.2.0.10 bP 208c

The primary in this system is known as UCAC4 178-222889. It was included as a β Pic candidate member in Elliott et al. (2016), but they did not obtain its spectral type. It is placed at a heliocentric distance of 128 pc according to *Gaia* DR2, which is not in good agreement with the association. Therefore, we consider that this catalogued candidate member is a dubious member to the association. We found a candidate companion placed at an angular separation of $4''$. Its *Gaia* DR2 astrometry is in very good agreement with the primary.

We obtained optical and near-infrared spectroscopy of both the primary and the companion using DuPont/B&C and NTT/SofI, and obtained spectral types of M2 and M3 respectively for the primary and secondary in the optical, and M3 for both components in the NIR.

B.2.0.11 bP 221 + bP 222

The primary in this candidate system is known as TYC 7443-1102-1. It is a K9 star (Pecaut & Mamajek 2013), identified as a β Pic candidate member by Lépine & Simon (2009). It is placed at a heliocentric distance of 51 pc according to its *Gaia* DR2 parallax.

The candidate companion is placed at an angular separation of $26''$, which corresponds to a projected physical separation of 1300 AU. It was identified as a β Pic candidate member, and as a proper motion companion to the primary by Lépine & Simon (2009). The *Gaia* DR2 astrometry of the two components are in good agreement with each other. The companion has unusually high astrometric errors for its brightness, although it is not marked as a duplicated source.

B.2.0.12 bP 251 + bP252

This pair is formed by the objects 2MASS J21103147−2710578 and 2MASS J21103096−2710513. They were proposed as β Pic candidate members by Malo et al. (2013), both with a 99.9% of membership probability. They are placed at a heliocentric distance of 40 pc according to their *Gaia* DR2 parallaxes, and they are separated $9''$, corresponding to a projected physical separation of 380 AU. This pair was proposed as candidate companions by Alonso-Floriano et al. (2015). Their spectral types are M4.5 and M5 (Riaz et al. 2006). Their *Gaia* DR2 PM and parallax are in very good agreement with each other.

B.2.0.13 bP 257c, bP 257c2

The primary in this system is called TYC 9486-927-1. Its *Gaia* DR2 parallax indicates a heliocentric distance of 34 pc. It was discovered to be a young star by Torres et al. (2006). They determined a spectral type of M1 for it. However, Deacon et al. (2016) later classified this object as an M2. Elliott et al. (2014) proposed it as a Carina Association member. However, Messina et al. (2017) included it in their study as a Beta Pic member. We found two candidate companions to this primary.

The faintest candidate, placed at 3.6′ from the primary, was reported as a wide companion by Deacon et al. (2016). It is an L3 object, formerly proposed as a THA candidate member by Gagné et al. (2014). However, Deacon et al. (2016) suggest that the lithium content of the primary indicates an age range of 10–45 Myr, and that the kinematics of both objects are closer to the Beta Pic moving group, although they do not fit perfectly. They estimated a mass of 11.6–15 M_{Jup} for the companion, and a separation of ∼6900 AU. Its *Gaia* DR2 PM and parallax are in perfect agreement with the primary, and this more recent parallax indicates a projected physical separation of 7400 AU.

The brightest candidate is placed at a higher separation of 15′ from the primary. It was proposed as a THA candidate member by Gagné et al. (2015b), although with a membership probability of only 35.7%, and an estimated spectral type of ∼M4.1 from its photometry. Its *Gaia* PM and parallax are in very good agreement with the primary and the faintest candidate. The projected physical separation considering this parallax is 31 200 AU. This object did not have a measured spectral type in the literature, so we observed it in the near-infrared, using NTT/SofI, and obtained a spectral type of M6.5.

There is an additional candidate companion in this system. It is known as 2MASS J21121598-8128452. This object was proposed as a THA candidate member by Gagné et al. (2015b), although with a membership probability of only 40.4%. It was observed by Gagné et al. (2015c), they obtained a spectral type of M5.5 and signs of having an intermediate gravity (β). It is placed at an angular separation from the primary of 31′, corresponding to a projected physical separation of >63 000 AU. It would also have a high separation of >70 000 AU to the L3 candidate companion. However, it would be placed at a separation of 35 200 from the bright candidate companion. Its *Gaia* DR2 astrometry is also in very good agreement with the other three objects. We observed this object in the NIR using NTT/SofI, and obtained a spectral type of M5.5.

B.2.0.14 bP264c

The catalogued member in this system (secondary) is also known as 2MASS J21551741−0045478. It is an M4.5 star (Riaz et al. 2006), proposed as a β Pic candidate member by Malo et al. (2013), with a membership probability of 95.9%. The primary in the system was also found as a companion candidate by Alonso-Floriano et al. (2015). It is also known as 2MASS J21551738−0046231. The *Gaia* DR2 astrometry of both components is in very good agreement with each other.

We obtained near-infrared spectroscopy of the candidate primary using NTT/SofI, and obtained a spectral type of M5 in the NIR. We also obtained optical spectroscopy of both components using NOT/ALFOSC, and obtained spectral types of M5 for both in the optical.

B.2.0.15 bP288c

The primary in this system was proposed as a β Pic candidate member by Gagné et al. (2015c), with a membership probability to the YMG of only 34.1%. Therefore, the membership of this candidate member is dubious. They did not obtain its spectral type through spectroscopy, but they estimated an expected spectral type of ∼M4 through its photometry.

Both the primary and the candidate companion have an entry in the *Gaia* DR2 catalogue, but do not have a parallax or PM measurement. The primary is marked as a duplicated source, and the candidate is marked as single source.

The two objects have similar proper motions according to the PPMXL catalogue, but they are discrepant in declination: (101.6, −74.1)±(5.4, 5.4) mas yr^{-1} for the primary, and (98.8, −115.9)±(4.1, 4.1) mas yr^{-1} for the companion.

The colours of these two objects in Pan-STARRS and SDSS are very similar, and they indicate a spectral type of ∼M5 for both the primary and the companion candidate. Considering that they have a difference in magnitude of ∼2 mag in the J-band, we would expect a later spectral type and redder colours for the candidate companion, even in the case that the primary is a close binary. Therefore, these colours may indicate that the candidate companion is a ∼M5 object which is placed a bit further away from our point of view than the primary.

B.3 Details on the individual THA candidate systems

B.3.0.1 THA 023c

The primary of this system is known as UCAC4 137-000439. It was proposed as a candidate member of THA by Kraus et al. (2014), they assigned a spectral type of M2.2 to it. It was discovered to be a close nearly equal-mass binary, with a separation of 0.1″, and masses of 0.54 and 0.49 $M_\odot$ (Janson et al. 2017; Shan et al. 2017). It has a third component placed at 4.6″, which we identified in this search. The system is placed at a heliocentric distance of 44 pc, which implies a separation of 4.4 AU for the close binary, and 200 AU for the wider companion.

The *Gaia* DR2 astrometry of the companion is in very good agreement with the primary. The astrometric errors of the binary primary are very high for its brightness, likely due to its binarity, although it is not marked as a duplicated source in *Gaia*.

We observed the primary and the candidate companion using NTT/SofI, and obtained a spectral type of M3 and M5 for them.

B.3.0.2 THA 051c

The primary in this system is a candidate member proposed by Torres et al. (2000). They estimated a spectral type of K1. It is placed at a heliocentric distance of 65 pc according to its *Gaia* DR2 parallax. Nevertheless, the membership of this object to the THA association is ambiguous, and the BANYAN Σ online tool gives a high probability of belonging to the field (66%), and a low probability of membership to the Carina Near association (33.9%).

We found a candidate companion at a separation of 3′, which at the distance of the primary translates into a physical projected separation of 11 700 AU. The expected spectral type for this object is late-K. This candidate companion does not have an entry in the *Gaia* DR2 catalogue, despite being bright enough for *Gaia* to detect it. It does have an entry in the *Gaia* DR1 catalogue, and its $G - J$ colour is in good agreement with a late-K spectral type. Regarding its proper motion, it has an entry in the PPMXL catalogue, and it indicates a proper motion of (73.1, 10.0)±(10.1,10.1) mas yr^{-1}, which is compatible with the *Gaia* measurement for the primary's PM, within its errors.

B.3.0.3 THA 359c

The primary in this candidate system was proposed as a candidate THA member by Gagné & Faherty (2018). According to its *Gaia* DR2 parallax, it is

placed at a heliocentric distance of 43 pc. Gagné & Faherty (2018) estimated an expected spectral type of ∼M5 from its photometry and parallax.

We found a very faint candidate companion, placed at a distance of 5′ from the primary. At the heliocentric distance of the primary, this would imply a projected physical separation of 13 300 AU. This object is too faint for *Gaia* DR2 to detect it. According to its magnitude, if it is placed at the same distance, we would expect a spectral type of ∼L6. It is detected by Spitzer, and its [3.6-4.5] colour is compatible with an ∼L1–L7 spectral type. However, its $J - w1$, $J - w2$ and $Ks - w1$ colours indicate a spectral type of around ∼L0–L2.

B.3.0.4 THA 099c

The primary in this candidate system is known as UCAC3 92-4597. It is placed at a heliocentric distance of 43 pc according to its *Gaia* DR2 parallax, and it has a spectral type of M3.5 (Riaz et al. 2006). It was proposed as a THA candidate member by Malo et al. (2013), they obtained a membership probability of 98.9% to the association. Malo et al. (2014) indicate that the primary is a single-line spectroscopic binary. Baron et al. (2019) indicates a total mass of 0.84 $M_\odot$ for it. We found a candidate companion placed at an angular separation of 7″. This object was reported as a common proper motion companion by Janson et al. (2014), and it has a spectral type of M5.5 Riaz et al. (2006).

We obtained near-infrared spectroscopy of both the primary and the candidate companion using NTT/SofI, and obtained spectral types of M3.5 and M5.5 for them.

B.3.0.5 THA 136, THA 141 and THA 142

The three components in this candidate system are previously reported THA candidate members. The primary is known as CD-53 544. It was proposed as a THA candidate member by Torres et al. (2008), its spectral type is K6 (Torres et al. 2006). Its heliocentric distance is 44 pc according to its *Gaia* DR2 parallax. The secondary is an M2 star placed at an angular distance of 22″. Both objects were discovered to be close nearly equal-mass binaries, with separations of 0.04″ and 0.08″, respectively, and masses of 0.7+0.7 $M_\odot$ and 0.56+0.54 $M_\odot$, respectively (Shan et al. 2017).

We found an additional candidate companion placed at an angular distance of 15′ from the primary, corresponding to a projected physical separation of 40 700 AU. This object was observed by Martín et al. (2010) in their search for ultracool objects, they measured a spectral type of M9.5. It was identified as a

THA candidate member by Gagné et al. (2015b), they obtained a membership probability of 99.9% to the association. They estimated a mass of 20 M_{Jup}. This object was not previously related as a candidate companion to any of the two close binaries in the literature. Its *Gaia* PM and parallax are in very good agreement with the two close binaries.

We observed THA 136 in the near-infrared using NTT/SofI, and obtained a spectral type of M9.5.

B.3.0.6 THA 143 and THA 144

The two components in this candidate system were previously proposed as THA candidate members. They are known as UCAC3 73-5378 and UCAC3 73-5376. Both were included in the THA census by Kraus et al. (2014), they obtained a spectral type of M4.3 for each one. They are placed at a heliocentric distance of 42 pc according to their *Gaia* DR2 parallax, and their angular separation is 23″, corresponding to a physical projected separation of 970 AU.

The *Gaia* DR2 astrometry of the two components is in very good agreement with each other. The astrometric error of the primary is slightly higher than expected for its brightness, but it is not marked as a duplicated source.

B.3.0.7 THA 157 and THA 158

The primary in this candidate system is known as GSC 08057-00342. It was proposed as a THA candidate member by Rodriguez et al. (2013). It is placed at a heliocentric distance of 44 pc according to its *Gaia* DR2 parallax. There are different spectral type estimations in the literature for this object, that classify it as an M1.1 (Kraus et al. 2014), M1.5 (Riaz et al. 2006) and even M3 (Torres et al. 2000). It was recently discovered to be a spectroscopic binary by Flagg et al. (2020), they estimated a spectral type of M2+M3. We found a candidate companion placed at an angular separation of 15″. This object was proposed as a THA member by Gagné et al. (2015b), they obtain a membership probability of 99.7% for it. It was also reported as a proper motion companion to the binary primary by Flagg et al. (2020).

The *Gaia* DR2 astrometry of both objects is in very good agreement with each other.

We obtained near-infrared spectroscopy of THA 158 using NTT/SofI and obtained a spectral type of M5.

B.3.0.8 THA 362 and THA 363

The two components in this system were proposed as THA candidate members by Gagné & Faherty (2018). They also present them as comoving companions, and estimate an expected spectral type of ∼M5 for both. Their heliocentric distance is 42 pc, according to their *Gaia* DR2 parallax, and their angular separation is 6″, corresponding to a projected physical separation of 260 AU. Their *Gaia* DR2 PM and parallaxes are in very good agreement between each other.

We acquired optical and near-infrared spectroscopy of both components, using DuPont/B&C and NTT/SofI, and obtained spectral types of M5.5 for both in the optical, and M5 for both in the NIR.

B.3.0.9 THA 207 and THA 364

The primary in this system is a visual binary formed by two very bright stars, HD 24072 (B9.5) and HD 24071 (A1). Their *Gaia* DR2 parallaxes and PMs are in very good agreement, and their heliocentric distance places them at 53 pc. Their angular separation is 8″, which corresponds to a projected physical separation of 420 AU.

We found a candidate companion placed at 1.4′ from this binary. This object was proposed as a THA candidate member by Elliott et al. (2016). Gagné & Faherty (2018) identified is as a comoving companion of the bright binary, and they estimated an expected spectral type of ∼M2 for the companion. The *Gaia* DR2 astrometry of this object is in good agreement with the brighter binary, although they have slight discrepancies. However, the astrometric errors of the brightest objects are higher than expected, and their astrometry is probably affected by their proximity.

We obtained near-infrared spectroscopy of THA 364 using NTT/SofI, and obtained a spectral type of M4.

B.3.0.10 THA 212 and THA 213

The components in this candidate system are known as HD 25284 and HD 25284 B. They are placed at a heliocentric distance of 49 pc. Their angular separation is 12″, corresponding to a projected physical separation of 570 AU. They were reported as common proper motion companions by Chauvin et al. (2010) and Benavides et al. (2010). Later, Kraus et al. (2014) included them as THA candidate members, they estimated spectral types of K4 and K5 for them. The secondary is reported as a close binary in the Tycho Double Star Catalogue, with a separation of 0.5″between the components. However, it is not

marked as a duplicated source in the *Gaia* DR2 catalogue, and its astrometric errors are not higher than the usual either.

The *Gaia* DR2 astrometry of these two objects is in very good agreement with each other. The astrometric errors of the primary are larger than expected for its brightness, but it is not marked as a duplicated source.

B.3.0.11 THA 367 and THA 368

The two components in this candidate system were identified as THA candidate members by Gagné & Faherty (2018). They also presented them as comoving candidate companions, and estimated expected spectral types of ∼M4 and ∼M5 for them from their photometry. They are placed at a heliocentric distance of 53 pc, according to their *Gaia* parallax. Their angular separation is 6″, corresponding to a projected physical separation of 300 AU.

The *Gaia* DR2 PM and parallax of both components is in very good agreement with each other. The primary has unusually high astrometric errors for its brightness, and is marked as a duplicated source.

We observed both components in the optical range using NOT/ALFOSC, and obtained spectral types of M4.5 and M6.5.

B.3.0.12 THA 238 and THA 239

This primary was discovered to be a young nearby star by Torres et al. (2006). They determined a spectral type of K7. Torres et al. (2008) proposed it as a THA candidate member, with a membership probability of 90%. Its *Gaia* DR2 parallax indicates a heliocentric distance of 60 pc. It was reported to be a close binary by Elliott et al. (2015), with an angular separation of 1″, and masses of 0.7+0.35 $M_{\odot}$.

We found a candidate companion placed at 6′ from this primary. At the heliocentric distance of the primary, this translates to a projected physical separation of 21 900 AU. The candidate companion is another compiled member of THA. It was confirmed as a THA candidate member by Kraus et al. (2014), and they determined a spectral type of M4.1. The secondary was discovered to be a close nearly equal-mass binary by Shan et al. (2017) and Janson et al. (2017), with an angular separation of 0.5″between its components. Shan et al. (2017) estimate a heliocentric distance of 55±3 pc, an a mass of 0.28+0.28 $M_{\odot}$ for it.

The binary secondary is detected in *Gaia* DR2, but it is marked as a duplicated source and does not include a complete 5-parameter astrometric solution. However, its PM is measured in the PPMXL catalogue, and this measurement

is in very good agreement with the binary primary within its errors. The primary shows only one entry in the *Gaia* DR2 catalogue, it is not marked as a duplicated source, and it shows astrometric errors which are not significatively high for its brightness.

B.3.0.13 THA 251c

The primary in this system is HD 53842, a well known F5 member of THA, placed at 58 pc according to its *Gaia* DR2 parallax. We found a candidate companion placed at a distance of 11′, which corresponds to a projected physical separation of 37 900 AU at the heliocentric distance of the primary.

The candidate companion has two very close entries in *Gaia* DR2 catalogue, both with similar brightness. One of them has a non-adequate parallax but similar PM, and the other one does not have a parallax or PM measurement. The parallax measurement of the first one could be affected by the proximity of the second object, and may not be reliable. Hence, we have two *Gaia* entries with similar magnitudes which could be two related objects, or a chance alignment of two objects with similar apparent brightness but placed at different heliocentric distances. These objects have a single PM measurement in the PPMXL catalogue of (1.8, 52.6) ±(11.5,11.5) mas yr^{-1}, which is similar to the primary but not coincident. The $G - J$ colour of the sources correspond to an ∼M4.5–M5.5 spectral type, which is in agreement with the expected if it is placed at the same heliocentric distance as the primary.

B.3.0.14 THA 271c

The compiled object in this system corresponds to the brown dwarf 2MASS J20334473−5635338. This object was proposed as a THA member by Gagné et al. (2015b), they estimated a spectral type of M9.8, a mass of 13.5 M_{Jup} and a statistical heliocentric distance of 55 pc, and give a moderate probability of membership to the THA association, of 49.8%. Therefore, the membership of this object to the THA association is dubious. They indicate a PM of (16.0, −73.1)±(6.1, 12.5) mas yr^{-1}. This object was later observed by Gagné et al. (2015c), they found a spectral type of L0 and signs of very low gravity in its spectrum. We found a brighter companion candidate at a separation of 13′ from it, with an expected spectral type of ∼M4.5.

The L0 does not have an entry in the *Gaia* DR2 catalogue, due to its faintness in the optical wavelength range. The brighter candidate companion does have an entry in *Gaia* DR2, its parallax indicates a heliocentric distance of 63 pc, which would indicate a projected physical separation with the L0 of

47 700 AU. Its PM is similar to the L0, although slightly higher in both RA and DEC. Its $G - J$ colour indicates a spectral type of ∼M4.5.

B.3.0.15 THA 273c

The compiled member in this system was proposed as a THA candidate member by Gagné et al. (2015b). They estimate an expected spectral type of ∼M5.3 from its photometry, and give a membership probability to the association of 68.6%. It is placed at a heliocentric distance of 55 pc according to its *Gaia* DR2 parallax.

We found a brighter object placed at an angular separation of 8′from this compiled member, which corresponds to a projected physical separation of 27 700 AU. This object was rejected as a THA candidate member by Kraus et al. (2014), due to its radial velocity of -9.7 km s^{-1}. They measured a spectral type of M2.3 for it, and they found Hα in its spectrum, with a pEW of -3.41 Å.

The *Gaia* DR2 astrometry of the two objects is in relatively good agreement.

We observed both the primary and the candidate in the near-infrared using NTT/SofI and obtained spectral types of M4.5 and M5.5 for the components.

B.3.0.16 THA 330 and THA 331

The primary in this system was proposed as a THA candidate member by Gagné et al. (2015b), with a membership probability of 98.7%. They obtained a spectral type of M5 for it. This object is placed at a heliocentric distance of 42 pc according to its *Gaia* DR2 parallax.

We found a candidate companion placed at an angular separation of 17″from it, corresponding to a projected physical separation of 700 AU. This object was originally identified by Cruz et al. (2009), they obtained a spectral type of L2, and signs of a very low gravity (γ) in its spectrum. It was proposed as a THA candidate member by Gagné et al. (2015b), with a membership probability of 99.9%. Faherty et al. (2016) obtained a near-infrared spectral type of L3γ. This object was included as a comoving companion to the M5 primary in Desrochers et al. (2018).

The *Gaia* DR2 astrometry of this pair is in very good agreement. The secondary has high astrometric errors, probably due to its faintness.

B.3.0.17 THA 333 and THA 335

The two components in this candidate system were previously proposed as candidate THA members in the literature. The brightest one (THA 333) was

proposed as a THA candidate by Gagné et al. (2015b), with a membership probability of 77.3% and an estimated expected spectral type of ∼M3.5 from its photometry. It is placed at a heliocentric distance of 49 pc according to its *Gaia* DR2 parallax. The faintest one (THA 335) is placed at 3′ from the primary, corresponding to a projected physical separation of 8600 AU. It was proposed as a THA candidate member by Kraus et al. (2014). They obtained a spectral type of M3.8.

The brightest component has two entries in the *Gaia* catalogue with similar G magnitude. One of them has a complete 5-parameter astrometric solution, which is in relatively good agreement with the faintest one, although its astrometric errors are slightly higher than expected for its brightness, probably due to the proximity of the other object. The second entry does not have a complete 5-parameter solution.

We observed the candidate "primary" using NTT/SofI, and obtained a spectral type of M6, which is later than the spectral type of the faintest component, despite being placed at a similar heliocentric distance according to their *Gaia* DR2 parallaxes. This fact, combined with the double entry in the *Gaia* DR2 catalogue indicates that the brightest component is most likely binary, and that the M3.8 would be the primary of the system.

B.3.0.18 THA 336 and THA 337

The two components in this candidate system were also previously identified as THA candidate members in the literature. The primary was proposed as a THA member by Malo et al. (2013), with a membership probability of 99.9%. Its spectral type is M2.5 (Riaz et al. 2006). It is placed at a heliocentric distance of 46 pc, according to its *Gaia* DR2 parallax. The secondary is placed at 13′ from it, corresponding to a projected physical separation of 35 100 AU. This object was proposed as a THA member by Kraus et al. (2014), they obtained a spectral type of M3.5.

The *Gaia* DR2 astrometry of these two objects is in perfect agreement with each other. The astrometric errors for both objects are low, and they are not marked as duplicated sources.

B.4 Details on the individual TWA candidate systems

B.4.0.1 TWA 020 and TWA 021

The primary in this system is the star TW Hya. It is placed at a heliocentric distance of 60 pc according to its *Gaia* DR2 parallax, and its spectral type is

K6 (Torres et al. 2006). We found a candidate companion placed at an angular separation of 12′ from it, corresponding to a projected physical separation of 44 200 AU. This object is known as TWA 28. It was identified as a TWA member by Scholz et al. (2005), they determined a spectral type of M8.5 in the optical, and also proposed it as a wide companion to the star TW Hya. They estimated a mass of 20 M_{Jup} for it. The *Gaia* DR2 astrometry of both objects is in very good agreement with each other.

B.4.0.2 TWA 023c

The primary in this system was proposed as a TWA candidate member by Gagné et al. (2015b). They estimated a spectral type of M5.3 from its photometry, a membership probability of 84.8% to TWA, a statistical distance of 50.6 pc, and a mass of 31.6 M_{Jup}. However, according to *Gaia* DR2, it is placed a bit further away, at a heliocentric distance of 85 pc. We found a candidate companion placed at a distance of 6.4′, which, at the distance of the primary would correspond to a projected physical separation of 32 700 AU.

The companion has an entry in *Gaia* DR2, but does not have parallax or PM measurement. It is also marked as a duplicated source. Its $G - J$ colour indicates an ∼M5.5 spectral type. It does have an entry in the PPMXL catalogue, and its PM is slightly discrepant in right ascension with the primary. The primary's $G - J$ colour also indicates an ∼M5.5 spectral type.

We obtained optical spectroscopy using DuPont/B&C of both the primary and the candidate companion, and found spectral types of M5.5 for both components. These spectral types indicate that they cannot be placed at the same heliocentric distance, as the faintest one is also a possible binary, indicating that it must be placed at a larger heliocentric distance.

B.4.0.3 TWA 038 and TWA 039

The two components in this candidate system are known as CD-34 7390 A and CD-34 7390 B. They are also known as TWA 13A and TWA 13B. They are placed at a heliocentric distance of 60 pc, and their angular separation is 5″, corresponding to a projected physical separation of 300 AU. They were identified as TWA candidate members and as a visual binary by Sterzik et al. (1999), who obtained a spectral type of M1 and M2 for them. Later, Torres et al. (2006) obtained spectral types of M1 and M1. Their *Gaia* DR2 astrometry of the two components is in very good agreement with each other.

B.4.0.4 TWA 046c

The primary in this candidate system is known as TWA 30. Its heliocentric distance is 48 pc according to its *Gaia* DR2 parallax. It was identified as a TWA candidate member by Looper et al. (2010b), they obtained a spectral type of M5 for it and a strong variability, due to the presence of an accretion disk. We found a candidate companion placed at a separation of 1.3′ from it, corresponding to a projected physical separation of 3800 AU. This object is known as TWA 30B. It was identified as a wide companion by Looper et al. (2010a). They obtained a spectral type of M4 for the secondary, and evidence of the presence of an accretion disk around it. They found evidence that the reason for the secondary to appear several magnitudes underluminous despite its earlier spectral type is the fully edge-on orientation of its accretion disk.

The *Gaia* DR2 astrometry of the two components is in very good agreement with each other.

B.4.0.5 TWA 047 and TWA 048

The components in this candidate system are known as CD-26 8623 and CD-26 8623 B, or TWA 8A and TWA 8B. Their heliocentric distance is 46 pc according to their *Gaia* DR2 parallax, and their angular separation is 13″, corresponding to a projected physical separation of 610 AU. They were identified as candidate members to TWA and also as comoving companions by Webb et al. (1999). They determined spectral types of M2 and M5 for them.

The *Gaia* DR2 astrometry of both components is in very good agreement with each other. None of them is marked as a duplicated source.

B.4.0.6 TWA 049c

The catalogued member in this candidate system is known as 2MASS J11353003-1947062. It was proposed as a TWA candidate member by Gagné et al. (2017), with a moderate membership probability of 52.7%, an expected spectral type of ∼M6, and a statistical heliocentric distance of 34 pc. However, according to its *Gaia* DR2 parallax it is placed further away, at a heliocentric distance of 91 pc. Its $G - J$ colour indicates a spectral type of ∼M3.

We found a brighter candidate companion to this object. This object is not previously known in the literature. It is placed at an angular separation of 16″, which corresponds to a projected physical separation of 1500 AU. Its *Gaia* DR2 astrometry is in very good agreement with the known TWA candidate member (secondary), and its $G - J$ colour indicates a spectral type of ∼M4.

B.4.0.7 TWA 050c

The primary in this system was proposed as a TWA member by Gagné et al. (2015b). They estimated a spectral type of ∼M3.9 from its photometry, a statistical distance of 63 pc, a mass of 90.7 M_{Jup}, and a membership probability of 98.9% to TWA. Gagné et al. (2017) later updated its statistical heliocentric distance to 59.8 ± 7.2 pc. The primary is marked in *Gaia* DR2 as a duplicated source, and does not show a parallax or PM measurement. Therefore, it is a possible binary source.

We found a candidate companion placed at 1.4′ from this primary. This object was proposed as a TWA candidate member by Gagné et al. (2015b), with a membership probability of 99.0%, and a statistical distance of 60.2 pc. However, Gagné et al. (2017) measured a spectral type of M5 for it, and updated its membership probability to low-likelihood candidate member. The candidate companion has two entries in *Gaia* DR2, very close to each other, which are also almost coincident in brightness. Therefore, the secondary is also probably a close binary, with similar mass components. Neither of the two entries has a parallax or PM measurement in the *Gaia* DR2 catalogue. However, they do have a PM measurement in the PPMXL catalogue, and the PM of both the (possibly binary) primary and the (possibly binary) secondary are in perfect agreement between each other.

Acknowledgements / Agradecimientos

Al futuro doctorando que sostenga este ejemplar entre sus manos. ¡Huye, estás a tiempo! Es broma. Si yo he podido, tú puedes también :)

Al equipo de Objetos Subestelares del IAC, por los consejos y discusiones interesantes sobre ciencia, y por su ayuda inestimable. En especial, a mi supervisor, Víctor: gracias por tu paciencia infinita y tu apoyo incondicional. Eres el mejor. ¡Sin ti jamás habría sido capaz de conseguirlo! Al personal del IAC, por hacerme sentir siempre como en casa. Al personal de los Observatorios de Canarias, y de La Silla, en Chile, por lo mismo. A mi familia, por apoyar siempre a esta joven sub-estelar eyectada a una órbita a muy alta separación de casa, y mantener nuestra energía de ligadura siempre estable a pesar del tiempo y la distancia. A Ray, por sufrir esta tesis más que yo (¡vámonos de vacaciones, por favor! <3). Te quiero muchísimo. A mis compañeras de The Healers, por enseñarme lo que significa tener una banda de rock de verdad (ha sido la caña!!), y a los compañeros músicos del IAC de las bandas sin nombre por los buenos ratos.

Y sobre todo, a mis compañeros de reparto de "Doctorandos", la mejor sitcom de la vida real. Si todo esto en algún momento mereció la pena, fue gracias a vosotros. Gracias por las cenas, las cervezas, las excursiones, los conciertos, los almuerzos en la cafetería (¡la mejor parte del día!), las fiestas, las risas, los desahogos y el apoyo moral. Gracias por enseñarme tantísimo y por ser tan auténticos. También a esas personitas especiales (doctorandos o no) que con una cerveza, un abrazo y sus palabras me empujaron día a día a seguir avanzando, y a llevar mejor las rayadas y los dilemas de la vida. Y en especial, a Rebeca, a quien dedico esta tesis. Sé que tú lo habrías conseguido también, y tu tesis habría sido genial. No puedo sino dedicarte la mía, con todo mi corazón. Te echaré muchísimo de menos.